

AD-A115 395

FOREIGN TECHNOLOGY DIV WRIGHT-PATTERSON AFB OH
OPTIMUM FILTERS AND PULSED SIGNAL STORAGE DEVICES, (U)
MAY 82 Y S LEZIN
FTD-ID(RS)T-0182-81

F/8 9/5

UNCLASSIFIED

NL

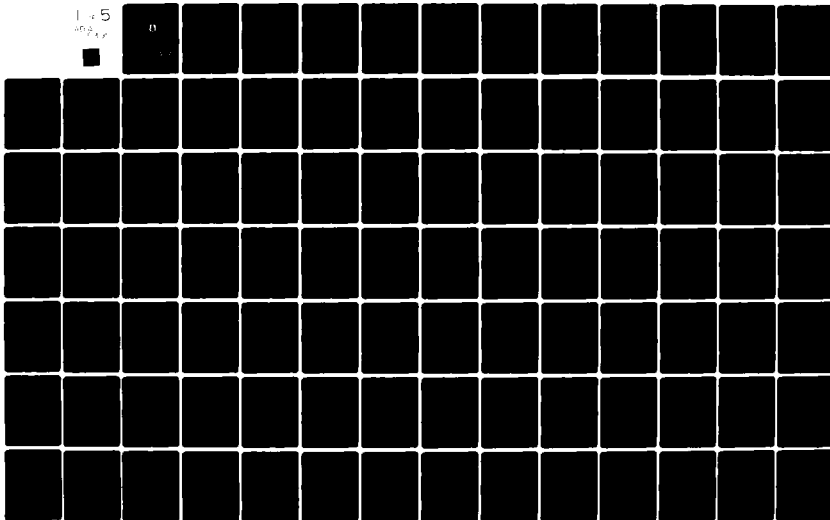
145

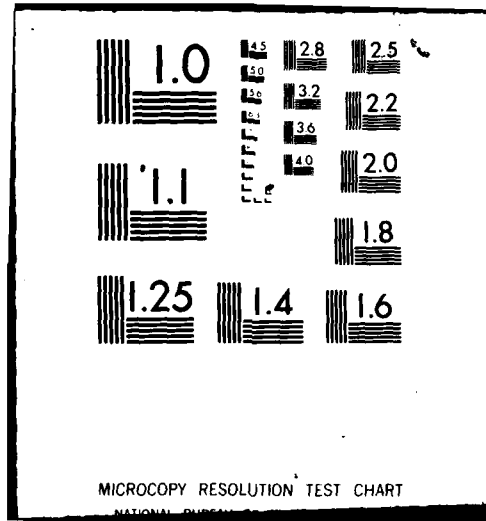
402

414



0





2

FTD-ID(RS)T-0182-81

AD A115395

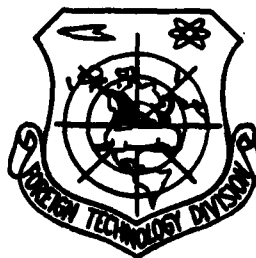
FOREIGN TECHNOLOGY DIVISION



OPTIMUM FILTERS AND PULSED SIGNAL STORAGE DEVICES

by

Yu.S. Lezin



DTIC
ELECTE
JUN 10 1982
S D D

DTIC FILE COPY

Approved for public release;
distribution unlimited.



82 06 10 125

Accession For	
NTIS GRA&I	<input checked="" type="checkbox"/>
DTIC TAB	<input type="checkbox"/>
Unannounced	<input type="checkbox"/>
Justification	
By	
Distribution/	
Availability Codes	
Dist	Avail and/or Special
A	



FTD-ID(RS)T-0182-81

EDITED TRANSLATION

FTD-ID(RS)T-0182-81

5 May 1982

MICROFICHE NR: FTD-82-C-000589

OPTIMUM FILTERS AND PULSED SIGNAL STORAGE DEVICES

By: Yu.S. Lezin

English pages: 395

Source: Optimal'nyye Fil'try i Nakopiteli
Impul'snykh Signalov, Publishing House
"Sovetskoye Radio", Moscow, 1969, pp. 1-445

Country of origin: USSR

Translated by: SCITRAN

F33657-81-D-0263

Requester: USAMICOM

Approved for public release; distribution unlimited.

THIS TRANSLATION IS A RENDITION OF THE ORIGINAL FOREIGN TEXT WITHOUT ANY ANALYTICAL OR EDITORIAL COMMENT. STATEMENTS OR THEORIES ADVOCATED OR IMPLIED ARE THOSE OF THE SOURCE AND DO NOT NECESSARILY REFLECT THE POSITION OR OPINION OF THE FOREIGN TECHNOLOGY DIVISION.

PREPARED BY:

TRANSLATION DIVISION
FOREIGN TECHNOLOGY DIVISION
WP-AFB, OHIO.

FTD-ID(RS)T-0182-81

Date 5 May 19 82

Table of Contents

U.S. Board on Geographic Names Transliteration System	iii
Preface	1
Introduction	3
Part One, Optimum Filters	7
Chapter 1, Properties of Optimum Filters	8
Chapter 2, Optimum Filters for the Simplest Pulsed Signals	47
Chapter 3, Optimum Filters for Pulsed Signals with Linear Frequency Modulation	89
Chapter 4, Optimum Filters for Phase-Manipulated Signals	127
Chapter V, Optimum Filters for Sequences of Pulsed Signals	159
Part 2, Pulsed Signal Storage Devices	196
Chapter VI, Threshold Signals with Coherent Storage of Pulsed Signal Sequences	197
Chapter VII, A Coherent Single-Stage Storage Device	232
Chapter VIII, A Coherent Double Storage Device	258
Chapter IX, Coherent Two-Stage Storage Device	272
Chapter X, Noncoherent Exponential-Weight Storage Device	287
Chapter XI, Problems of Practical Realization of Analog Pulsed Signal Storage Devices	334
Chapter XII, Digital Storage Devices	356

References	379
List of Notations	390
Abbreviations Used in Text and on Block Diagrams	393
Notations of Block-Diagram Components Used in Figures	394

U. S. BOARD ON GEOGRAPHIC NAMES TRANSLITERATION SYSTEM

Block	Italic	Transliteration	Block	Italic	Transliteration
А а	<i>А а</i>	A, a	Р р	<i>Р р</i>	R, r
Б б	<i>Б б</i>	B, b	С с	<i>С с</i>	S, s
В в	<i>В в</i>	V, v	Т т	<i>Т т</i>	T, t
Г г	<i>Г г</i>	G, g	У у	<i>У у</i>	U, u
Д д	<i>Д д</i>	D, d	Ф ф	<i>Ф ф</i>	F, f
Е е	<i>Е е</i>	Ye, ye; E, e*	Х х	<i>Х х</i>	Kh, kh
Ж ж	<i>Ж ж</i>	Zh, zh	Ц ц	<i>Ц ц</i>	Ts, ts
З з	<i>З з</i>	Z, z	Ч ч	<i>Ч ч</i>	Ch, ch
И и	<i>И и</i>	I, i	Ш ш	<i>Ш ш</i>	Sh, sh
Й й	<i>Й й</i>	Y, y	Щ щ	<i>Щ щ</i>	Shch, shch
К к	<i>К к</i>	K, k	Ъ ъ	<i>Ъ ъ</i>	"
Л л	<i>Л л</i>	L, l	Ы ы	<i>Ы ы</i>	Y, y
М м	<i>М м</i>	M, m	Ь ь	<i>Ь ь</i>	'
Н н	<i>Н н</i>	N, n	Э э	<i>Э э</i>	E, e
О о	<i>О о</i>	O, o	Ю ю	<i>Ю ю</i>	Yu, yu
П п	<i>П п</i>	P, p	Я я	<i>Я я</i>	Ya, ya

*ye initially, after vowels, and after ъ, ь; e elsewhere.
When written as ě in Russian, transliterate as yě or ě.

RUSSIAN AND ENGLISH TRIGONOMETRIC FUNCTIONS

Russian	English	Russian	English	Russian	English
sin	sin	sh	sinh	arc sh	sinh ⁻¹
cos	cos	ch	cosh	arc ch	cosh ⁻¹
tg	tan	th	tanh	arc th	tanh ⁻¹
ctg	cot	cth	coth	arc cth	coth ⁻¹
sec	sec	sch	sech	arc sch	sech ⁻¹
cosec	csc	csch	csch	arc csch	csch ⁻¹

Russian English

rot curl
lg log

GRAPHICS DISCLAIMER

All figures, graphics, tables, equations, etc. merged
into this translation were extracted from the best
quality copy available.

UDC 621.391.272;621.374.325;621.396.96

Lezin, Yu. S. Optimum Filters and Pulsed Signal Storage Devices. Second edition, revised and supplemented. Izdatel'stvo "Sovetskoye radio," 448 pages, 11,400 copies, price 1 ruble 48 kopecks

The book is a monograph in which the properties of optimum (matched) signal detection filters on a background of gaussian noise, methods of building them, the operating mechanism and efficiency of these filters, their practical approximations and specifically of analog and digital storage devices of repeated pulsed signals are outlined. The problems of practical realization of the devices indicated above are also discussed in detail.

The methods considered in the book are reduced to engineering formulas. The results of calculations made by these formulas are presented in the form of a large number of graphs and tables which permit rather simple comparison of different systems and selection of their individual parameters. Therefore, the book may be used as a reference manual when designing noiseproof radio apparatus.

The book is intended for a wide range of radio engineers involved in development, design, production and operation of radar and other pulsed systems and for teachers, graduate students and students of radio engineering specialties of higher educational institutions.

167 figures, 18 tables and 219 references.

PREFACE

3

The given book is the second, revised and supplemented edition of a book of the same name published in 1963. Approximately 60 percent of the text was rewritten during preparation of the second edition. It is devoted to problems of increasing the noise stability of radar systems by means of optimum (matched) filters and pulsed signal storage devices. Main attention is devoted to applied problems of efficient construction and calculation of the indicated devices.

The results of the author's investigations, conducted during the period 1957-1966 are systematically outlined in the book. Moreover, the papers of other authors published in the Soviet and foreign press were also used. The latter is related mainly to Chapters 1, 3, 4, 6, 11 and 12.

The author is deeply grateful to Corresponding Member of the USSR Academy of Sciences Yu. B. Kobzarev, who turned the author's attention during many conversations to a number of unresolved problems in the indicated field of electronics and made valuable comments on the results of solving them.

The materials outlined in the book have been repeatedly reported at scientific conferences, seminars and meetings.

The author is truly grateful to all those who sent their comments on the first edition of the book and who participated in discussion of it and especially to Yu. B. Kobzarev, A. Ye. Basharinov, B. R. Levin, N. I. Chistyakov, A. P. Manovtsev, N. T. Petrovich, A. G. Saybel',

M. Stanecu and K. P. Polov. Moreover, gratitude is expressed to Yu. I. Pakhomov, who together with the author wrote section 3.5 and item 2 of section 6.5 of the book and made a number of interesting comments on the first edition of the book, and to M. M. Leshchinskiy, who participated in writing Chapter 12 and who kindly offered to the author the materials outlined in section 10.6.

The author is deeply grateful to B. N. Mutyashev and V. I. Tikhonov for very careful review of the manuscript of the second edition of the book and for useful advice directed toward improving it.

All remarks on the book's contents will be gratefully accepted by the author.

INTRODUCTION

5

Increasing the noise stability of radio reception has always been one of the most important problems of electronics [1]. The noise which inevitably enters a receiver together with signals or that occurs in it distorts the transmitted messages and thus limits its sensitivity. By attenuating the harmful effect of noise, one can increase the reliability of message transmission and the effective range of radio engineering systems.

The problem of a significant increase of the effective range of radar systems, which can be solved only by significantly increasing the average power of transmitting devices, increasing the overall dimensions of antennas and increasing the sensitivity of receivers of these systems, is specifically very timely. However, a further increase of transmitter power and the overall dimensions of antennas is fraught with such extensive engineering difficulties [2, 3] that significant results should not be expected in this direction. Moreover, increasing transmitter power inevitably leads to the following undesirable consequences:

- complication of the design of the SHF generator, pulsed modulator, power supply device, and antenna-feeder waveguide devices;

- an increase of operating expenses due to an increase of energy consumption and complication of maintenance;

--an increase of the noise level created by the given RLS [radar station] to other detection, control, communications and television systems and so on;

--an increase of the electromagnetic field intensity and consequently of the degree of the harmful effect on maintenance personnel and other people located nearby.

Therefore, increasing the noise stability (sensitivity) of radio receivers is one of the promising, economically feasible and practically possible methods of significantly increasing the effective range of radar systems.

6

One can achieve an increase of receiver sensitivity by different methods: by cooling their input circuits to temperatures close to absolute zero, by using quantum-mechanics and parametric amplifiers and by using devices that carry out optimum separation (filtration) of pulsed signals from noise.

Among these methods, the use of optimum filters that accomplish optimum separation of pulsed signals from noise [4-6] and devices that are practical approximations of these filters [7] occupies an important position.

The abundance of articles in Soviet and foreign periodical literature on these problems specifically indicates the timeliness of optimum filtration problems.

The first edition of the book [7] was written in 1961-1962 when the properties of optimum filters, like the capabilities provided by using them, were known to a comparatively small range of radio engineers. The situation has now changed fundamentally. The main concepts of optimum filtration theory and pulsed signal storage have become generally known and have become part of many textbooks of vuzes [higher educational institutions] [8-10], while optimum filters and storage devices have achieved wide application.

A large number of monographs on statistical methods of signal separation from noise has been published during the past few years. The most significant of them are the book of L. A. Vaynshteyn and V. D. Zubakov [11], S. Ye. Fal'kovich [12], L. S. Gutkin [13], Ya. D. Shirman and V. N. Golikov [10], a collective of authors with editing by G. P. Tartakovskiy [14] and V. I. Tikhonov [15]. The very interesting books of Woodward [16], Middleton [17], Davenport and Ruth [18] and Helstrom [19] have been translated into Russian and published. However, the "engineering direction of theoretical investigations is still inadequately expressed" [10] in most of the published papers.

The first edition of the book was written with regard to the fact that we did not know of a single book in which the statistical methods of signal separation from noise could be considered in detail with an engineering, applied slant. The following hypothesis of the authors of [11] is very typical in this regard: "To avoid confusion, let us note that optimum filters and optimum detectors have been investigated in the book only from the viewpoint of their mathematical operations which filters and detectors should perform on the received mixture of signals and noise; problems related to practical realization of the corresponding circuits remain beyond the scope of the given book."

The first edition of the book was sold out rapidly and the need for a book in which problems of optimum filtration of signals from their mixture with random noise, storage of repeated pulsed signals and building of corresponding devices would be considered from the engineering viewpoint, increased even more. The second edition was prepared in this respect.

It has as its purpose a systematic outline of the properties of optimum filters and building of these filters for single pulsed signals and sequences of them, to determine the operating mechanism of these filters and to discuss possibilities of practical realization of them, to consider the properties of storage systems with delayed feedback, which are a practical approximation of optimum filters for sequences of pulsed signals, and to outline threshold signal theory during storage of sequences of pulsed signals by means of these systems and also to discuss problems of practical realization of pulsed signal storage devices.

The book was fundamentally revised during preparation of the second edition, which mainly had two purposes.

The first purpose was to increase the theoretical level and to utilize more complex mathematical apparatus of the probability ratio, bell functions and the theory of recurrent events. This made it possible to outline more strictly the problem of optimum detection of various signals: precisely known, with random initial phase and with random initial phase and amplitude, to find and outline new interesting and important results on the efficiency of analog and digital pulsed signal storage devices. In increasing the theoretical level of the book, we attempted to preserve the accessibility of the outline in brevity and compressiveness determined by the limited volume of the book.

The second purpose of revising the book was to amplify its applied direction. The structure of the book was changed, several new chapters, paragraphs and sections of an applied nature were written, the number of examples and figures was increased and so on for this purpose.

Chapters 7, 8, 9, 11 and 12 were rewritten during the revision and Chapters 1, 2, 3 and 5 were completely revised. The remaining chapters were supplemented with new materials.

Main attention is turned toward the physical aspect of the outlined processes with regard to the fact that the book is intended for a wide range of readers. The mathematical apparatus used was therefore selected as simply as possible. This made it possible to avoid to a significant degree duplication of the material contained in other books mentioned above.

Despite the considerable simplification of the mathematical apparatus employed in the book, familiarity with the main concepts of probability theory and the theory of random processes is required of the reader (for example, Chapters 2, 3, 4 and 8 of B. R. Levin's book [20] of Chapters 1, 2, 3, 6 and 7 of V. I. Tikhonov's book [15]). The book has been illustrated with a large number of figures, on which are shown the block-diagrams of the considered devices and the time diagrams of voltages at their different points to facilitate understanding.

PART ONE

OPTIMUM FILTERS

CHAPTER 1

11

PROPERTIES OF OPTIMUM FILTERS

1.1. Characteristic Features and Problems of Radar Reception. Nature of Considered Noise

The shape of the received signal reflected from a point object coincides with the shape of the transmitted signal and is therefore previously known in active radar. Information about the object that caused reflection of the transmitted signal is primarily included in the delay time of the received signal with respect to the transmitted signal and also in the frequency bias of the received signal with respect to the transmitted frequency.

However, the fact itself of a reflected signal in the received oscillation is previously unknown. The latter can be represented as both random noise and a mixture of this noise with the reflected signal. The first problem of radar reception also includes determination of the presence of a reflected signal in the received oscillation. This problem is called the detection problem.

The other problem of radar reception is measurement of the parameters of a reflected signal distorted by random noise. These parameters are most frequently the delay time and Doppler frequency shift.

The problem of signal resolution, i.e., the problem of separate detection of several simultaneous reflected signals with parameters that hardly differ and analysis of the parameters of these signals, is also very important to radar.

Main attention is subsequently devoted to consideration of devices to solve the first problem, i.e., signal detection devices on a random noise background. However, the results obtained in this case are applicable both in measurement of parameters and in signal resolution. 12

In this case only noise of the normal fluctuating type is studied. This is explained by at least two factors.

First, fluctuating noise is the main type of noise in the range of ultrashort waves used for radar. Actually, as is known, the level of atmospheric pulsed noise in the indicated band is insignificant and one can essentially avoid the pulsed noise of industrial origin by installing a radar system at a sufficient distance from the source of this noise, which is always possible in the case of detection (especially of long-range) systems. Mutual interference (i.e., noise from other radio engineering systems) can be reduced considerably by separating the systems in frequency and space.

Second, and this is very important, the fluctuating noise that is interference of a purely random nature is a very harmful type of interference [21]. Because of its random nature, it is essentially impossible to completely eliminate it since there always exists the finite probability that noise causes such a distortion of the received signal that the oscillation formed as a result of this will coincide with a completely different signal. In this case the detection error will be inevitable.

Thus, the probability of error (distortion) only to some specific level, which cannot be overcome by any means whatever, can be reduced by improving the receivers. The latter was also strictly proved by V. A. Kotel'nikov, who developed the theory of potential noise stability [22].

When considering the effect of normally fluctuating noise, there is the possibility of applying the comparatively well-developed apparatus of probability theory and the theory of random processes, which permits one to simplify this consideration and to obtain a number of quantitative results.

1.2. The Cross-Correlation Device--the Most Important Part of Optimum Signal Detectors, Signal Identification and Measurement of Parameters

1

1. Detection of Precisely Known Signal

The received oscillation $u_1(t)$ * is either noise $n_1(t)$ or the sum of the signal $v_1(t)$ and noise $n_1(t)$. In the general case one can write

$$u_1(t) = xv_1(t) + n_1(t),$$

where the parameter $x = 1$ in the presence of a signal and $x = 0$ in its absence.

The signal $v_1(t)$, probability distribution of parameter $P(x)$ and probability distribution of noise $P(n_1)$ are assumed to be known. Unknown is only the fact of whether there is a signal in the received oscillation, i.e., the value of parameter x . The receiver should provide an answer on the value of this parameter on the basis of analysis of the received oscillation during the observation interval $t = 0-T$.

No receiver can determine the value of x with absolute accuracy and with total confidence due to the distorting effect of noise and the finite nature of analysis time--there will always be the finite probability of an erroneous decision.

Therefore, the most important thing that can be required of a receiver is to determine the probability of one or another value of x with given realization of the received oscillation $u_1(t)$. In other

*The subscript 1 denotes that the voltages at the receiver input are considered (the receiver is denoted by point 1 and the output of its linear part is denoted by point 2).

words, an optimum receiver based on analysis of the received oscillation should calculate the a posteriori (post experimental) probability distribution $P_{u_1}(x)$ for all possible values (two in the considered case) of parameter x with given received oscillation $u_1(t)$ [13, 16, 22].

A posteriori distribution of $P_{u_1}(x)$ is the distribution of x provided that realization u_1 is received. Since the unconditional probability of the appearances of events x and $u_1(t)$ is

$$P(x, u_1) = P(x) P_x(u_1) = P(u_1) P_{u_1}(x),$$

where $P(u_1)$ is the probability that realization $u_1(t)$ will appear and $P_x(u_1)$ is the conditional probability that this realization will appear at given value of x , then the a posteriori probability is

$$P_{u_1}(x) = \frac{1}{P(u_1)} P(x) P_x(u_1). \quad (1.2.1)$$

The conditional probability $P_x(u_1)$ is the probability that the model of noise $n_1(t) = u_1(t) - xv_1(t)$ will appear, i.e.,

$$P_x(u_1) = P\{n_1(t) = u_1(t) - xv_1(t)\}.$$

According to (1.2.1), the probability that the received oscillation contains a signal ($x = 1$) comprises

$$P_{u_1}(1) = \frac{1}{P(u_1)} P(1) P\{n_1(t) = u_1(t) - v_1(t)\},$$

and the probability that there is no signal ($x = 0$) in the received oscillation,

$$P_{u_1}(0) = \frac{1}{P(u_1)} P(0) P\{n_1(t) = u_1(t)\}.$$

The ratio of these probabilities

$$\frac{P_{u_1}(1)}{P_{u_1}(0)} = \frac{P(1)}{P(0)} \frac{P\{n_1(t) = u_1(t) - v_1(t)\}}{P\{n_1(t) = u_1(t)\}} \quad (1.2.2)$$

is the product of the ratio of a priori probabilities of signal and noise reception and the ratio of probabilities that the received oscillation contains a signal and that this oscillation is only noise.

Unfortunately, a priori probabilities of radar signal reception and its absence in the received oscillation are usually unknown.

Therefore, the value of (1.2.2) is judged only by the value of the so-called probability ratio

$$\Lambda(u_i) = \frac{P[n_i(t) = u_i(t) - v_i(t)]}{P[n_i(t) = u_i(t)]}, \quad (1.2.3)$$

that shows the extent to which the statement of signal reception is more probable than the alternative statement of its absence.

15

If the received noise is white normal noise and has spectral intensity (energy spectrum)

$$F_1(\omega) = 2a^*, \quad (1.2.4)$$

then the probability of noise model $n_1(t)$ having length t and band ΔF comprises [8, 10]

$$P(n_i) = \left(\frac{1}{\sqrt{2\pi \cdot 2a\Delta F}} \right)^{2aFT} \exp \left[-\frac{1}{2a} \int_0^T n_i^2(t) dt \right].$$

In this case, according to (1.2.3),

$$\begin{aligned} \Lambda(u_i) &= \exp \left\{ -\frac{1}{2a} \int_0^T [u_i(t) - v_i(t)]^2 dt \right\} / \exp \left[-\frac{1}{2a} \int_0^T u_i^2(t) \times \right. \\ &\quad \left. \times dt \right] = \exp \left[-\frac{E_i}{2a} + \frac{1}{a} \int_0^T u_i(t) v_i(t) dt \right], \end{aligned} \quad (1.2.5)$$

where $E_i = \int_0^T v_i^2(t) dt$ is the signal energy.

It is interesting to note that the probability ratio (1.2.5) is independent of the width of the noise bandpass. Therefore, it is also valid for the case of white normal noise which is formed as a result of passage to the limit $\Delta F \rightarrow \infty$.

Since the signal is fully known in the considered case, the probability ratio (1.2.5) is dependent only on the value of the

* The value of a is the spectral intensity (i.e., the power for the spectral interval of 1 Hz) of noise if one takes into account both positive and negative frequencies. Since only positive frequencies are subsequently considered according to physical concepts, the spectral noise intensity is assumed equal to $2a$ [11, 20].

integral $\int_0^T u_1(t) v_1'(t) dt$. The latter is a partial value (at $\tau = 0$) of the cross-correlation function of the received oscillation $u_1(t)$ and of the anticipated signal $v_1(t)$ [6, 20]:

$$R_{\nu}(\tau) = \int_0^T u_1(t) v_1(t - \tau) dt, \quad (1.2.6)$$

and is calculated by a cross-correlation device (VKU; Vzaimno korrelyatsionnoye ustroystvo).

Thus, an optimum detector should calculate the a posteriori probability distribution of parameter x with given model of the received oscillation or the ratio of these a posteriori probabilities (1.2.3). Calculation of the latter reduces to calculation of the probability ratio (1.2.5), which is carried out with the cross-correlation device. Consequently, the cross-correlation device is the main component of an optimum detector.

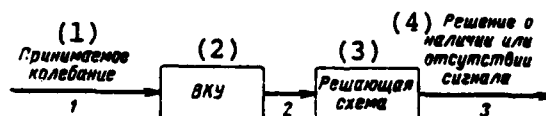


Fig. 1. Block diagram of optimum receiver to detect precisely known signal.

Key: (1) received oscillation; (2) cross-correlation device; (3) resolving circuit; (4) decision on presence or absence of signal.

Its output voltage may coincide with accuracy to the constant multiplier and constant term both with probability ratio $\Lambda(u_1)$ and with any monotonic (for example, logarithmic) function of this ratio. In this case

$$u_2 = k[\ln \Lambda(u_1) + b],$$

where k and b are arbitrary constants.

Selecting $k = a$ and $b = E_1/2a$, we find according to (1.2.5)

$$u_2 = \int_0^T u_1(t) v_1(t) dt = R_{\nu}(0).$$

As already indicated, a detector is designed to analyze the received oscillation to determine whether this oscillation consists only of noise (and there is no signal in this case) or whether it is a mixture of signal and noise. Consequently, this detector is a resolving device.

Besides a purely resolving (logic) circuit, which is essentially a nonlinear device, an optimum detector should contain, as indicated above, a cross-correlation device (Figure 1.2.1). The resolving circuit is most simply made in the form of a threshold device (minimum limiter) which generates a voltage at the output that indicates whether a decision is made on signal reception only if the voltage at its input exceeds some level U_0 , called threshold voltage (Figure 1.2.2). The presence of voltage at the output of the threshold device indicates signal reception and its absence indicates reception of noise alone. Thus, if the voltage of the input of the threshold device u_2^* exceeds the threshold U_0 :

$$u_2 > U_0$$

then a decision is made on the presence of a signal and in the opposite case

$$u_2 < U_0$$

a decision is made on its absence.

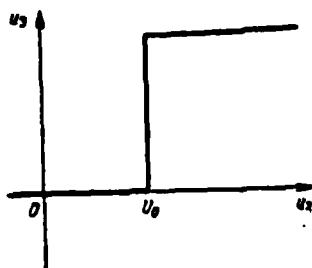


Fig. 1.2.2. Characteristics of threshold device.

* Here and further the subscripts coincide on the corresponding figure to the number of the point to which the considered physical value is related (in the given case u_2 is voltage at point 2 of the block diagram shown in Figure 1.2.1).

Voltage is fed from the output of the threshold device to the information receiver, which may be a digital computer or computing system. If the information receiver is an operator observing reflected signals on a radar screen, the cathode-ray tube of this screen, which reproduces only those voltages on the screen which exceed the cut-off voltage according to its value, due to the nonlinearity of its characteristic, is used as the threshold device.

18

Two types of errors may be observed in operation of the detector.

An error of first kind includes the fact that the voltage at the input of the threshold device (i.e., at the output of the linear filter) exceeds the threshold voltage when noise alone is received, due to which an incorrect decision is made about signal reception. This error is called a false alarm or false detection.

An error of second kind consists in loss of a signal due to the fact that a voltage whose value is less than threshold voltage is formed at the output of the linear filter due to interaction of signal and noise, which is the basis for an erroneous conclusion about reception of noise alone (i.e., about the absence of a signal). It is called signal loss.

The foregoing is illustrated by Figure 1.2.3,* in which the time diagrams of the signal, noise and signal-noise mixture are shown at the input of the threshold device. The response voltage of the threshold device is also shown in Figure 1.2.3, c. It is obvious from consideration of these time diagrams that correct detection of a signal is observed at moment t_1 (i.e., the receiver generates a correct decision on signal reception), the false alarm phenomenon occurs at moment t_2 and signal loss occurs at moment t_3 .

Since both errors are caused by the effect of fluctuating noise, which is a random process subject only to statistical (probability)

* Figure 1.2.3 is drawn for the case when an optimum filter is used as the cross-correlation device in an optimum detector (Figure 1.2.1) (see section 1.3).

laws, the problem of radar signal detection is statistical and can be solved only by using methods of probability theory or the theory of random processes.

19

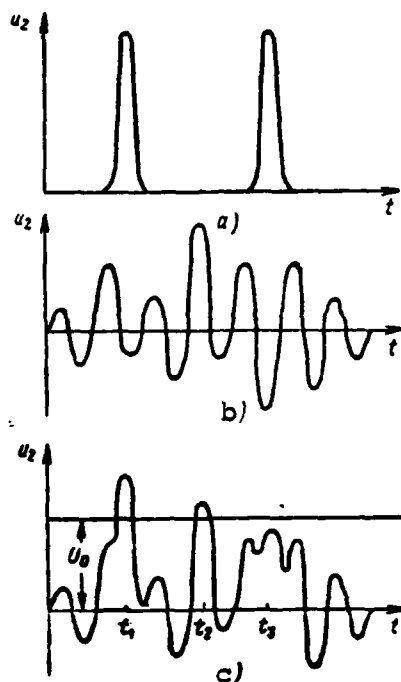


Fig. 1.2.3. Time diagrams of signal (a), noise (b) and signal-noise mixture (c).

Let us determine the error probability of radar reception.

The probability of a false alarm F is equal to the probability that the noise oscillation at the output of the VKU exceeds the threshold voltage:

$$F = \text{Bep}(n_2 > U_0) = \int_{U_0}^{\infty} W(n_2) dn_2,$$

where $W(n_2)$ is the probability distribution density of output noise.

Since

$$n_2 = \int_0^T n_1(t) v_1(t) dt = \lim_{N \rightarrow \infty} \sum_{k=1}^N n_1\left(\frac{kT}{N}\right) v_1\left(\frac{kT}{N}\right) \frac{T}{N},$$

and each term of this sum is distributed by normal law (input noise $n_1(t)$ is a normal random process), then output noise n_2 also has normal

20

distribution. Its mean value is

$$m_1(n_2) = \int_0^T m_1[n_1(t)] v_1(t) dt = 0,$$

since $m_1[n_1(t)] = 0$. The variation of this noise is

$$\begin{aligned} \sigma_1^2 &= m_1(n_2^2) - [m_1(n_2)]^2 = m_1(n_2^2) = m_1 \left[\int_0^T n_1(t) \times \right. \\ &\quad \times v_1(t) dt \int_0^T n_1(x) v_1(x) dx \left. \right] = \int_0^T v_1(t) dt \times \\ &\quad \times \int_0^T m_1[n_1(t) n_1(x)] v_1(x) dx = \int_0^T v_1(t) dt \int_0^T R_n(t-x) v_1(x) dx, \end{aligned} \quad (1.2.7)$$

where $R_n(t)$ is the autocorrelation function of input noise.

Since input noise is considered white noise having spectral intensity (1.2.4), then its autocorrelation function is

$$R_n(\tau) = a\delta(\tau),$$

where $\delta(\tau)$ is a delta-function or single pulse.

Substituting this function into (1.2.7) and using the filter device of the delta-function [23], we find

$$\sigma_1^2 = a \int_0^T \sigma_1^2(t) dt = aE_1. \quad (1.2.8)$$

Consequently, the probability density of the output noise is

$$W(n_2) = \frac{1}{\sqrt{2\pi aE_1}} \exp\left(-\frac{n_2^2}{2aE_1}\right)$$

and the probability of a false alarm is

$$F = \int_0^\infty \frac{1}{\sqrt{2\pi aE_1}} \exp\left(-\frac{n_2^2}{2aE_1}\right) dn_2 = \frac{1}{2} [1 - \Phi(l)], \quad (1.2.9)$$

where $\Phi(l) = \frac{2}{\sqrt{\pi}} \int_0^l e^{-t^2} dt$ is the integral, error function and Kramp's function [20];

$$l = \frac{U_0}{\sqrt{2aE_1}} = \frac{U_0}{\sqrt{2\sigma_1^2}}$$

is the relative response threshold.

Considering the dependence of the probability of a false alarm on the relative threshold (Figure 1.2.4), we arrive at the obvious conclusion that the threshold voltage must be increased compared to the effective (mean square) value of noise at the VKU output to reduce the probability of a false alarm.

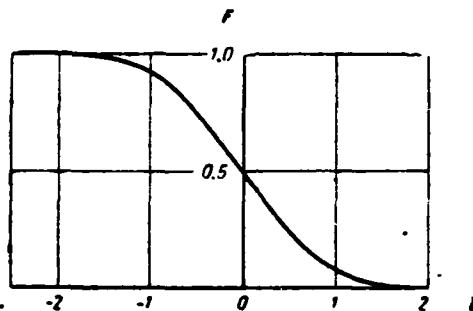


Fig. 1.2.4. Probability of false alarm as function of relative threshold.

Since the voltage of the signal-noise mixture at the VKU output has the mean value

$$\begin{aligned} m_1(u_{\Sigma}) &= m_1(n_1 + v_1) = \int_0^T m_1[n_1(t) + v_1(t)] v_1(t) dt = \\ &= \int_0^T v_1^2(t) dt = E_1 \end{aligned}$$

and variation $\sigma_1^2 = m_1[(n_1 + v_1)^2] - [m_1(n_1 + v_1)]^2 = aE_1$, then the probability density of the output voltage of the signal-noise mixture is

$$W(u_{\Sigma}) = \frac{1}{\sqrt{2\pi aE_1}} \exp \left[-\frac{(u_{\Sigma} - E_1)^2}{2aE_1} \right]$$

and the probability of signal loss is

$$\begin{aligned}
 H &= \text{Bep}(u_{sc} < U_0) = \int_{-\infty}^{U_0} W(u_{sc}) du_{sc} = \\
 &= \frac{1}{2} \left[1 - \Phi\left(\frac{q_1}{\sqrt{2}} - l\right) \right],
 \end{aligned}
 \tag{1.2.10}$$

where

$$q_1^2 = \frac{m_1^2(u_{sc})}{\sigma_2^2} = \frac{E_1}{a} \tag{1.2.11}$$

is the output signal/noise ratio for power.

The dependence of signal loss probability on the difference of the signal/noise ratio and the relative threshold completely coincides with the dependence of the probability of a false alarm on the relative threshold (Figure 1.2.4).

We are usually concerned in practice with the probability of correct detection D rather than with the signal loss probability.

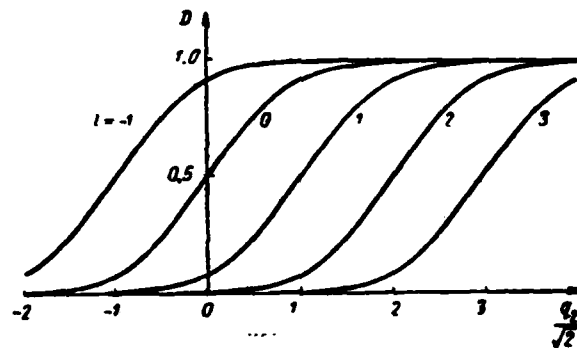


Fig. 1.2.5. Characteristics of detecting a precisely known signal.

Obviously,

$$D = 1 - H = \frac{1}{2} \left[1 + \Phi\left(\frac{q_1}{\sqrt{2}} - l\right) \right]. \tag{1.2.12}$$

It follows from consideration of the dependence of the probability of correct signal detection on the signal/noise ratio at different values of relative threshold (Figure 1.2.5), which is called the detection characteristic, that the signal/noise ratio must be increased

universally compared to relative threshold to increase the probability of correct detection.

It is easy to see from (1.2.9) and (1.2.10) that the relative threshold affects both the probability of a false alarm and the probability of signal loss. However, if the relative threshold must be increased to reduce the probability of an error of first kind, its value must on the contrary be decreased to reduce the probability of signal loss. Therefore, it would seem that the value of this threshold should be selected from compromise concepts to achieve minimum total probability of error. However, this approach, called the ideal observer criterion [11, 17], is most typical for communications systems [24] in which both false detection and signal loss are undesirable to the same degree.

A different approach, called the Neiman-Pearson criterion [10, 11, 17], is more correct in the case of radar detection systems. The fact is that false detection of a radar signal is an exceptionally dangerous phenomenon since it can cause very undesirable consequences and therefore the probability of this event should be very low (on the order of 10^{-6} to 10^{-10}). An increase of this value cannot be permitted even by reducing the probability of signal loss.

If the Neiman-Pearson criterion is used, the probability of a false alarm F is previously fixed. Since it is functionally related to the relative threshold [see (1.2.9) and Fig. 1.2.5], then the latter is also previously given. The problem of a designer of the receiver of a radar detection system reduces to development of devices that permit one to reduce the signal loss probability and consequently to increase the probability of correct detection of the signal.

It follows from (1.2.12) that since the relative threshold is given by the level of the probability of the false alarm, then the only possibility to increase the probability of correct detection is a universal increase of the signal/noise ratio at the input of the threshold device. If it is preceded by the VKU (Fig. 1.2.1), then this ratio, according to (1.2.11), is equal to the ratio of signal energy to half the spectral intensity of noise. If the probability of a false alarm

and the spectral intensity of noise are given, then the probability of a false alarm can be increased only by increasing the signal energy.

With given signal energy, its shape does not affect the probability of correct detection and therefore is insignificant from the viewpoint of solving the detection problem and should be selected from engineering concepts or of achieving high quality characteristics when measuring the signal parameters.

2. Detection of a Signal with Random Parameters

The signal received by the receiver is usually not known precisely. Its amplitude, initial phase, delay time and other parameters are usually previously unknown. Two methods of receiving signals with unknown parameters are possible. The first method includes preliminary conversion of this signal to a totally known signal by measuring (analyzing) all its unknown parameters and subsequent reception of it as a completely known signal. This method requires special time to make the measurements indicated above, complication of the receiver and increased signal/noise ratio. Therefore, it is usually not employed but is replaced with another method in which the unknown parameters of the signal are assumed random and it is received while disregarding their specific values by statistical averaging of the received oscillation for all possible values of these random parameters. In this case the received oscillation is

$$u_1(t) = n_1(t) + xv_1(t, \alpha_1, \alpha_2, \dots),$$

where $\alpha_1, \alpha_2, \dots$ are random unmeasured signal parameters. Let us fix their values. The considered signal then becomes precisely known. According to (1.2.3), the probability ratio for this case 25

$$\Lambda(u_1, \alpha_1, \alpha_2, \dots) = \frac{P[n_1(t) = u_1(t) - v_1(t, \alpha_1, \alpha_2, \dots)]}{P[n_1(t) = u_1(t)]}$$

is a function of these fixed parameters. Carrying out statistical averaging of this conditional probability ratio for all possible values of random parameters with regard to the distribution of these values $W(\alpha_1, \alpha_2, \dots)$, we find the unconditional probability ratio

$$\Lambda(u_1) = \int_0^\infty \int_0^\infty \dots W(a_1, a_2, \dots) \frac{P[n_1(t) = u_1(t) - v_1(t, a_1, a_2, \dots)]}{P[n_1(t) = u_1(t)]} \times \quad (1.2.13)$$

$$\times da_1 da_2 \dots$$

Let us consider as a first example detection of the signal $v_1(t, \varphi) = V_1(t) \cos(\omega_0 t + \varphi)$ with random uniformly distributed phase $W(\varphi) = \frac{1}{2\pi}$. Having substituted the expression for the signal into (1.2.5), we find after elementary transformations

$$\ln \Lambda(u_1, \varphi) = -\frac{E_1}{2a} + \frac{1}{a} Z \cos(\varphi + \psi),$$

where

$$Z^2 = z_1^2 + z_2^2; \quad z_{1,2} = \int_0^T u_1(t) V_1(t) \begin{Bmatrix} \cos \omega_0 t \\ \sin \omega_0 t \end{Bmatrix} dt \quad (1.2.14)$$

and

$$\psi = \arctg \frac{z_2}{z_1}.$$

Then according to (1.2.13) we will have

$$\Lambda(u_1) = \frac{1}{2\pi} \int_0^{2\pi} \exp \left[-\frac{E_1}{2a} + \frac{1}{a} Z \cos(\varphi + \psi) \right] d\varphi = \quad (1.2.15)$$

$$= e^{-\frac{E_1}{2a}} I_0 \left(\frac{Z}{a} \right),$$

since

26

$$\int_0^{2\pi} \exp[-a \cos(\varphi + \psi)] d\varphi = 2\pi I_0(a),$$

where $I_0(a)$ is a zero-order modified Bessel function. Since this function is monotonic [25], the optimum detector of the considered signal should calculate the value $Z^2 = z_1^2 + z_2^2$ and according to (1.2.14), z_1 and z_2 are the voltages at the output of 2 VKU controlled by two frequency ω_0 and amplitude $V_1(t)$ oscillations shifted by $\pi/2$.

Consequently, an optimum receiver for a signal with random initial phase consists of two VKU controlled by quadrature oscillations, two square-law function generators (squaring devices), an adder and threshold device (Fig. 1.2.6).

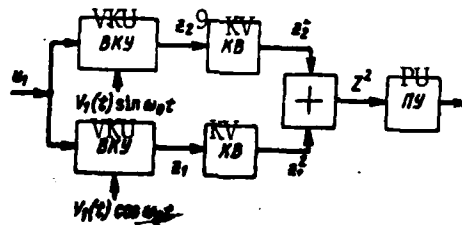


Fig. 1.2.6. Block diagram of optimum receiver for signal with random phase.

Let us then determine the structure of an optimum receiver for a signal with random unmeasurable amplitude and initial phase. Let us find for this purpose the probability ratio for the signal, assuming that its relative amplitude A is distributed by Raleigh law

$$W(A) = 2A \exp(-A^2) I(A),$$

where $I(x) = 1$ at $x > 0$, and the initial phase is distributed according to uniform law. Then

27

$$W(A, \varphi) = \frac{1}{\pi} \exp(-A^2) I(A).$$

Moreover,

$$u_1(t) = n_1(t) + x A V_1(t) \cos(\omega_0 t + \varphi).$$

Substituting this expression into (1.2.5) and repeating the calculations made during consideration of the previous example, we find

$$\ln \Lambda(u_1, A, \varphi) = -\frac{A^2 E_1}{2a} + \frac{1}{a} A Z \cos(\varphi + \psi),$$

where Z and ψ are the same as previously. Having carried out statistical averaging of the conditional probability ratio $\Lambda(u_1, A, \varphi)$, first with respect to φ and then with respect to A , we will have

$$\Lambda(u_1) = \frac{2a}{E_1 + 2a} \exp \left[\frac{Z^2}{2a(E_1 + 2a)} \right]. \quad (1.2.16)$$

Thus, the optimum receiver for a signal with random amplitude and initial phase should calculate, as in the case of a signal with random initial phase, the value of Z^2 . Therefore, the block diagram of the

receiver shown in Fig. 1.2.6 is also optimum for a signal with random amplitude and initial phase.

3. Detection of Some Other Signals. Signal Identification and Measurement of Their Parameters

Since the purpose of the given book is not to outline the theory of optimum radio receiving methods, which has been quite fully and successfully outlined in other monographs [10-19], let us limit ourselves to enumeration (see, for example, [13] for proof) of some signals whose optimum detectors contain VKU as one of the basic components.

Thus, a VKU is used as the main part of optimum detectors for the following signals (to supplement the foregoing):

1) coherent pulsed sequences: a) precisely known, b) with random initial phase and c) with random amplitude and initial phase;

2) noncoherent pulse sequences: a) with random initial phases, b) with random initial phases and amplitudes fluctuating in unison and c) with random initial phases and independently fluctuating amplitudes;

3) with random amplitude;

4) of a weak precisely known signal with phase detection;

5) with many possible values of parameters and so on.

VKU are widely used not only in optimum detectors, as noted above, but also in optimum signal identification detectors and receivers for measuring their parameters.

As examples let us point out that VKU are the most important components of optimum receivers designed to perform the following tasks [13]:

1) identification of two signals;

2) identification of m orthogonal signals;

3) identification of signals with many possible values of parameters;

4) measurement of signal amplitude;

5) measurement of signal delay time, i.e., range to the target;

6) measurement of signal frequency and consequently of the radial velocity of the target and so on.

Thus, a VKU is the main part of optimum receivers designed to solve the most diverse problems.

Therefore, the problem of realizing a VKU is very important, especially in practice, which is also considered below.

1.3. Realization of Cross-Correlation Device in the Form of an Optimum Filter. Pulse Characteristics of Optimum Filter

By definition, a VKU is a device for calculation of the function

$$R_s(\tau) = \int_{-\infty}^{\infty} f_1(x) f_2(x - \tau) dx,$$

that establishes the degree of cross-correlation (relationship) of the functions $f_1(x)$ and $f_2(x - \tau)$. 29

With optimum reception of a precisely known signal, the received oscillation $u_1(t)$ performs the role of the first function and the emitted signal $v_1(t)$ and consequently the signal anticipated upon reception, performs the second function. In this case

$$R_s(\tau) = \int_{-\infty}^{\infty} u_1(x) v_1(x - \tau) dx. \quad (1.3.1)$$

which differs from (1.2.6) only by integration limits.

A computing system (Fig. 1.3.1), consisting of a delay device for time τ , multiplier device and integrating device, can calculate this function. This device calculates only one value of the

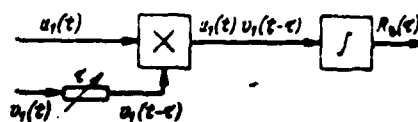


Fig. 1.3.1. Block diagram of cross-correlation device.

cross-correlation function each time, corresponding to the specific delay time τ . To investigate the entire course of the cross-correlation function of the signal and input oscillation, one must calculate many values of this function corresponding to different delays τ . And this first of all requires multiple repetition of the input voltage and second considerably longer analysis time.

Another solution of this problem is to use a multichannel system in the form of parallel connection of a large number of computing systems with different delay times τ . The structure of the entire device thus naturally becomes very cumbersome and complicated for analyzing the cross-correlation function.

If the signal arrival time is previously known, then it is no longer necessary to calculate the entire cross-correlation function but it is sufficient to determine its value at $\tau = 0$. However, this case is usually not observed in practice. Thus, for example, the signal arrival time in any rangefinders carries information about the range to the target and is therefore not previously known. 30

Being a linear system with variable parameters [26], the computing cross-correlation device has no invariance with respect to arrival time (see section 1.6) and therefore should be multichannel with unknown signal arrival time.

In this regard let us consider a capability, very important to practice, of realizing a cross-correlation device in the form of a simpler single-channel linear device with constant parameters that generates the function $R_0(\tau)$ continuously at its own output during the time that the input signal time delay only introduces the corresponding delay to the signal at the output of this device.

Formula (1.3.1) for the cross-correlation function has the nature of a convolution which establishes contact between the voltages at the input and output of the linear system (a linear filter). Actually, the voltage at the output of the linear filter is described by the convolution

$$u_2(t) = \int_{-\infty}^t u_1(x) h(t-x) dx, \quad (1.3.2)$$

where $h(t)$ is the pulse characteristic of the filter, i.e., its response to a single pulse $\delta(t)$.

Since $h(t) = 0$ at $t < 0$ in physically realized filters, then $h(t-x) = 0$ at $x > t$, due to which (1.3.2) can be represented in the form:

$$u_2(t) = \int_{-\infty}^{\infty} u_1(x) h(t-x) dx. \quad (1.3.3)$$

Let us select a linear system such that the voltage at its output produces the following cross-correlation function with accuracy to arbitrary multiplier C and with some time delay t_0 :

$$u_2(t) = C R_2(t-t_0). \quad (1.3.4)$$

It follows from (1.3.3) and (1.3.1) that this equality is equivalent to the following:

$$\int_{-\infty}^{\infty} u_1(x) h(t-x) dx = C \int_{-\infty}^{\infty} u_1(x) v_1(x-t+t_0) dx,$$

for fulfillment of which it is sufficient that

$$h(t) = C v_1(t_0-t). \quad (1.3.5)$$

A linear system having such a pulse characteristic is called an optimum filter since it fulfills according to (1.3.3) the most important operation of optimum reception--calculation of the cross-correlation function. As will be shown below, an optimum filter (OF; Optimal'nyy fil'tr) is the best even in the sense of producing at its output the maximum possible signal/noise ratio with given signal shape and white noise intensity at its input.

Optimum detection filters should be distinguished from filters optimum in the sense of the mean square error criterion. These filters, unlike those considered, are used to reproduce a signal in the presence of random noise and are used extensively in automatic regulation and control systems [18, 29]. The latter are also contained in radar counters of moving target parameters [14].

In the case of radio signals, expression (1.3.5) can be represented in the following complex form:

$$\bar{H}(t) = C \bar{v}_1(t - t_0) e^{-j\omega_0 t}, \quad (1.3.6)$$

where $\bar{H}(t)$ is the complex amplitude of the pulse characteristic; $\bar{v}_1(t)$ is the complex signal amplitude; and ω_0 is the signal carrier frequency, while the asterisk denotes a complex conjugate function, i.e., a function with opposite sign of the imaginary part.

One can ascertain the equivalents of formulas (1.3.5) and (1.3.6) in the following manner. If both sides of equality (1.3.6) are multiplied by $e^{j\omega_0 t}$ and if one converts in them from complex to real values, then we find (1.3.5).

It follows from (1.3.5) that the pulse characteristic of a filter optimum to signal $v_1(t)$ differs from the function that describes this signal only by constant multiplier C with a time shift to value t_0 and with sign of the independent variable of time t . To emphasize the latter it is said that the pulse characteristic of the OF is a mirror image of the function that describes the instantaneous values of the signal.

One of the signals (a), its mirror image (b) and one of the possible pulse characteristics of the realized optimum filter (c) are shown in Fig. 1.3.2. In this case $C = 2$ and $t_0 = t_k$ are selected, where t_k is the moment of time that the signal ends at the input.

The need for time delay t_0 , whose value should not be less than the moment of time of the end of the input signal

$$t_0 \geq t_k \quad (1.3.7)$$

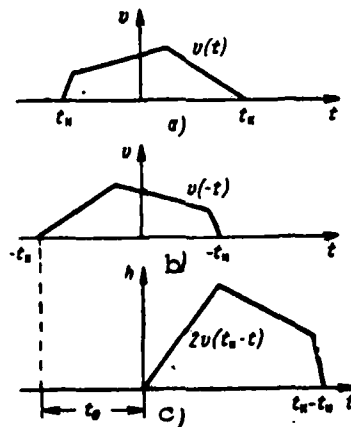


Fig. 1.3.2. Time diagrams of signal (a), of its mirror image (b) and of pulse characteristic of OF (c).

can be easily seen from this figure. If the latter condition were not observed, then the OF would generate voltage $h(t)$ at its output even before the single pulse $\delta(t)$ was fed to its input at moment $t = 0$. It is clear that this filter cannot be realized.

It is feasible to select $t_0 = t_k$ to avoid excess signal delay at the output and to simplify the structure of the OF.

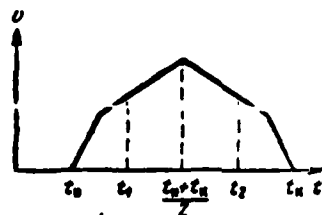


Fig. 1.3.3. Symmetrical signal.

For signals whose shape is symmetrical with respect to the mean position (Fig. 1.3.3), the following relation is valid

$$v_1(t_2) = v_1(t_1), \quad (1.3.8)$$

where moments of time t_1 and t_2 are related by the function

$$t_n - t_1 = t_2 - t_n,$$

and t_n is the moment of time of the beginning of the signal.

It follows from the latter equality that:

$$t_2 = t_H + t_K - t_1,$$

due to which expression (1.3.8) assumes the form

$$v_1(t_1) = v_1(t_H + t_K - t_1).$$

Since it is valid for any moment of time t_1 , subscript 1 can be omitted:

$$v_1(t) = v_1(t_H + t_K - t).$$

As a result of the latter relation and (1.3.5), a filter optimum to a symmetrical signal has the pulse characteristic

$$h(t) = Cv_1(t + t_H + t_K - t_0).$$

Hence we conclude that the pulse characteristic of a filter optimum to a symmetrical signal differs from the function that describes the signal only by the constant coefficient C and the time shift by value $t_C = t_H + t_K - t_0$.

If the signal delay of the output of this filter is selected as the minimum possible $t_0 = t_K$, then the value of the indicated shift will be equal to the moment of the beginning of the signal t_H and the pulse characteristic will assume the form

$$h(t) = Cv_1(t + t_H). \quad (1.3.9)$$

Specifically, at $t_H = 0$

$$h(t) = Cv_1(t). \quad (1.3.10)$$

i.e., the pulse characteristic of a filter optimum to the signal, which is symmetrical with respect to the mean position and begins at moment of time $t = 0$, reproduces the shape of this signal on scale C .

Let us note in conclusion that optimum filters are also usually employed as cross-correlation devices in radar systems. However, in those cases when the signals have very complex shape or extremely long duration (on the order of seconds), it practically becomes impossible to build optimum filters, whereas realization of a computing

cross-correlation device in the form of a digital correlator presents no special difficulties.

1.4. Signal Storage in an Optimum Filter

It follows from (1.3.5) and (1.3.1) that:

$$u_2(t) = C \int_{-\infty}^{\infty} u_1(x) v_1(x - t + t_0) dx. \quad (1.4.1)$$

If the voltage of a signal optimum to the filter is fed to its input, i.e., if $u_1(t) = v_1(t)$, then the following voltage will occur at its output

$$v_2(t) = C \int_{-\infty}^{+\infty} v_1(x) v_1(x - t + t_0) dx = CR_1(t - t_0), \quad (1.4.2)$$

where

$$R_1(\tau) = \int_{-\infty}^{+\infty} v_1(t) v_1(t - \tau) dt = \int_{-\infty}^{+\infty} v_1(t) v_1(t + \tau) dt \quad (1.4.3)$$

is the autocorrelation function of the signal $v_1(t)$.

Accordingly, this filter is an autocorrelation device with respect to a signal optimum to the given filter.

Due to the evenness of the autocorrelation function, the output signal voltage (1.4.2) is an even time function with respect to moment t_0 . Therefore, if the beginning of counting time is converted to this moment, the output signal spectrum will consist of only cosine waves.

It is well known that autocorrelation function $R_1(\tau)$ is maximum at $\tau = 0$. Therefore, the voltage at the output of an optimum filter reaches a maximum value at moment $t = t_0$. This maximum (peak) in value of the output signal has the value

$$v_2(t_0) = CR_1(0) = C \int_{-\infty}^{+\infty} v_1^2(t) dt = CE_1. \quad (1.4.4)$$

Thus, the peak value of signal voltage at the output of an optimum filter is proportional to the total signal energy at the input. 35

The signal voltage is processed by an optimum filter by time t_0 , which cannot be earlier than the moment the signal ends at the input due to (1.3.7), so as to store all components of this signal and by adding them to form a peak signal pip at the output.

Thus, the operating mechanism of an optimum filter includes signal storage (in the broad sense).^{*} Therefore, an optimum filter can be called an ideal storage device. It must be constructed so that signal storage is best.

For this purpose the pulse characteristic of the optimum filter should have the shape of a signal due to which this filter acquires the capability of analyzing the degree of proximity of the input oscillation and of the anticipated signal. This is accomplished by multiplying the instantaneous value of the input oscillation by the shape of the signal and subsequent integration [see (1.4.1)]. In the case of reception of the anticipated signal, the result of this analysis will be very significant since the signal is stored in the best manner. This also ensures the maximum possible probability of its detection.

Specifically, if the signal is a square-wave video pulse:

$$\begin{aligned} v(t) &= V & \text{at } 0 < t < \tau, \\ v(t) &= 0 & \text{at } t < 0 \text{ and } t > \tau. \end{aligned}$$

then it follows from (1.4.1) at $t_0 = \tau$ that the output voltage

$$u_s(t) = VC \int_{t-\tau}^t u_i(\tau) d\tau \quad (1.4.5)$$

is an integral, increased VC times, of the input voltage in the range of duration τ preceding the given moment of time t . Consequently, the optimum filter integrates the input voltage during the signal length and produces the result of this integration continuously at its own output.

^{*} Unlike adding the input voltage samples (for example, separated by a time interval multiple to the repetition rate), which is also called storage.

If the signal has a more complex shape, then a filter optimum to it will produce the weight integration of the input oscillation during the duration of the signal and the weight function is the function that describes the signal, i.e., determined by its shape.

Let, for example, a signal have triangular shape:

$$\left. \begin{aligned} v_1(t) &= \frac{V}{\tau} t & \text{at } 0 < t < \tau, \\ v_1(t) &= 0 & \text{at } t < 0 \text{ and } t > \tau. \end{aligned} \right\}$$

Then, having assumed that $t_0 = \tau$, we find according to (1.4.1)

$$u_1(t) = \frac{CV}{\tau} \int_{t-\tau}^t [x - (t - \tau)] u_1(x) dx.$$

The weight function of integration

$$\left. \begin{aligned} f(x, t) &= x - (t - \tau) & \text{at } t - \tau < x < t, \\ f(x, t) &= 0 & \text{at } x < t - \tau \text{ and } x > t \end{aligned} \right\}$$

also has the form of a triangle (Fig. 1.4.1). Consequently, the values of the received oscillation $u_1(x)$ with this input signal should be multiplied by the corresponding values of the weight function whose value is greater at $x < t$, the closer moment of time x is to moment t and the product of these functions should be integrated in the range of duration τ ended at the considered moment of time t .

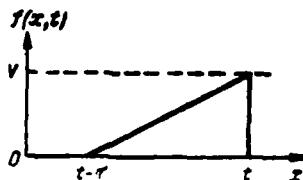


Fig. 1.4.1. Weight function of input voltage integration with triangular signal.

Let us note that there is no better procedure for processing a signal-noise mixture than signal storage when receiving a signal of known shape on a background of random fluctuating noise.

Actually, it is impossible to use the second method of separating signal from noise--interference compensation--in the given case since the interference is a random oscillation with previously unknown shape. Therefore, it is essentially impossible to construct a device to compensate for interference. 37

1.5. Spectral Characteristics of the Optimum Filter

It is easy to determine the transfer function $\bar{K}(\omega)$, which is the ratio of complex amplitudes of harmonic frequency oscillations ω at the output and input of this filter, from the known pulse characteristic of the optimum filter. As is known [9],

$$\bar{K}(\omega) = \int_{-\infty}^{\infty} h(t) e^{-j\omega t} dt.$$

Having substituted (1.3.5) into this expression, we find

$$\bar{K}(\omega) = C \int_{-\infty}^{\infty} v_1(t_0 - t) e^{-j\omega t} dt = C e^{-j\omega t_0} \int_{-\infty}^{\infty} v_1(x) e^{j\omega x} dx.$$

Comparing the derived integral to the expression for spectral density of the signal

$$\bar{S}_1(\omega) = \int_{-\infty}^{\infty} v_1'(t) e^{-j\omega t} dt,$$

we conclude that they are complex conjugate functions, due to which

$$\bar{K}(\omega) = C \bar{S}_1^*(\omega) e^{-j\omega t_0}. \quad (1.5.1)$$

Thus, the transfer function of an optimum filter differs from function $\bar{S}^*(\omega)$, complex conjugate to the signal spectrum $\bar{S}(\omega)$ only by a multiplier of form $C e^{-j\omega t_0}$, where C and t_0 are constants as was established in section 1.4 and t_0 is the moment of time at which the maximum instantaneous value (i.e., the peak value) of the signal is observed [30,31]. 38

The complex equality (1.5.1) is equivalent to the two real equalities:

$$K(\omega) = CS_1(\omega) \quad (1.5.2)$$

and

$$\psi(\omega) = -[\varphi(\omega) + \omega t_0], \quad (1.5.3)$$

where $K(\omega)$ is the amplitude-frequency characteristic of the filter; $\psi(\omega)$ is its phase characteristic; $S_1(\omega)$ is the modulus of the spectral density of the signal or its amplitude spectrum; and $\phi(\omega)$ is the independent variable (phase) of the spectral density of the signal or its phase spectrum.

It follows from consideration of the first of these equalities that the amplitude-frequency characteristic of an optimum filter is distinguished only by multiplier C from the amplitude spectrum of the signal to which this filter is optimum. Because of this, there is relative attenuation of the spectral components of the signal and noise corresponding to the less intensive sections of the signal spectrum. This attenuation is greater, the less the intensity of the signal components on these frequencies. The latter play a lesser role in formation of the peak value of the output signal than more intensive components. Attenuation of the noise spectrum, uniform at the input, is observed on all frequencies, with the exception only of those which correspond to the maximum signal spectrum.

The foregoing concepts are illustrated by Fig. 1.5.1 for the case of a square-wave video pulse. It is easy to note from consideration of it that the amplitude spectrum of the output signal $S_2(\omega)$ coincides in shape with the energy spectrum of output noise $F_2(\omega)$. This is confirmed by the following relations:

$$S_2(\omega) = S_1(\omega) K(\omega) = CS_1^2(\omega)$$

and

$$F_2(\omega) = F_1(\omega) K^2(\omega) = 2\alpha C^2 S_1^2(\omega),$$

hence, it follows:

$$F_2(\omega) = 2\alpha CS_2(\omega), \quad (1.5.4)$$

i.e., the amplitude spectrum of the signal at the output of an optimum filter differs from the energy spectrum of output noise only by the multiplier.

39

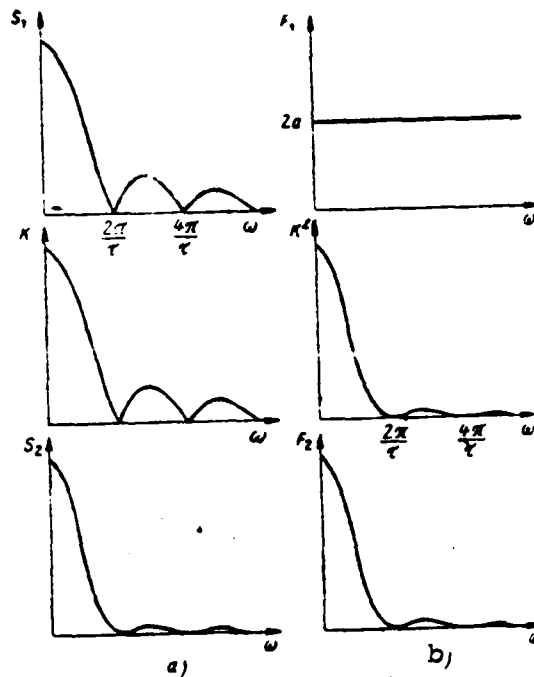


Fig. 1.5.1. Conversion of signal (a) and white noise (b) spectrum in optimum filter.

Let us return to interpretation of equality (1.5.3). It means that the phase characteristic of an optimum filter $\psi(\omega)$ differs only by sign from the sum of the phase spectrum of the signal $\phi(\omega)$ and the linear frequency function ωt_0 (Fig. 1.5.2).

With regard to the fact that the phase characteristic of an optimum filter satisfies equality (1.5.3), all the spectral components of the signal at the output of this filter, being cosine curves, have the same zero phase at moment $t = t_0$. Actually, the harmonic component of the frequency signal ω at the output of an optimum filter at moment t has the complete phase

40

$$\theta(t) = \omega t + \phi(\omega) + \psi(\omega) = \omega t + \phi(\omega) - \phi(\omega) - \omega t_0 = \omega(t - t_0),$$

which approaches zero at $t = t_0$ regardless of the value of frequency. Being added in phase, the spectral components of the signal also form the highest peak horn of the signal at this moment.

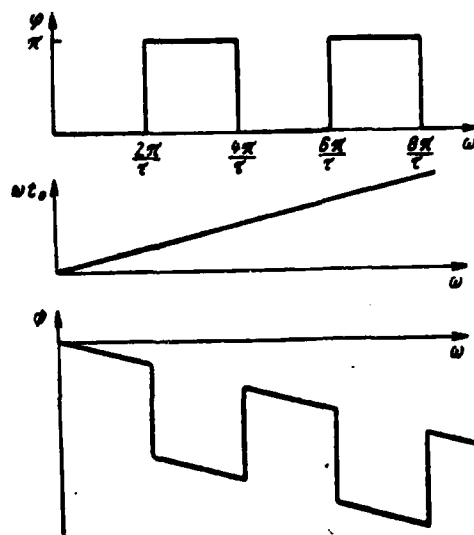


Fig. 1.5.2. Plotting of phase characteristic of optimum filter

Reversal of the phase of the spectral components of noise with an optimum filter does not change their random nature, due to which the result of adding these components will also be random at the output. In this case the probability that the noise components will be added at some moment of time in phase and form a very large noise horn is very low as at the filter input.

With regard to the fact that the characteristics of an optimum filter are matched in the best manner to the signal characteristics (specifically to its spectral characteristics), an optimum filter is frequently called a matched filter in the literature [5, 32].

Using the relations derived above, let us establish the relationship between signal voltage and the autocorrelation function of noise at the output of an optimum filter. It follows from (1.5.1) that the signal at the output of an optimum filter has the spectral density

$$S_s(\omega) = S_n(\omega) K(\omega) = CS_n^2(\omega) e^{-j\omega t_0}$$

and the instantaneous value

$$v_2(t) = \frac{C}{2\pi} \int_{-\infty}^{\infty} S_1^2(\omega) e^{j\omega(t-t_0)} d\omega = \frac{C}{\pi} \int_0^{\infty} S_1^2(\omega) \cos \omega(t-t_0) d\omega. \quad (1.5.5)$$

Consequently, the output signal is dependent only on the amplitude spectrum of the input signal and is independent of its phase signal. This is explained by the fact that an optimum filter compensates for phase shifts between the spectral components of the input signal.

Since output noise has energy spectrum (1.5.4), then its autocorrelation function is

$$R_2(t) = \frac{1}{2\pi} \int_0^{\infty} F_2(\omega) \cos \omega t d\omega = \frac{aC^2}{\pi} \int_0^{\infty} S_1^2(\omega) \cos \omega t d\omega.$$

Comparing this expression to (1.5.5), we find

$$R_2(t-t_0) = aCv_2(t), \quad (1.5.6)$$

i.e., the autocorrelation function of noise at the output of an optimum filter differs from the output signal only by constant multiplier aC and by the time shift by value t_0 .

Specifically, assuming that $t = t_0$, we will have

$$\sigma_2^2 = R_2(0) = aCv_2(t_0). \quad (1.5.7)$$

Accordingly, the standard deviation of output noise is aC times greater than the peak value of the output signal reached at $t = t_0$.

It follows from (1.5.7) and (1.4.4) that:

$$\sigma_2^2 = aC^2 E_1. \quad (1.5.8)$$

1.6. Invariance of the Optimum Filter

42

It follows from (1.5.1) that a filter optimum to the signal $v(t)$ is optimum for all other signals of the same shape, i.e., those differing from signal $v(t)$ only by amplitude, time position and initial phase. Actually, if one signal differs from another only by the fact that its amplitude is μ times greater and it is arranged in time later

by t_1 , then as is known [44], the spectral density of this signal differs from the spectral density of the second signal only by the multiplier $\mu e^{-j\omega t_1}$. Therefore, complete identity of the transfer functions of filters optimum to these signals can be achieved in (1.5.1) by the appropriate selection of constants C and t_0 . This also proves the optimum nature of the filter for all signals of given shape simultaneously.

This result can easily be found by the time method. Actually, let the filter be optimum to some signal $v_1(t)$, due to which the pulse characteristic of the filter meets condition (1.3.5). This same filter is also optimum to signal $\mu v_1(t - t_1)$ having the same shape and differing only by the fact that its amplitude is μ times greater and it is delayed by time t_1 compared to the first signal. The optimum nature of this filter for this signal follows from the fact that its pulse characteristic satisfies condition (1.3.5) for the second signal as well, but only at values of constants C and t_0 other than for the first signal.

Accordingly, an optimum filter has the property of invariance with respect to amplitude and time position.

With regard to the problem of the invariance of an optimum filter with respect to the initial phase, then one should bear in mind the following. If there is a filter optimum to some signal with specific initial phase, the effect of a signal of the same shape but with different initial phase on it leads to variation of the output signal phase by the value θ , equal to the difference of the initial phases of the effective and optimum signal. This can easily be seen from the expression [10]

$$\bar{U}_2(t) = \frac{1}{2} C e^{-j\omega t_0} \int_{-\infty}^{\infty} \bar{U}_1(x) \bar{V}_1^*(x - t + t_0) dx, \quad (1.6.1)$$

that establishes the relationship between the complex amplitudes of output voltage $\bar{U}_2(t)$, input voltage $\bar{U}_1(t)$ and optimum signal voltage $\bar{V}_1(t)$ and which is a complex analog of the real integral (1.4.1). If the input oscillation is varied in phase by angle θ , then its complex

amplitude will acquire an additional multiplier $e^{j\theta}$, which, being carried out beyond the sign of the integral, indicates variation of the phase of the output oscillation by the same angle. The value of the amplitude of the output oscillation also remains the same:

$$U_1(t) = |\bar{U}_1(t)| = \frac{1}{2} C \left| \int_{-\infty}^{\infty} \bar{U}_1(x) V^*_{s_1}(x - t + t_0) dx \right|. \quad (1.6.2)$$

In this case the peak value of the output oscillation essentially does not vary, but the moment of time this value is reached is shifted by value θ/ω_0 .

If the initial phase of the signal is varied by a random value, then the time shift of the maximum output signal will also be random. Therefore, the optimum receiver for a signal with random unmeasured initial phase, except an optimum filter for a signal with some initial phase, should contain a device that eliminates the dependence of the output voltage on the random initial phase. This device can be an amplitude detector that retains information about the signal amplitude and that eliminates information about its phase.

It is interesting to note that the modulus of voltage at the output of an optimum filter at moment $t = t_0$ differs only by multiplier C from value Z , which should calculate the optimum detector for a signal with random initial phase (see item 2, section 1.2). Actually, relations (1.2.14) can be represented in the following form:

$$z_1 = \operatorname{Re} \int_{-\infty}^{\infty} \bar{U}_1(x) V^*_{s_1}(x) dx$$

and

$$z_2 = \operatorname{Im} \int_{-\infty}^{\infty} \bar{U}_1(x) V^*_{s_1}(x) dx,$$

due to which

$$Z = \sqrt{z_1^2 + z_2^2} = \left| \int_{-\infty}^{\infty} \bar{U}_1(x) V^*_{s_1}(x) dx \right|.$$

Comparing this expression to (1.2.6) we find

$$U_s(t_0) = CZ = C\sqrt{z^2 + z^2},$$

which also proves the previous statement.

Accordingly, an optimum receiver for a signal with random initial phase can be constructed from a block-diagram differing from that previously considered (Fig. 1.2.6) with two quadrature channels and consisting of a filter optimum to a signal with arbitrary initial phase, amplitude detector and threshold device (Fig. 1.6.1).



Fig. 1.6.1. Second block-diagram of optimum receiver for signal with random phase.

Key: (1) optimum filter; (2) amplitude detector; (3) threshold device

Thus, the combination of the filter optimum to a signal with arbitrary initial phase and an amplitude detector is optimum for signals of the same shape, but having any value of initial phase, i.e., invariant with respect to the initial phase. The property of invariance of an optimum filter is very important, especially for practice. Actually, the amplitude, delay and initial phase of the received signal are not usually known. However, instead of building a large number of filters, each of which would be optimum for a signal with specific values of amplitude, delay and initial phase, it is sufficient to design only one filter which will be optimum for all signals of given shape to accomplish optimum reception.

45

Such signal parameters as amplitude and initial phase frequently assume random values in radar and carry no useful information, i.e., they are spurious. It follows from the foregoing that the presence of these random parameters does not change the structure of an optimum filter, but the presence of a random initial phase in the received signals leads to the need to use an amplitude detector (or two quadrature channels) after the optimum filter.

1.7. Signal/Noise Ratio at Output of Optimum Filter

According to (1.4.4) and (1.5.8), the ratio of the square of the peak value of an output signal to the noise output comprises

$$q_{\text{max}}^2 = \frac{v_2^2(t_0)}{\sigma_2^2} = \frac{E_1}{a}.$$

This result completely coincides with (1.2.11) and means that the ratio of the square of the peak value of the signal to the noise output at the output of an optimum filter is equal to the signal energy at its input, divided by half the spectral noise intensity at the input.

Thus, the signal/noise ratio at the output of an optimum filter is dependent only on the signal energy at its input and is totally independent of its shape (see item, section 1.2).

Let us ascertain that an optimum filter, which was selected in section 1.3 so that the voltage at its output reproduced the cross-correlation function, provides the maximum possible signal/noise ratio at its own output when a signal optimum to it and white noise are fed to its input.

When a signal $v_1(t)$ is fed to the input of a linear system with pulse characteristic $h(t)$, the voltage at its output, according to (1.3.3), is

$$v_2(t) = \int_{-\infty}^{\infty} v_1(x) h(t-x) dx.$$

The noise at the output of this system, caused by white noise with spectral intensity (1.2.4) being fed to the input, has the autocorrelation function [20]

$$R_2(\tau) = a \int_{-\infty}^{\infty} h(t) h(t+\tau) dt \quad (1.7.1)$$

and output (variance)

$$\sigma_2^2 = R_2(0) = a \int_{-\infty}^{\infty} h^2(t) dt. \quad (1.7.2)$$

Therefore, the ratio of the square of the peak signal value (at moment $t = t_0$) to noise output at the output of a linear system comprises

$$q_s^2 = \frac{\left[\int_{-\infty}^{\infty} v_1(x) h(t_0 - x) dx \right]^2}{a \int_{-\infty}^{\infty} h^2(t) dt}.$$

According to Bunyakovskiy's inequality [33]

$$\begin{aligned} \left[\int_{-\infty}^{\infty} v_1(x) h(t_0 - x) dx \right]^2 &< \int_{-\infty}^{\infty} v_1^2(x) dx \int_{-\infty}^{\infty} h^2(t_0 - x) dx = \\ &= E_1 \int_{-\infty}^{\infty} h^2(t) dt, \end{aligned}$$

due to which

$$q_s^2 < \frac{E_1}{a} = q_{\text{max}}^2.$$

Bunyakovskiy's inequality and the latter equality following from it are transformed to equalities provided that the integral functions differ only by an arbitrary constant multiplier (for example, C):

$$C v_1(x) = h(t_0 - x),$$

which is completely equivalent to (1.3.5). This also proves the most important property of an optimum filter--an optimum filter permits one to achieve the maximum possible ratio of the square of the peak signal value to noise output at its own output with given signal shape and noise level at the input and thus to achieve the maximum probability of correct detection of this signal with given level of false alarm probability [34].

47

1.8. Characteristics of Optimum Filter When Input Noise is Correlated

The characteristics of an optimum filter were considered above for the case of white gaussian noise at the input. Let us generalize the results for the case of correlated noise.

Thus, let the noise at the input have energy spectrum $F_1(\omega)$, which is a function of frequency, i.e., $F_1(\omega) \neq \text{const}$. To determine the characteristics of an optimum filter, let us use the method developed by V. A. Kotel'nikov [22] and that includes division of the optimum filter ("ideal receiver" in V. A. Kotel'nikov's terminology) into two linear components with transfer functions $\bar{K}_1(\omega)$ and $\bar{K}_2(\omega)$ (Fig. 1.8.1).

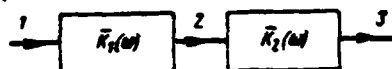


Fig. 1.8.1. Representation of optimum filter in form of two linear filters

Let us select the transfer function of the first component $\bar{K}_1(\omega)$ such that the noise at its output become white noise, i.e., its intensity be identical at all frequencies (both positive and negative):

$$F_2(\omega) = a = \text{const.}$$

Since $F_2(\omega) = F_1(\omega)K_1^2(\omega)$, then to do this it is necessary that

$$K_1^2(\omega) = \frac{a}{F_1(\omega)}.$$

If the signal at the input has spectral density $\bar{S}_1(\omega)$, it will be as follows at the output of the first filter:

48

$$\bar{S}_2(\omega) = \bar{S}_1(\omega)K_1(\omega).$$

The transfer function of the second linear component $\bar{K}_2(\omega)$ must be selected according to (1.5.1) for optimum filtration of a mixture of this signal and white noise, i.e.,

$$K_2(\omega) = CS_s^*(\omega)e^{-j\omega t_0},$$

where C and t_0 are some constants.

The entire optimum filter, consisting of the two indicated linear components, obviously has the transfer function

$$K(\omega) = K_1(\omega)K_2(\omega).$$

Having used the three previous relations, let us rewrite the latter equality in the following form:

$$\begin{aligned} K(\omega) &= \bar{K}_1(\omega) C S_1^*(\omega) \bar{K}_1^*(\omega) e^{-j\omega t_0} = \\ &= C K_1^2(\omega) S_1^*(\omega) e^{-j\omega t_0} = a C \frac{S_1^*(\omega)}{F_1(\omega)} e^{-j\omega t_0} \end{aligned}$$

if finally

$$K(\omega) = C_1 \frac{S_1^*(\omega)}{F_1(\omega)} e^{-j\omega t_0}, \quad (1.8.1)$$

where $C_1 = aC$.

Accordingly, the transfer function of a filter optimum to a signal which is mixed with noise whose intensity is dependent on frequency is directly proportional to a function complex conjugate to the spectral density of the signal and is inversely proportional to the energy spectrum of the input noise [35].

Specifically, at $F_1(\omega) = a$, formula (1.8.1) is degenerate at (1.5.1) if one assumes that $C = C_1/a$.

Let us determine the signal/noise ratio at the output of an optimum filter in this case.

It follows from (1.8.1) that a signal at the output of this filter has the spectrum

$$S_2(\omega) = S_1(\omega) K(\omega) = C_1 \frac{S_1^2(\omega)}{F_1(\omega)} e^{-j\omega t_0},$$

instantaneous value

$$v_2(t) = \frac{C_1}{2\pi} \int_{-\infty}^{\infty} \frac{S_1^2(\omega)}{F_1(\omega)} e^{j\omega(t-t_0)} d\omega$$

and peak value

$$V_2 = v_2(t_0) = \frac{C_1}{2\pi} \int_{-\infty}^{\infty} \frac{S_1^2(\omega)}{F_1(\omega)} d\omega.$$

The noise at the filter output comprises

$$\sigma_1^2 = \frac{1}{2\pi} \int_{-\infty}^{\infty} F_1(\omega) K^2(\omega) d\omega = \frac{C_1^2}{2\pi} \int_{-\infty}^{\infty} \frac{S_1^2(\omega)}{F_1(\omega)} d\omega.$$

Therefore, the ratio of the square of the peak signal to noise at the filter output is

$$q_1^2 = \frac{V_3^2}{\sigma_3^2} = \frac{1}{2\pi} \int_{-\infty}^{\infty} \frac{S_1^2(\omega)}{F_1(\omega)} d\omega. \quad (1.8.2)$$

If one assumes that $F_1(\omega) = a$ in this formula, then we again find the result (1.2.11), valid for the case of white noise.

Using (1.8.1), it is easy to show [7, 18] that the pulse characteristic of an optimum filter satisfies the following integral equation:

$$\int_{-\infty}^{\infty} h(\tau) R_{11}(t - \tau) d\tau = C_1 v_1(t_0 - t), \quad (1.8.3)$$

where $R_{11}(t)$ is the autocorrelation function of input noise and $v_1(t)$ is the input signal voltage.

Specifically, if the noise is white noise, i.e., if $R_{11}(\tau) = a\delta(\tau)$, then, using the filtering property of the delta-function and assuming that $C_1 = aC$, we again find (1.3.5) from (1.8.3).

OPTIMUM FILTERS FOR THE SIMPLEST PULSED SIGNALS

2.1. Design of Filters Optimum to Single Video Pulse Signal

1. Methods of Optimum Filter Design

The properties of optimum filters were considered in the previous chapter. For practical purposes, it is very important not only to know these properties but also to know how to design optimum filters based on elementary radio engineering devices.

Two methods of designing optimum filters are possible--time and spectral (frequency) [36]. The time method is based on the use of the relationship between the pulse characteristic of an optimum filter and the function that describes this signal. This relationship is established in the general case by the relation (1.3.5) and in the special case of a signal symmetrical with respect to its own mean position by relation (1.3.10). In this case design of an optimum filter includes construction of a linear system whose pulse characteristic reproduces on some scale and with some delay the function which is a near image of the signal, which coincides with this signal in the case of a symmetrical signal.

The use of the relationship between the transfer function of an optimum filter and the signal spectrum is the basis of the second,

spectral or frequency method of designing optimum filters. This relationship is described by equality (1.5.1).

The spectral method of designing optimum filters consists in building a linear system whose transfer function differs from that complex conjugate to the signal spectrum only by a multiplier of type $Ce^{-j\omega t_0}$. 51

The latter method requires a knowledge of the signal spectrum in the case when the signal is controlled by a time function rather than spectrum and is therefore somewhat more complicated.

Optimum filters are designed below by both methods.

2. Building a Filter Optimum to a Square-Wave Video Pulse

A square-wave video pulse of amplitude V and length τ (Fig. 2.1.1) is described by the function

$$\left. \begin{aligned} v(t) &= V & \text{at } -\frac{\tau}{2} < t < \frac{\tau}{2}, \\ v(t) &= 0 & \text{at } |t| > \frac{\tau}{2}. \end{aligned} \right\}$$

Using the time method of design and taking into account that the signal is symmetrical with respect to its own mean position, let us select a linear system whose pulse characteristic would be a square-wave video pulse of length τ . In other words, a linear system must be constructed which would generate a video pulse of indicated shape and length at the output when a single pulse acts on its input.

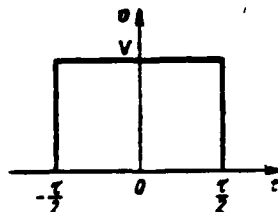


Fig. 2.1.1. Square-wave video pulse.

First, let us note that a single voltage jump $l(t)$ is formed at the output when a single pulse acts on the input of an integrating device. A square-wave pulse of single amplitude and length τ is the

difference of unit jumps $l(t)$ and $l(t - \tau)$ shifted with respect to each other by time τ .



Fig. 2.1.2. Block diagram of optimum filter for square-wave video pulse.

Therefore, a linear system whose pulse characteristic is a square-wave pulse of length τ is a combination of the following three devices: an integrating device, delay device by time τ and a subtraction device (Fig. 2.1.2). This system is also an optimum filter for the considered pulse. The time diagrams of the voltages at the output of its individual components when a single pulse acts on the input are shown in Fig. 2.1.3.

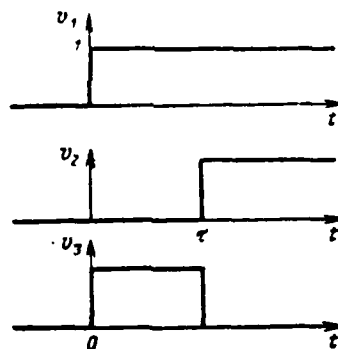


Fig. 2.1.3. Time diagrams of voltages in optimum filter.

Let us construct an optimum filter by the spectral method. The considered signal has the spectrum

$$S(\omega) = V \frac{e^{j\omega \frac{\tau}{2}}}{j\omega} - V \frac{e^{-j\omega \frac{\tau}{2}}}{j\omega} = V e^{-j\omega \frac{\tau}{2}} \frac{e^{j\omega \tau} - 1}{j\omega}.$$

A function complex conjugate to this spectrum has the form

$$\bar{S}^*(\omega) = V e^{j\omega \frac{\tau}{2}} \frac{1 - e^{-j\omega \tau}}{j\omega}.$$

Due to (1.5.1), an optimum filter has the transfer function

$$\bar{K}(\omega) = Ce^{-j\omega t_0} V e^{j\omega \frac{\tau}{2}} \frac{1 - e^{-j\omega \tau}}{j\omega}$$

or, having assumed for simplification that $C = 1/V$ and $t_0 = \tau/2$,

5

$$\bar{K}(\omega) = \frac{1}{j\omega} (1 - e^{-j\omega \tau}). \quad (2.1.1)$$

Since the linear component with transfer function $1/j\omega$ is an integrating device and since $e^{-j\omega \tau}$ describes the transfer function of the delay device by time τ , an optimum filter consists of an integrating device, delay device by time τ and subtraction device [37].

Accordingly, the same result was achieved by the spectral method as by the time method.

3. Building a Filter Optimum to a Trapezoidal Video Pulse

A trapezoidal video pulse (Fig. 2.1.4, a) having amplitude V , length τ and length of plane part τ_1 can be represented in the form of the algebraic sum of four voltages which, beginning at moments of time equal to $-(\tau/2)$, $-(\tau_2/2)$, $\tau_1/2$ and $\tau/2$, respectively, vary linearly with law $2V/(\tau - \tau_1)$ and up to these moments of time are identically equal to zero (Fig. 2.1.4, b). Therefore,

$$\begin{aligned} v(t) &= v_1(t) + v_2(t) + v_3(t) + v_4(t) = \\ &= \frac{2V}{\tau - \tau_1} \left[\left(t + \frac{\tau}{2} \right) \wedge \left(t + \frac{\tau}{2} \right) - \left(t + \frac{\tau_1}{2} \right) \wedge \left(t + \frac{\tau_1}{2} \right) - \right. \\ &\quad \left. - \left(t - \frac{\tau_1}{2} \right) \wedge \left(t - \frac{\tau_1}{2} \right) + \left(t - \frac{\tau}{2} \right) \wedge \left(t - \frac{\tau}{2} \right) \right]. \end{aligned} \quad (2.1.2)$$

Since the signal is symmetrical with respect to its own mean position and $t_H = -(\tau/2)$, then according to (1.3.10), the pulse characteristic of a filter optimum to the signal should in the case of minimum delay (memory) have the form

54

$$h(t) = C v \left(t - \frac{\tau}{2} \right).$$

Having assumed for further simplification that $C = (\tau - \tau_1)/2V$, we find

$$h(t) = t \cdot 1(t) - \left(t - \frac{\tau - \tau_1}{2}\right) 1\left(t - \frac{\tau - \tau_1}{2}\right) - \left(t - \frac{\tau + \tau_1}{2}\right) 1\left(t - \frac{\tau + \tau_1}{2}\right) + (t - \tau) 1(t - \tau). \quad (2.1.3)$$

It is easy to note that the pulse characteristic consists of four terms of identical nature differing (except for sign) only by the time delay. Therefore, any other term can be formed from the first term of this function by the corresponding delay (and if necessary inversion as well).

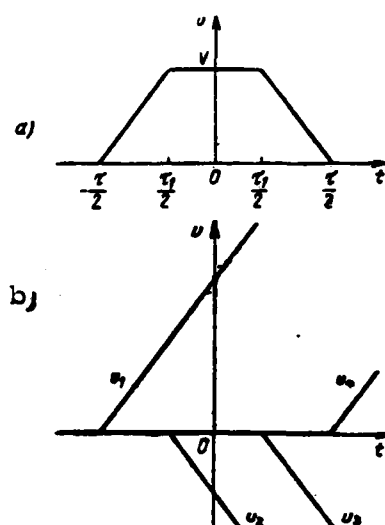


Fig. 2.1.4. Trapezoidal video pulse (a) and its terms (b).

The first term of this function $t \cdot 1(t)$ is formed as a result of the action of a single pulse on two series-connected integrating devices. Therefore, an optimum filter for a trapezoidal video pulse consists of two-series-connected integrating devices, three time delay devices equal to $(\tau - \tau_1)/2$, $(\tau + \tau_1)/2$ and τ , respectively, and an adding device (Fig. 2.1.5, a).

55

Instead of the three indicated delay devices, it is feasible to have only one of them with maximum time delay and two leads or three delay devices with delay times equal to $(\tau - \tau_1)/2$, τ_1 and $(\tau + \tau_1)/2$, respectively (Fig. 2.1.5, b). The block diagram of an optimum filter can be converted to an even simpler diagram (Fig. 2.1.5, c). Its

56

simplicity includes the presence of only two delay devices and the use of subtraction devices simpler in circuitry and design.

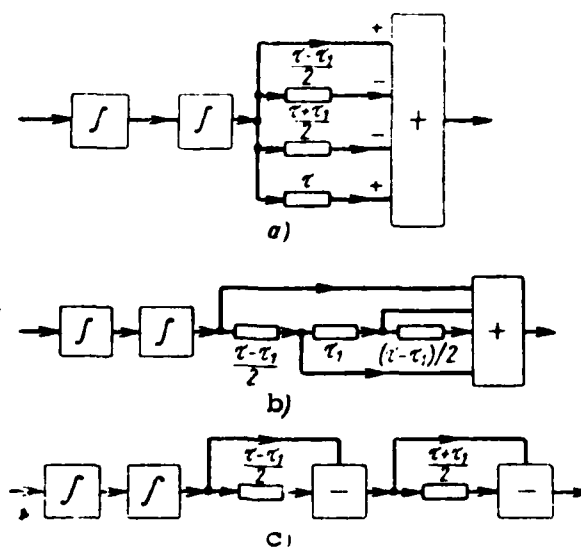


Fig. 2.1.5. Block diagram of optimum filter for trapezoidal video pulse.

Let us construct an optimum filter by the spectral method. Since a trapezoidal video pulse has the spectrum [27]

$$S(\omega) = \frac{8V}{(\tau - \tau_1)\omega^2} \sin \frac{\omega(\tau + \tau_1)}{4} \sin \frac{\omega(\tau - \tau_1)}{4} =$$

$$= \frac{2V}{\tau - \tau_1} e^{-j\omega \frac{\tau}{2}} \frac{1}{(j\omega)^2} \left(1 - e^{j\omega \frac{\tau - \tau_1}{2}}\right) \left(1 - e^{j\omega \frac{\tau + \tau_1}{2}}\right),$$

then, making use of (1.5.1) and assuming for simplification that $C = (\tau - \tau_1)/2V$ and $t_0 = t_H = \tau/2$, we find that an optimum filter should have the transfer function

$$K(\omega) = \frac{1}{(j\omega)^2} \left(1 - e^{-j\omega \frac{\tau - \tau_1}{2}}\right) \left(1 - e^{-j\omega \frac{\tau + \tau_1}{2}}\right). \quad (2.1.4)$$

By consideration of this expression we again arrive at the conclusion that an optimum filter consists of two integrating, two delay and two subtraction devices (Fig. 2.1.5, c).

Since a triangular video pulse is a special case of a trapezoidal video pulse when the length of its plane part is selected equal to zero ($\tau_1 = 0$), then a filter optimum to a triangular video pulse can

easily be produced from a filter optimum to a trapezoidal video pulse, having assumed in the latter case that $\tau_1 = 0$.

4. Building a Filter Optimum to a Video Pulse of More Complex Shape

By using the foregoing method, one can build an optimum filter for any pulse whose envelope consists of some number of segments of straight lines, parabolas and algebraic lines of as high an order as desired. This optimum filter will contain only integrating, delay, addition-subtraction and amplifying devices [7].

The number of integrating devices in this filter is a unit greater than the highest order of the algebraic lines whose segments comprise the pulse envelope (in this case the horizontal straight line must be regarded as a zero-order line). The number of delay devices (without leads) is equal to the number of segments of which the pulse envelope is comprised (if one does not consider segments corresponding to a signal identical to zero). The total delay time provided by these devices is equal to the length of the pulse signal. There can be several addition-subtraction devices. The number of amplifiers is not greater than the number of segments. In principle all the amplifiers can be omitted. It is sufficient to provide voltage dividers in the corresponding circuits in this case.

As indicated below (see section 2.4), the structure of an optimum filter is weakly dependent on slight changes of signal shape. Because of this, one cannot fail but take into account the small details of signal shape when designing optimum filters. Taking this circumstance into account permits one to considerably simplify the construction of filters sufficiently close to optimum.

5. Building Optimum Filters for Correlated Noise

Let us consider construction of an optimum filter for detecting a square-wave video pulse (Fig. 2.1.1) on a background of noise whose spectral intensity is a function of frequency $F_1(\omega)$ (this noise is called "colored" or correlated). This construction can be accomplished most simply by the spectral method [38].

Let the spectral intensity of input noise be a decreasing frequency function (curve 1 in Fig. 2.1.6):

$$F_1(\omega) = \frac{2ag^2}{\omega^2 + g^2}$$

where $2a$ is the spectral noise intensity on the zero frequency and g is a constant that characterizes the width of the energy spectrum of input noise and is numerically equivalent to the frequency on which the spectral intensity is one-half that on the zero frequency. 58

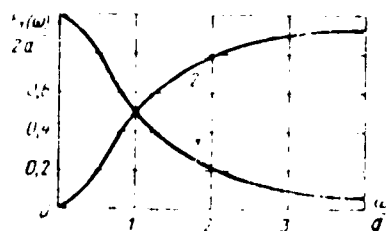


Fig. 2.1.6. Energy spectra of noise.

The considered noise has the autocorrelation function

$$R_1(t) = \frac{ag}{2} e^{-g|t|}$$

and accordingly can be produced by passing white noise with intensity (1.2.4) through a low-frequency RC filter with time constant $g^{-1} = RC$ [17]. This normal noise is a Markov process [39].

According to (1.8.1), an optimum filter should have the following transfer function in the given case

$$A(\omega) = C_1 \frac{1}{j\omega} (1 - e^{-j\omega t}) \frac{\omega^2 + g^2}{2ag^2}. \quad (2.1.5)$$

Assuming for simplification that $C_1 = 2ag^2$, we find

$$A(\omega) = \left(\frac{t^2}{j\omega} + t \right) (1 - e^{-j\omega t}). \quad (2.1.6)$$

Since $j\omega$ is the transfer function of differentiating device D , an optimum filter in the considered case consists of a combination of an integrating device, device with transfer coefficient g^2 and 59

differentiating and subtraction devices and also a combination of a time delay device equal to pulse length τ and subtraction device (Fig. 2.1.7, a).

With an unlimited increase of g , i.e., with expansion of the energy spectrum of input noise, (2.1.5) changes to (2.1.1) and the derived block diagram of an optimum filter degenerates to the block diagram of an optimum filter for white input noise (Fig. 2.1.2).

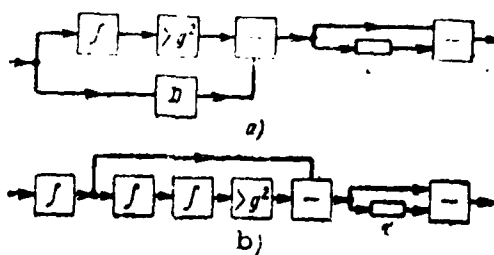


Fig. 2.1.7. Block diagrams of optimum filters for square-wave pulse with uncorrelated noise.

Let us consider the second case when the spectral intensity of the input noise increases with an increase of frequency by the law

$$F_1(\omega) = \frac{2a\omega^2}{\omega^2 + g^2},$$

approaching the constant $2a$ (Fig. 2.1.6, curve 2). Here constant g has the meaning of the frequency on which the energy spectrum of noise is one-half its own maximum value at $\omega = \infty$. The autocorrelation function of this noise is

$$R_1(t) = a\delta(t) - \frac{ag}{2} e^{-g|t|}.$$

It can be regarded as the result of passage of white noise with intensity (1.2.4) through a CR filter of upper frequencies with time constant $g^{-1} = RC$. The transfer function of an optimum filter is then

$$\begin{aligned} K(\omega) &= \frac{1}{j\omega} (1 - e^{-j\omega\tau}) \frac{\omega^2 - g^2}{\omega^2} = \\ &= \frac{1}{j\omega} \left[1 - \frac{g^2}{(j\omega)^2} \right] (1 - e^{-j\omega\tau}). \end{aligned} \quad (2.1.7)$$

Accordingly, in the given case an optimum filter consists of an integrating device, a combination of two integrating devices, a device with transfer coefficient g^2 and a subtraction device and a combination of a delay device by time τ and subtraction device (Fig. 2.1.7, b).

This optimum filter degenerates into an optimum filter (Fig. 2.1.2) constructed for the case of white noise with an unlimited decrease of g .

It follows from comparison of the block diagrams of optimum filters (Figs. 2.1.2 and 2.1.7) that the nonuniformity of the energy spectrum of input noise may lead to appreciable variation of the structure of an optimum filter. The structure of an optimum filter is complicated even more if the length of its pulse characteristic is limited [40].

2.2. Design of Filters Optimum to a Single Radio Pulse Signal of Specific Shape

1. Transfer Function of a Filter Optimum to Radio Pulse Signal

Construction of filters optimum to video pulse signals received on a normal noise background was considered above. However, radio pulse signals are usually fed to a receiver. They can be optimally filtered in some cases in the radio channel of the receiver, i.e., at the high or intermediate frequency. A very important property of filters optimum to radio signals is their invariance with respect to the initial phase (see section 1.6).

In this regard let us consider the construction of filters optimum to a radio pulse signal of specific shape. This construction can be simplified considerably by using the mutual conformity of optimum filters for video and radio pulse signals. The latter follows from the relationship between the transfer functions of these filters. Let us establish this relationship.

It is well known [44] that the spectral density of a radio pulse $\bar{S}_p(\omega)$ is about equal to half the product of the spectral intensity of its envelope $\bar{S}(\omega)$ in which the independent variable ω is replaced by $\omega - \omega_0$ and the phase multiplier $e^{j\psi}$:

$$\bar{S}_p(\omega) \approx \frac{1}{2} \bar{S}(\omega - \omega_0) e^{j\psi},$$

where ω_0 is the carrier frequency of the radio pulse and ψ is the initial phase of oscillations of this frequency.

Because of (1.5.1), a filter optimum to a radio pulse signal has the transfer function

$$K_p(\omega) = C_1 S_p^*(\omega) e^{-j\omega t_1} = \frac{1}{2} C_1 S^*(\omega - \omega_0) e^{-j(\omega t_1 + \psi)},$$

where C_1 and t_1 are constants.

Since the transfer function of a filter optimum to the envelope of this signal is:

$$K(\omega) = C S^*(\omega) e^{-j\omega t_0},$$

then assuming that $C = \frac{1}{2} C_1 e^{-j\psi}$ and $t_0 = t_1$, we find the relation

$$K_p(\omega) = K(\omega - \omega_0), \quad (2.2.1)$$

that establishes the relationship between the transfer functions of filters optimum to a radio pulse signal and its envelope, respectively.

Thus, it is sufficient in the transfer function of a filter optimum to its envelope to replace independent variable ω by $\omega - \omega_0$ to produce a transfer function of a filter optimum to a radio pulse of a given shape.

2. Congruence of Filters Optimum to Radio Pulse Signal and Its Envelope, Respectively

Because of (2.2.1), filters, one of which is optimum to a radio pulse signal and the other of which is optimum to its envelope, have the property of congruence.

Congruence is also inherent to the components of these filters. One or several components of an optimum filter for a radio pulse corresponds to each component of the filter optimum to the envelope of this pulse.

62

It was shown in the previous section that the components of filters optimum to video pulse signals can be integrating, delay by time t_3 , amplifying and addition-subtraction devices. The transfer functions of the latter two types of devices are independent of frequency in the working frequency band. Therefore, their notations coincide on the

working frequency band. Therefore, their notations coincide on the functional diagrams of optimum filters.

The first two types of devices have frequency-dependent transfer functions:

$$K(\omega) = \frac{1}{j\omega} \text{ и } K(\omega) = e^{-j\omega t_0}.$$

The corresponding components in an optimum filter for a radio pulse have according to (2.2.1) the transfer functions

$$K(\omega) = \frac{1}{j(\omega - \omega_0)} \quad (2.2.2)$$

and

$$K(\omega) = e^{-j(\omega - \omega_0)t_0} = e^{-j\omega t_0} e^{j\omega_0 t_0}.$$

Since the phase angle $\omega_0 t_0$ is much greater than 2π and if the phase of harmonic oscillation is inverted to any number which is a multiple of 2π , its value does not change and then

$$e^{j\omega_0 t_0} = e^{j2\pi \left[E\left(\frac{\omega_0 t_0}{2\pi}\right) + R\left(\frac{\omega_0 t_0}{2\pi}\right) \right]} = e^{j \left[2\pi E\left(\frac{\omega_0 t_0}{2\pi}\right) + \chi(t_0) \right]} = e^{j\chi(t_0)}$$

and

$$K(\omega) = e^{-j\omega t_0} e^{j\chi(t_0)},$$

where

$$\chi(t_0) = \omega_0 t_0 - 2\pi E\left(\frac{\omega_0 t_0}{2\pi}\right) = 2\pi R\left(\frac{\omega_0 t_0}{2\pi}\right);$$

$E(x)$ is the whole part of the number x and $R(x)$ is the fractional part of this number;

$$f_0 = \frac{1}{2\pi} \omega_0.$$

Therefore, the combination of the same series-connected delay device and phase shifting device by angle $\chi(t_0)$ corresponds in an optimum filter for this radio pulse to the delay device by time t_0 used in an optimum filter for the video pulse envelope of the radio pulse. 63

It is further shown (in item 5 of the given section) that transfer function (2.2.2) is approximately realized by a highly selective resonance amplifier. Therefore, a highly selective resonance

amplifier corresponds to the integrating device in a filter optimum to the video pulse envelope of a radio pulse.

3. Building Optimum Filters for Radio Pulses

Using the congruence of the components of optimum filters for a radio pulse and its envelope indicated above, it is easy to construct an optimum filter for a radio pulse by the known structure of an optimum filter for its envelope.

To do this, every integrating device in the block diagram of a filter optimum to the envelope of the considered radio pulse should be replaced by a highly selective resonance amplifier, the time delay device t_3 should be supplemented with a phase-shifting device by angle $\chi(t_3)$ and the amplifier and addition-subtraction devices should be left unchanged.

Using these rules and the results of the previous section in which optimum filters were designed for video pulses of different shape, let us construct optimum filters for radio pulses of square-wave and rectangular shape. As a result we find the following results.

An optimum filter for a square-wave radio pulse (Fig. 2.2.1, a) consists of a highly selective resonance amplifier, a delay device by time τ equal to its length, a phase-shifting device by angle $\chi(\tau)$ and a subtraction device. A somewhat different solution of this problem belongs to Rochefort [45] and to Ya. D. Shirman.

In the case of a trapezoidal radio pulse, an optimum filter is a combination of two highly selective resonance amplifiers, two delay devices by time $(\tau - \tau_1)/2$ and $(\tau + \tau_1)/2$, phase-shifting devices by angles $\chi(\frac{\tau - \tau_1}{2})$ and $\chi(\frac{\tau + \tau_1}{2})$ and subtraction devices (Fig. 2.2.1, b).

If the time parameters of the envelopes of radio pulses (length τ , length of plane part τ_1 and so on) are selected as multiple to the period of their carrier oscillation $T_0 = 1/f_0$, then the product of this time parameter of envelope t_i by the carrier frequency f_0 of the

radio pulse will be a whole number, as a result of which the corresponding phase inversion angle $\chi(t_i) = 2\pi R(f_0 t_i)$ approaches zero. In this case it is no longer necessary to use phase-shifting devices when constructing optimum filters and their block diagrams are simplified somewhat.

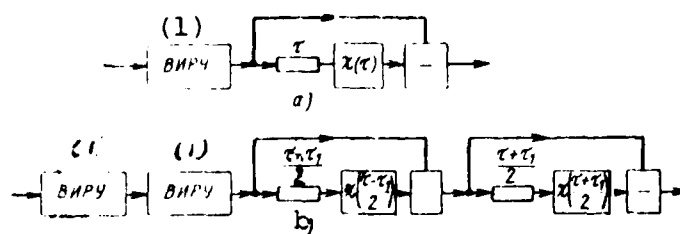


Fig. 2.2.1. Block diagrams of optimum filters for radio pulses.

Key: (1) highly selective resonance amplifier

However, the phase shifters indicated above must still be used in practice to compensate for the inaccuracy of manufacturing the delay devices, which may provide a delay of oscillations by values somewhat different from the calculated values.

4. Characteristics of Highly Selective Resonance Amplifier

Based on the equivalent circuit of a highly selective resonance amplifier (Fig. 2.2.2) and assuming that a generator (pentode or transistor) is used in it with high wave impedance R_i , it is easy to write the expression for the transfer function of this amplifier

$$K(\omega) = \frac{I_2}{I_1} = \frac{S}{\frac{1}{R_i} + \frac{1}{Z_0}} \approx S Z_0$$

$$= S \frac{(R + j\omega L) \frac{1}{j\omega C}}{R + j\left(\omega L - \frac{1}{\omega C}\right)} \frac{SR_0 \left(1 - j \frac{1}{Q} \frac{1}{1 + \frac{\omega}{\omega_0} \frac{1}{\omega_0}}\right)}{1 + jQ \frac{\omega}{\omega_0} \left(1 + \frac{1}{1 + \frac{\omega}{\omega_0} \frac{1}{\omega_0}}\right)}$$

where \bar{Z}_0 is the equivalent impedance of the circuit; $R_0 = \frac{L}{CR}$ is the equivalent wave impedance of the circuit; $Q = \frac{1}{2} \sqrt{\frac{L}{C}}$ is the Q-factor of the circuit and $\omega_0 = \frac{1}{\sqrt{LC}}$ is the resonance frequency of the circuit.

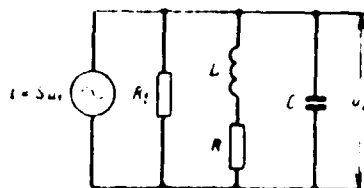


Fig. 2.2.2. Equivalent circuit of highly selective resonance amplifier (VIRU; Vysokoizbiratel'nyy rezonansnyy usilitel').

On frequencies that satisfy the condition

$$\frac{\omega_0}{Q} \ll |\omega - \omega_0| \ll \omega_0 \quad (2.2.3)$$

(for which it is necessary that the amplifier circuit have high Q -factor and that the resonance amplifier have high selectivity), the following approximate expression is valid:

$$A(\omega) \approx \frac{N}{2C} \frac{1}{j(\omega - \omega_0)} \quad (2.2.4)$$

Thus, in the frequency band considerably wider than the amplifier bandpass $\Delta\omega = \omega_0/Q$ but narrow compared to the mean (resonance) frequency ω_0 , the transfer function of a highly selective resonance amplifier is approximately but sufficiently reliably described by function (2.2.4), which differs from function (2.2.2) only by the constant coefficient.

Based on this, one can state that a highly selective resonance amplifier corresponds to an integrating device in an optimum filter for the envelope. Therefore, it is natural to call it a high-frequency integration device.

The radio signals in which the carrier frequency coincides with the resonance frequency of this amplifier and the width of the spectrum is much greater than its bandpass are integrated in this amplifier. The need for the latter follows from the fact that the harmonic components of the signals within the bandpass are transmitted with slight frequency distortions and therefore they are not integrated, unlike those components which fall on the slopes of the resonance curve of the amplifier. In this regard it is necessary for integration of the radio signal in a resonance amplifier that the relative fraction of its harmonic components impinging in the bandpass be low.

As is known, a resonance amplifier has the pulse characteristic

$$h(t) = \frac{S}{L} e^{-\zeta t} \cos \omega_p t \cdot I(t) \approx \frac{S}{L} e^{-\zeta t} \cos \omega_0 t \cdot I(t),$$

where $\omega_p = \sqrt{\omega_0^2 - \zeta^2}$ is the frequency of free oscillations of the circuit approximately equal to its resonance frequency ω_0 and $\zeta = R/2L$ is the attenuation factor of oscillations.

For time intervals whose length satisfies the condition $\zeta t \ll 1$, 67
attenuation can be disregarded. Therefore, the pulse characteristic of a highly selective resonance amplifier has the form

$$h(t) = \frac{S}{L} \cos \omega_0 t \cdot I(t). \quad (2.2.5)$$

Making use of this expression, it is easy to show that the pulse characteristic of a filter, whose block diagram is shown in Fig. 2.2.1, a, is a square-wave radio pulse of length τ and frequency ω_0 at $\zeta \tau \ll 1$, which also confirms the optimum nature of this filter.

2.3. Operating Mechanism of Optimum Filter for Square-Wave Video Pulse

1. Preliminary Remarks

Construction of filters optimum to single pulse signals was considered above. It is very important to understand why one or another optimum filter consists of these rather than different components, i.e., to determine its operating mechanism.

To do this, one must analyze the passage of the pulse signal and noise through different components of the optimum filter and combinations of them.

The passage of noise is analyzed by the time method (using correlation functions). The same results are found when this problem is considered by the spectral method.

The passage of signal and noise through an optimum filter for a square-wave video pulse is analyzed below. It is shown in item 2,

section 2.1 that this filter consists of an integrating device, time delay device equal to the pulse length and subtraction device (Fig. 2.1.2).

Both an integrating RC-circuit and an integrating amplifier [185] whose time constants $\beta = RC$ and $\beta = (1 + K)RC$ are much greater than the length of a square-wave video pulse, can be used as the integrating device. Here K is the amplification factor of the UPT contained in the integrating amplifier. Let us subsequently assume that an integrating device is a combination of an integrating amplifier, a special case of which is an integrating circuit at $K = 0$, and an auxiliary amplifier with amplification factor RC . The latter is not required and is introduced only to simplify the following expressions.

68

The integrating device then has the transfer function

$$A(t) = \beta \left(1 - e^{-\frac{t}{\beta}}\right) \cdot I(t) = \beta \sum_{i=1}^{\infty} \frac{(-1)^{i+1}}{i!} \left(\frac{t}{\beta}\right)^i \cdot I(t), \quad (2.3.1)$$

where

$$\beta = KRC \gg \tau. \quad (2.3.2)$$

2. Passage of Signal

If a pulse signal acts at the input of an optimum filter (Fig. 2.1.2) only from $t = 0$ to $t = \tau$ and has amplitude V_1 (Fig. 2.3.1, a), then the signal voltage at the output of the integrating device varies by the law (Fig. 2.3.1, b)

$$\left. \begin{aligned} v_s(t) &= V_1 \beta \left(1 - e^{-\frac{t}{\beta}}\right) \approx V_1 t \left(1 - \frac{t}{2\beta}\right) && \text{at } 0 \leq t \leq \tau, \\ v_s(t) &= V_1 \beta \left(1 - e^{-\frac{t}{\beta}}\right) e^{-\frac{t-\tau}{\beta}} \approx && \\ &\approx V_1 \tau \left(1 - \frac{2t-\tau}{2\beta}\right) && \text{at } \tau \leq t \leq \beta. \end{aligned} \right\} \quad (2.3.3)$$

After passage through the delay line, this oscillation is delayed by time τ (Fig. 2.3.1, c). We find at the output of the subtraction device a pulse of approximately triangular shape (Fig. 2.3.1, d):

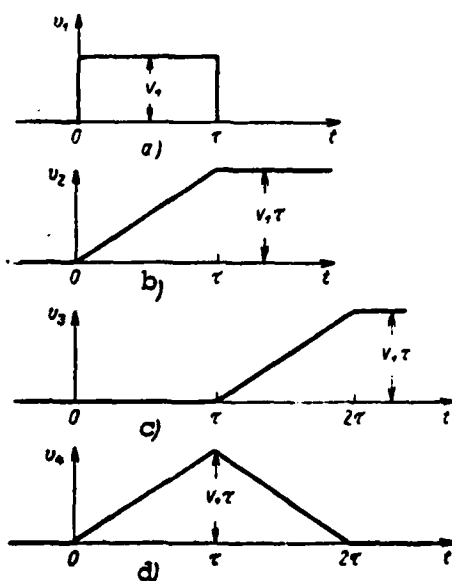
69

$$\left. \begin{aligned} v_1(t) &= V_1 \beta \left(1 - e^{-\frac{t}{\beta}} \right) \approx V_1 t \left(1 - \frac{t}{2\beta} \right) \approx V_1 t & \text{at } 0 \leq t \leq \tau, \\ v_2(t) &= V_1 \beta \left(2e^{-\frac{t-\tau}{\beta}} - e^{-\frac{t}{\beta}} - 1 \right) \approx \\ &\approx V_1 \left(2\tau - t + \frac{t^2 - 4t\tau + 2\tau^2}{2\beta} \right) \approx V_1 (2\tau - t) & \text{at } \tau \leq t \leq 2\tau, \\ v_3(t) &= -V_1 \beta \left(1 - e^{-\frac{t-\tau}{\beta}} \right) e^{-\frac{t-\tau}{\beta}} \approx \\ &\approx -V_1 \frac{\tau^2}{\beta} \left(1 - \frac{t-2\tau}{\beta} \right) \approx -V_1 \frac{\tau^2}{\beta} \approx 0 & \text{at } 2\tau \leq t \leq \beta. \end{aligned} \right\} \quad (2.3.4)$$

It has amplitude

$$V_s \approx V_1 \tau \left(1 - \frac{\tau}{2\beta} \right) \approx V_1 \tau \quad (2.3.5) \quad 70$$

and a length approximately equal to 2τ .



69

Fig. 2.3.1. Time diagrams of voltages in optimum filter for video pulse.

The transfer coefficient of the peak signal with optimum filter comprises

70

$$g = \frac{V_i}{V_i} \approx \tau \left(1 - \frac{\tau}{2\beta}\right) \approx \tau. \quad (2.3.6)$$

3. Passage of Noise

Let us assume that the noise at the input is white noise and has spectral density (1.2.4). Let us use formula (1.7.1) to calculate the autocorrelation function and noise at the output of the integrating device.

Since the pulse characteristic is a time derivative of the transfer function, in the considered case due to (2.3.1),

$$h(t) = \frac{dA(t)}{dt} = e^{-\frac{t}{\beta}} \cdot l(t),$$

and therefore, according to (1.7.)

$$R_s(t) = a \int_0^{+\infty} e^{-\frac{u}{\beta}} e^{-\frac{u+|t|}{\beta}} du = \frac{a\beta}{2} e^{-\frac{|t|}{\beta}}. \quad (2.3.7)$$

Hence, it follows that the noise at the output of the integrating device has output

$$\sigma_s^2 = R_s(0) = \frac{a\beta}{2} \quad (2.3.8)$$

and a normalized correlation function

$$r_s(t) = \frac{R_s(t)}{\sigma_s^2} = e^{-\frac{|t|}{\beta}}. \quad (2.3.9)$$

Thus, the integrating device converts the uncorrelated noise to a noise oscillation with correlation time equal to the very large time constant of this device β . In other words, the integrating device causes strong correlation of the noise passing through it. This is physically explained by the fact that the integrating device eliminates rapid variations of input noise oscillation, filtering its high-frequency components. As will be seen from the following, this is also used to attenuate noise with an optimum filter.

The oscillation from the output of the integrating device (Fig. 2.1.2) is fed directly to the subtraction device and with delay by τ , i.e.,

$$u_4(t) = u_2(t) - u_3(t) = u_2(t) - u_2(t - \tau). \quad (2.3.10)$$

Therefore, the output noise is

$$\begin{aligned} \sigma_4^2 &= m_1(u_4^2) - [m_1(u_4)]^2 = m_1(u_4^2) = \\ &= m_1[u_2^2(t) + u_2^2(t - \tau) - 2u_2(t)u_2(t - \tau)] = \\ &= m_1[u_2^2(t)] + m_1[u_2^2(t - \tau)] - 2m_1[u_2(t)u_2(t - \tau)]. \end{aligned}$$

Since steady noise is being considered, then

$$m_1[u_2^2(t)] = m_1[u_2^2(t - \tau)] = \sigma_2^2; \quad m_1[u_2(t)u_2(t - \tau)] = R_2(\tau)$$

and

$$\sigma_4^2 = 2\sigma_2^2 - 2R_2(\tau) = 2\sigma_2^2 [1 - r_2(\tau)] = a\beta (1 - e^{-\frac{\tau}{T}}) \approx a\tau. \quad (2.3.11)$$

It follows from (2.3.5) and (2.3.11) that the signal/noise ratio at the output of an optimum filter comprises

$$q_4^2 = \frac{V_4^2}{\sigma_4^2} \approx \frac{V_1^2 \tau}{a}, \quad (2.3.12)$$

which is found to be in complete agreement with formula (1.2.11).

4. Operating Mechanism of Operating Filter for Single Pulse

The pulse signal is stored by the integrating device to level (2.3.5). A delay of this signal by time τ and subsequent subtraction of it from the oscillation fed directly from the integrating device does not alter the peak value (amplitude) of the signal.

72

The white noise passing through the integrating device is strongly correlated. It is fed to the subtraction device directly and with delay by time τ much less than its correlation time. The level of output noise is reduced considerably as a result of subtraction of the two strongly correlated noise oscillations. Indeed, it follows from (2.3.11) that the noise output is transmitted by a combination of the delay and subtraction defices with coefficient

$$Q = \frac{\sigma_4^2}{\sigma_2^2} = 2(1 - e^{-\frac{\tau}{T}}) \approx 2\frac{\tau}{T},$$

whose value, due to (2.3.2), is very low.

The noise suppression by combination of the delay and subtraction devices can also be explained by the spectral method [46].

If the integrating device is used for continuous integration of the input oscillation of both the signal and noise, then a combination of the delay and subtraction devices limits the time of this integration to the length of the signal at the input. If these devices are absent, the signal would be stored (integrated) only during its length while the noise would be stored for a considerably longer time. The signal/noise ratio at the output would be very low.

Thus, the combination of delay and subtraction devices performs the functions of automatic integration time limiter of the input oscillation up to the length of the pulse signal.

The concepts presented above are essentially the development and concrete definition of the remarks made in section 1.4.

Let us note that the considered optimum filters consist of linear components, the order of arrangement of which can be varied. Thus, for example, an optimum filter (Fig. 2.1.2) in which the integrating device precedes the combination of delay and subtraction devices is fully equivalent to an optimum filter in which the integrating device is preceded by a combination of delay and subtraction devices. Moreover, preference is frequently given to this circuitry of an optimum filter in practice since the level of processed signals and noise decreases in it as a result of subtraction, due to which the integrating device operates in a lighter mode.

73

2.4. Reduction of Signal/Noise Ratio Due to Deviation of Filter and Signal Characteristics From Optimum

1. Preliminary Remarks

It was shown above that a filter hardly differing from an optimum filter can be constructed for a signal with as complex a shape as desired. Very important for practice is the problem of how significant deviations of its characteristics from the optimum and also variation

of the shape of the signals received by this filter are for efficient operation of the optimum filter. Slight deviations of the characteristics of an optimum filter, like slight variation of signal shape that lead in both cases to a mutual error of the filter and signal, are always observed in practice.

This problem is also considered below for different special cases.

2. Variation of Shape of Video Signal or Envelope of Radio Signal With Retention of Signal Length at 0.5 Level

Let a symmetrical trapezoidal video pulse having the same length τ at 0.5 level act on the input of a filter (Fig. 2.1.2) optimum to a square-wave video pulse of length τ (Fig. 2.1.1):

$$\left. \begin{aligned} v_1(t) &= 0 & \text{at } t \leq 0 \text{ и } t \geq 2\tau - \tau_1 \\ v_1(t) &= \frac{V_1' t}{\tau - \tau_1} & \text{at } 0 \leq t < \tau - \tau_1 \\ v_1(t) &= V_1' & \text{at } \tau - \tau_1 \leq t < \tau \\ v_1(t) &= \frac{V_1'}{\tau - \tau_1} (2\tau - \tau_1 - t) & \text{at } \tau \leq t < 2\tau - \tau_1 \end{aligned} \right\}$$

where V_1' is the amplitude of this pulse and τ_1 is the length of its plane part (vertex).

74

Since the peak value of the signal at the output of an optimum filter is dependent on the input signal energy [see (1.4.4)], then let us select the amplitude of the trapezoidal pulse such that its energy

$$E_1 = \int_{-\infty}^{\infty} v_1^2(t) dt = \frac{V_1'^2}{3} (2\tau + \tau_1)$$

is equal to the energy of a square-wave pulse with amplitude V_1 optimum to the filter. Then

$$V_1' = V \left(\frac{3\tau}{2\tau + \tau_1} \right)^{1/2}. \quad (2.4.1)$$

The voltage at the output of the integrator (Fig. 2.1.2) is an integral of input voltage:

$$u_1(t) = \int_{-\infty}^t u_1(x) dx,$$

due to which

$$\left. \begin{aligned} v_2(t) &= 0 & \text{at } t < 0, \\ v_2(t) &= \frac{V'_1}{\tau - \tau_1} \frac{t^2}{2} & \text{at } 0 < t < \tau - \tau_1, \\ v_2(t) &= V'_1 \left(t - \frac{\tau - \tau_1}{2} \right) & \text{at } \tau - \tau_1 < t < \tau, \\ v_2(t) &= \frac{V'_1}{2} \left[\tau + \tau_1 + \frac{t - \tau}{\tau - \tau_1} (3\tau - 2\tau_1 - t) \right] & \text{at } \tau < t < 2\tau - \tau_1, \\ v_2(t) &= V'_1 \tau & \text{at } t \geq 2\tau - \tau_1. \end{aligned} \right\}$$

The voltage is fed to the lower output of the subtraction device with delay by τ , due to which

$$\left. \begin{aligned} v_3(t) &= 0 & \text{at } t < \tau, \\ v_3(t) &= \frac{V'_1}{\tau - \tau_1} \frac{(t - \tau)^2}{2} & \text{at } \tau < t < 2\tau - \tau_1. \end{aligned} \right\}$$

The following voltage acts at the output of an optimum filter

75

$$v_4(t) = v_2(t) - v_3(t) = v_2(t) - v_2(t - \tau),$$

which is described on interval $\tau \leq t \leq 2\tau - \tau_1$ by the expression

$$v_4(t) = V'_1 \left[\frac{\tau + \tau_1}{2} + \frac{t - \tau}{\tau - \tau_1} (2\tau - \tau_1 - t) \right].$$

Investigating it for the extreme value, let us determine the moment that the output voltage reaches the maximum value

$$t_m = \frac{3\tau - \tau_1}{2}.$$

At this moment the voltage at the input of the filter passes through level $0.5V'_1$ and reaches a maximum value at the output

$$V_4 = \frac{V'_1}{4} (3\tau + \tau_1).$$

In the case of a square-wave pulse optimum to it acting on the filter, the output voltage has a maximum value of (2.3.5). It follows from (2.3.5), (2.4.1) and the last expression that the loss in the signal/noise ratio in output due to the mutual nonoptimum nature of the filter and signal comprises

$$G = \frac{V_{\text{out}}^2}{V_4^2} = \frac{16}{3} \frac{2+x}{(3+x)^2}, \quad (2.4.2)$$

where $x = \tau_1/\tau$ is the relative length of the pulse peak.

The loss in power decreases monotonically (approximately linearly) with an increase of the relative length of the peak (Fig. 2.4.1). When the pulse peak has the same length as the pulse at the 0.5 level, i.e., $\tau_1 = \tau$ and $x = 1$, a trapezoidal pulse degenerates to a square-wave pulse and there is no loss ($G = 1$). At zero length of the peak, the pulse acquires a triangular shape and the loss comprises only 1.185 in this case.

Accordingly, if the pulse shape varies from square-wave to triangular but its energy and length are retained at the 0.5 level, the signal/noise ratio in power at the filter output, optimum to a square-wave pulse, deteriorates by only a total of 18.5 percent.

This permits one to conclude that the structure of a nonoptimum filter is not critical to variation of signal shape. The reason for this is that the criterion of the maximum signal/noise ratio is integral. Therefore, the signal at the optimum filter output is an integral of the input signal taken on a segment of length τ , which characterizes the length of the input signal at the 0.5 level. The value of this integral is hardly dependent on the signal shape if its energy is kept constant.

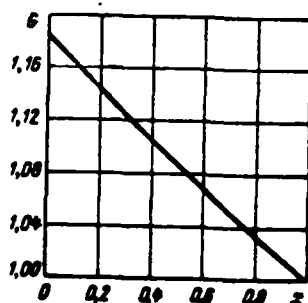


Fig. 2.4.1. Dependence of loss due to relative length of pulse peak

The foregoing is illustrated by Fig. 2.4.2, in which square-wave and triangular video pulses of equal energy are shown and the part of the triangular pulse which participates in formation of the maximum signal at the matched filter output is cross-hatched. One can clearly see from the figure that the areas (integrals) of the square-wave and

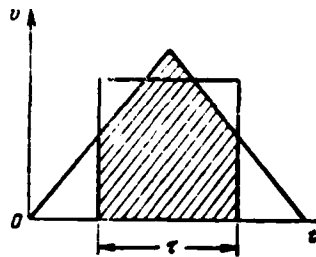


Fig. 2.4.2. Time diagrams of square-wave and triangular pulses of equal energy.

cross-hatched part of the triangular pulses differ comparatively little.

Due to the noncritical nature of the structure of optimum filters to variations of signal shape, there is no need to take into account small details of the shape of the video signal or the envelope of the radio signal when designing them.

3. Variation of Signal Length

77

If a square-wave video pulse of different length τ_1 and amplitude V_1 acts on the input of a filter (Fig. 2.1.2) optimum to a square-wave video pulse of length τ , then the voltage at the output comprises

and

$$\left. \begin{aligned} V_4 &= V_1 \tau_1, & \text{if } \tau_1 < \tau, \\ V_4 &= V_1 \tau, & \text{if } \tau_1 \geq \tau. \end{aligned} \right\}$$

If there is an optimum signal, $V_4 = V_1 \tau$. If the energy of these two signals is equal, $V_1 = V_1 \left(\frac{\tau}{\tau_1} \right)^{1/2}$.

Therefore, the power loss in signal/noise ratio due to variation of signal length is

$$\left. \begin{aligned} G &= \left(\frac{V_4}{V_1} \right)^2 = \frac{\tau}{\tau_1} & \text{at } \tau_1 < \tau \\ G &= \frac{\tau_1}{\tau} & \text{at } \tau_1 \geq \tau \end{aligned} \right\} \quad (2.4.3)$$

Accordingly, if the signal length varies n times, there is a decrease of signal/noise ratio by the same number of times.

Specifically, variation of signal length by ± 10 percent leads to 10 percent power losses in signal/noise ratio.

Thus, an optimum filter is weakly critical to slight variations of signal length.

4. Variation of Signal Amplitude Spectrum

Let us assume that the signal was deformed due to some reason or other, which caused variation in the signal spectrum. In this case the spectrum of the received signal is

$$\bar{S}'_1(\omega) = \bar{D}(\omega) \bar{S}_1(\omega),$$

where $\bar{S}_1(\omega)$ is the spectrum of the undistorted signal, $\bar{D}(\omega) = A(\omega)e^{jB(\omega)}$ is a function of distortions of the signal spectrum and $A(\omega)$ and $B(\omega)$ are a function of distortions of the amplitude and phase spectra, respectively, of the signal.

The signal at the output of an optimum filter then has the spectrum

78

$$\begin{aligned} \bar{S}'_1(\omega) &= \bar{S}'_1(\omega) \bar{K}^*(\omega) = \bar{S}'_1(\omega) C \bar{S}_1^*(\omega) e^{-j\omega t_0} = \\ &= C \bar{D}(\omega) \bar{S}_1^2(\omega) e^{j\omega t_0} \end{aligned}$$

and an instantaneous value of

$$v'_s(t) = \frac{C}{2\pi} \int_{-\infty}^{\infty} \bar{D}(\omega) \bar{S}_1^2(\omega) e^{j\omega(t-t_0)} d\omega. \quad (2.4.4)$$

Specifically, in the absence of spectral distortions we find (1.5.5).

Let us first consider the case when only the amplitude spectrum of the signal is distorted while the law of these distortions is harmonic [48]:

$$D(\omega) = A(\omega) = a_0 + a_1 \cos \omega c = a_0 + \frac{a_1}{2} (e^{j\omega c} + e^{-j\omega c}). \quad (2.4.5)$$

Then the output voltage, according to (2.4.4), is

$$v'_s(t) = \frac{a_1}{2} \frac{C}{2\pi} \int_{-\infty}^{\infty} \bar{S}_1^2(\omega) e^{j\omega(t-t_0+c)} d\omega +$$

$$+ a_0 \frac{C}{2\pi} \int_{-\infty}^{\infty} S_1^2(\omega) e^{j\omega(t-t_0)} d\omega + \frac{a_1}{2} \frac{C}{2\pi} \int_{-\infty}^{\infty} S_1^2(\omega) e^{j\omega(t-t_0-c)} d\omega.$$

Comparing the terms of this expression to (1.5.5), we find

$$v'_1(t) = \frac{a_1}{2} v_1(t+c) + a_0 v_1(t) + \frac{a_1}{2} v_1(t-c). \quad (2.4.6)$$

Accordingly, the signal at the output of an optimum filter is increased a_0 times and two additional signals of the same shape appear with relative amplitude $a_1/2$, shifted in time with respect to the main signal by $\pm c$, as a result of the cosine amplitude-frequency distortions.

Since the signal length at the filter output is double the length τ_1 of a signal optimum to it, then signals (2.4.6) do not overlap provided that

$$c > 2\tau_1. \quad (2.4.7)$$

These signals partially overlap at $c > \tau_1$. However, it does not affect the peak value of the output signal, which is a_0 times greater than an undistorted signal. In this case the signals at the filter input

$$v_1(t) = \frac{1}{2\pi} \int_{-\infty}^{\infty} A(\omega) S_1(\omega) e^{j\omega t} d\omega = \frac{a_1}{2} v_1(t+c) + a_0 v_1(t) + \frac{a_1}{2} v_1(t-c)$$

79

do not overlap at all. Squaring this expression and integrating the result in infinite time limits, we find with regard to the absence of overlapping that the total energy of the input signal is $E'_1 = \left(a_0^2 + \frac{a_1^2}{2}\right) E_1$, where E_1 is the energy of an undistorted signal.

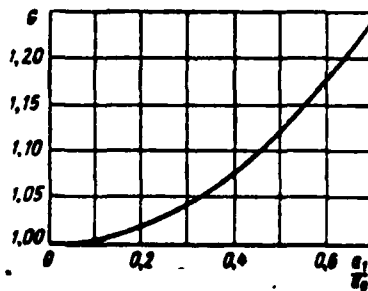


Fig. 2.4.3. Loss as function of relative amplitude of frequency distortions.

Accordingly, the square of the peak value of the output signal increases a_0^2 times due to amplitude-frequency distortions by law (2.4.5) and should have been increased with optimum filtration in proportion to the signal energy, i.e., $a_0^2 + a_1^2/2$ times. Therefore, the power loss in signal/noise ratio due to mutual nonoptimum nature of the signal and filter comprises

80

$$G = 1 + \frac{a_1^2}{2a_0^2} \quad (2.4.8)$$

and increases with an increase of the relative amplitude of frequency distortions (Fig. 2.4.3). Specifically, a 10% power loss corresponds to $a_1 = 0.472 a_0$. Accordingly, an optimum filter is weakly critical to slight harmonic variations of the signal amplitude spectrum.

5. Variation of Signal Phase Spectrum

Let us consider the case of sine-curve phase-frequency variations of the signal [48]:

$$D(\omega) = e^{jB(\omega)} = e^{jb \sin \omega c}$$

Then according to (2.4.4), the output signal is

$$v_s(t) = \frac{C}{2\pi} \int_{-\infty}^{\infty} S_1^2(\omega) e^{j[\omega(t-t_0) + b \sin \omega c]} d\omega.$$

Since [25, 48]

$$e^{jb \sin \omega c} = \sum_{k=-\infty}^{\infty} J_k(b) e^{j k \omega c},$$

where $J_k(b)$ is a k -order Bessel function of first kind, then by substituting this expression into the previous one and changing the order of integration and adding, using (1.5.5) and taking into account that $J_{-k}(b) = (-1)^k J_k(b)$, we find

$$v_s(t) = \sum_{k=-\infty}^{\infty} J_k(b) v_s(t + kc) + J_0(b) v_s(t) + \sum_{k=1}^{\infty} (-1)^k J_k(b) v_s(t - kc). \quad (2.4.9)$$

Accordingly, harmonic phase-frequency variations of the input signal lead to the fact that the main output signal is multiplied by $J_0(b)$ and an infinite number of pairs of satellite signals having the same shape as the main signal, shifted in time with respect to the main signal by $\pm kc$, where k is a whole number, and multiplied by $J_k(b)$,

81

appears around it; moreover, all the satellite signals shifted toward an advance have the same initial phase while the phases of any two adjacent delaying signals differ by 180° .

If amplitude b of the phase-frequency variations is low, then since [25]

$$J_0(b) \approx 1 - \frac{b^2}{4} \quad \text{and} \quad J_n(b) \approx \frac{1}{n!} \left(\frac{b}{2} \right)^n \quad \text{at } n \geq 1,$$

expression (2.4.9) is simplified:

$$v_2(t) \approx \frac{b}{2} v_2(t+c) + \left(1 - \frac{b^2}{4} \right) v_2(t) - \frac{b}{2} v_2(t-c),$$

and mainly has the same nature as output signal (2.4.6) with cosine amplitude-frequency distortions.

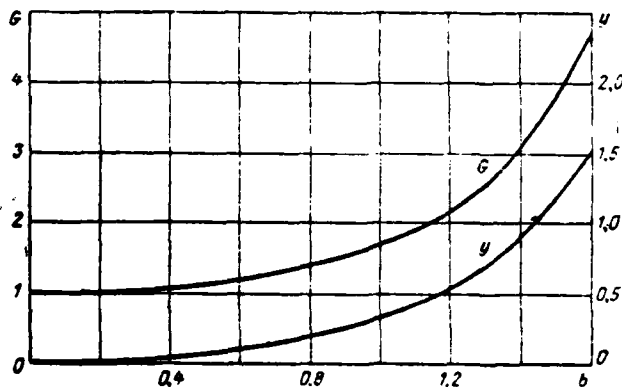


Fig. 2.4.4. Loss and relative output of satellite signal as functions of amplitude of phase distortions.

If condition (2.4.7) is fulfilled, the peak value of the signal in the case of phase-frequency distortions differs from that of an undistorted signal $J_0(b)$ times. Therefore, the power loss in signal/noise ratio due to phase-frequency variations of the signal is

$$G = [J_0(b)]^{-2}. \quad (2.4.10)$$

The relative peak output of the first satellite signal comprises

$$y = \frac{J_1^2(b)}{J_0^2(b)}. \quad (2.4.11)$$

These two values increase (Fig. 2.4.4) as the amplitude of the

phase-frequency variations increase, reaching 1.72 and 0.333 at $b = 1$ and 4.83 and 1.57 at $b = 1.6$, respectively.

Accordingly, the effect of phase-frequency distortions of the signal is insignificant only with relatively small value of them. It is significant that the degree of distortions of the output signal depends on the absolute (rather than the relative) value of the phase-frequency variations.

6. Linear Phase Changes of Signal

By analogy with (1.3.3), the complex voltage envelope at the output of a linear selective system can be represented in the form of a Duamel integral for envelopes [10, 28, 49]

$$\bar{U}_2(t) \approx \frac{1}{2} \int_{-\infty}^{\infty} \bar{U}_1(x) \bar{H}(t-x) dx, \quad (2.4.12)$$

where $\bar{U}_1(t)$ and $\bar{H}(t)$ are the complex envelopes of the input voltage and pulse characteristic of the system, respectively. Specifically, for an optimum filter, according to (1.3.6),

$$\bar{U}_2(t) \approx \frac{C}{2} e^{-j\omega_0 t} \int_{-\infty}^{\infty} \bar{U}_1(x) \bar{U}_1^*(t_0 - t + x) dx. \quad (2.4.13)$$

If the voltage of the signal is fed to its input, we find at the output

$$V_2(t) \approx \frac{C}{2} e^{-j\omega_0 t} \int_{-\infty}^{\infty} V_1(x) V_1^*(t_0 - t + x) dx,$$

$$V_2(t_0) = \frac{C}{2} e^{-j\omega_0 t_0} \int_{-\infty}^{\infty} V_1^2(x) dx = CE_1 e^{-j\omega_0 t_0},$$

$$v_2(t_0) = \operatorname{Re}(V_2(t_0) e^{j\omega_0 t_0}) = CE_1.$$

Let the input voltage differ from the optimum signal only by phase $\psi(t)$, i.e., $\bar{U}_1(t) = V_1(t) e^{j\psi(t)}$

Then

$$\bar{U}_2(t) \approx \frac{C}{2} e^{-j\omega_0 t} \int_{-\infty}^{\infty} V_1(x) V_1^*(x - t + t_0) e^{j\psi(x)} dx.$$

and specifically at $t = t_0 - \epsilon = \tau - \epsilon$

$$U_2(\tau - \varepsilon) \approx \frac{C}{2} e^{-j\omega_0 \tau} \int_{-\infty}^{\tau} V_1(x) V_1^*(x + \varepsilon) e^{j\psi(x)} dx.$$

If $V_1(t) = V_1(t) e^{j\psi(t)}$, where $V_1(t)$ and $\psi(t)$ are the amplitude and phase functions of the signal, respectively, and the signal has constant output over its entire length τ , i.e.,

$$\text{and } \left. \begin{aligned} V_1(t) &= \left(\frac{2E_1}{\tau} \right)^{1/2} \text{ at } 0 < t < \tau \\ V_1(t) &= 0 \text{ at other values of } t \end{aligned} \right\}$$

then

$$\left. \begin{aligned} u_2(\tau - \varepsilon) &= \frac{CE_1}{\tau} \int_0^{\tau - \varepsilon} \cos \theta(x, \varepsilon) dx \text{ at } \varepsilon > 0, \\ u_2(\tau - \varepsilon) &= \frac{CE_1}{\tau} \int_{-\varepsilon}^{\tau} \cos \theta(x, \varepsilon) dx \text{ at } \varepsilon < 0, \end{aligned} \right\}$$

where $\theta(x, \varepsilon) = \psi(x) - \psi(x + \varepsilon) = \varphi'(x) - \omega_0 \varepsilon$.

If $\psi(t) = \psi_0$ at $0 < t < \tau$ and $|\psi_0| \leq \pi$, then assuming that ε is small and comprises a fraction of the period of the carrier oscillation $2\pi/\omega_0$, we have

$$\theta(x, \varepsilon) \approx \psi_0 - \omega_0 \varepsilon - \varphi'(x) \varepsilon = \psi_0 - [\omega_0 + \varphi'(x)] \varepsilon \approx \psi_0 - \omega_0 \varepsilon,$$

since the rate of variation of the phase function is usually small compared to the carrier frequency. Therefore

$$u_2(\tau - \varepsilon) \approx CE_1 \left(1 - \frac{|\varepsilon|}{\tau} \right) \cos(\psi_0 - \omega_0 \varepsilon).$$

At $\varepsilon = \frac{\psi_0}{\omega_0}$ this expression reaches a maximum:

$$U_2 = u_2 \left(\tau - \frac{\psi_0}{\omega_0} \right) \approx CE_1 \left(1 - \frac{|\psi_0|}{\omega_0 \tau} \right) \approx CE_1,$$

since

$$\omega_0 \tau \gg 2\pi > 2|\psi_0|.$$

Accordingly, inversion of the phase of input oscillation by angle π essentially leads only to a shift of the moment of the maximum output oscillation by the time $\varepsilon = \frac{\psi_0}{\omega_0}$.

Subsequently assuming that the constant phase shifts of the input are eliminated, we will be interested in the output voltage when the signal ends

$$u_2(\tau) = \frac{CE_1}{\tau} \int_0^\tau \cos \psi(t) dt. \quad (2.4.14)$$

Let the distorting phase function be linear over the signal length:

$$\psi(t) = \psi_m \left(\frac{t}{\tau} - \frac{1}{2} \right) \text{ at } 0 < t < \tau, \quad (2.4.15)$$

where ψ_m is the incident wave of phase during the length of the pulse. Then, substituting this expression into the previous one and calculating, we find

$$u_2(\tau) = CE \frac{\sin \frac{1}{2} \psi_m}{\frac{1}{2} \psi_m}.$$

Accordingly, the loss in signal/noise ratio comprises

$$G = \left(\frac{\frac{1}{2} \psi_m}{\sin \frac{1}{2} \psi_m} \right)^2 = \frac{\psi_m^2}{2(1 - \cos \psi_m)} \quad (2.4.16) \quad 85$$

and increases with an increase of the incident wave of the phase (see curve 1 in Fig. 2.4.5). At $\psi_m = 0.5\pi$ and 0.9π the loss comprises 1.25 and 2.05, respectively.

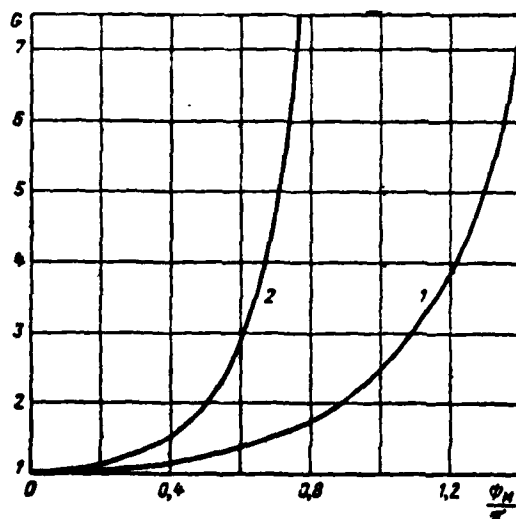


Fig. 2.4.5. Dependence of loss on incident wave of phase.

A linear varying deviation of phase (2.4.15) is obviously equivalent to detuning $F = \frac{\psi_m}{2\pi\tau}$. If one assumes that a power loss on the

order of 20% is permissible, then the permissible detuning is

$$F_{\text{don}} = \frac{0.25}{\tau},$$

which is rather difficult to provide, especially in the case of signals of great length.

Thus, an optimum filter is very critical to variation of the carrier frequency of the received signal.

We note that in some cases of angular modulation (for example, with linear frequency modulation), the requirements on the frequency stability of the received signal can be sharply attenuated (see section 3.8). However, in this case the maximum output signal is observed with a considerable time shift rather than at the moment the signal ends, as was considered above.

86

One can also consider other laws of phase variation of the input oscillation and one can determine the laws achieved in this case. It is obvious that one of the worst cases (in the sense of a decrease of output signal amplitude) will be intermittent variation of phase:

$$\left. \begin{aligned} \psi(t) &= -\frac{\psi_m}{2} \quad \text{at } 0 < t < \frac{\tau}{2}, \\ \psi(t) &= \frac{\psi_m}{2} \quad \text{at } \frac{\tau}{2} < t < \tau. \end{aligned} \right\}$$

In this case according to (2.4.14), the power loss is

$$G = \frac{2}{1 + \cos \psi_m}.$$

comprising 1.25 at $\psi_m = 0.28$ (see curve 2 in Fig. 2.4.5).

However, consideration of random variation of output signal phase, which is done below, is of great interest.

7. Random Variation of Signal Phase

Let variation of the input signal phase be a steady random process with zero mean and normal law of probability distribution and known autocorrelation function $R(t) = \sigma^2 r(t)$, where $r(t)$ is a normalized autocorrelation function. Let us determine the statistical

characteristics of voltage at the output of an optimum filter [see (2.4.14)]*:

$$u_2(\tau) \approx \frac{CE_1}{\tau} \int_0^{\tau} e^{j\psi(t)} dt.$$

8

The mean value of this expression is

$$m_1(u_2) \approx \frac{CE_1}{\tau} \int_0^{\tau} m_1[e^{j\psi(t)}] dt.$$

Since the mean value $m_1(e^{j\psi})$ is a value at $v = 1$ of the characteristic function of the normally distributed value [15, 20]:

$$\theta_v(v) = m_1(e^{jv\psi}) = \exp \left[jm_1(\psi)v - \frac{1}{2} \sigma^2 v^2 \right],$$

then

$$m_1(e^{j\psi}) = \exp \left[jm_1(\psi) - \frac{1}{2} \sigma^2 \right] = \exp \left(-\frac{\sigma^2}{2} \right)$$

and

$$m_1(u_2) = CE_1 \exp \left(-\frac{\sigma^2}{2} \right).$$

due to which the power loss is

$$G = \exp \sigma^2, \quad (2.4.17)$$

comprising 1.1, 1.2 and 1.5, respectively, at $\sigma = 0.309, 0.427$ and 0.637 radian. Accordingly, the permissible variations are random phase variations on the order of half a radian.

The square of the output voltage is

$$\begin{aligned} u_2^2 &= \left(\frac{CE}{\tau} \right)^2 \int_0^{\tau} \exp j\psi(t) dt \int_0^{\tau} \exp [-j\psi(x)] dx = \\ &= \left(\frac{CE}{\tau} \right)^2 \int_0^{\tau} dx \int_0^{\tau} \exp j[\psi(t) - \psi(x)] dx. \end{aligned}$$

and its mean value is

$$m_1(u_2^2) = \left(\frac{CE_1}{\tau} \right)^2 \int_0^{\tau} dt \int_0^{\tau} m_1(\exp j[\psi(t) - \psi(x)]) dx.$$

Since, due to the normal nature of processes $\psi(t)$ and $\psi(x)$,

88

*See [50] for solution of a similar problem with respect to antennas by the statistical modelling method.

$$\begin{aligned}
m_1 \{ \exp j [\psi(t) - \psi(x)] \} &= \exp \left\{ j [m_1(\psi(t)) - m_1(\psi(x))] - \frac{1}{2} \times \right. \\
&\times \left. \left\{ m_1 [\psi(t) - \psi(x)]^2 - m_1^2 [\psi(t) - \psi(x)] \right\} \right\} = \exp \left\{ - \frac{1}{2} \times \right. \\
&\times \left. \left\{ m_1 [\psi^2(t)] - 2m_1 [\psi(t)\psi(x)] + m_1 [\psi^2(x)] \right\} \right\} = \\
&= \exp \{ -\sigma^2 [1 - r(t-x)] \}.
\end{aligned}$$

then

$$m_1(u_2^2) = \left(\frac{CE_1}{\tau} \right)^2 \int_0^1 dt \int_0^1 \exp \{ -\sigma^2 [1 - r(t-x)] \} dx.$$

Changing the variable in the internal integral and then the order of integration, we find

$$m_1(u_2^2) = 2(CE_1)^2 \int_0^1 (1-y) \exp \{ -\sigma^2 [1 - r(\tau y)] \} dy. \quad (2.4.18)$$

The mean square was calculated on the Minsk-1 ETsVM [digital computer] for two types of normalized autocorrelation function:

$$r_1(t) = \exp \left(-\frac{|t|}{\sigma\tau} \right) \text{ и } r_2(t) = \exp \left(-\frac{t^2}{\sigma^2\tau^2} \right).$$

where σ is the ratio of the correlation time of the process to the signal length (see Fig. 2.4.6), on which the solid curves show exponential functions and the dashed lines show bell functions).

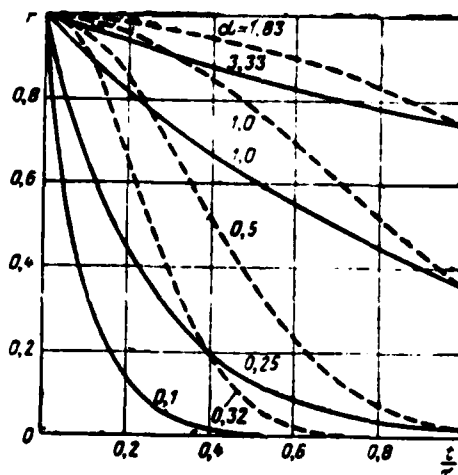


Fig. 2.4.6. Autocorrelation functions of signal phase variation.

The results of calculation (Fig. 2.4.7) show that there is a rapid decrease of the mean square as the deviation of phase variation increases and the more rapid it is, the less correlated the input signal

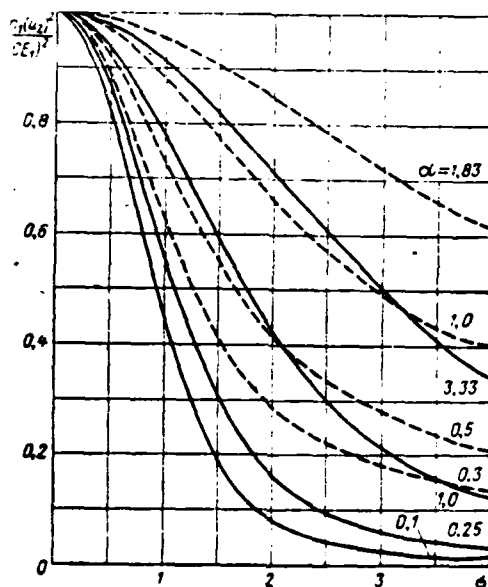


Fig. 2.4.7. Dependence of mean square of output voltage on mean square deviation of phase.

phase is. On the contrary, very strongly correlated phase variations essentially do not change the value of the mean square of output voltage. This is easily explained physically since completely correlated phase variations correspond to inversion of the carrier oscillation phase of the input voltage which, as was established above, essentially does not change the value of the output voltage. Random variations with mean square value on the order of half a radian are permissible in the case of weak correlation of phase changes. It is very complicated to provide the latter in systems with wideband signals (see Chapters 3 and 4), in which phase variation of the spectral components during signal length reaches very large values.

8. Random Variations of Signal Amplitude

Let the complex voltage amplitude at the input of an optimum filter be the product of the complex amplitude of an optimum signal by the real random time function $1 + v(t)$:

$$U_1(t) = [1 + v(t)]V_1(t).$$

The output voltage, according to (2.4.13), is then

$$u_s(\tau) = \frac{C}{2} \int_{-\infty}^{\infty} [1 + v(t)] V_1^2(t) dt$$

and if

$$\left. \begin{aligned} V_1^2(t) &= \frac{2E_1}{\tau} \quad \text{at } 0 < t < \tau, \\ V_1^2(t) &= 0 \quad \text{at other values of } t, \end{aligned} \right\}$$

$$u_s(\tau) = \frac{CE_1}{\tau} \int_0^{\tau} [1 + v(t)] dt.$$

Assuming that random process $v(t)$ is steady with zero mean and autocorrelation function $R(t) = \sigma^2 r(t)$, we find that the output voltage has the mean value

$$\begin{aligned} m_1[u_s(\tau)] &= \frac{CE_1}{\tau} \int_0^{\tau} \{1 + m_1[v(t)]\} dt = CE_1 \{1 + \\ &+ m_1[v(t)]\} = CE_1, \end{aligned} \quad (2.4.19)$$

and the mean square is [29, 51]

91

$$\begin{aligned} m_2[u_s^2(\tau)] &= \left(\frac{CE_1}{\tau}\right)^2 \left[\tau^2 + 2 \int_0^{\tau} (\tau - x) R(x) dx\right] = \\ &= (CE_1)^2 [1 + \sigma^2 f(\alpha)], \end{aligned}$$

where

$$f(\alpha) = \frac{2}{\alpha^2} \int_0^{\alpha} (\alpha - x) r(x, \alpha) dx,$$

α is the ratio of the correlation time of amplitude changes of signal to its length.

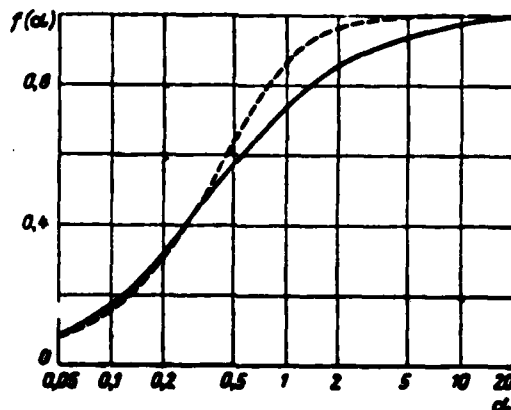


Fig. 2.4.8. Dependence of variation of output voltage on relative correlation time of amplitude variations of signal. The solid curve corresponds to an exponential function while the dashed curve corresponds to a bell autocorrelation function.

Specifically, for the considered exponential autocorrelation function

$$f(a) = 2a [1 - a(1 - e^{-\frac{1}{a}})] \quad (2.4.20)$$

and for a bell autocorrelation function

$$f(a) = a \left[\sqrt{\pi} \Phi\left(\frac{1}{a}\right) + a(1 - e^{-\frac{1}{a^2}}) \right] \quad (2.4.21)$$

Consideration of these functions (Fig. 2.4.8) shows that rapid, weakly correlated amplitude changes of the input signal cause a comparatively small increase of the mean square of the output voltage, while slow, strongly correlated changes are transferred almost without attenuation to the mean square of the output voltage.

92

The energy of the signal $E_{12} = \frac{1}{2} V_1^2 (1 + \sigma^2)$ increases due to random amplitude variations of the input signal. Since the mean value of output voltage (2.4.19) does not vary, this is equivalent to a power loss.

$$G_1 = 1 + \sigma^2 \quad (2.4.22)$$

If one proceeds from the mean square value of the output voltage, the loss comprises

$$G_2 = \frac{1 + \sigma^2}{1 + \sigma^2 f(a)} \quad (2.4.23)$$

Its value is less than G_1 , especially with strongly correlated amplitude variations of the input signal.

The results permit one to conclude the weak critical nature of the optimum filter structure to both random and regular (see item 2) small amplitude variations of the input signal and its length (item 3) and also to sufficiently small random and regular phase variations (items 6 and 7).

2.5. Comparison of Optimum Filter for Simplest Signals With Resistance-Coupled and Other Amplifiers

Let us consider passage of a square-wave video pulse signal and noise through a resistance-coupled amplifier without correction.

If only the effect of spurious capacitance C_0 is taken into account, then the transient function of this amplifier is also described by an expression of type (2.3.1). Only in the given case are there no

auxiliary amplifier and time constant $\beta = C_0 R_a$, where R_a is the load resistance of the anode circuit.

Therefore, the output signal has a peak value of

93

$$V_2 = KV_1 (1 - e^{-\frac{\tau}{\beta}}),$$

where V_1 is the pulse amplitude at the input, τ is the pulse length and K is the amplification factor.

By analogy with (2.3.8), the noise at the output has power

$$\sigma_2^2 = \frac{aK^2}{2\beta}.$$

Therefore, the ratio of the square of the peak signal value to noise at the output of the resistance-coupled amplifier comprises

$$q_2^2 = \frac{U_2^2}{\sigma_2^2} = \frac{U_1^2 \tau}{a} \frac{2\beta}{\tau} (1 - e^{-\frac{\tau}{\beta}})^2.$$

Using (2.3.12), let us determine the loss in the signal/noise ratio when using a resistance-coupled amplifier compared to an optimum filter:

$$G = \frac{q_2^2_{\text{opt}}}{q_2^2} = \frac{\tau}{2\beta (1 - e^{-\frac{\tau}{\beta}})^2}.$$

Since the time constant of the amplifier is related to its bandpass at the $1/\sqrt{2}$ level by the function $\beta = 1/2\pi\Delta F$, the latter equality can be rewritten in the following form:

$$\frac{1}{G} = \frac{1}{\pi b} (1 - e^{-\pi b})^2, \quad (2.5.1)$$

where $b = \Delta F\tau$ is the product of the bandpass by the pulse length, which is naturally called the dimensionless bandpass.

Investigating (2.5.1) for the maximum with respect to b , we find the equation

$$1 + 4\pi b = e^{2\pi b},$$

the root of which is

$$b_1 = \Delta F_1 \tau = 0.200$$

(2.5.2)

and is an optimum value of the dimensionless bandpass.*

The dependence of the signal/noise ratio at the output of a resistance-coupled amplifier (in fractions of the similar ratio at the output of an optimum filter) on the bandpass of the amplifier is shown by curve 1 in Fig. 2.5.1. Curve 2 reproduces the similar function for a system of two series-connected resistance-coupled amplifiers. Consideration of them shows the low critical nature of the optimum values of the bandpass of a resistance-coupled amplifier.

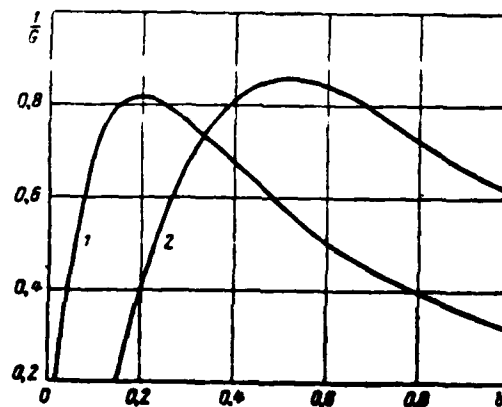


Fig. 2.5.1. Dependence of value inverse to loss on bandpass of amplifier.

The loss is minimum with optimum bandpass and comprises for a single resistance-coupled amplifier

$$G_{\min} = G(b = b_1) = \frac{1}{0.815} = 1.227. \quad (2.5.3)$$

Accordingly, the signal/noise power ratio at the output of a single resistance-coupled amplifier with optimum bandpass is only 18.5% (i.e., 0.9 dB) less than that at the output of an optimum filter. It follows from consideration of curve 2 in Fig. 2.5.1 that the indicated ratio at the output of resistance-coupled amplifiers with optimum bandpass is only 14.3% less than at the output of an optimum filter.

*The optimum values of the bandpasses of an ideal filter when receiving a square-wave pulse and of a filter with bell-shaped frequency characteristic when receiving a bell-shaped pulse were first calculated by V. I. Siforov [52] and A. P. Belousov [53], respectively.

Calculations show that in the case of a triangular shape of the video pulse signal, a resistance-coupled amplifier whose bandpass is selected as optimum $b_2 = 0.3$, provides a power loss on the order of 22% (i.e., 1.1 dB) in the signal/noise ratio compared to a filter optimum to this signal.

Based on the foregoing and also based on the mutual conformity of filters optimum to radio and video pulse signals of the same shape (see section 2.2, item 3) and on the equivalence of resonance and resistance-coupled amplifiers [54], one can state that the loss in signal/noise ratio compared to an optimum filter is approximately 1 dB for a square-wave radio pulse when using a tuned amplifier with optimum bandpass of $b_1 = 0.4$. The latter is valid both for a multistage tuned amplifier and for signals of different shape [15, 55].

Calculations performed using the results obtained by S. I. Yev-tyanov [49] and A. A. Kolosov [56] for the case of a square-wave radio pulse and bandpass amplifier with critical relationship between its circuits and bandpass of $b = 1$ show that the loss in the signal/noise ratio comprises 0.6 dB in this case.

It follows from the investigations of N. A. Semenov [57] that the signal/noise ratio at the output differs from the maximum possible by no more than 0.5 dB, i.e., insignificantly, with the effect of bell-shaped, trapezoidal, triangular and square-wave pulses on a UPCh [intermediate-frequency amplifier] with bell-shaped ("probability") frequency characteristic.

Accordingly, the use of an optimum filter for single pulse signals of simple shape, related to some complication of the circuit and design, permits one to achieve a comparatively small advantage in noise stability and is usually unfeasible. This is explained by the noncritical nature of the optimum filter to variation in the shape of the video signal or the shape of the envelope of the radio signal (see section 2.4).

However, one should bear in mind that the pulse at the output of a resistance-coupled amplifier with optimum bandpass (curve a in

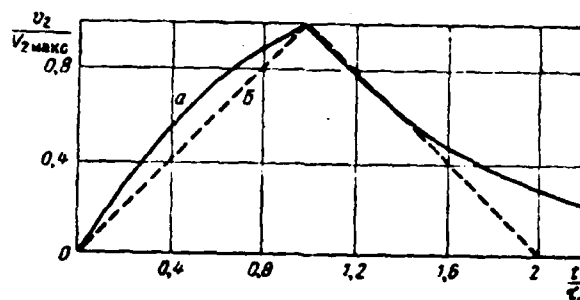


Fig. 2.5.2. Voltages at output of amplifier (a) and optimum filter (b)

Fig. 2.5.2) has a length 57% greater at the 0.1 readout level and 78% greater at the 0.05 readout level than at the output of an optimum filter (dashed curves b in the same figure). Therefore, the time resolution (in range) of the radio engineering pulse system deteriorates in the case of using resistance-coupled and other amplifiers with optimum bandpass (from the viewpoint of signal/noise ratio).

OPTIMUM FILTERS FOR PULSED SIGNALS WITH LINEAR FREQUENCY MODULATION

3.1. Broadening of Signal Spectrum to Increase Range Resolution

It was assumed previously that the range resolution of radar systems cannot be made less than the distance corresponding to the length of the emitted pulse [58-59]:

$$\Delta r = \frac{ct}{2}.$$

From this follows the conclusion that an increase of range resolution requires shortening of the length of the emitted pulses, which is accompanied by a decrease of the energy of emitted signals with existing restrictions on the peak transmitted power and because of this is accompanied by a decrease of the effective range of these systems.

However, if the signal/noise ratio is sufficiently high, the range resolution is determined by the pulse length at the output of the linear part of the receiver. Therefore, the statement presented above is valid 98 only if shortening of the pulse length of the signal is not provided in the receiver by corresponding processing of it. An example of the latter may be high-frequency differentiation (Fig. 3.1.1).

It permits a considerable increase of the resolution, which is mainly limited by the receiver bandpass. In this case two pulses correspond to each input pulse. The second pulse can be eliminated by

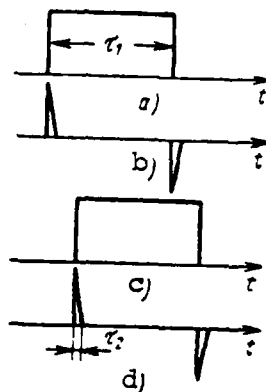


Fig. 3.1.1. Resolution of time-overlapped pulsed signals a and c in system with differentiation (signals b and d are the result of differentiation of signals a and c).

adding it to the first pulse delayed by time τ_1 using an adding device with feedback delayed by τ_1 (Fig. 3.1.2, a and b). An attenuator with transfer factor m whose value is somewhat less than unity (Fig. 3.1.2, c) can be connected to the feedback circuit to eliminate its self-excitation. Having taken $m = 0.99$, we find 100-fold attenuation of the second pulse at the output.

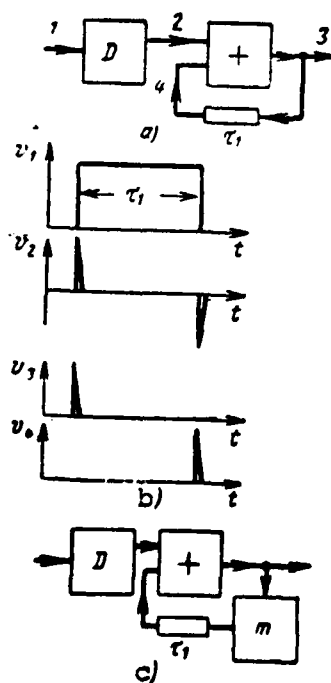


Fig. 3.1.2. Block diagrams of Urkovits optimum filters (a) and (c) and time diagrams of voltages (b)

AD-A115 395

FOREIGN TECHNOLOGY DIV WRIGHT-PATTERSON AFB OH
OPTIMUM FILTERS AND PULSED SIGNAL STORAGE DEVICES, (U)

F/G 9/5

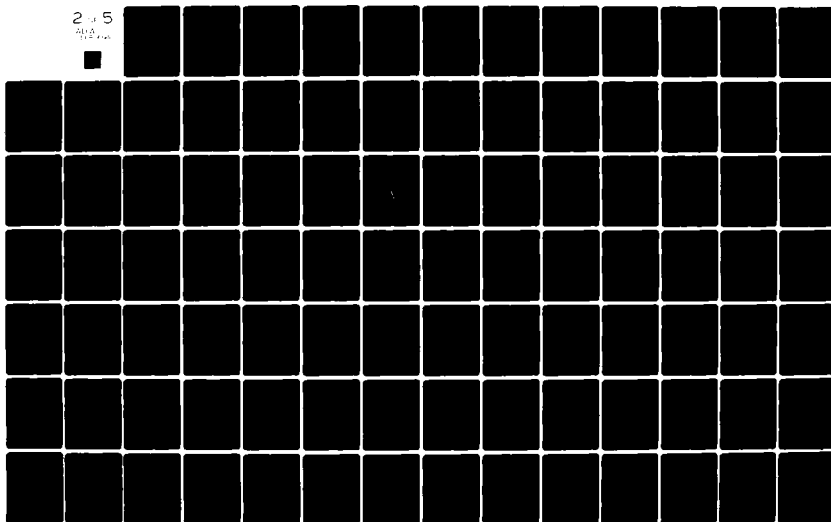
MAY 82 Y S LEZIN
FTD-ID(RS)T-0182-81

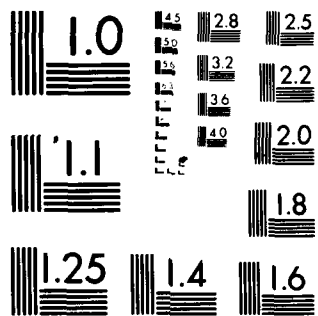
UNCLASSIFIED

NL

2-5

AD-A115 395





MICROCOPY RESOLUTION TEST CHART
NATIONAL BUREAU OF STANDARDS-1963-A

The device shown in Fig. 3.1.2, a has the transfer function

$$K(\omega) = \frac{j\omega}{1 - e^{-j\omega\tau_1}}, \quad (3.1.1)$$

which is inverse to the spectrum of a video pulse of length τ_1 and of single amplitude and coincides with the transfer function of an optimum Urkovits filter [11, 60]. The latter is designed for optimum separation of radar signals from noise formed by reflection from a large number of randomly arranged local objects. The spectral intensity of this noise is proportional to the square of the modulus of the emitted pulse spectrum $F_1(\omega) = \mu |\bar{S}(\omega)|^2$. Based on (1.8.1), the optimum filter for separation of the signals of this noise has the transfer function

$$K(\omega) = C \frac{\bar{S}^*(\omega)}{F_1(\omega)} e^{-j\omega t_0} = C \frac{\bar{S}^*(\omega)}{\mu |\bar{S}(\omega)|^2} = \frac{C}{\mu} \frac{e^{-j\omega t_0}}{\bar{S}(\omega)}.$$

Having assumed that $t_0 = 0$ and $C = \mu V$, for a square-wave pulse of length τ_1 we find (3.1.1).

This also shows that the device (Fig. 3.1.2, a) is an optimum Urkovits filter. It did not find application in radar receivers due to the fact that the effective range would be sharply reduced due to the increased effect of white input noise. The latter is explained by the fact that the modulus of the transfer function (3.1.1) is comparatively small at low frequencies at which the spectrum of the received signal is also mainly concentrated. The modulus of the transfer function is appreciably higher at higher frequencies corresponding to less intensive sections of the signal spectrum. As a result the noise level at the output will be very high and it will be infinitely high with unlimited bandpass.

If the filter bandpass is appreciably limited, this leads to significant broadening of the output pulses of the signal.

Thus, the contradiction indicated above between the effective range of the system and its range resolution does not find satisfactory resolution even in this case.

It was shown in the first chapter that optimum filtration of signals must be used to ensure the greatest effective range. The output signal should reproduce in this case the autocorrelation function of

the input signal. To achieve high range resolution, one must have this function in the form of a short pulse concentrated in the vicinity of $t = 0$ and having short length τ_2 . Therefore, the pulse spectrum at the output of an optimum filter should be on the order of $1/\tau_2$ and that at its input should be on the order of $\sqrt{2}/\tau_2$. Accordingly, the spectrum of emitted pulses should be rather broad to achieve high range resolution. 100

This can be achieved both by shortening the length of the emitted pulses (which is unfeasible) and by angular (frequency or phase) modulation of them by some law.

The emitted pulses should have high energy, which is achieved by increasing the length with the usually existing restrictions of peak power, to achieve high effective range. Therefore, the emitted signals should have sufficiently high product of the width of the spectrum by length to ensure both high range resolution and high effective range. These signals are called wideband, complex modulated or complex.

The requirement of the wideband nature of the signal spectrum to achieve high range resolution is necessary, but insufficient. And if the signal spectrum is wide, its correlation function may essentially have either a single wide central pip in the vicinity of point $t = 0$ or, along with a narrow central pip, several additional pips. The uniqueness of range measurement cannot be provided in the latter case.

The indicated circumstance, on the one hand, considerably complicates selection of the shape of received signals and on the other hand determines this selection.

3.2. Pulse Spectrum With Linear Frequency Modulation

One of the simplest methods of broadening the spectrum of an emitted radio pulse [61] is percentage modulation of its carrier frequency by linear law within the range of length:

$$\omega = \omega_0 + \frac{\Delta\omega}{\tau_1} t \quad \text{at } |t| < \frac{\tau_1}{2}, \quad (3.2.1)$$

where $\Delta\omega = 2\pi\Delta f$ is frequency deviation and ω_0 is mean frequency. This

pulse has phase

101

$$\varphi = \int \omega dt + C = \omega_0 t + \frac{\Delta\omega}{2\tau_1} t^2 + C.$$

Having assumed that $\phi = 0$ at $t = 0$, we find $C = 0$. The instantaneous pulse voltage at $|t| < \frac{\tau_1}{2}$ is then

$$v_1 = V_1 \cos \left(\omega_0 t + \frac{\Delta\omega}{2\tau_1} t^2 \right) = \frac{V_1}{2} \left[\exp j \left(\omega_0 t + \frac{\Delta\omega}{2\tau_1} t^2 \right) + \exp -j \left(\omega_0 t + \frac{\Delta\omega}{2\tau_1} t^2 \right) \right]. \quad (3.2.2)$$

This pulse has the spectral density

$$S_1(\omega) = \frac{V_1}{2} \int_{-\tau_1/2}^{\tau_1/2} \left\{ \exp j \left[(\omega_0 - \omega) t + \frac{\Delta\omega}{2\tau_1} t^2 \right] + \exp -j \left[(\omega_0 + \omega) t + \frac{\Delta\omega}{2\tau_1} t^2 \right] \right\} dt.$$

The second term is a rapidly oscillating function, due to which the integral of it is much less than the integral of the first term [10]. Therefore, assuming that

$$x = \sqrt{\frac{2\Delta f}{\tau_1}} \left(t + \frac{\omega_0 - \omega}{\Delta\omega} \tau_1 \right),$$

we find

$$S_1(\omega) = \frac{V_1}{2} \sqrt{\frac{\tau_1}{2\Delta f}} \exp \left[-j \frac{(\omega_0 - \omega)^2}{2\Delta\omega} \tau_1 \right] \int_{-x_1}^{+x_2} e^{j \frac{\pi}{2} x^2} dx,$$

where

$$x_1 = \sqrt{\frac{D}{2}} \left(1 - 2 \frac{\omega_0 - \omega}{\Delta\omega} \right); \quad (3.2.3)$$

$$x_2 = \sqrt{\frac{D}{2}} \left(1 + 2 \frac{\omega_0 - \omega}{\Delta\omega} \right);$$

$$D = \Delta f \tau_1.$$

At the beginning of the pulse $(t = -\frac{\tau_1}{2})$, when $\omega = \omega_0 - \frac{\Delta\omega}{2}$, $x_1 = 0$ and $x_2 = \sqrt{2D}$ and at the end of the pulse $(t = \frac{\tau_1}{2})$, when $\omega = \omega_0 + \frac{\Delta\omega}{2}$, $x_2 = 0$ and $x_1 = \sqrt{2D}$. Since

$$\int_0^y e^{j \frac{\pi}{2} x^2} dx = Z(y) = \int_0^y \cos \frac{\pi}{2} x^2 dx + j \int_0^y \sin \frac{\pi}{2} x^2 dx = C(y) + jS(y).$$

where $\bar{Z}(y)$ is a complex Fresnel integral, $C(y)$ and $S(y)$ are Fresnel cosine and sine integrals, respectively [25], we finally write

$$\begin{aligned} S_1(\omega) &= V_1 \sqrt{\frac{\tau_1}{8\Delta f}} \exp\left[-j \frac{(\omega_0 - \omega)^2}{2\Delta\omega} \tau_1\right] [\bar{Z}(x_1) + \bar{Z}(x_2)] = \\ &= V_1 \sqrt{\frac{\tau_1}{8\Delta f}} \exp\left[-j \frac{(\omega_0 - \omega)^2}{2\Delta\omega} \tau_1\right] [C(x_1) + C(x_2) + jS(x_1) + \\ &\quad + jS(x_2)]. \end{aligned} \quad (3.2.4)$$

Accordingly, the amplitude spectrum [62] is

$$\begin{aligned} S_1(\omega) &= V_1 \sqrt{\frac{\tau_1}{8\Delta f}} \{ [C(x_1) + C(x_2)]^2 + \\ &\quad + [S(x_1) + S(x_2)]^2 \}^{1/2} \end{aligned} \quad (3.2.5)$$

and the phase spectrum is

$$\varphi(\omega) = -\frac{(\omega_0 - \omega)^2}{2\Delta\omega} \tau_1 + \operatorname{arctg} \frac{S(x_1) + S(x_2)}{C(x_1) + C(x_2)}. \quad (3.2.6)$$

Analysis of relation (3.2.5) and consideration of the curves in Fig. 3.2.1, a show that the ChM (frequency-modulated) amplitude spectrum of the pulse becomes even more uniform as coefficient D increases in the range of the band from $\omega_0 - (\Delta\omega/2)$ to $\omega_0 + (\Delta\omega/2)$ and decreases sharply on the boundaries of this band. Thus, the signal spectrum is concentrated 103 within the indicated band with sufficiently large values of coefficient D (which are also of the greatest interest). Calculations show that almost 95% of all the signal energy is included in this band at $D = 10$ and this fraction exceeds 98% at $D = 100$ [63].

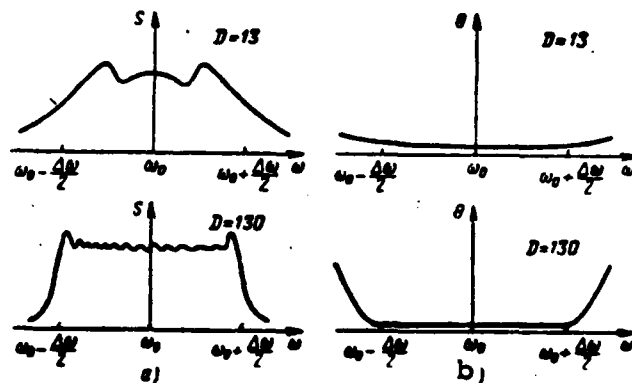


Fig. 3.2.1. FM amplitude spectrum of pulse (a) and component of its phase spectrum (b).

The second term of the phase spectrum

$$\theta(\omega) = \text{arctg} \frac{S(x_1) + S(x_2)}{C(x_1) + C(x_2)}$$

in the range of the same band is essentially constant, especially at large values of D (Fig. 3.2.1, b).

Therefore, at large values of D when

$$[C(x_1) + C(x_2)]^2 + [S(x_1) + S(x_2)]^2 \approx 2 \text{ при } |\omega - \omega_0| < \frac{\Delta\omega}{2},$$

one can assume approximately that the amplitude spectrum is directly angular:

$$\left. \begin{aligned} S_1(\omega) &\approx \frac{V_1}{2} \sqrt{\frac{\tau_1}{\Delta f}} & \text{at } |\omega - \omega_0| < \frac{\Delta\omega}{2}, \\ S_1(\omega) &\approx 0 & \text{at } |\omega - \omega_0| > \frac{\Delta\omega}{2}, \end{aligned} \right\} \quad (3.2.7)$$

and that the phase spectrum is quadratic

$$\varphi(\omega) \approx \theta_0 - \frac{(\omega_0 - \omega)^2}{2\Delta\omega} \tau_1 \quad \text{at } |\omega - \omega_0| < \frac{\Delta\omega}{2}, \quad (3.2.8)$$

where θ_0 is a constant phase angle.

3.3. Characteristics of Optimum Filter. Signal at Its Output

Substituting (3.2.4) into (1.5.1) and assuming that $C = \frac{2}{V_1} \sqrt{\frac{\Delta f}{\tau_1}}$ is constant, we find the following expression for the transfer function of an optimum filter

$$K(\omega) = \frac{1}{\sqrt{2}} [Z^*(x_1) + Z^*(x_2)] \exp j \left[\frac{(\omega_0 - \omega)^2}{2\Delta\omega} \tau_1 - \omega t_0 \right].$$

Specifically, at large value of D, according to (3.2.7) and (3.2.8),

$$\left. \begin{aligned} K(\omega) &= \exp j \left[\frac{(\omega_0 - \omega)^2}{2\Delta\omega} \tau_1 - \omega t_0 \right] & \text{at } |\omega - \omega_0| < \frac{\Delta\omega}{2}, \\ K(\omega) &= 0 & \text{at other values of } \omega. \end{aligned} \right\}$$

In this case the spectrum of the output signal is

$$\left. \begin{aligned} S_2(\omega) &= S_1(\omega) K(\omega) = \frac{V_1}{2} \sqrt{\frac{\tau_1}{\Delta f}} \exp(-j\omega t_0) & \text{at } |\omega - \omega_0| < \frac{\Delta\omega}{2}, \\ S_2(\omega) &= 0 & \text{at other values of } \omega. \end{aligned} \right\} \quad (3.3.1)$$

Accordingly, the amplitude spectra of the signal at the input and output of an optimum filter coincide at large value of D and with selection of constant C made above.

The instantaneous value of the output signal is

$$\begin{aligned} v_s(t) &= \operatorname{Re} \left\{ \frac{1}{\pi} \int_0^{\infty} \tilde{S}_s(\omega) e^{j\omega t} d\omega \right\} \cong \\ &\cong \operatorname{Re} \left\{ \frac{V_1}{2\pi} \sqrt{\frac{\tau_1}{2f}} \int_{\omega_0 - \frac{\Delta\omega}{2}}^{\omega_0 + \frac{\Delta\omega}{2}} \exp j\omega(t - t_0) d\omega \right\} = \\ &= V_1 \sqrt{D} \frac{\sin \pi \Delta f (t - t_0)}{\pi \Delta f (t - t_0)} \cos \omega_0 (t - t_0). \end{aligned} \quad (3.3.2)$$

It no longer has frequency modulation. Its complex amplitude (Fig. 3.3.1)

$$V_s(t) = V_1 \sqrt{D} \frac{\sin \pi \Delta f (t - t_0)}{\pi \Delta f (t - t_0)} \quad (3.3.3)$$

has the form of the function $\sin x/x$.

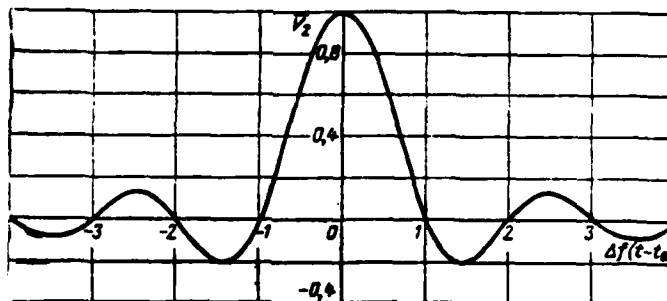


Fig. 3.3.1. Time variation of complex amplitude of output pulse.

The output pulse at the 0.637 level of the maximum value has length $\tau_2 = 1/\Delta f$. Therefore, the ratio of the pulse lengths at the input and output of an optimum filter comprises $\tau_1/\tau_2 = \Delta f \tau_1 = D$. Due to this, D is called a pulse length compression coefficient.

The output signal is symmetrical with respect to $t = t_0$ and reaches a peak value at this moment of $v_{2\text{max}} = V_1 \sqrt{D}$, which is \sqrt{D} times greater than the signal amplitude at the input.

It follows from (1.3.5) and (3.2.2) that the pulse characteristic of an optimum filter is

$$\left. \begin{aligned} h(t) &= CV_1 \cos \left[\omega_0(t-t_0) - \frac{\Delta\omega}{2\tau_1}(t-t_0)^2 \right] \\ &\quad \text{at } |t-t_0| < \frac{\tau_1}{2}, \\ h(t) &= 0 \text{ at other values of } t. \end{aligned} \right\} \quad (3.3.4)$$

and its complex amplitude is

$$\left. \begin{aligned} H(t) &= CV_1 \exp \left\{ -j \left[\frac{\Delta\omega}{2\tau_1}(t-t_0)^2 \right] + \omega_0 t_0 \right\} \\ &\quad \text{at } |t-t_0| < \frac{\tau_1}{2}, \\ H(t) &= 0 \text{ at other values of } t. \end{aligned} \right\} \quad (3.3.5)$$

Substituting this expression and also the expression for the complex amplitude of the input signal into (2.4.12)

$$\left. \begin{aligned} U_1(t) &= V_1(t) = V_1 \exp \left(j \frac{\Delta\omega}{2\tau_1} t^2 \right) \\ &\quad \text{at } |t| < \frac{\tau_1}{2}, \\ U_1(t) &= V_1(t) = 0 \text{ at other values of } t \end{aligned} \right\}$$

and taking into account that the integral function $V_1(x)\bar{H}(t-x)$ is distinct from zero in the given case only in the range $-\frac{\tau_1}{2} < x < t-t_0+\frac{\tau_1}{2}$, if $t_0-\tau_1 < t < t_0$, and in the range $t-t_0-\frac{\tau_1}{2} < x < \frac{\tau_1}{2}$, if $t_0 < t < t_0+\tau_1$, let us determine the complex amplitude of the output signal*:

$$\begin{aligned} &\text{at } |t-t_0| > \tau_1 \quad V_2(t) = 0, \\ &\text{at } t_0 - \tau_1 < t < t_0 \\ &\quad V_2(t) = \frac{CV_1^2}{2} \times \\ &\quad \times \int_{-\frac{\tau_1}{2}}^{t-t_0+\frac{\tau_1}{2}} \exp \left\{ j \left[\frac{\Delta\omega}{2\tau_1} x^2 - \frac{\Delta\omega}{2\tau_1}(t-x-t_0)^2 - \omega_0 t_0 \right] \right\} dx = \\ &\quad = \frac{CV_1^2}{2} \frac{\sin \pi \Delta f (t-t_0) \left(1 - \frac{t_0-t}{\tau_1} \right)}{\pi \Delta f (t-t_0)} e^{-j\omega_0 t_0}, \\ &\text{at } t_0 < t < t_0 + \tau_1 \\ &\quad V_2(t) = \\ &\quad = \frac{CV_1^2}{2} \int_{t-t_0-\frac{\tau_1}{2}}^{\frac{\tau_1}{2}} \exp \left\{ j \left[\frac{\Delta\omega}{2\tau_1} x^2 - \frac{\Delta\omega}{2\tau_1}(t-x-t_0)^2 - \omega_0 t_0 \right] \right\} dx = \end{aligned}$$

10

* See [64] for the effect of a pulse of arbitrary length on an LChM [linear frequency-modulated] optimum filter.

$$= \frac{CV_1^2}{2} \frac{\sin \pi \Delta f (t - t_0) \left(1 - \frac{t - t_0}{\tau_1}\right)}{\pi \Delta f (t - t_0)} e^{-j\omega_0 t}.$$

Selecting constant C the same as above, combining the two derived expressions into one and writing them in real form, we find at

$$v_s(t) = V_1 \sqrt{D} \frac{\sin \left[\pi \Delta f (t - t_0) \left(1 - \frac{|t - t_0|}{\tau_1}\right) \right]}{\pi \Delta f (t - t_0)} \times \cos \omega_0 (t - t_0). \quad (3.3.6)$$

The amplitude of the output signal

$$V_s(t) = V_1 \sqrt{D} \left| \frac{\sin \left[\pi \Delta f (t - t_0) \left(1 - \frac{|t - t_0|}{\tau_1}\right) \right]}{\pi \Delta f (t - t_0)} \right| \quad (3.3.7)$$

$$V_s(t) = 0 \quad \begin{array}{l} \text{at } |t - t_0| < \tau_1, \\ \text{at other values of } t \end{array}$$

differs somewhat from the amplitude of (3.3.3) which was found by the approximate method (we assumed that the amplitude spectrum of the input and accordingly of the output pulse is square-wave). However, if the compression coefficient is sufficiently high, this difference is very small, since in the range of the length of the main pip of the output pulse $\frac{|t - t_0|}{\tau_1} < \frac{1}{2D} \ll 1$. Because of this, (3.3.7) essentially coincides with (3.3.3) in the indicated case.

Thus, the assumption of the square-wave nature of the frequency-modulated amplitude spectrum of the pulse is rather precise with large compression factor. Therefore, one can assume that the amplitude-frequency characteristic of an optimum filter is square-wave with a high degree of accuracy:

$$\left. \begin{array}{l} K(\omega) = 1 \quad \text{at } |\omega - \omega_0| < \frac{\Delta \omega}{2}, \\ K(\omega) = 0 \quad \text{at other values of } \omega, \end{array} \right\} \quad (3.3.8)$$

and that the phase-frequency characteristic is a second-degree parabola (Fig. 3.3.2, a):

$$\varphi(\omega) = -\omega t_0 + \frac{(\omega - \omega_0)^2}{2\Delta \omega} \tau_1 - \theta_0. \quad (3.3.9)$$

Thus, an optimum filter for a linear frequency-modulated pulse consists in the first approximation of an ideal bandpass filter and one with quadratic phase-frequency characteristic.

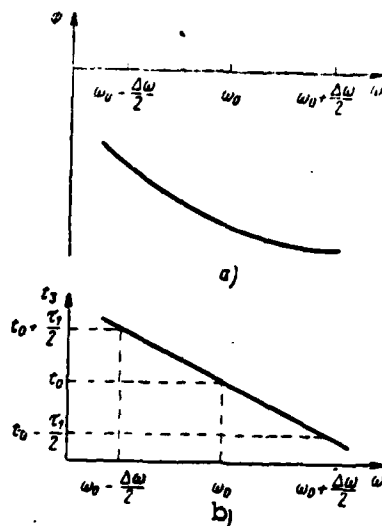


Fig. 3.3.2. Phase-frequency characteristic of optimum filter (a) and dependence of its delay time on frequency (b).

3.4. Mechanism of Signal Compression in Optimum Filter

It follows from (3.3.9) that an optimum filter delays the spectral components by the time

$$t_s = -\frac{d\phi(\omega)}{d\omega} = t_0 - \frac{\omega - \omega_0}{\Delta\omega} \tau_1, \quad (3.4.1)$$

which is a linear decreasing frequency function (Fig. 3.3.2, b). This phenomenon of the dependence of delay time on frequency is called dispersion, characteristic (3.4.1) is called the dispersion characteristic and a device with this characteristic is called a dispersion filter. 109

Let us present a clear explanation* of LChM compression of the signal in an optimum filter. At moment of time t the instantaneous signal frequency at the filter input is equal to ω . Oscillation of this frequency is fed to the filter output with delay by $t_s(\omega)$, i.e., at moment $t + t_s(\omega)$, whose value according to (3.4.1) and (3.2.1) comprises

* This explanation can be strictly substantiated by means of the steady phase method [9, 82].

$$t + t_3(\omega) = t + t_0 - \frac{\omega - \omega_0}{\Delta\omega} \tau_1 = t + t_0 - \frac{\tau_1}{\Delta\omega} \left[\left(\omega_0 + \frac{\Delta\omega}{\tau_1} t \right) - \omega_0 \right] = t_0.$$

Accordingly, all the spectrum components of the signal (regardless of their frequency value) are delayed in the optimum filter by such time that they are fed to its output simultaneously at moment t_0 . Being cosine components and having the same zero phase, they also form the peak pip of the signal as a result of arithmetic addition. The significant increase of the output signal amplitude is also explained by this [10, 87].

The circumstance that the output signal amplitude increases \sqrt{D} times can be explained in the following manner. Let us replace the linear frequency-modulated pulse (3.2.2) by a combination of N impulses having the same amplitude, less than length by a factor of N and following each other.

Let the k -th pulse (where $k = 1-N$) of this combination have frequency $f_k = f_0 - \frac{f_0}{2} + \frac{(2k-1)\Delta f}{2N}$, coinciding with the frequency of a linear frequency-modulated pulse at moment of time $t_k = -\frac{\tau_1}{2} + \frac{(2k-1)\tau_1}{2N}$.

Let us select the number of pulses such that on the one hand their spectra do not overlap and on the other hand there are no gaps in the spectrum of their combination. In this case the spectrum of the totality of pulses will essentially coincide with the spectrum of a linear frequency-modulated pulse. 11

The conditions indicated above are fulfilled if the width of the spectrum of any pulses is equal to the absolute frequency difference of the given and adjacent pulses, i.e., $\frac{1}{(\tau_1/N)} = \frac{\Delta f}{N}$, hence $N = \sqrt{\Delta f \tau_1} = \sqrt{D}$.

Thus, a linear frequency-modulated pulse is equivalent in the first approximation to the totality \sqrt{D} of unmodulated pulses of the same amplitude and total length following each other whose carrier frequencies are shifted by linear law with respect to each other. These pulses are combined in time in an optimum filter, which also leads to an increase of the output signal amplitude by a factor of \sqrt{D} equal to the number of these pulses.

Let us attempt to explain physically the process of shortening the pulse length in an optimum filter and also the shape of the output pulse.

It was already indicated above [see (3.2.7) and (3.3.1)] that the signal on both the input and output of an optimum filter has a square-wave amplitude spectrum. In other words, it is the totality of an infinitely large number of spectral components of identical intensity in the range of the band $\omega_0 - \frac{\Delta\omega}{2} < \omega < \omega_0 + \frac{\Delta\omega}{2}$ (let us assume for concreteness that the spectral density at extreme frequencies of $\omega = \omega_0 \pm \frac{\Delta\omega}{2}$ is one-half that at medium frequencies).

It was established in section 1.5 that the spectral component of any frequency of a signal at the output of an optimum filter has the phase

$$\theta(\omega) = \omega(t - t_0). \quad (3.4.2)$$

The latter approaches zero at moment t_0 of the maximum signal and increases linearly as the time from the moment of the maximum decreases and also with an increase of the frequency of this harmonic component of the signal.

Therefore, the vector diagram of the voltages at the output of an optimum filter is a "fan" of the vectors of these harmonic components (Fig. 3.4.1). These vectors (except the two outer ones) have identical amplitudes and at $t = t_0$ coincide (Fig. 3.4.1, a), forming a very large total voltage vector. As time increases, beginning at $t = t_0$, the phase of all the vectors, according to (3.4.2), will increase by linear law. 111

Assuming that the vector diagram (Fig. 3.4.1), on which only nine vectors of harmonic oscillations differing from each other in frequency by the value $k \frac{\Delta\omega}{8}$, where $k = 1-8$, is shown instead of an infinitely large number of vectors of the harmonic components of the signal according to the accepted reasons, rotates counterclockwise with mean frequency $\omega = \omega_0$, we find that the fan of vectors will unfold at $t > t_0$.

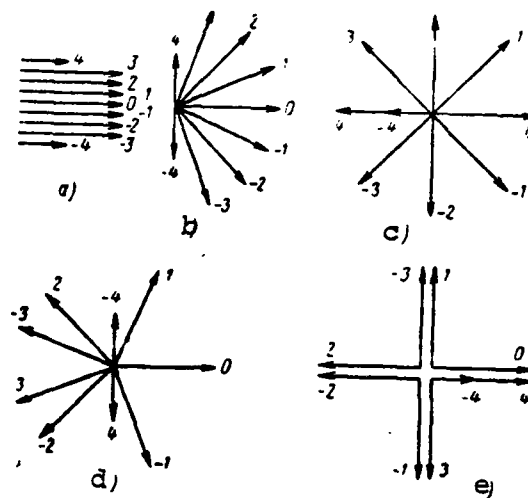


Fig. 3.4.1. Vector diagrams of voltages at optimum filter output

The vectors of the minimum $\omega_0 - \frac{\Delta\omega}{2}$ and maximum $\omega_0 + \frac{\Delta\omega}{2}$ frequencies will occupy the extreme positions and the vectors of all the other frequencies will occupy the intermediate positions.

112

The angle between the vectors of the maximum and mean frequencies comprises

$$\beta = \frac{1}{2} \Delta\omega (t - t_0),$$

while the angle between the vectors of the minimum and mean frequencies will differ from the indicated value only by sign. Since these angles are less than $\pi/2$ in absolute value, all the vectors of the harmonic components of the signal are arranged in the right half-plane. This corresponds to the time interval $t_0 < t < t_0 + \frac{1}{2\Delta f}$.

At $t = t_0 + \frac{1}{2\Delta f}$ the vectors of the extreme frequencies will be perpendicular to the vector of the mean frequency (Fig. 3.4.1, b) and at $t = t_0 + \frac{1}{\Delta f}$ they will become opposite to this vector (Fig. 3.4.1, c). In the latter case there is mutual compensation of the individual vectors of the signal components and the vector of their sum approaches zero, like the output voltage. Similar compensation of the vectors of the components will occur at moments of time $t = t_0 + \frac{2k-1}{\Delta f}$, where k is any whole number.

At moment of time $t = t_0 + \frac{2}{\Delta f}$, the incident wave of the phases of the extreme vectors will comprise 2 with respect to the mean vector since these vectors coincide (Fig. 3.4.1, e). In this case there will also be mutual compensation of the vectors of the spectral components. A similar situation will also occur at moments of time $t = t_0 + \frac{2k}{\Delta f}$, where k is any whole number, with the exception of zero.

Accordingly, at moments of time

$$t = t_0 + \frac{k}{\Delta f},$$

where, as above, k is any whole number (except zero), the output voltage approaches zero due to the mutual compensation of its spectral components.

11

There is only partial compensation of the spectral components of the signal at all other intermediate moments of time. The quadrature components of the signal will be mutually compensated for at any moment of time. The latter indicates that the instantaneous frequency of the output voltage is constant, i.e., this voltage has no angular modulation. The uncompensated spectral components of the signal will also form output voltage distinct from zero.

The vectors of the extreme frequencies change places (Fig. 3.4.1, d) at moment $t = t_0 + \frac{3}{2\Delta f}$ compared to the case of $t = t_0 + \frac{1}{2\Delta f}$ (Fig. 3.4.1, b). In this case two-thirds of the vectors will be located in the left half-plane and the remaining ones will be located in the right half-plane. The latter will be compensated by half the vectors located in the left half-plane while the uncompensated vectors will form the total output voltage vector. If its value is one-third as much and the direction is opposite to that which occurred at $t = t_0 + \frac{1}{2\Delta f}$, since a fewer number of vectors participate in its formation which remained uncompensated and they are located in the left rather than in the right half-plane. One can thus explain the polarity and decrease (compared to the case of $t = t_0 + \frac{1}{2\Delta f}$) of the amplitude of output voltage by a factor of n for moments of time $t = t_0 + \frac{2n-1}{2\Delta f}$, where n is any whole number. An ever-smaller (1/n-th) part of the spectral components of the signal is

uncompensated for as n increases, due to which the amplitude of the output signal also decreases by the indicated factor.

Thus, the nature of the output signal with complex amplitude (3.3.3) is fully determined by the uniformity of the amplitude spectrum of this signal and by the equality of the phases of its spectral components at moment $t = t_0$. If this uniformity of the amplitude spectrum or the cophasality (at $t = t_0$) its components is violated in any way, the shape of the output signal changes.

3.5. Practical Circuits of Optimum Filters

It was indicated above that a practical approximation of an optimum filter for a linear frequency-modulated pulse is combination of the ideal frequency filter with characteristic (3.3.8) and dispersion filter with characteristic (3.3.9) or (3.4.1).

It was initially suggested that a phase-compensating filter consisting of series-connected bridge quadrapoles (Fig. 3.5.1) [66] be used as the dispersion filter [65]. Their number is on the order of several hundred [12]. Therefore, this filter is a very cumbersome and unreliable device complicated to regulate and operate.

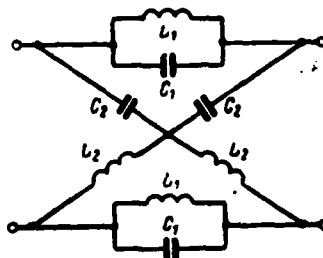


Fig. 3.5.1. Phase-compensating filter.

It was then proposed that a diagram (Fig. 3.5.2) consisting of an ordinary (nondispersion) delay line with $(N - 2)$ uniformly arranged leads, N frequency filters with bandpass of $\Delta f/N$ and uniformly biased resonance frequencies overlapping the frequency band from $f_0 - \Delta f/2$ to $f_0 + \Delta f/2$ and an adder [67], be used as a dispersion filter. As follows from section 3.4, $N = \sqrt{D}$. This diagram is used to compress linear

frequency-modulated pulses of comparatively short length, on the order of units of microseconds, and with high frequency deviation (on the order of tens and hundreds of megahertz).

1.

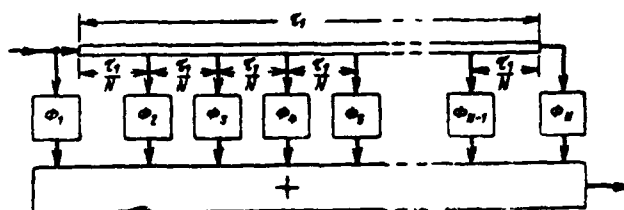


Fig. 3.5.2. Block diagram of dispersion filter on delay line with leads.

A dispersion ultrasonic delay line (DULZ; Dispersionnaya ul'trazvukovaya liniya zaderzhki) [68-70] is usually employed for optimum filtration of the most narrow band signals of greater length. It is an ultrasonic waveguide in the form of a thin flat aluminum or steel plate with electric to ultrasonic oscillation piezoconverters soldered to its ends and vice versa (Fig. 3.5.3, a). Several types of oscillations--longitudinal, transverse and so on--may propagate in this waveguide. The first longitudinal type of these oscillations has dispersion, i.e., the rate of their propagation in the waveguide is dependent on frequency [68, 70].

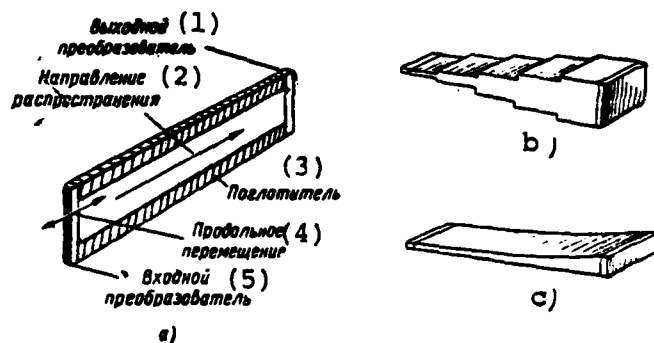


Fig. 3.5.3. Dispersion ultrasonic delay lines.
Key: (1) output converter; (2) direction of propagation; (3) absorber; (4) longitudinal motion; (5) input converter.

The typical dispersion characteristic of a DULZ operating with the first longitudinal type of oscillations is shown in Fig. 3.5.4 and has a linear segment in the frequency range (f_1, f_2) . The median frequency

1

of this segment is inversely proportional to the length d of the acoustic line: $f_0 = \alpha/d$, where for the usually employed acoustic line materials $\alpha = 2-2.2$ MHz·mm. The width of this segment (along the axis of delay time) is proportional to the length of the acoustic line l : $\Delta t_g = \beta l$, where $\beta = 1.5-3$ μ s/cm. The width of the linear segment for frequency $\Delta F = f_2 - f_1$ for a line with constant thickness comprises 10-14% of the median frequency. As an example let us point out that a steel tape 198 mm long, 12.7 mm wide and 0.076 mm thick is used in a typical DULZ with $f_0 = 30$ MHz, $\Delta F = 3$ MHz and $\Delta t_g = 33.3$ μ s [68].

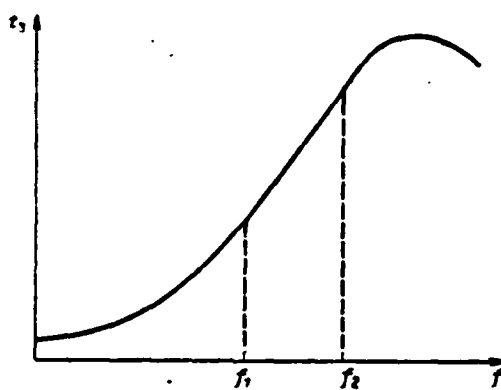


Fig. 3.5.4. Dispersion characteristic of ultrasonic dispersion delay line.

The disadvantage of the DULZ with constant thickness of the acoustic line is a comparatively small band ΔF of the linear segment of the dispersion characteristic. Its broadening by increasing the median frequency f_0 requires a decrease of the acoustic line thickness, which is fraught with great technological difficulties in manufacture (provision of the required tolerance in thickness, attachment of the transducers and so on) and also with an increase of signal attenuation in the line.

The thickness of the DULZ acoustic line is varied intermittently or smoothly in length (Fig. 3.5.3, b and c) to expand the frequency band corresponding to the linear segment of the dispersion characteristic [71]. This DULZ is equivalent to series connection of several lines, each of which has a constant thickness but different from other lines. Because of this, the median frequencies of the linear segments of the dispersion characteristics of these lines will be different.

The dispersion characteristic of a line with variable thickness, equal to the sum of the dispersion characteristics of the components of the line, has a linear segment broad in frequency. Its width is $\Delta F = (0.3-0.5) f_0$. In this case deviations from linearity are less than $\pm 1.5\%$ on this segment.*

The compression coefficient of this DULZ cannot be more than 300-500 due to the increase of nonlinearity of the dispersion characteristic, which is determined by the inaccuracy of calculation and manufacture of the line profile.

Dispersion filters based on parallel connection of two or more DULZ that provide less compression, with heterodyning of individual segments of the signal spectrum (Fig. 3.5.5), are used to achieve greater compression [72].

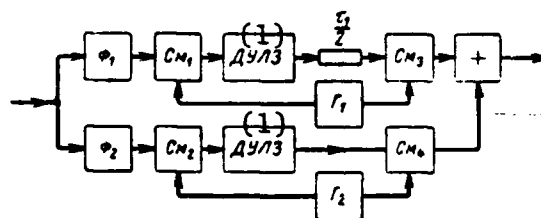


Fig. 3.5.5. Dispersion filter with two ultrasonic dispersion delay lines and heterodyning. (1) - DULZ

A linear frequency-modulated pulse with length τ_1 , frequency deviation Δf and median frequency f_0 , acting on the input of this circuit, is separated in frequency by filters F_1 and F_2 whose bandpasses are arranged from $f_0 - \Delta f/2$ to f_0 and from f_0 to $f_0 + \Delta f/2$, respectively. In this case a linear frequency-modulated pulse with length $\tau_1/2$, frequency deviation $\Delta f/2$ and median frequency $f_0 - \Delta f/4$ is formed at the output of F_1 . The pulse at the output of F_2 differs only by the median frequency, which is equal to $f_0 + \Delta f/2$ and by the additional delay by time $\tau_1/2$.

11

* Diffraction delay lines also have good dispersion characteristics [86].

Since heterodyne frequencies f_1 and f_2 are equal to $f_0 - F_0 - \frac{\Delta f}{4}$ and $f_0 - F_0 + \frac{\Delta f}{4}$, respectively, and since only the difference frequencies are separated at the output of mixers Cm_1 and Cm_2 , the pulse spectra are heterodyned to the band of the linear section of the DULZ dispersion characteristic from $F_0 - \frac{\Delta f}{4}$ to $F_0 + \frac{\Delta f}{4}$. As a result of passing through these DULZ, the pulses are compressed to length of $2/\Delta f$, i.e., $\Delta f \tau_1/4$ times. They are then shifted in time by the delay line by $\tau_1/2$ and are fed to mixers Cm_3 and Cm_4 , controlled by the same heterodyne oscillations. The sum frequencies have already been separated at the output of these mixers, due to which the initial spectra are restored and random initial phases of heterodyne oscillations are eliminated. In this case two compressed pulses of length $2/\Delta f$ and frequencies equal to $f_0 - \Delta f/4$ and $f_0 + \Delta f/4$, respectively, are formed.

Being added in the adder, these pulses form a double amplitude pulse of one-half the length with the correct phase relations. The phase relations between the added pulses required for this are achieved by slight tuning of the frequency of one of the heterodynes. It is easy to make the latter automatic. Use of this FAPCh (automatic phase frequency control) considerably increases the operating stability of the circuit.

To achieve a very large compression coefficient D of a linear frequency-modulated pulse using DULZ that permit pulses to be compressed only D_1 times, one should use N parallel channels and 119

$$N = E\left(\sqrt{\frac{D}{D_1}}\right) + 1 \approx \sqrt{\frac{D}{D_1}}.$$

A compression coefficient up to 10^5 can be achieved in this circuit [72].

Besides the passive methods of optimum processing of LChM pulses considered above, the active method using a multichannel correlator, which is a circuit with a mixer controlled by a long LChM heterodyne pulse and with separation of signals at the mixer output, distinguished by time position using frequency filters [73]. The disadvantage of this circuit, caused by its multichannel nature, includes the complexity and cumbersomeness of the apparatus.

3.6. Attenuation of Side Pips of the Output Pulse

The signal envelope at the output of an optimum filter (Fig. 3.3.1) has, along with a large main (central) pip, other weaker, but still sufficiently intensive side pips. This is the consequence of the square-wave nature of the amplitude spectrum of the output signal (see section 3.4).

To improve the shape of the envelope of this signal by attenuation of its side pips, one can use a filter with smooth but sharply decreasing amplitude-frequency characteristic instead of an ideal filter. An example of this characteristic may be a bell-shaped characteristic:

$$K(\omega) = e^{-a(\omega - \omega_0)^2},$$

where

$$a = \frac{0.0351}{\Delta F^2},$$

and ΔF is the filter bandpass at the $1/\sqrt{2}$ level.

As a result of passage by FM signal (3.2.2) through a device with quadratic phase-frequency characteristic (3.3.9) and bell filter, the signal will have the spectrum

12

$$S_2(\omega) = e^{j \left[-\omega t_0 + \frac{(\omega - \omega_0)^2}{2\Delta\omega} \tau_1 - \theta_0 \right]} e^{-a(\omega - \omega_0)^2} V_1 \times \\ \times \int_{-\tau_1/2}^{\tau_1/2} e^{j \left[(\omega_0 - \omega) y + \frac{\Delta\omega}{2\tau_1} y^2 \right]} dy$$

and the instantaneous value

$$v_2(t) = \frac{V_1}{2\pi} \int_{-\infty}^{+\infty} \exp \left\{ -a(\omega - \omega_0)^2 + j \left[\omega(t - t_0) + \right. \right. \\ \left. \left. + \frac{(\omega - \omega_0)^2}{2\Delta\omega} \tau_1 - \theta_0 \right] \right\} d\omega \int_{-\tau_1/2}^{\tau_1/2} \exp j \left[(\omega_0 - \omega) y + \frac{\Delta\omega}{2\tau_1} y^2 \right] dy.$$

Changing the order of integration and carrying out the calculations, we find

$$v_2(t) = 0.754 V_1 n \sqrt{B} \left\{ \Phi \left[\frac{1}{2} \sqrt{\frac{n}{c}} (1 - j4.54 n^2 \Delta f (t - t_0)) \right] + \right. \\ \left. + \Phi \left[\frac{1}{2} \sqrt{\frac{n}{c}} (1 - j4.54 n^2 \Delta f (t - t_0)) \right] \right\} \times \\ \times \exp \left\{ -7.14 n^2 \Delta f^2 (t - t_0)^2 + j \left[2\pi f_0 (t - t_0) + \frac{\pi}{4} - \theta_0 \right] \right\},$$

where $n = \Delta F / \Delta f$ is the ratio of the filter bandpass to frequency

deviation, $\Phi(z)$ is the probability integral of the complex variable [25] and

$$c = 2,27n^2 + jD^{-1} \approx 2,27n^2,$$

since D is on the order of hundreds and n is on the order of 0.5.

Accordingly, the signal at the output has the complex amplitude

$$V_s(t) \approx 0,754V_1 n \sqrt{D} \left\{ \Phi \left[\frac{0,588}{n} - j2,67n\Delta f(t-t_0) \right] + \right. \\ \left. + \Phi \left[\frac{0,588}{n} + j2,67n\Delta f(t-t_0) \right] \right\} \exp[-7,14n^2\Delta f^2(t-t_0)^2],$$

which at $t = t_0$ assumes the maximum value

12

$$V_{s,max} = 1,508n \sqrt{D} \Phi \left(\frac{0,588}{n} \right) V_1.$$

The expression for the complex amplitude of the output signal is easily converted to the form

$$V_s(t) = 1,508V_1 n \sqrt{D} \{1 - \operatorname{Re} [e^{z^2} \omega(z)]\} e^{-7,14n^2\Delta f^2(t-t_0)^2},$$

where

$$z = 2,67n\Delta f(t-t_0) + j \frac{0,588}{n};$$

$$\omega(z) = e^{-z^2} \left(1 + \frac{2j}{\sqrt{\pi}} \int_0^z e^{t^2} dt \right)$$

is the tabulated function of the complex independent variable [74].

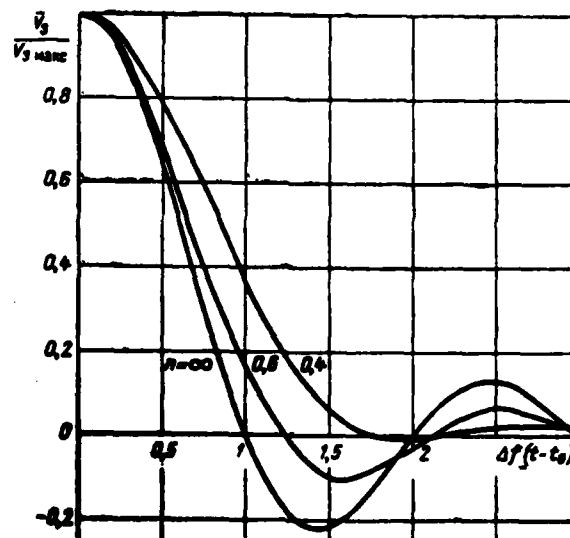


Fig. 3.6.1. Time variation of complex amplitude of output pulse.

Consideration of the shape of the output signal envelope (Fig. 3.6.1) shows that the level of side pips decreases appreciably as the bandpass of the bell filter is constricted. Thus, the relative value of the first side pip decreases more than one-half even at $n = 0.6$ compared to the pulse at the output of an optimum filter (which essentially coincides with a pulse at $n = \infty$). At $n = 0.4$ the value of the first side pip decreases by a factor of 38 and that of the second (which is greater than the first in this case) decreases by a factor of 5.8. 122

Attenuation of the side pips is accompanied by an increase of the length of the main pip. However, this increase is comparatively small and comprises 8 and 26%, respectively, in the cases indicated above (at a pulse length readout level equal to $1/\sqrt{2}$).

Moreover, constriction of the filter bandpass also leads to variation of both the peak signal value and the noise at the output and accordingly to variation of the signal/noise ratio.

Since the output noise has output

$$\sigma_3^2 = \frac{a}{\pi} \int_0^{\infty} e^{-2a(a-\omega)^2} d\omega \approx \frac{a}{\sqrt{2\pi a}} = 2.13a\Delta f,$$

then the following signal/noise ratio is observed at the output

$$q_3^2 = \frac{V_{3\text{max}}^2}{\sigma_3^2} = 1.065n \frac{V_{11}^2}{a} \Phi^2\left(\frac{0.588}{n}\right).$$

Accordingly, the power loss in the signal/noise ratio compared to an optimum filter comprises

$$G = \frac{0.4697}{n\Phi^2\left(\frac{0.588}{n}\right)} \quad (3.6.1)$$

The minimum value of this loss is observed at $n = 0.62$ and is equal to only 12%. If the filter bandpass varies from $0.38 \Delta f$ to $0.96 \Delta f$, the value of this loss does not exceed 30% (Fig. 3.6.2).

Thus, replacement of an ideal filter with a bell filter having bandpass on the order of $(0.4-0.5) \Delta f$ permits one to considerably reduce the level of the side pips with comparatively slight expansion of the main pip and essentially indiscernible decrease of signal/noise ratio. 12

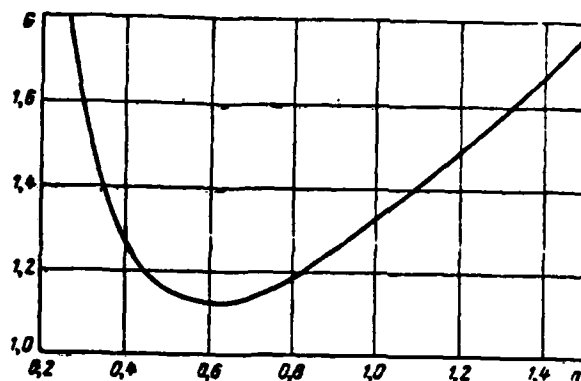


Fig. 3.6.2. Dependence of loss on ratio of filter bandpass to frequency deviation.

Greater attenuation of the side pips of the output signal can be achieved by means of special weight processing. It is based on the use of results obtained when solving a similar problem of greater attenuation of the side lobes of the antenna radiation pattern with minimum expansion of the main lobe by the Dolf-Chebyshev method [67, 75]. Specifically, truncated pulse bandpass (3.3.2) yields very good results through a filter with the transfer function

$$K(\omega) = 1 + 2 \sum_{k=1}^N \mu_k \cos \frac{\pi}{2f} (\omega - \omega_0) = \sum_{k=-N}^N \mu_k e^{j \frac{k(\omega - \omega_0)}{\Delta f}}, \quad (3.6.2)$$

where N is a whole number that determines the accuracy of approximation of the best Dolf-Chebyshev filter to the given filter (the accuracy of approximation increases with an increase);

12

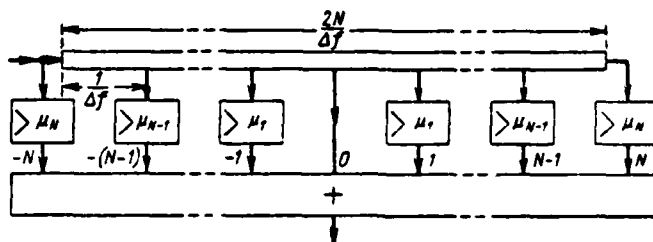
$$\mu_0 = 1; \mu_k = \mu_{-k} = \frac{0.5(-1)^{k+1}}{\prod_{n=1}^N \left(1 - \frac{k^2}{n^2}\right)} \times \prod_{n=1}^N \left[1 - \left(\frac{k}{N+1}\right)^2 \frac{A^2 + \left(N + \frac{1}{2}\right)^2}{A^2 + \left(n - \frac{1}{2}\right)^2} \right],$$

at $k = 1-N$ (the product $\prod_{n=1}^N$ does not contain any term with $n = k$);

$$A = \frac{1}{\pi} \operatorname{arch} \frac{1}{\gamma};$$

and γ is the ratio of the value of the first side lobe, which is the largest of the side lobes, to the value of the main pip.

Since the transfer function $\mu_k e^{i \frac{k\omega}{\Delta f}}$ is realized by combining a device with transfer coefficient μ_k and a delay device by time $k/\Delta f$, then if the median signal frequency f_0 is a multiple of frequency deviation Δf , weight processing (3.6.2) is accomplished by a system of a delay device by time $2N/\Delta f$ with $2N - 1$ uniformly arranged leads and an adder with weights μ_k of the voltages taken from these leads and also from the input and output of the delay device (Fig. 3.6.3).



125

Fig. 3.6.3. Block diagram of weight processing device.

The pulse achieved as a result of this weight processing has the following length at the $1/\sqrt{2}$ level

124

$$\tau_3 = \frac{2(N+1)}{\Delta f} \left[\frac{\left(\operatorname{arch} \frac{1}{\gamma} \right)^2 - \left(\operatorname{arch} \frac{1}{\sqrt{2}\gamma} \right)^2}{\left(\operatorname{arch} \frac{1}{\gamma} \right)^2 + \pi^2 \left(N + \frac{1}{2} \right)^2} \right]^{1/2}.$$

The mechanism of weight processing of a truncated signal is illustrated by the time diagrams shown in Fig. 3.6.4, a, where the simplest case is taken: $N = 1$ and $\mu_1 = 0.4$. The shape of the output pulse achieved as a result of quasi-optimum weight processing by law (3.6.2) at $\gamma = 0.01$ and $N = 5$ is shown in Fig. 3.6.4, b.

126

Weight processing of a pulse shortened in an optimum filter worsens the signal/noise ratio. However, this deterioration is comparatively small and at $\gamma \geq 0.01$ does not exceed 30% of power [63]. The weight processing device should be made from sufficiently stable components and requires very careful adjustment.

More detailed methods of side pip attenuation are considered in [76].

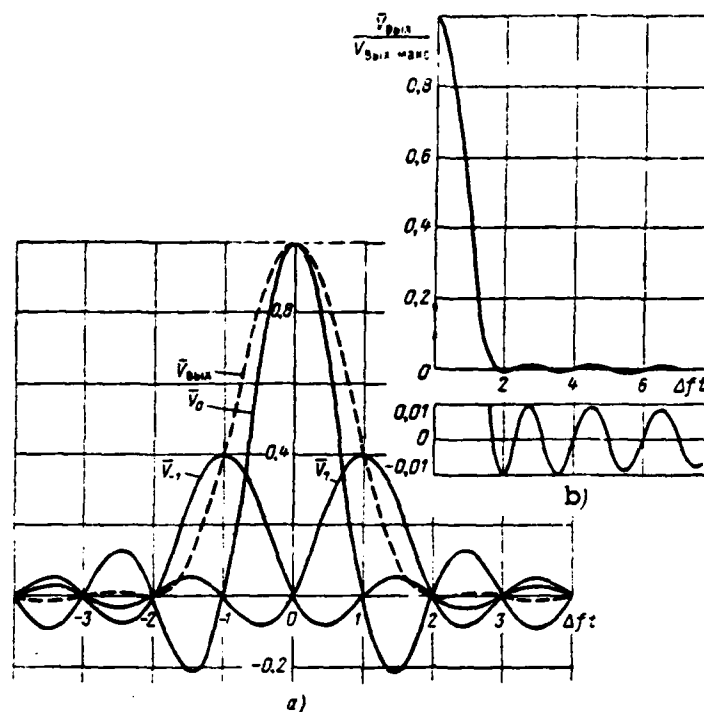


Fig. 3.6.4. Time variation of complex signal amplitudes during weight processing

3.7. Phase Distortions of Signal and Compensation of Their Even Components

The effect of both determined and random phase and amplitude distortions of the signal on the nature of the signal at the optimum filter output was considered in detail in section 2.4. This consideration was carried out in general form and therefore its results are also valid in the case of an LChM signal [77-80]. It is important only to note that in this case the signal is very wideband and therefore the difference of the phase variations of its extreme spectral components during the pulse duration comprises a very large value $-2\pi\Delta f\tau_1 = 2\pi D$. Phase distortions of no more than $1/2$ rad are permissible, which correspond to a relative error of no more than $1/4\pi D$. This is a very rigid requirement and one very difficult to fulfill.

With regard to the extremely harmful effect of phase distortions, let us consider one of the systems of [81] (Fig. 3.7.1) in which even phase distortions are compensated.

Optimum filtration of a wideband radio signal can be regarded as compensation of phase predistortions intentionally introduced into the signal during its shaping. Let a signal be shaped by feeding a single (practically rather short) pulse to the input of a dispersion filter (DF; *dispersionnyy fil'tr*) with transfer function 127

$$\left. \begin{aligned} K(\omega) &= K_0 \exp j\psi(\omega) \text{ at } \omega_1 < \omega < \omega_2, \\ K(\omega) &= 0 \text{ on other frequencies.} \end{aligned} \right\} \quad (3.7.1)$$

where K_0 is a constant and $\psi(\omega)$ is the nonlinear phase-frequency characteristic. It can differ somewhat from the quadratic characteristic (3.3.9). Since a single pulse is the sum of an infinitely large number of harmonic components of any frequencies, then all the harmonic components lying in its bandpass are fed to the filter output. But they are fed with delay by time

$$t_s(\omega) = -\frac{d\psi(\omega)}{d\omega},$$

which, in view of the nonlinearity of $\psi(\omega)$, is different for different frequencies. Therefore, the voltage at the filter output will have a frequency whose value is different for different moments of time, i.e., it will be modulated in frequency and accordingly in phase. Specifically, if the phase-frequency characteristic is quadratic [see (3.3.9)] and if the dispersion frequency is linear [see (3.4.1)], the output voltage frequency will vary by linear law.

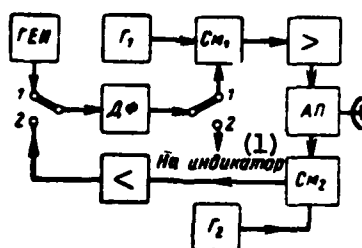


Fig. 3.7.1. System for generation and optimum filtration of frequency-modulated signal (ГЕН--single pulse generator; АП--antenna switch; 1--transmission; 2--reception.
Key: (1) to display.

The process of angular modulation being formed during shaping of the signal can be interpreted as inversion of the phase of the harmonic frequency component ω by angle $\psi(\omega)$. 128

Let us feed the signal shaped in this manner to mixer Cm_1 controlled by heterodyne oscillation Γ_1

$$v_3(t) = V_3 \cos(\omega_3 t + \alpha).$$

The following component will be formed at its output from the harmonic frequency component ω

$$v_4(t) = V_4 \cos[(\omega + \omega_3)t + \alpha + \psi(\omega)].$$

After the corresponding amplification, the signal is emitted in the form of the sum of these components (where $\omega_1 < \omega < \omega_2$) as a probing signal, is reflected from the target (which we shall assume is fixed to simplify the analysis) and is fed to the input of the receiver, where it is amplified and fed to mixer Cm_2 , controlled by heterodyne oscillation Γ_2 :

$$v_5(t) = V_5 \cos(\omega_5 t + \beta).$$

If the time delay and phase variation of the reflected signal are disregarded, the signal component considered above will create the following oscillation at the output of this mixer

$$\begin{aligned} v_6(t) &= 2V_4 \cos[(\omega_3 + \omega)t + \psi(\omega) + \alpha] \cos(\omega_5 t + \beta) = \\ &= V_4 \cos[(\omega_3 - \omega_5 - \omega)t - \psi(\omega) - \alpha + \beta] + \\ &+ V_4 \cos[(\omega_3 + \omega_5 + \omega)t + \psi(\omega) + \alpha + \beta]. \end{aligned}$$

Unlike the first mixer, a difference frequency is generated in the second mixer and the heterodyne frequencies are selected so that $\omega_5 - \omega_3 = 2\omega_0$, where

$$\omega_0 = \frac{\omega_1 + \omega_2}{2}$$

is the median frequency of the probing signal (and of the filter). Then

$$v_6(t) = V_4 \cos[(2\omega_0 - \omega)t - \psi(\omega) - \alpha + \beta].$$

Having fed this oscillation to a filter with transfer function (3.7.1), we find at its output at $\omega_1 < \omega < \omega_2$

$$v_7(t) = k V_4 \cos[(2\omega_0 - \omega)t - \psi(\omega) + \psi(2\omega_0 - \omega) - \alpha + \beta].$$

In view of the linearity of the considered system, consisting of a filter, frequency mixers and amplifiers, all the harmonic components pass

quite independently through the output. Their sum is also the output signal.

According to (1.5.3), this signal will be processed in an optimum manner provided that the phase shifts are compensated when

$$\psi(2\omega_0 - \omega) - \psi(\omega) - \alpha + \beta = \omega t_0 + \gamma,$$

where γ and t_0 are the constant phase shift and signal delay, respectively.

Since the linear and constant terms of the phase-frequency characteristic in this equation can always be compensated for by appropriate selection of the constants, let us rewrite it in the following form:

$$\begin{aligned} \text{or} \quad \psi_1(2\omega_0 - \omega) &= \psi_1(\omega) & \text{at } \omega_1 < \omega < \omega_2, \\ \psi_1(\omega_0 - \Omega) &= \psi_1(\omega_0 + \Omega) & \text{at } \omega_1 - \omega_0 < \Omega < \omega_2 - \omega_0, \end{aligned} \quad (3.7.2)$$

where $\psi_1(\omega)$ is the phase-frequency characteristic of the filter with eliminated linear and constant terms.

It follows from the latter equation that the effect of phase distortions is absent if phase-frequency characteristic (3.7.2) of the shaping and processing filters is even with respect to the median frequency.

In the special case of linear frequency modulation which is formed if the phase-frequency characteristic of the shaping filter has the form of (3.3.9), i.e.,

$$\psi_1(\omega) = \frac{(\omega - \omega_0)^2}{2\Delta\omega} \tau_1,$$

and condition (3.7.2) of the absence of phase distortions is fulfilled.

If the harmonic component is superimposed on the quadratic phase-frequency characteristic of the filter

$$\psi_1(\omega) = \pm \frac{(\omega - \omega_0)^2}{2\Delta\omega} \tau_1 + c \sin(\omega T + s) \quad \text{at } \omega_1 < \omega < \omega_2,$$

where c and T are constants, then the phase distortions will be compensated according to (3.7.2) provided that

$$\begin{aligned}\psi_1(2\omega_0 - \omega) - \psi_1(\omega) &= c \sin[(2\omega_0 - \omega)T + \varepsilon] - \\ &- c \sin(\omega T + \varepsilon) = 2c \cos(\omega_0 T + \varepsilon) \sin(\omega_0 - \omega)T = 0,\end{aligned}$$

hence it follows that $\omega_0 T + \varepsilon = \pm \left(k + \frac{1}{2}\right)\pi$, where k is any whole number. 130

Accordingly, any even distortions of the phase-frequency characteristic and specifically distortions of type

$$\Delta\psi_1(\omega) = \sum c_i \cos(\omega - \omega_i) T_i \quad \text{at } \omega_1 < \omega < \omega_2,$$

where c_i and T_i may assume any values, are completely compensated for in the considered system.

One can arrive at similar results by considering the problem of compensation of phase distortion by the time method. Using the steady phase method [9, 82], one can show that the shaping filter with transfer function (3.7.1) is optimum for a signal reflected from a fixed target and subject to double frequency conversion only in the case when a signal whose phase modulation law is even with respect to the moment of time corresponding to the middle of the signal pulse and accordingly the frequency modulation law is odd, is formed during shaping.

In other words, even distortions of the signal phase-modulation law (and odd distortions of the signal frequency-modulation law) are totally mutually compensated during shaping of it and processing in the considered system.

Thus, the main task in designing a signal shaping and processing system is not to eliminate phase distortions but to eliminate their odd components, which can be done rather simply.

3.8. Effect of Detuning Linear Frequency-Modulated Signal on Output Signal

If, unlike the case considered in section 3.3, a signal mixed in frequency by the value $\Omega = 2\pi F$ is fed to the input of an optimum filter

$$\begin{aligned}v_1(t) &= V_1 \cos \left[(\omega_0 + \Omega)t + \frac{\Delta\omega}{2\pi} t^2 \right] \quad \text{at } |t| < \frac{t_1}{2}, \\ v_1(t) &= 0 \quad \text{at other values of } t.\end{aligned}$$

then, having made similar transformations, we find at $|t-t_0| < \tau_1$

13.

$$v_s(t) = V_s(t) \cos \left[2\pi \left(f_0 + \frac{F}{2} \right) (t - t_0) \right],$$

where

$$V_s(t) = V_1 \sqrt{D} \frac{\sin \left\{ \pi [\Delta f (t - t_0) + F \tau_1] \left(1 - \frac{|t - t_0|}{\tau_1} \right) \right\}}{\pi [\Delta f (t - t_0) + F \tau_1]}. \quad (3.8.1)$$

This amplitude reaches a maximum at moment of time t_m (Fig. 3.8.1) in which the denominator of the latter expression approaches zero, i.e.,

$$t_m = t_0 - \frac{F}{\Delta f} \tau_1. \quad (3.8.2)$$

This expression can also be found directly from formula (3.4.1) if $\omega = \omega_0 + 2\pi F$ is substituted into it.

The maximum amplitude of the output signal is

$$V_{sm} = V_s(t_m) = V_1 \sqrt{D} \left(1 - \frac{|F|}{\Delta f} \right) \text{ at } |F| < \Delta f \quad (3.8.3)$$

and is reduced by linear law with an increase of the absolute value of detuning to Δf . At $|F| \geq \Delta f$, the output signal is approximately equal to zero. This is explained by the fact that the main part of the input signal spectrum is located outside the bandpass of the optimum filter.

If the input linear frequency-modulated signal is detuned with respect to the median frequency, the optimum filter shifts the spectrum of this signal with respect to the filter bandpass, which causes constriction of the output signal spectrum. If the output signal spectrum and the amplitude-frequency characteristic of the filter are regarded as square-wave, then the width of the signal spectrum at the filter output comprises $\Delta f - |F|$ at $|F| < \Delta f$.

This constriction of the output signal spectrum also causes both the decrease of the maximum output signal indicated above and expansion of its length* (Fig. 3.8.1).

* In order that frequency detuning not cause an increase in the length of the output pulse, linear frequency modulation is replaced by logarithmic phase modulation [72].

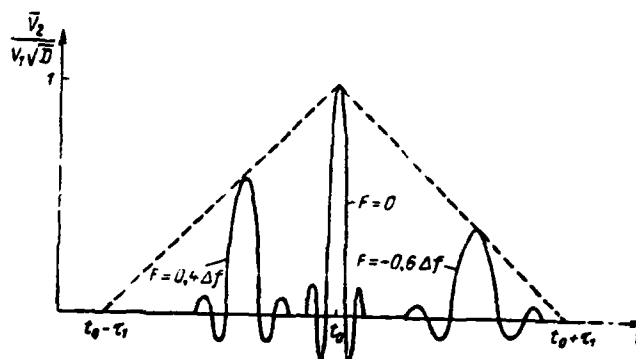


Fig. 3.8.1. Effect of detuning on shape and position of output pulse.

Using (3.8.1), it is easy to show that the length τ_2 of the output signal (at the 0.637 level) satisfies the quadratic equation

$$\tau_2^2 + \tau_1 \left(1 - \frac{|F|}{\Delta f}\right) \tau_2 - \frac{\tau_1}{\Delta f} = 0,$$

solution of which has the form

$$\tau_2 = \frac{\tau_1 (\Delta f - |F|)}{2\Delta f} \left\{ \left[1 + \frac{4\Delta f}{\tau_1 (\Delta f - |F|)^2} \right]^{1/2} - 1 \right\}. \quad (3.8.4)$$

With comparatively slight detuning when the following condition is fulfilled

$$|F| < (1 - 2D^{-1/2}) \Delta f,$$

formula (3.8.4) is simplified:

$$\tau_2 \approx \frac{1}{\Delta f - |F|}. \quad (3.8.5)$$

This expression is also easily found directly from the width of the output signal spectrum.

Calculations show that formula (3.8.5) yields an error of 3.3, 5.9, 9.3 and 17.2%, respectively, ^{when $D=100$ and} at relative detuning $|F|/\Delta f$ equal to 0.5, 0.6, 0.7 and 0.8, respectively.

If frequency detuning is caused by the Doppler effect:

13:

$$F = F_d = \frac{2v_r}{\lambda_0},$$

where λ_0 is the mean wave length and v_r is the radio velocity, then since the velocity and consequently the Doppler shift of frequency are

previously unknown, according to (3.8.2), the so-called velocity error of determining the delay time of the reflected signal appears

$$\Delta t = -\frac{F}{\Delta f} \tau_1 = -\frac{2v\tau_1}{\Delta f \lambda_0},$$

which leads to the range measurement error

$$\Delta r = \frac{c\Delta t}{2} = -\frac{cv\tau_1}{\Delta f \lambda_0}.$$

The target covers this range segment during the time

$$\nabla t = \frac{\Delta r}{v} = -\frac{\tau_1}{\Delta f}.$$

Accordingly, a range finder with linear frequency-modulated signal measures the range to the target at the following moment of time rather than the moment t_{00n} of the end of irradiation of the target by the signal pulse

$$t_{\text{new}} = t_{00n} + \nabla t = t_{00n} - \frac{\tau_1}{\Delta f}. \quad (3.8.6)$$

Thus, the extent of the time shift of the moment of range measurement is determined only by the parameters of the range finder and is totally independent of the speed of the target. Therefore, motion of the target does not lead to any error in determination of the target [10, 83].

3.9. Achieving High Accuracy and Resolution in Range and Speed

To estimate the accuracy and resolution of a system in range and speed, (i.e., the time position t and frequency F), the joint correlation function of modulation of the signal being used in it is usually analyzed [10-16, 32, 84, 85]

$$\begin{aligned} \bar{V}(t, F) &= \int_{-\infty}^{+\infty} \bar{V}(x) \bar{V}^*(x-t) e^{j2\pi Fx} dx = \\ &= \int_{-\infty}^{+\infty} \bar{S}^*(2\pi f) \bar{S}[2\pi(f-F)] e^{j2\pi ft} df, \end{aligned}$$

where $\bar{S}(\omega)$ is the frequency spectrum of the complex signal amplitude $\bar{V}(t)$.

Since $\bar{S}^*(2\pi f)$ is the transfer function of a filter optimum to the signal $\bar{V}(t)$, $\bar{S}[2\pi(f-F)]$ is the modulation spectrum of the signal

shifted in frequency by F and their product is the spectrum of the optimum filter response to the frequency-shifted signal, then the joint correlation function, being a Fourier transform of this product, is also the indicated response. This function is a generalization of the concept of a correlation function for the case of two variables t and F .

The normalized joint correlation function of modulation is usually employed

$$\Psi_0(t, F) = \frac{1}{2E} \int_{-\infty}^{+\infty} V(x) V^*(x-t) e^{j2\pi Fx} dx,$$

where

$$E = \frac{1}{2} \Psi(0, 0) = \frac{1}{2} \int_{-\infty}^{+\infty} V(x) V^*(x) dx$$

is the signal energy.

This function shows the relative value of the optimum filter response to a signal shifted in time by t and in frequency by F with respect to a signal optimum to this filter. In other words, it characterizes the degree of distinction of the filter responses to the two signals indicated above.

In the case considered above, linear frequency modulation is

$$V(t) = V_1 e^{j\pi \frac{\Delta f}{\tau_1} t^2} \cdot 1\left(\frac{\tau_1}{2} - |t|\right),$$

due to which after calculations we find

$$|\Psi_0(t, F)| = \left| \frac{\sin \left[\pi \left(D \frac{t}{\tau_1} + F \tau_1 \right) \left(1 - \frac{|t|}{\tau_1} \right) \right]}{\pi \left(D \frac{t}{\tau_1} + F \tau_1 \right)} \right| \cdot 1(\tau_1 - |t|). \quad (3.9.1)$$

The range of values of variables t and F in which $\frac{1}{2} < |\Psi_0(t, F)| < 1$ is naturally called the range of high correlation of signals. Two signals mutually shifted in time by t and in frequency by F , which correspond in the plane of variables t, F to points lying within this region, cannot be separately identified. 13

Since accurate measurement of the parameters of the received signal t and F within the range of high correlation is essentially

impossible in the presence of noise, it is sometimes called the region of ambiguity. The smaller this region, the higher the accuracy of measuring the indicated parameters.

To eliminate the ambiguity of measuring the parameters, it is necessary that the region of high correlation be unique. This requirement is essentially fulfilled in the case of a periodic or quasi-periodic signal. Therefore, one must satisfy the requirements so that different regions of high correlation be sufficiently separated from each other.

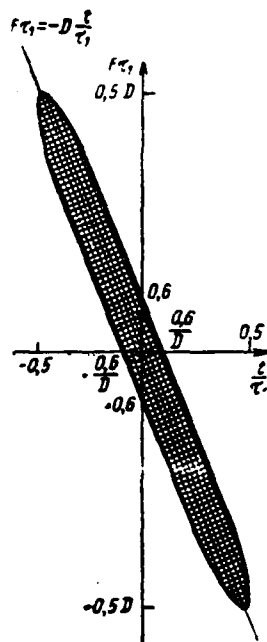


Fig. 3.9.1. Region of high correlation of linear frequency-modulated pulse.

A region of high correlation of signals with linear frequency-modulation (Fig. 3.9.1) is strongly extended in the direction of straight line $F\tau_1 = -D \frac{\xi}{\tau}$ and has width on the order of $\frac{1.2}{D}$ and length on the order of D . Its area is on the order of unity and is independent of the compression coefficient. Consideration of this region shows that the time (range) resolution is determined by the value

136

$$\Delta t = \frac{1.2}{\Delta f}, \quad (3.9.2)$$

inversely proportional to frequency deviation and accordingly to the width of the signal spectrum.

If there is no time shift between signals ($t = 0$)

$$\Psi_0(0, F) = \frac{\sin \pi F \tau_1}{\pi F \tau_1}. \quad (3.9.3)$$

The latter, like (3.9.1), has the form of function $\sin x/x$. Since (3.9.3) lies in the range of 0.5-1 at $|F\tau_1| < 0.6$, the frequency (velocity) resolution of the system is then characterized by the value

$$\Delta F = \frac{1.2}{\tau_1}, \quad (3.9.4)$$

inversely proportional to the length of the pulse signal.

These results, found for the special case, are rather general and are qualitatively valid for signals of different shape as well.

Let us explain the latter result physically. The capability of a system to distinguish two signals in frequency is determined by the time of analyzing these signals, which cannot be greater than their length. The greater the length of the signals being analyzed, the greater the difference their output effects is in the form of a different incident wave of phases. Therefore, the frequency resolution is determined by the length of the signals being used.

Having assumed in (3.9.1) that $\Delta f = 0$, we find the modulus of normalized correlation function of an unmodulated pulse of length τ :

$$|\Psi_0(t, F)| = \left| \frac{\sin \pi F \tau \left(1 - \frac{|t|}{\tau}\right)}{\pi F \tau} \right| \cdot 1(\tau - |t|). \quad (3.9.5)$$

At $t = 0$ we again find (3.9.3), hence it follows that the frequency resolution is characterized by the value of (3.9.4). At $F = 0$, we find the correlation function of the envelope of this signal

$$\Psi_0(t, 0) = \left(1 - \frac{|t|}{\tau}\right) 1(\tau - |t|),$$

which is a triangular function. Therefore, the time resolution comprises

137

$$\Delta t \approx \tau. \quad (3.9.6)$$

Since the width of the signal spectrum under consideration has the order $1/\tau$, it is easy to conclude that (3.9.2) and (3.9.6) are special cases of a more general formula

$$\Delta t \approx \frac{1}{\Pi}, \quad (3.9.7)$$

which is in complete agreement with the physical concepts outlined at the end of section 3.1. Comparing the region of high correlation of an unmodulated pulse (Fig. 3.9.2) to a similar region for a linear frequency-modulated pulse (Fig. 3.9.1), we note that the latter is strongly lengthened and rotated counterclockwise by an angle whose cotangent is equal to the compression coefficient. Its area also has an order of unity.

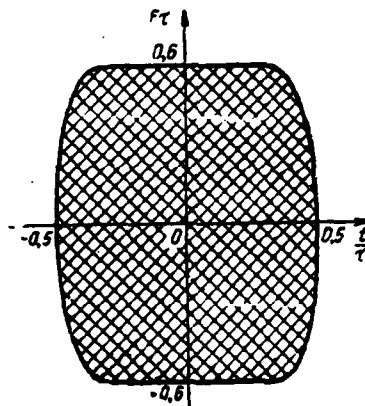


Fig. 3.9.2. Region of high correlation of unmodulated pulse.

To achieve high range and velocity resolution, one must use the shapes of signals whose normalized joint correlation function of modulation meets two requirements: 1) it is close to unity only in the small vicinity of point $t = F = 0$ and 2) the modulus of this function is considerably less than unity in all other regions of the plane t, F .

138

Unfortunately, it is impossible to achieve simultaneous concentration of the region of high correlation in the infinitely small vicinity of the origin and to achieve equality of the joint correlation function to zero in all other regions of the plane t, F . The fact is that this function satisfies the condition [16, 32, 85]

$$\int_{-\infty}^{\infty} dF \int_{-\infty}^{\infty} |\Psi_0(t, F)|^2 dt = 1, \quad (3.9.8)$$

which describes the so-called principle of ambiguity in radar. It means that any constriction of the central region of high correlation inevitably leads to an increase in the values of the joint correlation function in other regions and may even cause the appearance of new regions of high correlation. The latter may be the cause for ambiguity in measurement of signal parameters.

The joint correlation function of the noise signal meets the requirements indicated above. But use of it is related to great difficulties when accomplishing optimum filtration.

Attempts to select a satisfactory shape of a signal resulted in some success. Three types of signals that meet to a considerable degree the requirements indicated above are also considered in the following chapter.

OPTIMUM FILTERS FOR PHASE-MANIPULATED SIGNALS

4.1. Signals Manipulated in Phase According to Barker's Code

1. The concept of Barker's Code. Properties of Signals

Two signals having identical output and differing only in phase by π have the maximum possible degree of difference. The mutual correlation function in the absence of a time shift is equal to -1. Therefore, it is the use of these signals in transmission of digital messages (for example, in telegraphy, which is called phase in this case) that provides the highest noise stability [22, 24].

Let us take N pulse signals of length τ_0 and amplitude V , which differ from each other in time shift by a value multiple of length and may differ in initial phase by π . Let us form from these elementary pulsed signals the phase-manipulated signal (Fig. 4.1.1):

$$\begin{aligned} v &= V \cos [\omega_0 t + \theta(t)] \text{ at } 0 < t < N\tau_0 = \tau_1, \\ v &= 0 \text{ at } t < 0 \text{ or } t > N\tau_0, \end{aligned} \quad (4.1.1)$$

where $\theta(t) = \theta_i = \text{const}$ at $(i-1)\tau_0 < t < i\tau_0$ and $i = 1-N$ and θ_i is equal to either zero or π as a function of the code being used. It is assumed here and further that $\omega_0 \tau_0$ is a multiple of 2π . Having denoted $\cos \theta_i = d_i$, let us rewrite (4.1.1) as follows

$$v = V d_i \cos \omega_0 t \text{ at } (i-1)\tau_0 < t < i\tau_0,$$

where $i = 1-N$ and d_i is equal to either +1 or -1.

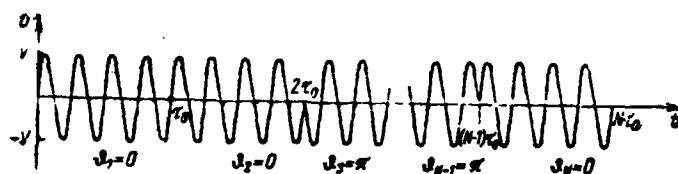


Fig. 4.1.1. Phase-manipulated signal consisting of elementary pulsed signals with four of the indicated initial phases.

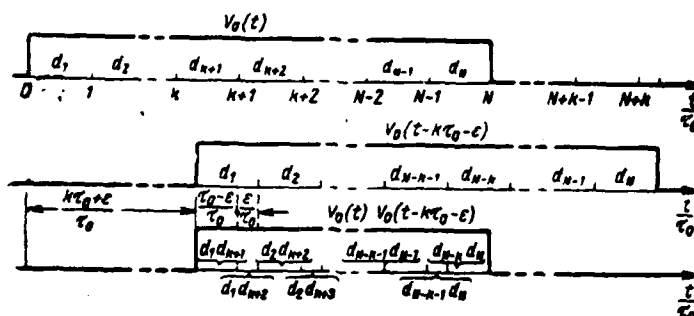


Fig. 4.1.2. Time diagram that explains calculation of correlation function.

The normalized complex envelope of this signal can be represented in the form of the following sum:

$$V_0(t) = \sum_{i=1}^N d_i \{1 [t - (i-1)\tau_0] - 1 [t - i\tau_0]\}. \quad (4.1.2)$$

The normalized correlation function of the complex envelope with a time shift of $t = k\tau_0 + \epsilon$, where k is a whole negative number and $0 \leq \epsilon \leq \tau_0$, is equal to (Fig. 4.1.2)

$$\begin{aligned} \psi_0(k\tau_0 + \epsilon) &= \frac{1}{N\tau_0} \int_{-\infty}^{+\infty} V_0(t) V_0^*(t - k\tau_0 - \epsilon) dt = \\ &= \frac{1}{N} \left[\left(1 - \frac{\epsilon}{\tau_0}\right) \sum_{i=1}^{N-k} d_i d_{i+k} + \frac{\epsilon}{\tau_0} \sum_{i=1}^{N-k-1} d_i d_{i+k+1} \right]. \end{aligned} \quad (4.1.3)$$

Specifically, with a time shift multiple of the length of the elementary pulse τ_0 ,

$$\psi_0(k\tau_0) = \frac{1}{N} \sum_{i=1}^{N-k} d_i d_{i+k}. \quad (4.1.4)$$

In the absence of a time shift $\psi_0(0) = \frac{1}{N} \sum_{i=1}^N d_i^2 = 1$, with a time shift of

$(N-1)\tau_0 - \psi_0[(N-1)\tau_0] = \frac{1}{N} d_1 d_N$ and with positive value of m , beginning at zero, and with any positive value of ε

$$\psi_0[(N+m)\tau_0 + \varepsilon] \equiv 0.$$

Let us select the sequence $\{d_i\}$, where $i = 1-N$ such that the normalized autocorrelation function lies within the range from $-\frac{1}{N}$ to $+\frac{1}{N}$ at values of the independent variable whose absolute value is greater than the length of the elementary pulse τ_0 :

$$-\frac{1}{N} < \psi_0(t) < \frac{1}{N} \quad \text{at } |t| \geq \tau_0.$$

Since d_i can assume values of only ± 1 , then as follows from (4.1.4), with even value of N , the following conditions should be fulfilled for this

$$\left. \begin{aligned} \sum_{i=1}^{N-2m} d_i d_{i+2m} &= 0 \quad \text{at } m=1, 2, \dots, \frac{N}{2}-1, \\ \sum_{i=1}^{N-2m-1} d_i d_{i+2m+1} &= \pm 1 \quad \text{at } m=0, 1, \dots, \frac{N}{2}-1. \end{aligned} \right\} \quad (4.1.5)$$

In like fashion with odd value of N

$$\left. \begin{aligned} \sum_{i=1}^{N-2m} d_i d_{i+2m} &= \pm 1 \quad \text{at } m=1, 2, \dots, \frac{N-1}{2}, \\ \sum_{i=1}^{N-2m-1} d_i d_{i+2m+1} &= 0 \quad \text{at } m=0, 1, \dots, \frac{N-3}{2}. \end{aligned} \right\} \quad (4.1.6)$$

One of the unknown values of d_i can be selected arbitrarily, having assumed, for example, that $d_1 = +1$. Then each of systems (4.1.5) and (4.1.6) consists of a $(N-1)$ -th equation with $(N-1)$ -th unknown.

It follows from (4.1.5) and (4.1.6) that expression (4.1.3) can be simplified. Thus, at $k = 0$ and with odd value of N 142

$$\sum_{i=1}^{N-1} d_i d_{i+1} = 0 \quad \text{or} \quad \sum_{i=1}^N d_i^2 = N,$$

due to which

$$\psi_0(\varepsilon) = 1 - \frac{\varepsilon}{\tau_0},$$

and with even value of N due to the fact that $\sum_{i=1}^{N-1} d_i d_{i+1} = \pm 1$,

$$\psi_0(s) = 1 - \frac{s}{\tau_0} + \frac{s}{N\tau_0} \operatorname{sign} \left(\sum_{i=1}^{N-1} d_i d_{i+1} \right).$$

At $1 < k < N - 1$ in the case of an even value of $N - k$

$$\sum_{i=1}^{N-k} d_i d_{i+k} = 0 \quad \text{and} \quad \sum_{i=1}^{N-k-1} d_i d_{i+k+1} = \pm 1,$$

hence it follows

$$\psi_0(k\tau_0 + s) = \frac{s}{N\tau_0} \operatorname{sign} \left(\sum_{i=1}^{N-k-1} d_i d_{i+k+1} \right).$$

In the case of an odd value of $N - k$ we have

$$\sum_{i=1}^{N-k} d_i d_{i+k} = \pm 1 \quad \text{and} \quad \sum_{i=1}^{N-k-1} d_i d_{i+k+1} = 0,$$

due to which

$$\psi_0(k\tau_0 + s) = \frac{1}{N} \left(1 - \frac{s}{\tau_0} \right) \operatorname{sign} \left(\sum_{i=1}^{N-k} d_i d_{i+k+1} \right).$$

With negative time shifts it is easy to determine the correlation function by using its property of evenness.

At $N = 2$ system (4.1.5) is the equation $d_1 d_2 = \pm 1$. Besides the two trivial solutions $d_1 = d_2 = 1$ and $d_1 = d_2 = -1$, there are two other solutions: $d_1 = +1$; $d_2 = -1$ and $d_1 = -1$; $d_2 = +1$. This system has eight solutions at $N = 4$ (Table 4.1.1).

Table 4.1.1

Index of Solution	d_1	d_2	d_3	d_4
a	+1	+1	-1	+1
b	+1	-1	+1	+1
c	-1	-1	+1	-1
d	-1	+1	-1	-1
e	+1	+1	+1	-1
f	-1	+1	+1	+1
g	-1	-1	-1	+1
h	+1	-1	-1	-1

It is easy to note that solutions b, d, f and h are mirror images of solutions a, c, e and g, respectively (i.e., the sequences that show them differ from each other by inverse order of succession of terms), while solutions c, d, g and h were found from solutions a, b, e and f, respectively, by multiplying each term of the sequence by -1. Therefore, only a and e are independent solutions. Comparison of their correlation functions (Fig. 4.1.3, a and b) shows that code a is somewhat better. Solutions of system (4.1.5) do not exist at other even values of N.

Solutions of system (4.1.6) exist only at $N = 3, 5, 7, 11$ and 13 with odd value of N (Table 4.1.2).

Table 4.1.2.

N	d_i												
	d_1	d_2	d_3	d_4	d_5	d_6	d_7	d_8	d_9	d_{10}	d_{11}	d_{12}	d_{13}
3	+1	+1	-1	0	0	0	0	0	0	0	0	0	0
5	+1	+1	+1	-1	+1	0	0	0	0	0	0	0	0
7	+1	+1	+1	-1	-1	+1	-1	0	0	0	0	0	0
11	+1	+1	+1	-1	-1	-1	+1	-1	-1	+1	-1	0	0
13	+1	+1	+1	+1	+1	-1	-1	+1	+1	-1	+1	-1	+1

The correlation function of signals at $N = 7, 11$ and 13 were plotted in Fig. 4.1.3, c, d, and e, respectively. It is interesting to note that they are negative everywhere at $N = 5$ and 13 , whereas they are negative at $N = 3, 7$ and 11 with the exception of segment $-\tau_0 < t < \tau_0$. 14

The sequences $\{d_i\}$ at $N = 3, 7$ and 11 were first suggested by Barker [88]. Because of this, the sequences that satisfy conditions (4.1.5) and (4.1.6) are called Barker codes.

Investigations [89, 90] and others showed that Barker codes unfortunately do not exist at $N > 13$. Because of this, it is impossible to find the excess of the main maximum modulus of the correlation function over simple maximums more than 13-fold with optimum filtration. In other words, when using a signal manipulated in phase according to Barker's code, the main maximum voltage at the output of an optimum

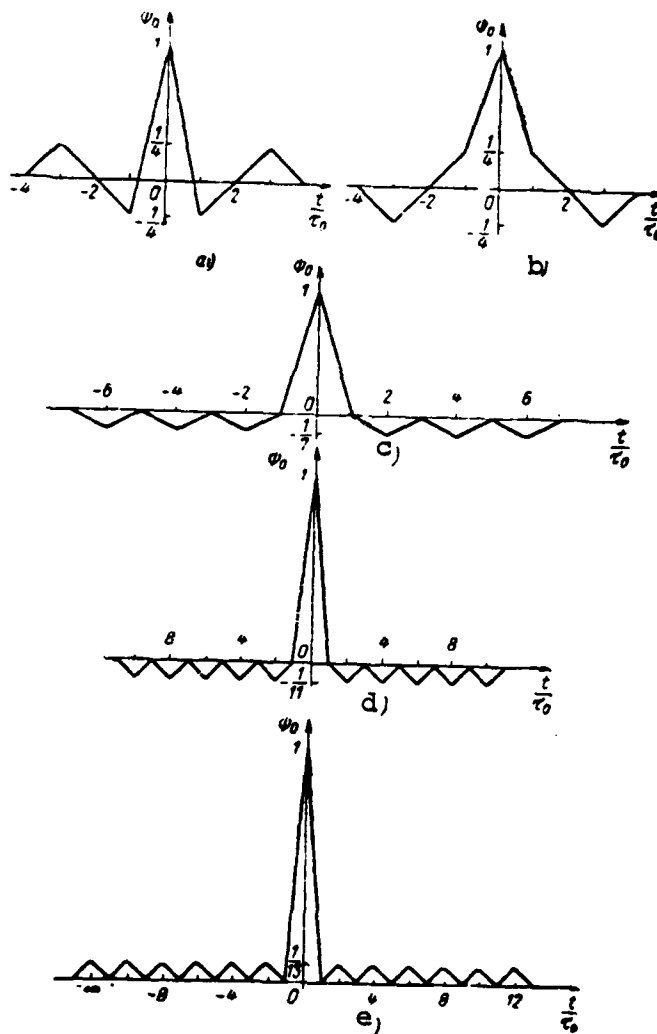


Fig. 4.1.3. Correlation function of Barker sequences.

filter is accompanied by collateral maximums whose relative value cannot be made less than $1/13$.*

145

The considered correlation function is a cross-section of the joint correlation function of modulation at $F = 0$. The other

* The relative value of the side maximums can be reduced below $1/N$ by using special weight processing of the signal after optimum filtration [15]. However, weight processing is related to complication of the circuit and leads to some (although small) losses in the signal/noise ratio and broadening of the main pip.

cross-section of this function (plane $t = 0$) is

$$\Psi_0(0, F) = \frac{1}{N\tau_0} \int_{-\infty}^{+\infty} V_0(x) \Psi_0^*(x) e^{i2\pi Fx} dx,$$

which leads to the equality

$$|\Psi_0(0, F)| = \left| \frac{\sin \pi F N \tau_0}{\pi F N \tau_0} \right|. \quad (4.1.7)$$

This expression coincides with (3.9.3) since $\tau_1 = N\tau_0$. Generally, formula (3.9.3) is valid for any signal with constant amplitude during its entire duration. As can be seen from Fig. 3.3.1, collateral maximum functions (3.3.3) or (3.9.3) are less than the main maximum by approximately a factor of 5.

Calculation of the autocorrelation function of a phase-manipulated 146 signal by a rather complicated law is a laborious and exhausting procedure if a digital computer is not used for this purpose. It can be simplified considerably by using the following method. Let us first note that, according to (4.1.3), the correlation function of a signal comprised of elementary pulses of identical length is a linear broken line whose break point corresponds to time shifts that are a multiple of length τ_0 . Therefore, calculation of the correlation function reduces to determination of its values at these discrete points. The latter is easily done by using a diamond-shaped table (see Table 4.1.3) constructed for a Barker sequence at $N = 7$). We write the considered sequence from bottom to top in the form of a vertical column on the left side of this table. If there is a plus in the top row, we rewrite this sequence unchanged in the horizontal row and if there is a minus at the indicated point, we change the signs of all its elements.

Table 4.1.3.

-	-	-	+	+	-	+													
+		+	+	+	-	-	+	-											
7			-	-	-	+	+	-	+										
-				-	-	-	+	+	-	+									
+					+	+	+	-	-	+	-								
+						+	+	+	-	-	+	-							
+							+	+	+	-	-	+	-						

-1, 0, -1, 0, -1, 0, +7, 0, -1, 0, -1, 0, -1

In other words, we write the sequence in the top row whose elements are a product of the corresponding element of the initial sequence for its last element (it is written in the top row of the vertical column). We write with one shift to the right a similar sequence of products of the elements of the initial sequence by its next to last element (it is written in the second row of the vertical column). We repeat this operation as many times as there are elements in the sequence. Having added the elements of each vertical column of the formed diamond-shaped table we determine the values of the autocorrelation function of this sequence at discrete points (they are written below the table). Having plotted these values on the graph and having connected adjacent values with straight-line segments, we find the autocorrelation function of the sequence which differs from the normalized autocorrelation function (Figure 4.1.3, c) only by the scale along the y-axis. The outlined method is essentially matrix representation of relation (4.1.4).

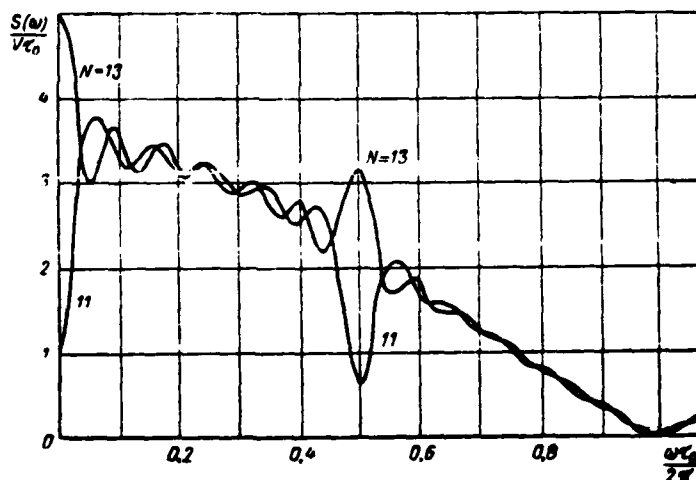


Fig. 4.1.4. Amplitude spectra of Barker sequences.

Making use of the fact that the autocorrelation function of the signal whose phase is manipulated by Barker's law, it is known that its amplitude spectrum can be easily determined [91]. Actually, the energy spectrum of the signal is related to its autocorrelation function by the Fourier transform:

$$F(\omega) = 4 \int_0^T \phi(\tau) \cos \omega \tau d\tau.$$

On the other hand, the energy spectrum is equal to double the square of the amplitude spectrum [27]:

$$F(\omega) = 2S_1(\omega).$$

Therefore, the signal amplitude spectrum is

$$S_1(\omega) = \left| \left[\frac{1}{2} F(\omega) \right]^{1/2} \right| = \left| \left[2 \int_0^{\infty} \psi(\tau) \cos \omega \tau d\tau \right]^{1/2} \right|. \quad (4.1.8)$$

In the given case the unnormalized autocorrelation function (see Fig. 4.1.3) of a Barker sequence with odd values of N (which are only of practical interest) consists of N symmetrical triangular pulses of length $2\tau_0$ shifted with respect to each other by a time which is a multiple of $2\tau_0$ and accordingly having complex amplitudes $NV_1^2\tau_0$ (central ejection) and $\pm V_1^2\tau_0$ (side ejections), and the positive sign corresponds to $N = 5$ and 13 while the negative sign corresponds to $N = 3, 7$ and 11.

14:

Since a triangular symmetrical pulse (with respect to $t = 0$) of amplitude U_n and length τ_n has spectral density [27]

$$S_0(\omega, U_n, \tau_n) = \frac{4U_n}{\omega^2 \tau_n} \left(1 - \cos \frac{\omega \tau_n}{2} \right),$$

then the spectral density of the autocorrelation function of a Barker sequence is

$$\begin{aligned} S_1(\omega) &= S_0(\omega, V^2\tau_0, 2\tau_0) \times \\ &\times \left(\pm \sum_{k=-\frac{N-1}{2}}^{-1} e^{-j2k\omega\tau_0} + N \pm \sum_{k=1}^{\frac{N-1}{2}} e^{-j2k\omega\tau_0} \right) = \\ &= \frac{2V^2}{\omega^2} (1 - \cos \omega\tau_0) \left(N \pm 2 \sum_{k=1}^{\frac{N-1}{2}} \cos 2k\omega\tau_0 \right). \end{aligned}$$

Accordingly, the considered sequence has the energy spectrum (positive frequencies)

14:

$$F(\omega) = S_1(\omega) + S_1(-\omega) = 2S_1(\omega).$$

Making use of formula (1.342.2) of [92] and making the elementary transformations, we find

$$F(\omega) = 2V^2\tau_0^2 \left[\frac{\sin(\omega\tau_0/2)}{\omega\tau_0/2} \right]^2 \left[N \pm \left(\frac{\sin N\omega\tau_0}{\sin \omega\tau_0} \right) \right].$$

Then according to (4.1.8) the amplitude spectrum of a Barker sequence is

$$S(\omega) = V\tau_0 \left| \frac{\sin(\omega\tau_0/2)}{\omega\tau_0/2} \left[N \pm \left(\frac{\sin N\omega\tau_0}{\sin \omega\tau_0} - 1 \right) \right]^{1/2} \right|.$$

Here as above, a positive sign in front of the parentheses occurs at $N = 5$ and 13 and a negative sign occurs at $N = 3, 7$ and 11.

Thus, the amplitude spectrum of a Barker sequence is the product of the amplitude spectrum of one of the pulsed signals which comprises this sequence and of the function (shape complexity factor)

$$R(\omega) = \left[N \pm \left(\frac{\sin N\omega\tau_0}{\sin \omega\tau_0} - 1 \right) \right]^{1/2}.$$

The latter is periodic with respect to ω having period π/τ_0 .

Consideration of the amplitude spectra of the two Barker sequences at $N = 11$ and 13 (Fig. 4.1.4) shows that they essentially coincide, with the exception of the very low-frequency region and the vicinity of frequency π/τ_0 . This difference of spectra is explained by the difference in the structure of Barker codes at the indicated values of N .

2. Signal Production. The Optimum Filter

A signal manipulated in phase by π according to the law of Barker's code can be found rather simply. A balanced modulator powered from a high-frequency generator and modulated by sequence of coded pulses can be used for this.

150

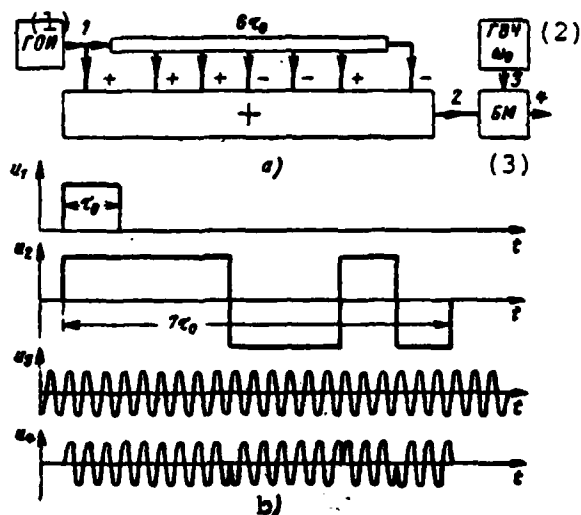


Fig. 4.1.5. Block diagram of FM signal generator at $N = 7$ (a) and time diagrams of voltages (b).

Key: (1) single video phase generator; (2) high-frequency generator; (3) balanced modulator.

The sequence of encoded pulses can be shaped by algebraic summation of the pulses taken from the leads of the delay line with total

length $(N - 1)\tau_0$ to whose input a square-wave pulse of length τ_0 is fed. The delay line has a total of $N - 2$ leads, ensuring a delay by a value that is a multiple of τ_0 . The pulses taken from the beginning of the line, from all the leads and from the end of the line are added in the adder with weights corresponding to the values of the terms d_i of the Barker code. The sequence of encoded pulses is thus shaped as a result of this summation (Fig. 4.1.5).

The pulse being fed to the input of the delay line can be produced either by means of an ordinary pulse circuit or by excitation of an optimum filter with a very short pulse for a video pulse of length τ_0 .

15

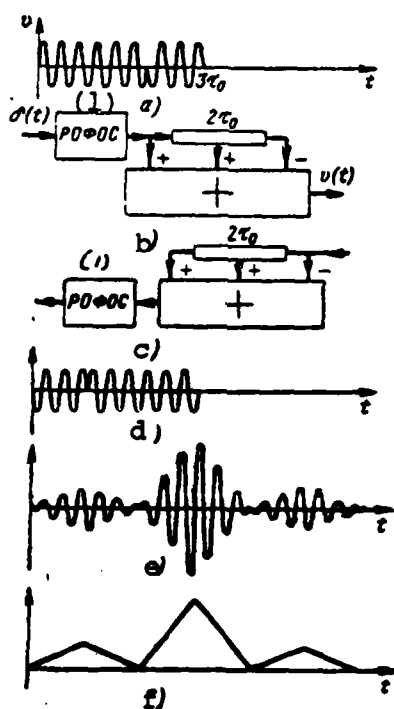


Fig. 4.1.6. FM signal at $N = 3$ (a), block diagrams of its generator (b) and optimum filter (c) and time diagrams of voltages (d, e and f).

Key: (1) RF optimum filter for single pulsed signal.

If a radio pulse of frequency ω_0 and length τ_0 , formed upon excitation of an optimum filter for the signal by a delta-pulse, is fed to the input of the delay line, then an FM encoded signal will be formed at the output of the adder (Fig. 4.1.6, a). Accordingly, the pulse characteristic of this system (Fig. 4.1.6, b) coincides with this signal. And as

shown in §1.3, the pulse characteristic differs from the function that represents the signal, mainly by the sign of the independent time variable. Therefore, if the input and output change places in the signal generation device (Fig. 4.1.6, b), i.e., if the direction of the signal is changed, then we find an optimum filter for the given signal (Fig. 4.1.6, c).

If a signal optimum to the filter is fed to its input (Fig. 4.1.6, d), a voltage is formed at its output that reproduces with some time shift the autocorrelation function of this signal (Fig. 4.1.6, e). A voltage (Fig. 4.1.6, f), which represents the modulus of the correlation function of the complex envelope of this signal in some scale and with some time shift, is formed as a result of its amplitude detection.

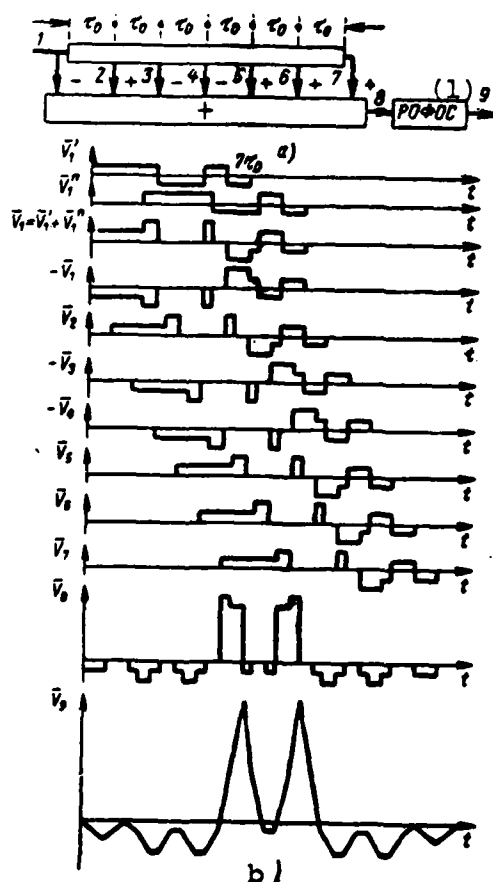


Fig. 4.1.7. Block diagram of optimum filter at $N = 7$ (a) and time diagrams of voltages (b). Key: (1) RF optimum filter for single pulsed signal.

If two signals overlapping in time, but separated by a time greater than τ_0 are fed to the input of the optimum filter, they form an output voltage with two separate main maximum values (Fig. 4.1.7), which also permit one to determine the time position of each of the signals. Accordingly, the system resolves these signals in time (by range).

Since Barker codes do not exist at $N > 13$, systems with signals manipulated by these codes have limited capabilities with respect to increasing the range resolution while retaining the same effective range and increasing the effective range while retaining the range resolution.

4.2. Signals Manipulated in Phase by Binary Pseudorandom Sequence

1. Concept of Binary Pseudorandom Sequence and Its Properties

When searching for the best signal shape, attention was turned toward signals manipulated in phase by π by so-called "linear recursion sequences" or "linear sequences of a shift register of maximum length" [15, 93-97], which were suggested when working out problems of coding in general message transmission theory.

These sequences are a set of N periodically repeated signals d_i , each of which can occupy one of two values: $+1$ or -1 . This value is determined by the product of the values of two or more previous symbols (but always odd) taken with opposite sign:

154

$$d_i = -d_{i-n}d_{i-m}\dots d_{i-k}, \quad \text{even number of factors} \quad (4.2.1)$$

where $n > m > \dots > 1 > k \geq 1$, while $i = (n + 1) - N$.

In the special case of two factors

$$d_i = -d_{i-n}d_{i-k}. \quad (4.2.2)$$

If we take for example $d_1 = d_2 = \dots = d_{n-1} = -1$ and $d_n = +1$, then an unrepeated elementary sequence $\{d_i\}$ of N symbols should be formed with proper selection of numbers $m, \dots, 1$ and k , where

$$N = 2^n - 1. \quad (4.2.3)$$

It should contain all combinations of n symbols of two elements -1 and $+1$, except the combination consisting of only negative ones. As a result, each sequence $\{d_i\}$, where $i = 1 - (2^n - 1)$, contains 2^{n-1} positive ones and $2^{n-1} - 1$ negative ones. Therefore,

$$\sum_{i=1}^N d_i = 1. \quad (4.2.4)$$

The symbols are repeated at $i > N$ in the same order, i.e., at any integer p

$$d_{i+pN} = d_i. \quad (4.2.5)$$

The same sequence of symbols is also formed at $t < 0$. It is obvious from (4.2.5) that the number N characterizes the period of an infinite sequence. The infinite sequence formed in this manner is called a binary pseudorandom sequence.

As an example let us first take the simplest case of $n = 2$:

$$d_i = -d_{i-2}d_{i-1}. \quad (4.2.6)$$

Then, if $d_1 = -1$ and $d_2 = +1$, then $d_3 = +1$, $d_4 = -1$, $d_5 = +1$, $d_6 = +1$, $d_7 = -1$ and so on.

Accordingly, the desired sequence has the form: $\dots, -1, +1, +1, -1, +1, +1, -1, +1, +1, \dots$. It contains all possible combinations of two symbols: -1 and $+1$, $+1, +1$ and $+1, -1$, except the "forbidden" combination $-1, -1$. The elementary sequence $-1, +1, +1$ is repeated every $N = 2^2 - 1 = 3$ symbols. It coincides with the Barker code at $N = 3$.

155

Two rules of (4.2.2) are possible at $n = 3$:

$$d_i = -d_{i-3}d_{i-2} \quad (4.2.7)$$

and

$$d_i = -d_{i-3}d_{i-1},$$

which accordingly lead to the following elementary sequences of $N = 2^3 - 1 = 7$ symbols: $-1, -1, +1, -1, +1, +1, +1$ and $-1, -1, +1, +1, +1, -1, +1$. The infinite sequences formed from these elementary

sequences differ from each other only by the order of the identical symbols, i.e., they are a mirror image of each other.

If $n = 4$ and $d_i = -d_{i-4}d_{i-3}$, then we find a sequence of $N = 2^4 - 1 = 15$ symbols: $-1, -1, -1, +1, -1, -1, +1, +1, -1, +1, -1, +1, +1, +1, +1$. According to the rule $d_i = -d_{i-4}d_{i-1}$, a "mirror" sequence is formed: $-1, -1, -1, +1, +1, +1, +1, -1, +1, -1, +1, +1, -1, -1, +1$.

The number of elements of sequence N increases sharply as n increases, essentially doubling with an increase of n by one (Table 4.2.1).

Table 4.2.1.

n	2	3	4	5	6	7	8	9	10	11	12
N	3	7	15	31	63	127	255	511	1023	2047	4095

Several numbers k , at which the considered sequence is formed by rule (4.2.2), corresponds to almost every integer n . Some of these combinations of n and k are placed in Table 4.2.2. If any value of k other than that indicated in this table is taken upon formation of a sequence by rule (4.2.2), then a double sequence will be formed, but its period will be less than (4.2.3).

Table 4.2.2.

n	5	5	6	6	7	7	9	9	10	10
k	2	3	1	5	1	6	4	5	3	7

n	11	11	14	14	15	15	17	17	18	18
k	2	9	5	9	1	14	3	14	3	15

No such integers k exist at $n = 8, 12, 13$ and 16 at which the considered sequence with maximum period $N = 2^n - 1$ is formed by the rule (4.2.2). A different combination $(n, n - k)$, which forms a sequence of the same period, being a mirror image of the first sequence, corresponds to each combination (n, k) , leading to a sequence of maximum period.

The latter is also valid for combinations of a different even number of integers, for example, for combinations of four integers (n, m, l, k) (Table 4.2.3), which correspond to the rule $d_i = -d_{i-n}d_{i-m}d_{i-l}d_{i-k}$ of formation of a considered sequence of maximum period. The combinations $(n, n - k, n - l, n - m)$, which leads to formation of a "mirror" sequence, corresponds to each such combination (These combinations are arranged in Table 4.2.3 in a row, occupying odd and even ordinal positions, respectively).

157

Table 4.2.3.

n	5	5	5	5	6	6	6	6	8	8
m	3	4	4	4	5	5	4	5	4	6
l	2	3	2	3	2	4	3	3	3	5
k	1	2	1	1	1	1	1	2	2	4

n	12	12	13	13	16	16	19	19
m	6	11	4	12	5	15	5	18
l	4	8	3	10	3	13	2	17
k	1	6	1	9	1	11	1	14

The total number of different combinations (and accordingly of sequences) for any value of n comprises

$$M = \frac{1}{n} \varphi(2^n - 1),$$

where $\varphi(x)$ is an Euler phi-function that determines the number of positive integers which are less than the given positive integer x and are relatively prime to x [98]. Those numbers which do not have common divisors or multipliers with it are called numbers relatively prime to the given number x . At $n = 10$ the number of types of sequences already comprises 60 (Table 4.2.4).

A binary pseudorandom sequence has a number of very interesting properties.

If an infinite sequence $\{d_i\}$ with period of N elements is shifted by k elements ($k \neq pN$) to the right or left, then the sequence $\{d_{i+k}\}$ is formed. Having multiplied the elements of the initial and shifted

Table 4.2.4.

n	2	3	4	5	6	7	8	9	10
M	1	2	2	6	6	12	16	48	60

n	11	12	13	14	15	16	17	18	19
M	176	144	630	756	1800	2048	7710	7776	27594

sequences d_i and d_{i+k} and having changed the sign of their product, we again find the same sequence shifted by a certain number of elements, i.e., $\{-d_i d_{i+k}\} = \{d_{i+m}\}$, where m is distinct from k and pN .

Multiplying the elements of sequences ($n = 2$) as an example

$$\dots, -1, +1, +1, -1, +1, +1, \dots \text{ and} \\ \dots, +1, -1, +1, +1, -1, +1, \dots,$$

we find

$$\dots, -1, -1, +1, -1, -1, +1, \dots$$

or after changing signs

$$\dots, +1, +1, -1, +1, +1, -1, \dots$$

This sequence differs from the initial one by a shift by two elements to the right.

Let us demonstrate the indicated property for a sequence plotted according to rule (4.2.7). Based on this rule, equality (4.2.5) and the obvious relation $d_i^2 = 1$, we have

$$\begin{aligned} -d_i d_{i+1} &= d_{i+2}, \\ -d_i d_{i+2} &= -d_i (-d_{i-1} d_i) = d_{i-1} = d_{i+3}, \\ -d_i d_{i+3} &= -d_i (-d_i d_{i+1}) = d_{i+1}, \\ -d_i d_{i+4} &= -(-d_{i+2} d_{i+3}) d_{i+4} = d_{i+5}, \\ -d_i d_{i+5} &= -(-d_{i+4} d_{i+5}) d_{i+6} = d_{i+6}, \\ -d_i d_{i+6} &= -d_i d_{i-1} = d_{i+7}. \end{aligned}$$

These equalities also prove the foregoing. The proof is similar for other values of n .

Since the sequence $\{-d_i d_{i+k}\}$ is totally equivalent to the sequence $\{d_i\}$ at $k \neq pN$, for which relation (4.2.4) is valid, then

$$\sum_{i=1}^N d_i d_{i+k} = -1 \quad \text{at } k \neq pN. \quad (4.2.8)$$

Moreover,

$$\sum_{i=1}^N d_i d_{i+pN} = \sum_{i=1}^N d_i^2 = N. \quad (4.2.9)$$

2. Correlation Function and Amplitude Spectrum of Sequence

Let us manipulate the high-frequency oscillation phase by π according to the law of variation of the integers of the binary pseudo-random sequence $\{d_i\}$. This signal will then have a normalized complex amplitude 15

$$V_0(t) = \sum_{i=-\infty}^{+\infty} d_i \{1 [t - (i-1)\tau_0] - 1 (t - i\tau_0)\}. \quad (4.2.10)$$

This expression differs from (4.1.2) only by the infinite limits of the sum. By analogy with (4.1.3), the normalized correlation function of the complex amplitude of this signal with time shift $t = k\tau_0 + \varepsilon$ has the form

$$\begin{aligned} \psi_0(k\tau_0 + \varepsilon) &= \frac{1}{N\tau_0} \int_0^{N\tau_0} V_0(x) V_0(x - k\tau_0 - \varepsilon) dx = \\ &= \frac{1}{N} \left[\left(1 - \frac{\varepsilon}{\tau_0}\right) \sum_{i=1}^N d_i d_{i+k} + \frac{\varepsilon}{\tau_0} \sum_{i=1}^N d_i d_{i+k+1} \right]. \end{aligned}$$

Due to (4.2.8) and (4.2.9), we find

$$\psi_0(s) = 1 - \frac{\varepsilon}{\tau_0} \left(1 + \frac{1}{N}\right),$$

and at $1 < k < N - 2$

$$\psi_0(k\tau_0 + \varepsilon) = -\frac{1}{N}$$

or otherwise

$$\left. \begin{aligned} \psi_0(t) &= 1 - \frac{|t|}{\tau_0} \left(1 + \frac{1}{N}\right) \quad \text{at } |t| \leq \tau_0, \\ \psi_0(t) &= -\frac{1}{N} \quad \text{at } \tau_0 < |t| < (N-1)\tau_0. \end{aligned} \right\} \quad (4.2.11)$$

Moreover,

$$\psi_0(t + pN\tau_0) = \psi_0(t). \quad (4.2.12)$$

The correlation function (Fig. 4.2.1) has one maximum on the order τ_0 wide for the period $T = N\tau_0$. Its absolute value is N times less than the maximum for the greater part of the period of length $(1 - \frac{2}{N})T$. Since the value of N can essentially be selected as large as desired, the correlation function of these signals may be found very close to ideal. 160

Due to the great affinity of this function to the correlation function of noise, the sequence of two discrete symbols that formed this signal is also called a binary pseudorandom sequence.

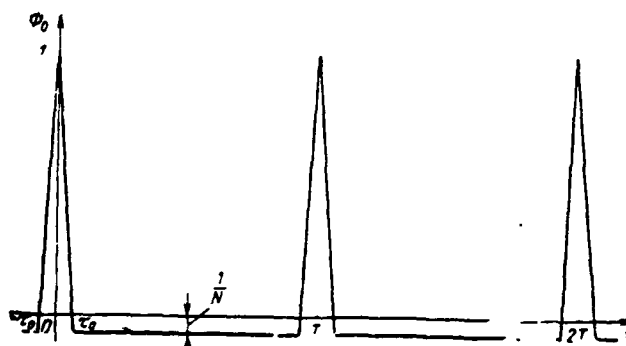


Fig. 4.2.1. Correlation Function of Binary Pseudorandom Sequence.

The additional maximums of the joint correlation function $\Psi_0(t, F)$ on plane t, F have a height on the order of $\frac{1}{\sqrt{N}}$, i.e., they can be made sufficiently small [15, 32].

Let us consider the method of calculating the values of the autocorrelation function of a binary pseudorandom sequence at discrete points by means of a matrix table. Due to the periodicity of the given sequence, this method differs somewhat from that outlined in item 1 of §4.1 for the case of an aperiodic sequence.

In the considered case according to the method outlined above, an auxiliary diamond-shaped matrix table is first compiled for a single period of the sequence (see Table 4.2.5, constructed for a binary pseudorandom sequence with $N = 7$). All the elements located to the right of the small diagonal of this table are then rewritten in the same 161

Table 4.2.5.

Figure 1 shows a 10x10 grid of symbols. The symbols are +, -, and dots. A dashed diagonal line runs from the top-left to the bottom-right. The x-axis is labeled with -1, -1, -1, -1, -1, -1, +7. The y-axis is labeled with +, +, +, -, +, -, -.

Due to (4.2.12), the autocorrelation function of the sequence is periodic and its spectrum, i.e., the energy spectrum of this sequence, is linear (discrete).

$$A\left(\frac{2\pi k}{N\tau_0}\right) = \frac{2}{N\tau_0} \int_0^{N\tau_0} \psi(t) \cos\left(\frac{2\pi k}{N\tau_0} t\right) dt = \frac{2V^2(N+1)}{\pi^2 k^2} \sin^2 \frac{\pi k}{N},$$
$$A(0) = \frac{1}{N\tau_0} \int_0^{N\tau_0} \psi(t) dt = \frac{V^2}{N^2}.$$
$$C(0) = |A(0)^{1/2}| = \frac{v}{N},$$
$$C \left(\frac{2\pi k}{N\epsilon_0} \right) = \left[2A \left(\frac{2\pi k}{N\epsilon_0} \right) \right]^{1/2} = \frac{2V}{\pi k} (N+1)^{1/2} \sin \frac{\pi k}{N}.$$

If we consider the periodic sequence whose period has the same length as the period of a binary pseudorandom sequence and which consists of a single square-wave pulse of the same amplitude and length as the pulses of the binary pseudorandom sequence, then using the results presented in [27], it is easy to establish that this sequence has the constant component

$$B(0) = \frac{V}{N}$$

and the amplitude of the k -th harmonic

$$B\left(\frac{2\pi k}{N\tau_0}\right) = \frac{2V}{\pi k} \left| \sin \frac{\pi k}{N} \right|.$$

It follows from pair comparison of the last four expressions that encoding the square-wave pulses by the binary pseudorandom sequence law does not change the constant component (which is explained by the structure of this sequence), but increases the amplitudes of all the harmonic components $|(N+1)^{1/2}| = |2^{n/2}|$ times (Fig. 4.2.2).

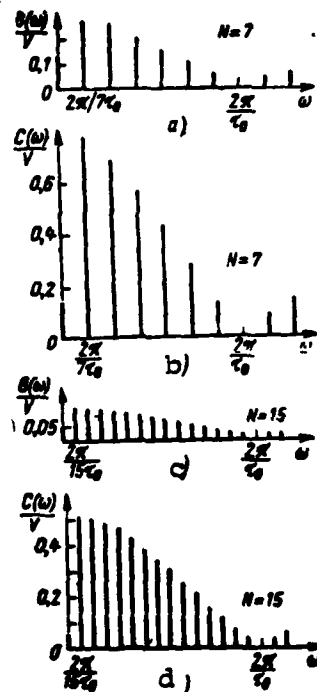


Fig. 4.2.2. Amplitude spectra of uncoded (a and c) and binary pseudorandom (b and d) sequences.

Signals manipulated in phase by binary pseudorandom sequences are used in wideband communications systems [96]. The capabilities of separating these signals are determined by their cross-correlation properties. Due to the pseudonoise nature of these sequences, one can expect that their different types have low cross-correlation. Actually, any two different binary pseudorandom sequences with periods $T_1 = N_1 \tau_0$ and $T_2 = N_2 \tau_0$, where N_1 and N_2 are relatively prime numbers, have a constant normalized cross-correlation function which is equal to the value inverse to the product $N_1 N_2$: 16

$$\psi_0(\tau) = \frac{1}{N_1 N_2 \tau_0} \int_0^{N_1 N_2 \tau_0} V_{10}(t) V_{20}(t + \tau) dt = \frac{1}{N_1 N_2} \text{ at any } \tau.$$

where τ_0 is the length of the elementary pulse of these sequences, $N_1 = 2^{n_1} - 1$ and $N_2 = 2^{n_2} - 1$ are the numbers of the elements in a single period of sequences, n_1 and n_2 are integers and $\bar{V}_{10}(t)$ is the normalized complex amplitudes of signals encoded in phase by these sequences.

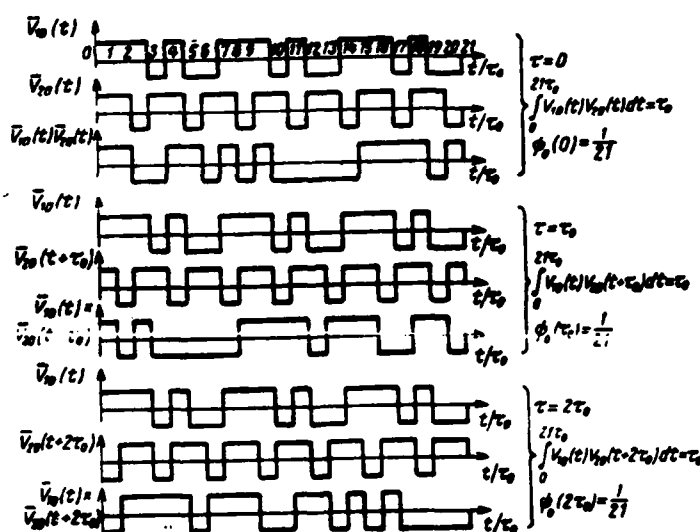


Fig. 4.2.3. Calculation of values of cross-correlation function of two binary pseudorandom sequences at three values of time shift.

The statement made above is illustrated by the example of calculating the cross-correlation function of two binary pseudorandom sequences with $N_1 = 7$ and $N_2 = 3$ for the time shift $\tau = 0, \tau_0$ and $2\tau_0$ (Fig. 4.2.3). Since the second sequence is repeated with period $3\tau_0$,

the time shifts $\tau = 3\tau_0, 4\tau_0, 5\tau_0, 6\tau_0, 7\tau_0, \dots$ reduce to the considered cases for $\tau = 0, \tau_0, 2\tau_0, 0, \tau_0, \dots$, respectively. With a shift by τ , differing from integer τ_0 , the normalized cross-correlation function has the same value. Thus, the normalized cross-correlation function is constant and equal to $1/2l$, which confirms the statement made above.

If N_1 and N_2 are taken as sufficiently large (and relatively prime) numbers, then the normalized cross-correlation function of the corresponding binary pseudorandom sequences will be as small as these sequences can be regarded as essentially uncorrelated.

3. Signal Production. Structure of Optimum Filter.

To produce a signal whose phase is manipulated by π by the law of a binary pseudorandom sequence, a modulating oscillation must be generated. It is simpler to form the latter by means of a nonequivalent circuit [99], since rules (4.2.2) and others are nonequivalence relations.

A block diagram of a device for generating an FM signal (Fig. 4.2.4, a) consists of a nonequivalent circuit (or adder modulo 2) made on two AND elements, an OR element and a NOT element, a generator for a single pulse with length τ_0 , an additional OR circuit, delay lines of $n\tau_0 = 2\tau_0$ with lead from the midpoint, a balanced modulator and high-frequency generator ω_0 .

If longer sequences formed by rule (4.2.2) are used, only the electrical length of delay line $n\tau_0$ and the position of the lead from this line that provides a delay by time $k\tau_0$ varies in the block diagram.

The number of inputs of the logic circuit that implements this rule and accordingly the number of leads of the delay line, which is one less than the number of cofactors (Fig. 4.2.5), is increased when a sequence is formed by rule (4.2.1) using a large number of cofactors. In this case the logic circuit consists of several nonequivalent circuits.

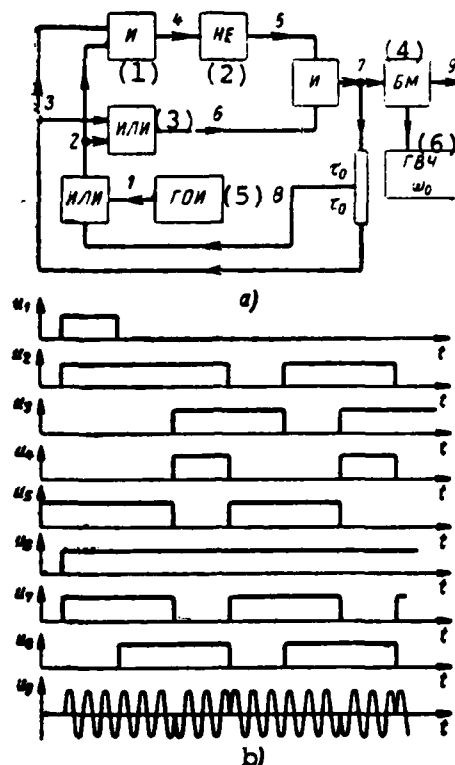


Fig. 4.2.4. Block diagram of signal generator with binary pseudorandom phase manipulation at $n = 2$ and time diagrams of voltages.

Key: (1) AND; (2) NOT; (3) OR; (4) Balanced modulator; (5) Single video pulse generator; (6) High-frequency generator.

The circuit of a binary sequence generator can also be made by using a shift register. In the simplest case ($n = 2$), it contains, besides the elements indicated above, two flip-flop stages of a shift register and a timing pulse oscillator (Fig. 4.2.6, a). The repetition rate of the latter is equal to the length of the elementary transmission.

166

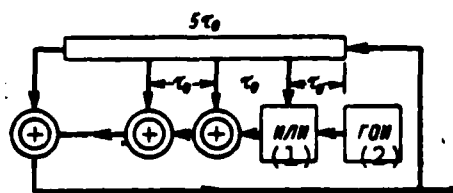


Fig. 4.2.5. Block diagram of binary pseudorandom sequence generator with delay line at $n = 5$, $m = 3$, $l = 2$ and $k = 1$.

Key: (1) OR; (2) Single video pulse generator.

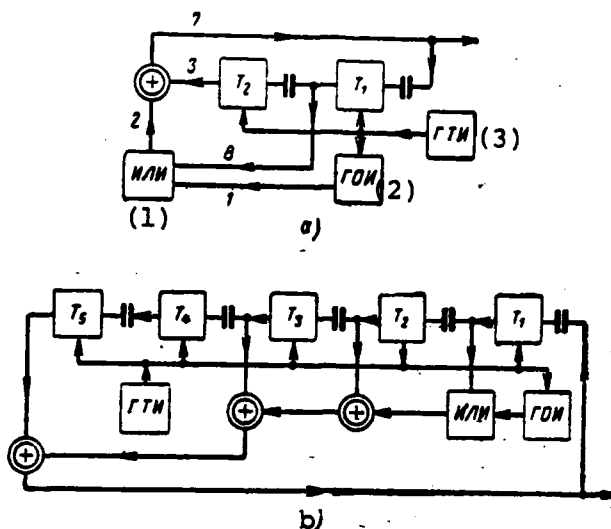


Fig. 4.2.6. Block diagram of binary pseudorandom sequence generator with shift register.

Key: (1) OR; (2) Single video pulse generator; (3) Timing pulse oscillator.

In the general case the shift register should have n flip-flops. When using rule (4.2.2), signals are fed to the nonequivalent circuit from the k -th and last flip-flops of the register and if the number of cofactors in (4.2.1) is equal to four, then it is fed from the k -th, 1-th, m -th and last flip-flops (see Fig. 4.2.6, b, where $k = 1$, $l = 2$, $m = 3$ and $n = 5$).

An optimum filter for a signal with pseudorandom phase manipulation law (Fig. 4.2.7, a) consists of one for a single radio pulse of length τ_0 , delay lines by time $(N - 1)\tau_0$ with $(N - 2)$ -th uniformly arranged leads, an adder and signal storage with period $N\tau_0 = T$. The latter accomplishes interperiod processing of the received signal (see the next chapter).

The considered optimum filter circuit (Fig. 4.2.7, a) operates on an intermediate frequency (PCh). Because of this, the requirements on the accuracy of maintaining the equivalence of the delay time between adjacent leads of the delay line and the length of the elementary pulse are very rigid (the time error should be much less than the period of the intermediate-frequency carrier oscillation). To significantly attenuate these requirements so that the time error is much less than

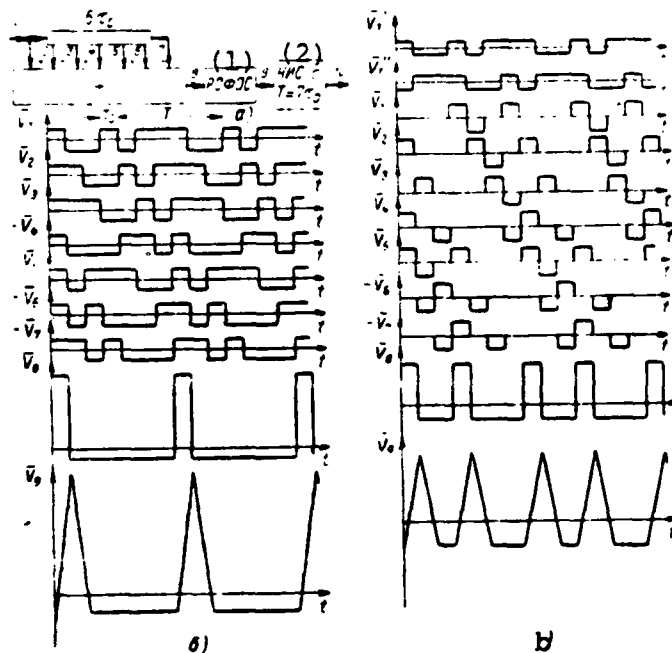


Fig. 4.2.7. Block diagram of optimum filter and FM signal (a) and time diagrams of voltages when one (b) and two (c) reflected signals are fed to the input.
Key: (1) RF optimum filter for single pulsed signal;
(2) Pulsed signal storage.

only the length of the elementary pulse, the optimum filter circuit must be altered so that the delay line (and storage device) operate on video frequency. Since the initial phase of the signal to be received is usually known beforehand, this optimum filter circuit should be quadrature (Fig. 4.2.8, a). It consists of two coherent detectors controlled by heterodyne oscillations shifted by 90° , two delay lines with leads, two storage devices, two square-law generators and an adder.

But in this case implementation of delay lines with leads causes the greatest difficulties. To avoid these difficulties, so-called discrete or digital optimum (matched) filters [100-102] are used in which shift registers consisting of N flip-flops are used instead of these lines (Fig. 4.2.8, b). A signal in the form of a video pulse sequence is fed to the input of the first flip-flop of the register from the output of one of the coherent detectors. The video pulse sequence is pushed by pulses of the timing pulse oscillator, following with period τ_0 , to the next flip-flops of the shift register. The

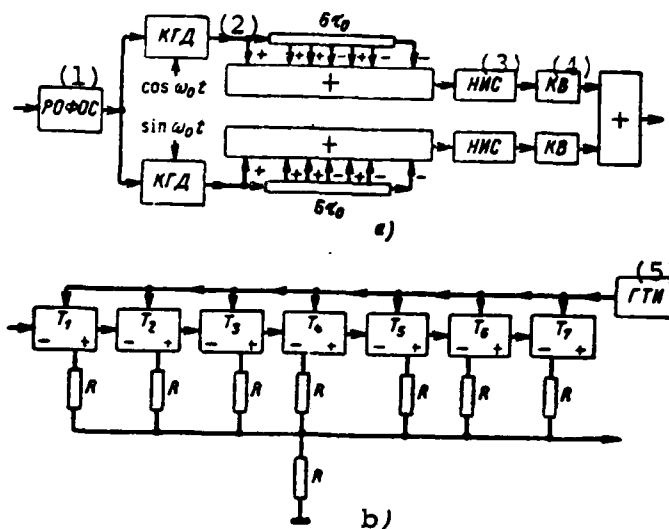


Fig. 4.2.8. Block diagrams of optimum receiver for FM signal and digital optimum filter.
Key: (1) RF optimum filter for single pulsed signal; (2) Coherent detector; (3) Pulsed signal storage; (4) Square-law generator; (5) Timing pulse oscillator.

voltages tapped from the output of one of the halves of each flip-flop are added in the output resistance as a function of the code to which this digital filter is tuned, forming a large voltage spike at the output only if a pulse sequence optimum to the given filter is recorded on the flip-flops of the shift register.

Before being fed to the coherent detectors, the signal is subjected to rigid restriction in the bandpass limiter, which leads to losses in the signal/noise ratio on the order of 1 dB with a weak signal [103-105].

The advantages of a digital optimum filter include its reliability, absence of restrictions on the length of the register (and accordingly of the number of N pulses in the period of the sequence), the absence of attenuation of the pulse sequence when moving along the register and the capability of changing the pulse shift rate in a simple manner.

4. Effect of Filter and Signal Error.

Analysis of the amplitude, phase and time distortions of the signal due to inaccuracy of the weights of the delay line leads in amplitude

and phase, inaccuracy of the moment of signal phase manipulation, inaccuracy of installing the delay line leads and so on shows [15, 106-109] that the effect of these distortions on the level of side lobes of the output signal decreases as the number of N elementary signal pulses increases. This is explained by the fact that the optimum filter, due to the pseudorandom nature of the signal, has a pseudorandom structure, as a result of which regular distortions of the signal after it passes through the optimum filter acquire a random nature and are added as random values [15]. Random signal distortions caused by random 170 deviations of the amplitudes and phases of the weights of the delay line leads will be added in the adder. Because of the independence of distortions at each lead, the standard deviation of the total distortions will be N times greater than those on each lead. The power of the output signal is N^2 times greater than the signal output on each lead. Therefore, the ratio of the standard deviation of distortions to signal output is N times less at the output than on the delay line lead.

Linear phase distortions caused by the time error between the length of the elementary pulse and the delay time between adjacent leads of the delay line are the most unfavorable. Unlike the distortions considered above, accumulation rather than averaging of these distortions occurs in an optimum filter. Therefore, the effect of these distortions increases with an increase of N . Because of this, special measures must be implemented to reduce these distortions.

Calculations show [109] that if a video frequency optimum filter is made on a delay line constructed on sections of capacitors and inductances with 2% tolerances and with temperature coefficients of capacitance and inductance equal to 10^{-5} for a signal with $N \leq 10^3$, then a decrease of the signal/noise ratio by voltage due to scattering of parts and variation of temperature by $\pm 50^\circ$ will not exceed 15%, which is quite acceptable.

5. Advantages and Disadvantages of System With Pseudorandom Phase Manipulation

Systems in which the signal has pseudorandom phase manipulation (PFM) permit one to achieve very high resolution both in range and

speed. However, the indicated factor is achieved at high values of N , on the order of 1,000. This requires selection of N on the order of 10.

With the same peak power and retention of the same range resolution, use of this system compared to the simplest pulsed system permits one to increase signal energy N -fold and accordingly the effective range $4\sqrt{N}$ times, which yields $4\sqrt{1023} = 5.655$ times at $N = 1,023$.

Apparently, no better codes than a binary pseudorandom sequence exists in general [85] since the systems that use them essentially realize their potential capabilities, which ensue from the uncertainty relation in radar (3.9.8). 17

No special difficulties arise when designing a transmitter (pulse sequence generator, balanced modulator and high-frequency generator).

However, implementation of a wideband delay line with $(N - 2)$ (i.e. on the order of 1,000) leads in an optimum filter is related to great engineering difficulties. To avoid them, digital optimum filters or integrated circuits are used. The second disadvantage of the system ensues from the continuous nature of signal emission and includes the need for very careful tie-in of the transmitter and receiver.

Despite the seriousness of these difficulties, they are surmountable. Radar systems with binary pseudorandom phase manipulation have already been described in the literature [110-111].

Besides the continuous operating mode of a system with pseudorandom phase manipulation, the pulsed mode is also possible. In this case the emitted pulse signal is phase manipulated throughout its length by a single period of a binary pseudorandom sequence. In this case the operation of the transmitter and receiver can be dispersed in time. The length of the signal comprises a fraction of the repetition period of the system. Therefore, it is considerably easier to implement an optimum filter for this signal.

However, in this case the signal energy and accordingly the effective range of the system are less with the same peak transmitter power. Moreover, the autocorrelation properties of this signal are considerably worse than those with analog operating mode--the excess of the maximum autocorrelation function of the signal above the highest absolute value of its side blips comprises approximately \sqrt{N} rather than N .*

These pseudo-noise signals are used not only in radar but in space radio communications as well [96].

We note in conclusion that the autocorrelation function of complex amplitude shown in Fig 4.2.1 has a signal whose phase is manipulated not only by a binary pseudorandom sequence but by quadratic residue (or Legendre) sequences and some others described in the books of V. I. Tikhonov [15] and S. Golomb [96]. As an example let us present two quadratic residue sequences: $++-++++---+-$ ($N = 11$) and $++---++++-+-+-----++-$ ($N = 19$). These sequences are generated by more complicated circuits than in the case of binary pseudorandom sequences. The optimum filters for these signals are constructed by the same block diagrams (Figs. 4.2.6 and 4.2.7). 17

4.3. Signals Manipulated in Phase by Frank Code Law

The digital analog of a signal whose frequency is modulated by linear law and accordingly whose phase is modulated by quadratic law is a multiphase Frank signal [112]. It has constant amplitude and carrier frequency and consists of $N = n^2$ elementary radio pulses of length τ_0 and initial phase constant during the length of each pulse. The value of the initial phase during the length of the k -th pulse ($k = 1-N$) is

$$\varphi(k) = 2\pi \frac{p}{n} \gamma(k), \quad (4.3.1)$$

where p and n are relatively prime whole numbers;

The regular method of synthesizing pulsed FM signals was developed by D. Ye. Vakman [214]. Phase manipulation by random law inside a pulse and from period to period is also of interest [215].

$$\gamma(k) = E\left(\frac{k-1}{n}\right) \left[k - E\left(\frac{k-1}{n}\right)n - 1 \right]; \quad (4.3.2)$$

and $E(x)$, as before, is the whole part of the number x .

Unfortunately, the complex formula (4.3.2) is insufficiently descriptive. Therefore, the values of coefficients $\gamma(k)$ that characterize the law of variation of the initial signal phase are usually written sequentially on the lines of the following matrix of rank $n \times n$:

$$\begin{bmatrix} 0 & 0 & 0 & \dots & 0 & 0 \\ 0 & 1 & 2 & \dots & n-2 & n-1 \\ 0 & 2 & 4 & \dots & 2(n-2) & 2(n-1) \\ 0 & 3 & 6 & \dots & 3(n-2) & 3(n-1) \\ \dots & \dots & \dots & \dots & \dots & \dots \\ 0 & n-2 & 2(n-2) & \dots & (n-2)(n-2) & (n-2)(n-1) \\ 0 & n-1 & 2(n-1) & \dots & (n-1)(n-1) & (n-1)(n-1) \end{bmatrix} \quad (4.3.3)$$

171

Thus, the initial signal phase varies intermittently at the moment one elementary pulse ends and the next one begins. The law of this variation approximates the quadratic law of phase variation of a signal with linear frequency modulation.

If this multiphase signal is repeated with period $T = N\tau_0$, then the autocorrelation function of this signal will also be periodic and equal to zero at any time shifts, with the exception of the neighborhoods (of width $2\tau_0$) of those points in which this function reaches a maximum.

A single period of a multiphase signal is used as the emitted pulse with pulsed operating mode. In this case the excess of the maximum autocorrelation function above the highest side blip increases with an increase of the number of elementary pulses in a multiphase signal (see the solid curve in Fig. 4.3.1, plotted on the basis of materials from [112]) and essentially does not differ from $3\sqrt{N}$ at $N \geq 9$ (see the dashed curve in the same figure). In this sense multiphase signals are considerably better than all other known discrete signals (with the exception of signals with phase manipulation by Barker code law) and specifically of signals manipulated in phase by a single period of a binary pseudorandom sequence.

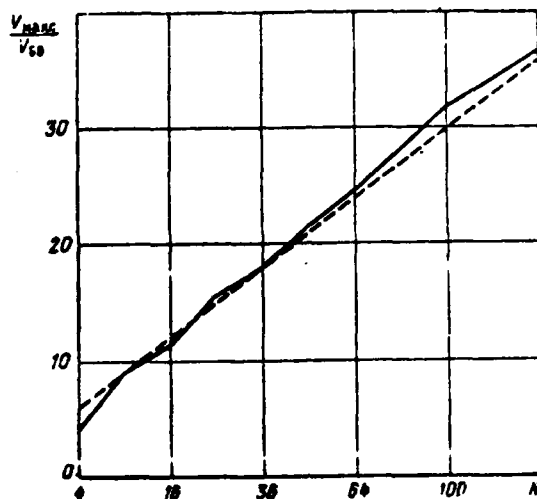


Fig. 4.3.1. Excess of maximum above highest side blip of correlation function of multiphase signal as function of N .

Multiphase code (4.3.2) or (4.3.3) consists of n groups, in each of which the phase shift varies at a constant rate, which increases uniformly from group to group. This property of the code permits one to construct very simple multiphase signal generators. Specifically, a combination of a single radio pulse generator of length τ_0 and an adder encompassed by feedback through an attenuator m times ($m < 1$), a delay device by time τ_0 and phase inverter by angle $\theta(l) = (2\pi p/n)l$ (where l is varied by a special program from group to group in the range from 0 to $n - 1$), an amplitude limiter that eliminates signal amplitude variations (which occur during circulation through the defect circuit of the adder) and an amplifier can be used as such a generator.

The optimum filter for these signals contains a delay device by time $(N - 1)\tau_0$ with $(N - 2)$ uniformly arranged leads and also in the general case N phase shifters by angle $\psi(i) = 2\pi - \phi(N - i)$, where $i = i - N$, and an adder. Essentially, the number of phase shifters is appreciably less than N since the phase rotation angle $\psi(i) = 2$ for values of i for which $\gamma(N - i) = 0$ modulo n according to (4.3.2) or (4.3.3), and there is no need for a phase shifter. A digital optimum filter can also be used along with an analog filter [113].

The optimum filter is unfortunately rather complicated at large value of N .

OPTIMUM FILTERS FOR SEQUENCES OF PULSED SIGNALS

5.1. DESIGN OF FILTERS OPTIMUM TO SEQUENCE OF VIDEO PULSED SIGNALS

1. Preliminary Remarks

In radar, the signal to be received is usually a pulse sequence (Fig. 5.1.1, a). Their repetition period (or quasi-period*) T is determined by the repetition period of pulses generated by the system transmitter. The envelope of the sequence of these pulses in the case of circular scanning accomplished by the radar system is determined by the shape of the antenna radiation pattern. If there is no circular scanning, the envelope of the sequence has a rectangular shape and the length of this sequence is equal to the time during which the transmitter emits sounding pulses while the receiver receives the reflected signals.

The design of optimum filters for sequences of video pulse signals formed by coherent detection of the corresponding sequences of radio pulse signals is considered in the given section.

*The term "quasi-period" is used with regard to the fact that the sequence of a limited number of repeated pulses is not, strictly speaking, periodic and therefore has no period.

The importance of this consideration follows from the fact that, as established in section 2.5, the use of optimum filters for single pulsed signals having no angular (i.e., frequency or phase) modulation permits one to achieve a comparatively slight gain in noise stability compared to the use of resistance-coupled, tuned and bandpass amplifiers. Devices similar in properties to an optimum filter for pulsed signal sequences permit a considerable increase of the noise stability of the system.

176

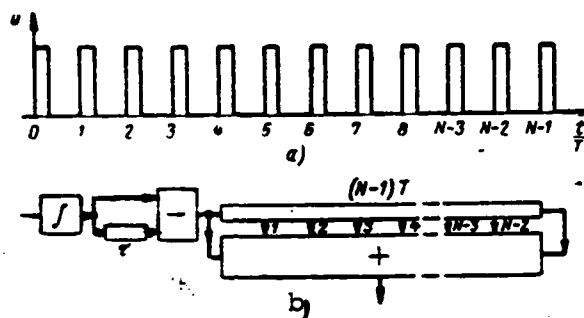


Fig. 5.1.1. Square-wave video pulse sequence (a) and block diagram of optimum filter (b).

Further, for brevity, the term "square-wave pulsed signal sequence" is used instead of the term "sequence of pulsed signals with square-wave envelope."

2. Design of Filter Optimum to Square-Wave Pulsed Signal Sequence

Let a signal be a square-wave sequence of N square-wave pulsed signals (Fig. 5.1.1, a). The problem is to select the linear device whose pulse characteristic reproduces the shape of this signal in some scale.

It was shown above (section 2.1, item 2) that a single square-wave video pulse is formed as a result of the effect of a single pulse on a filter optimum to this video pulse and consisting of an integrating, delay by pulse length τ and subtraction devices (Fig. 5.1.2).

1

The combination of a $N - 1$ delay device (each by the repetition period of pulsed signals T) and adder or an equivalent system of one delay device by time $(N - 1)T$ with $N - 2$ uniformly arranged leads and

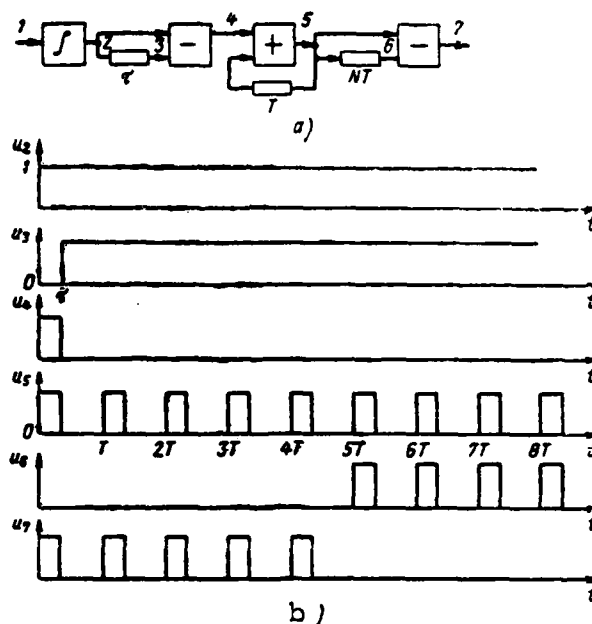


Fig. 5.1.2. Second block diagram of optimum filter and time diagrams of voltages.

an adder can be used to convert this video pulse to a sequence of N pulses (Fig. 5.1.1, b). Since the number of pulses N in the sequence is usually high and reaches several tens and even hundreds, then this optimum filter is very complicated and its use is unfeasible for this signal.

Therefore, let us attempt to obtain a different block-diagram of the optimum filter. We note that a single video pulse is converted to an infinite series of these pulses with repetition period T using an adder whose output is connected to the input by a delay device by time T (Fig. 5.1.2, a). To obtain a sequence of N video pulses from an infinite sequence (but existing only at $t > 0$), it is sufficient to feed an infinite sequence to the combination of the delay device by time NT and the subtraction device (Fig. 5.1.2, a).

17

Therefore, an optimum filter for a square-wave sequence of N video pulses consists of an optimum filter for a single video pulse, an adder included with feedback through a delay device by time T , a delay device by time NT and a subtraction device (Fig. 5.1.2, a). The time diagrams of voltages at different points of this optimum filter with a single pulse acting at the input are shown in Fig. 5.1.2, b).

The same structure of the optimum filter can also be achieved by the spectral method of design [114].

A square-wave sequence of N square-wave video pulses of amplitude V and length τ has the spectrum [115-116]

$$S(\omega) = 2V \frac{\sin \frac{\omega\tau}{2}}{\omega} \frac{\sin \frac{N\omega T}{2}}{\sin \frac{\omega T}{2}} =$$

$$= Ve^{-j\frac{\omega}{2}[\tau + (N-1)T]} \frac{e^{j\omega\tau} - 1}{j\omega} \frac{e^{j\omega NT} - 1}{e^{j\omega T} - 1}.$$

Using (1.5.1) and assuming that

$$C = \frac{1}{V} \quad \text{and} \quad t_0 = \frac{\tau + (N-1)T}{2},$$

we find the transfer function of the optimum filter

$$\bar{K}(\omega) = \frac{1}{j\omega} (1 - e^{-j\omega\tau}) \frac{1}{1 - e^{-j\omega T}} (1 - e^{-j\omega NT}). \quad (5.1.1)$$

The first two multipliers are the transfer function (2.1.1) of an optimum filter for a single video pulse. It is easy to see that $1/1 - e^{-j\omega T}$ is the transfer function of an adder with feedback through a delay device by time T and that $1 - e^{-j\omega NT}$ is the transfer function of the combination of a delay device by time NT and a subtraction device. Accordingly, we again find the same block diagram of an optimum filter (Fig. 5.1.2, a).

17'

An optimum filter can be constructed in similar fashion for trapezoidal, triangular and other sequences of video pulses [7, 114]. This construction is easiest by using the congruence of an optimum filter for a video pulse and a pulse sequence with envelope of the same shape.

3. Congruence of Optimum Filters for a Video Pulse and Pulse Sequence With Envelope of Same Shape. Relationship Between Spectra of These Signals.

Consideration of an optimum filter for pulse sequences of any shape shows that they consist of two parts. The first part is an optimum filter for a single pulse, from which the sequence is formed, and it is determined only by the shape of this pulse and its parameters.

The second part is not dependent on the pulse parameters and is determined by the shape of the envelope of the pulse sequence. Therefore, we feel that it can be called an optimum filter for the envelope of a sequence.

Comparing an optimum filter for a square-wave envelope of a sequence (Fig. 5.1.2, a) with optimum filter for a video pulse of the same shape (Fig. 2.1.2), it is easy to find the congruence of the components of these filters. Thus, an adder with delayed feedback in a filter optimum to the envelope of the sequence of the same shape conforms to the integrator in an optimum filter for a video pulse. This is quite natural since this adder is essentially the integrator of the envelope.

A delay device by the time of the length of the envelope of sequence NT (Fig. 5.1.2, a) and so on corresponds to a delay device by the time of the length of video pulse τ (Fig. 2.1.2).

This congruence permits one to construct a block diagram of an optimum filter for the envelope of a pulse sequence of the same shape from the block diagram of an optimum filter for a video pulse. 180

The reason for the indicated mutual correspondence consists in the fact that the video pulse and envelope of the sequence have identical shape [7, 117]. Therefore, there is coupling between their spectra.

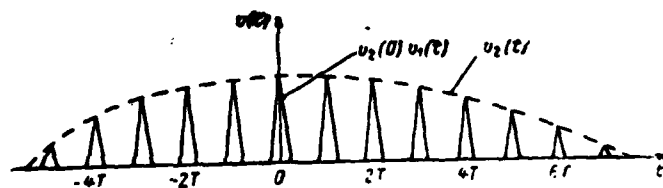


Fig. 5.1.3. Video pulse sequence.

Actually, let a signal $v(t)$ be a sequence of video pulses of identical shape $v_1(t)$, lagging behind each other by a time that is a multiple of T and that have amplitude which varies by the law of the envelope of the sequence $v_2(t)$ (Fig. 5.1.3):

$$v(t) = \sum_{n=-\infty}^{+\infty} v_2(nT) v_1(t - nT).$$

One can then show [7] that the spectrum of this sequence is

$$\bar{S}(\omega) = \bar{S}_1(\omega) \bar{S}_2(\omega), \quad (5.1.2)$$

where $\bar{S}_1(\omega)$ is the spectrum of a single pulse of the sequence having amplitude equal to 1;

$$\bar{S}_1(\omega) = \sum_{n=-\infty}^{\infty} v_1(nT) e^{-j\omega nT} = \sum_{k=-\infty}^{\infty} \bar{S}_1(\omega + k\Omega); \quad (5.1.3)$$

and $\bar{S}_2(\omega)$ is the spectrum of the envelope of sequence $v_2(t)$.

Function $\bar{S}_3(\omega)$ describes the spectrum which has period $\Omega = 2\pi/T$ and maximums at frequencies that are a multiple of this period, since for any integer k

18

$$\bar{S}_1(\omega + k\Omega) = \sum_{n=-\infty}^{\infty} v_1(nT) e^{(-j\omega + k\frac{2\pi}{T})nT} = \bar{S}_1(\omega)$$

and

$$\begin{aligned} \bar{S}_1(k\Omega) &= \bar{S}_1(0) = \sum_{n=-\infty}^{\infty} v_1(nT) = \sum_{n=-\infty}^{\infty} |v_1(nT)| = \\ &= S_{1, \max} > S_1(\omega). \end{aligned}$$

It follows from (5.1.3) that the spectrum $\bar{S}_3(\omega)$ of the lattice function $f[n] = v_2(nT)$ is equal to the sum of the spectra of its continuous envelope $v_2(t)$, shifted along the axis of frequencies by values k that are a multiple of the pulse repetition rate in the sequence, and k varies from $-\infty$ to $+\infty$.

The width of each of the spectra of sum (5.1.3) obviously has an order of magnitude inverse to the length of the envelope τ_2 , i.e., $\Delta\Omega_{3k} \approx 2\pi/\tau_2$. Since the length of the envelope of the sequence is usually much greater than the pulse repetition quasi-period in this sequence-- $\tau_2 \gg T$, then the width of each of the spectra of the sum is much less than the repetition rate Ω , which is equal to the period of this spectrum.

Thus, the spectrum $\bar{S}_3(\omega)$ is periodic, with comparatively narrow maximums at frequencies that are a multiple of the repetition rate, and the maximums are separated from each other by regions of very low values.

Thus, the spectrum $\bar{S}_3(\omega)$ has the shape of a comb (Fig. 5.1.4, a) and is therefore called a comb spectrum [116].

The spectrum of the pulse sequence $\bar{S}(\omega)$, which is the product of the uniform comb-shaped spectrum $\bar{S}_3(\omega)$ and the spectrum of a single pulse $\bar{S}_1(\omega)$ (Fig. 5.1.4, b) due to (5.1.2), is also comb-shaped (Fig. 5.1.4, c), but is no longer a uniform but a modulated spectrum $\bar{S}_1(\omega)$.

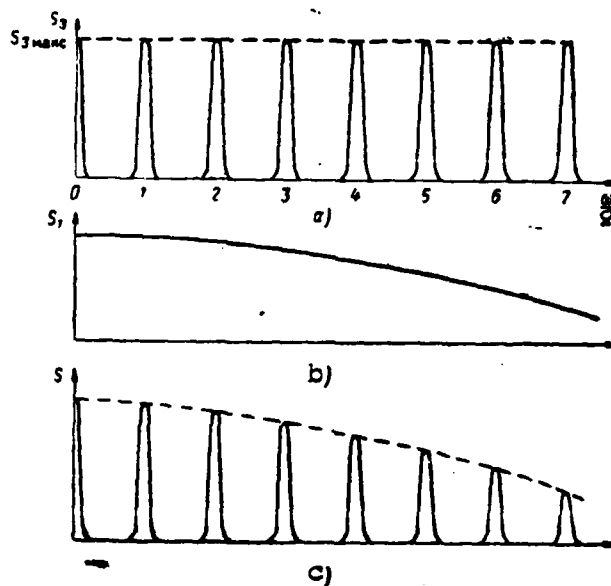


Fig. 5.1.4. Comb-shaped spectra (a and c) and single pulse spectrum (b).

As indicated above, this property of being comb-shaped is typical for the spectra of sequences of periodically repeated pulses with envelopes of any shape. Therefore, the optimum filter for any sequences of periodically repeated pulses should contain a device with a comb-shaped frequency characteristic, which is called a comb filter [116, 118, 119].

4. Identity of Filter Optimum to Pulse Sequence and of Ideal Comb Filter

A comb filter is, for example, an adder with feedback delayed by time T , supplemented with a delay device by time PT and a subtraction device (here P is some integer equal to, for example, the number of pulses in sequence N). A system of a delay device by time $(P - 1)T$

with $(P - 2)$ uniformly arranged leads and an adder is completely equivalent to this device (Fig. 5.1.1, b).

These comb filters have the transfer function

$$K(\omega) = \frac{1 - e^{-j\omega PT}}{1 - e^{-j\omega T}} = e^{-j\omega \frac{PT}{2}} f(\omega, T, P), \quad (5.1.4)$$

where

$$f(\omega, T, P) = \frac{\sin \frac{\omega PT}{2}}{\sin \frac{\omega T}{2}} \quad (5.1.5)$$

is an ideal comb function (Fig. 5.1.5). Its frequency period is equal to Ω at odd value of P and 2Ω at even value of P . The period of the transfer function of comb filter (5.1.4) is equal to the repetition rate Ω regardless of whether the number P is even or odd. The maximum values of this function increase as P increases, while the frequency zones corresponding to the higher values of the function are constricted.

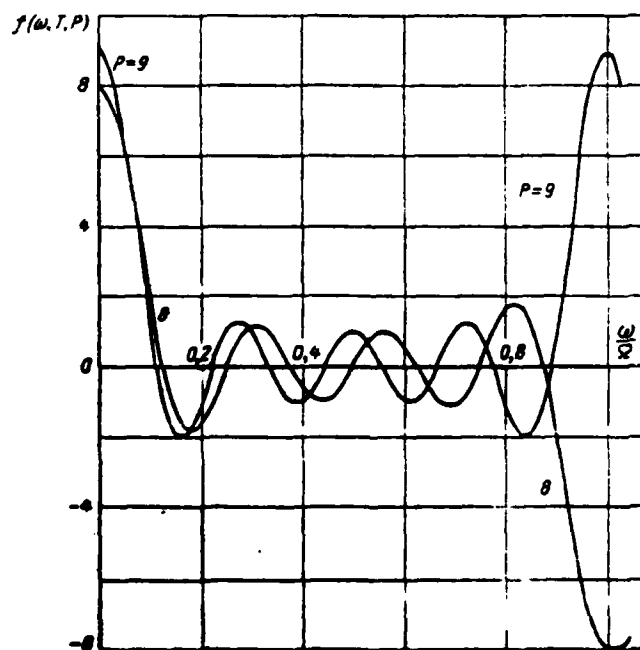


Fig. 5.1.5. Ideal comb functions.

Let us consider a simple example of a square-wave pulse sequence of any shape. In this case

$$\left. \begin{aligned} v_2(nT) &= V \quad \text{at } |n| \leq M, \\ v_2(nT) &= 0 \quad \text{at } |n| > M \end{aligned} \right\}$$

and

$$\begin{aligned} \bar{S}_1(\omega) &= \sum_{n=-\infty}^{+\infty} v_2(nT) e^{-j\omega nT} = V \frac{\sin \frac{2M+1}{2} \omega T}{\sin \frac{\omega T}{2}} = \\ &= V f(\omega, T, N), \end{aligned}$$

where $N = 2M + 1$.

Moreover,

$$S_{\text{max}} = \bar{S}_1(k\Omega) = VN \quad \text{and} \quad \bar{S}(\omega) = V \bar{S}_1(\omega) f(\omega, T, N).$$

The latter expression in the case of square-wave pulses coincides with that presented in section 2. The spectrum of a square-wave sequence of square-wave pulses is plotted in Fig. 5.1.6.

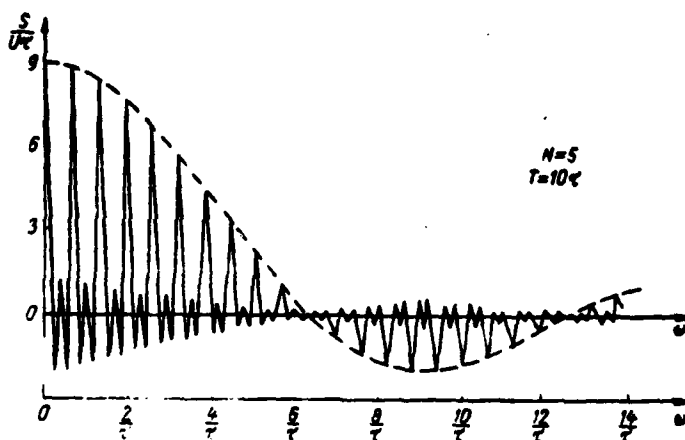


Fig. 5.1.6. Comb spectrum of pulse sequence.

Since the transfer function of an optimum filter differs only by the multiplier from the signal spectrum (of symmetrical shape), then the optimum filter for a pulse sequence is an ideal comb filter completely matched to the spectrum of this sequence. It is also distinguished by this from comb filters that are a set of ordinary resonance filters tuned to frequencies that are a multiple of the repetition rate [116, 120].

The number of these resonance filters is equal to the ratio of the bandpass to the repetition rate

$$\nu = \frac{\Delta\Omega}{\Omega} = \frac{\Delta F}{F} = \Delta FT.$$

The bandpass of a comb filter is selected from the condition of the permissible distortion of the pulse when it passes through the comb filter $\Delta F = b/\tau$, where b is a coefficient on the order of one or a fraction of it. Therefore,

$$\nu = \frac{bT}{\tau} = b Q, \quad (5.1.6)$$

where Q is the on-off time ratio of the pulses in the sequence, which has an order of a thousand in radar. Assuming that b is equal to a comparatively low value of 0.5 and that $Q = 1,000$, we find $\nu = 500$.

A comb filter in the shape of a set of this number of resonance filters tuned rather precisely to frequencies that are a multiple of the repetition rate is a very cumbersome device and one complicated to tune and operate. Specifically, the problem of precise phasing of the oscillations taken from the separate circuits during their addition in the adder is very complicated. The use of such a comb filter is feasible only if there is a low on-off time ratio of pulses in the sequence [120] and low requirements on the quality of the pulse at the output of this filter when coefficient b can be selected as sufficiently small. In this case the pulse will be strongly extended in time and its time position can be determined only with a large error.

5. Realizability of Optimum Filters for Sequence of Pulses

180

It was shown above that an optimum filter for a pulse sequence consists of one for a single pulse, an adder with delayed feedback, a delay device and a subtraction device.

All these components, with the exception of the adder with delayed feedback, can be accomplished. If an adder with delayed feedback is made, it is unstable and will be self-exciting since its feedback coefficient is equal to one. To eliminate the self-excitation of this device, one must reduce the value of its feedback coefficient. To do

this, a device with transfer coefficient m whose value is less than one is connected to its feedback circuit. It can be called an attenuator.

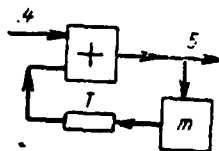


Fig. 5.1.7. Block diagram of recirculator.

If the coupling coefficient m of the device (Fig. 5.1.7) is selected rather close to one (but less than this value), then this device, called a recirculator, will be as close to the ideal in its properties that losses in the signal/noise ratio will be insignificant. This problem is investigated in detail in section 5.3.

5.2. Optimum Filters for Sequences of Radio Pulse Signals

1. Preliminary Remarks

Optimum filters for sequences of radio pulse signals have both the gains of optimum filters for radio pulses and the gains of those for pulse sequences in front of optimum filters for single pulses. Therefore, they are of great interest.

18

Let us distinguish radio pulse sequences of two kinds*:

1. A radio pulse sequence of first kind (Fig. 5.2.1, c), which is formed by amplitude pulse modulation of a continuous harmonic oscillation (Fig. 5.2.1, a) by a video pulse sequence (Fig. 5.2.1, b). In this case the initial phases of the different radio pulses of the sequence are different in the general case (if the product of the carrier frequency f_0 by the repetition quasi-period T differs from an integer).

*The given classification of radio pulse sequences is not generally accepted and is introduced only for convenience of exposition.

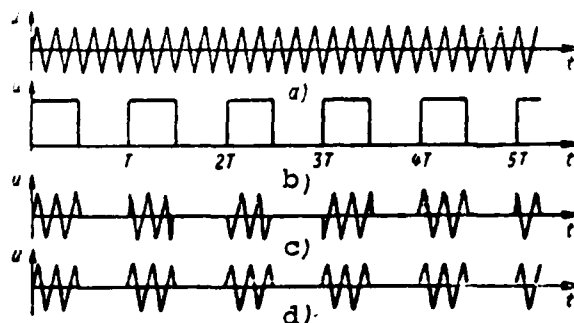


Fig. 5.2.1. Formation of radio pulse sequences.

2. Radio pulse sequence of second kind (Fig. 5.2.1, d), which consists of radio pulses with identical initial phases. These radio pulses differ by time position: they are delayed with respect to the first pulse by a time that is a multiple of the repetition quasi-period T .

If the product of the carrier frequency f_0 by the repetition quasi-period T is an integer, i.e., the repetition quasi-period is a multiple of the period of the carrier oscillation, these sequences are completely identical.

If the sequence consists of radio pulses with different initial phases, but the law of their variation is known (for example, in the case of a radar station when the difference of initial phases of the received radio pulses is determined by the difference of the initial phases of the emitted radio pulses), then this sequence can be converted by means of coherent-pulse equipment [154] to a radio pulse sequence of both the second and first kind.

188

Finally, if the sequence consists of radio pulses with random initial phases, then this sequence cannot be reduced to a sequence of the first or second kind and is noncoherent (see item 2, section 6.2). Optimum filtration of this sequence on a radio frequency is impossible and can be done only after it is converted by means of amplitude detection to a video pulse sequence.

2. Optimum Filters for Radio Pulse Sequences of First Kind

Using the congruence of an optimum filter for video and radio pulses, established in item 3, section 2.2, it is easy to construct an optimum filter for sequences of radio pulse signals of first kind from known optimum filters for sequences of video pulse signals (see section 5.1).

It is shown in item 2, section 5.1, that an optimum filter for a square-wave sequence of video pulse signals consists of an optimum filter for a single pulse of this sequence, an adder with feedback delayed by T , a delay device by time NT and a subtraction device (Fig. 5.1.2, a).

However, as follows from item 3, section 2.2, the combination of a delay device by time T and phase shifter by angle $\chi(T) = 2\pi R(f_0 T)$ in a radio-frequency optimum filter corresponds to a delay device by the same time in a video frequency optimum filter. In like fashion, the combination of the same delay device and phase shifter by angle $\chi(NT)$ corresponds to a delay device by time NT in a video frequency optimum filter. Moreover, an optimum filter for a single video pulse corresponds to one for a radio pulse (see section 2.2).

189

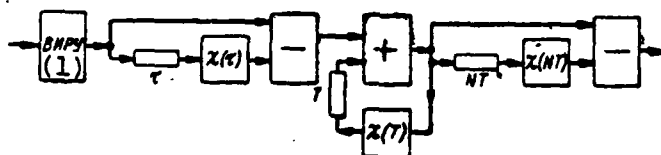


Fig. 5.2.2. Block diagram of optimum filter for radio pulse sequence of first kind.

Key: (1) Highly selective tuned amplifier.

Because of the foregoing, an optimum filter for a square-wave sequence of square-wave radio pulses consists of a highly selective tuned amplifier, a combination of delay device by time τ and phase shifter by angle $\chi(\tau)$, an adder encompassed with feedback through a delay device by time T and a phase shifter by angle $\chi(T)$, a combination of a delay device by time NT and a phase shifter by angle $\chi(NT)$ and two subtraction devices (Fig. 5.2.2).

In similar fashion, using an optimum filter for a trapezoidal video pulse sequence (item 3, section 2.4), and also the congruence of the

components of video and radio frequency optimum filters noted above, it is easy to construct an optimum filter for the indicated radio pulse sequence of first kind.

3. Optimum Filters for Radio Pulse Sequences of Second Kind

It is easy to see that the use of phase shifters by angles $\chi(T)$ and $\chi(NT)$ in an optimum filter for a square-wave radio pulse sequence of first kind (Fig. 5.2.2) is caused by the fact that the radio pulses being fed to the adder or subtraction device should have identical initial phases for normal operation of this filter.

In the case of radio pulse sequences of second kind, the initial phases of separate radio pulses are identical and therefore there is no need to use an optimum filter of the indicated phase shifters (however, a phase shifter that rotates the phase by angle $\chi(\tau)$ should be retained in the general case). 190

Accordingly, the block diagram of an optimum filter for the envelope of a radio pulse sequence of second kind coincides completely with that of an optimum filter for the envelope of the corresponding sequence of video pulse signals.

The block diagram of an optimum filter for a radio pulse sequence of second kind differs from that of an optimum filter for the corresponding video pulse sequence by the presence of an optimum filter for a radio pulse instead of one for a video pulse.

The difference in the circuits and designs of these filters is more significant since the adder and subtraction devices, designed to admit video pulses, will differ considerably from similar devices designed to operate with radio pulses.

Incomparably more rigid requirements are placed on delay devices used in optimum filters for radio pulse sequences (and for radio pulses) in the ratio of accuracy and stability of delay time T (and τ) than in the case of optimum filters for video pulse sequences (and for video pulses) [13].

Whereas instability of delay time Δt_3 should be much less in the latter case than the pulse length τ :

$$\Delta t_3 \ll \tau,$$

the following condition must be fulfilled in the case of radio pulses:

$$\Delta t_3 \ll T_0 = \frac{1}{f_0}.$$

If this condition is observed, pulses being fed to the adder (subtraction device) will not be in phase, which disrupts normal operation of an optimum filter. Because of this, optimum filters for radio pulse sequences are considerably more difficult to accomplish than optimum filters for video pulse sequences.

It is for this reason that optimum processing of radio pulse sequences is usually carried out by preliminary conversion by means of detection to a video pulse sequence and subsequent optimum filtration on the video frequency rather than by direct optimum filtration on the radio frequency. In order that these methods of processing be equivalent, it is necessary that detection be a linear operation, i.e., that the detector be cophasal (coherent). This problem is discussed in more detail in the next chapter.

5.3. Operating Mechanism of Optimum Filter for Square-Wave Sequence Square-Wave Pulses

1. Signal Transmission

If the indicated sequence acts on the input of an optimum filter for a square-wave pulse sequence (Fig. 5.1.2, a), the voltages at different points of this filter vary according to the time diagrams shown in Fig. 5.3.1, where $T = 3\tau$ and $N = 5$ are selected to simplify the p

An optimum filter for a single pulse, by accomplishing optimum matched processing of the signal, converts each square-wave pulse of the sequence to a triangular pulse of double length (Fig. 5.3.1, b). The first pulse of this sequence is transmitted to the first input of the adder, and the second pulse is fed to the second input of the adder. The output of the adder coincides in this case in time with the

second pulse of the sequence. A pulse of double amplitude is formed at the output as a result of their addition. A pulse of triple amplitude is generated at the output after delay by T and addition with the third pulse.

This process of a sequential increase (storage) of pulse amplitude (and generally of voltage) in the adder is continued until pulses are fed to its input. After the last (n -th) pulse arrives, the pulse amplitude at the output of the adder will be N times greater than that at the input. This pulse will then be repeated with quasi-period T (Fig. 5.3.1, c). 192

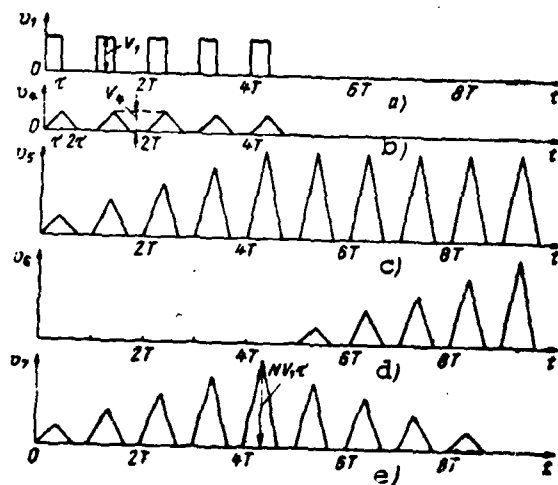


Fig. 5.3.1. Time diagrams of voltages in optimum filter for pulse sequence.

The sequence formed in this manner is fed directly to the subtraction device with delay by time NT (Fig. 5.3.1, d). As a result, a triangular sequence $(2N - 1)$ of triangular pulses will be formed at the output of the subtraction device (Fig. 5.3.1, e). The middle pulse of this sequence has the greatest amplitude

$$V_{T \text{ max}} = NV_{1T}, \quad (5.3.1)$$

which does not differ from the pulse amplitude of the sequence at the output of the adder after completion of the signal at the output.

Thus, the combination of the delay device by time NT and of the subtraction device does not change the signal amplitude and, as will 193

be shown further, it is required only to attenuate the noise output.

2. Noise Transmission

Using (1.7.1), it is easy to show that the noise at the output of an optimum filter for a single pulse (Fig. 5.1.2, a) has the autocorrelation function (Fig. 5.3.2)

$$\begin{aligned} R_n(t) &= a(\tau - |t|) \text{ at } |t| \leq \tau, \\ R_n(t) &= 0 \text{ at } |t| > \tau. \end{aligned} \quad (5.3.2)$$

and output $\sigma_i^2 = a\tau$ (see 2.3.11)).

Accordingly, the two instantaneous values of noise separated by a time interval whose value is greater than the pulse length are completely uncorrelated.

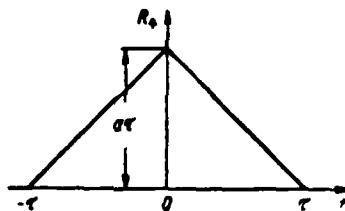


Fig. 5.3.2. Correlation function of noise at output of optimum filter for pulse.

The noise at the output of the adder is obviously the sum of the noise oscillations being fed to its input at a given moment and at moments of time that precede it by a time that is a multiple of the duration of the delay in the feedback circuit:

$$u_n(t) = \sum_{k=0}^{\infty} u_n(t - kT).$$

The number of these noise components is infinitely high since noise is fed continuously to the optimum filter. As a result of (5.3.2) and the fact that the repetition quasi-period is considerably greater than the pulse length:

$$T \gg \tau, \quad (5.3.3)$$

these components are uncorrelated with each other. Therefore, their outputs are added. Since the number of terms is infinitely great, the noise output at the output of the adder is an infinite number of times greater than the output at its input (2.3.11), i.e.,

$$\sigma_s^2 = \infty. \quad (5.3.4)$$

Because of this, the signal/noise ratio at the output of the adder is equal to zero with any finite number of pulse signals N .

However, noise has a finite output after further transmission of the combination of delay device by time NT and subtraction device. This is explained by the fact that the noise at the output of the adder is repeated with quasi-period T and therefore its values for two moments of time separated by an interval that is a multiple of T are completely correlated. Because of this, two oscillations of infinite output, but completely correlated, are subtracted in the subtraction device. In this case the noise output is reduced an infinite number of times and as will be shown below, becomes finite.

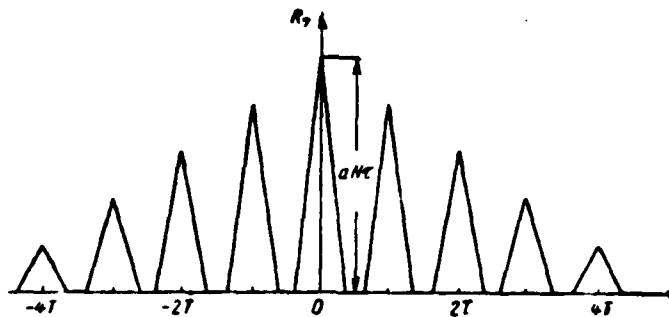


Fig. 5.3.3. Correlation function of noise at output of optimum filter for pulse sequence.

To determine the value of this output, let us calculate the autocorrelation function of output noise, making use of (1.7.1) and the previously found pulse characteristic of an optimum filter (u_7 in Fig. 5.1.2, b). The autocorrelation function of noise calculated in this manner at the output of an optimum filter (Fig. 5.3.3) differs from the signal voltage at the output of an optimum filter (Fig. 5.3.1, e) only by scale and shift toward a decrease of time by the value $t_0 = (N - 1)T + \tau$.

The maximum achieved by this function at $t = 0$ also characterizes the noise output

$$\sigma_f^2 = R_f(0) = aN\tau. \quad (5.3.5)$$

The latter is N times greater than the noise output (2.3.11) at the input of the adder. This is equivalent to addition of the output of noise oscillations during N repetition periods, i.e., during the duration of the signal at the input.

Thus, the combination of the delay device by time NT and the subtraction device, without changing the signal level, considerably reduces the noise output, limiting the time of its storage by the signal length. Because of this, the indicated combination can be called the limiter of the storage time of input oscillations up to the expected signal length.

The signal/noise ratio at the output of an optimum filter

$$q_z^2 = \frac{V_{\text{max}}^2}{\sigma_f^2} = N \frac{V_s^2}{a} \quad (5.3.6)$$

is N times greater than this ratio at the input of the adder (2.3.12) and fully agrees with the general formula (1.2.11).

The same finite results are also found when considering the transmission of a square-wave sequence of pulse signals and noise through an optimum filter made by a different block diagram (Fig. 5.1.1, b). A total of N determinant pulse signals and the same number of uncorrelated noise oscillations is added in the adder of this filter. As a result the signal at the output is increased N times in voltage, i.e., N^2 times in output, while noise increases N times in output. Accordingly, the signal/noise ratio in output increases N times.

We note that the order of the arrangement of the components can be changed due to the linearity of the different components of an optimum filter (Fig. 5.1.2, a). Thus, for example, an adder with delayed feedback can be placed after a combination of delay device by time NT and a subtraction device. This block diagram of an optimum filter is easiest to accomplish in practice since the noise output stored in the

adder in it will not reach an infinitely large level, but will be finite and equal to (5.3.5). In this case the different components of the optimum filter will operate in a considerably easier mode and therefore they are simpler to realize.

5.4. Operating Mechanism of Systems That are Practical Approximations of Optimum Filter for Pulse Sequence

1. System with Recirculator

The simplest practical approximation of an optimum filter for a pulse sequence is a system which differs from this filter (Fig. 5.1.2, a) by the fact that a recirculator is used in it instead of an unstable adder with delayed feedback (Fig. 5.1.7).

The process of signal transmission through this system differs only by the fact that the signal at the output of the recirculator is stored by exponential rather than by linear law and its amplitude at the output also decreases by exponential law after the end of the signal at the input (Fig. 5.4.1):

$$\left. \begin{aligned} V_s(k) &= v_s[(k-1)T + \tau] = \frac{V_{1\tau}}{1-m} (1-m^k) \\ V_s(k) &= \frac{V_{1\tau}}{1-m} (1-m^N) m^{k-N} \end{aligned} \right\} \begin{array}{l} \text{at } 1 \leq k \leq N, \\ \text{at } k > N. \end{array} \quad (5.4.1)$$

At moment of time $t_0 = (N-1)T + \tau$, the signal reaches maximum amplitude

$$V_{s, \max} = \frac{V_{1\tau}}{1-m} (1-m^N). \quad (5.4.2)$$

Specifically, at $m = 1$ we find (5.3.1).

As in the previous ideal case, further signal transmission through delay device by time NT and the subtraction device causes no variation of the maximum signal level. 19

Since a system of optimum filters for a square-wave pulse and recirculator has the pulse characteristic (Fig. 5.4.2, a)

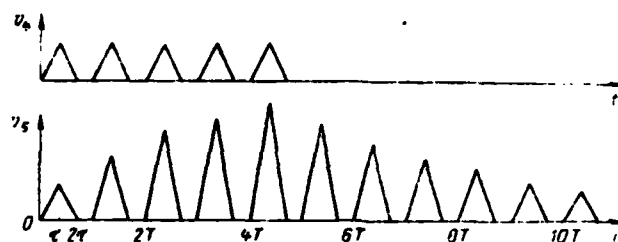
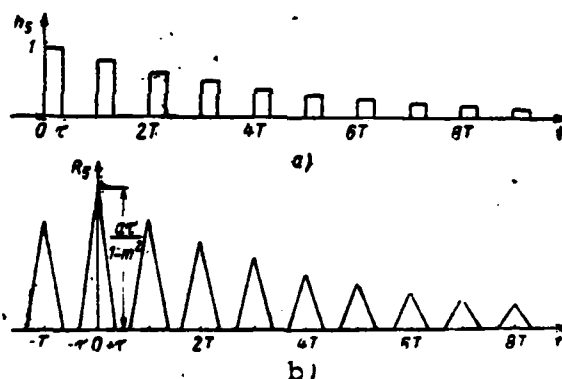


Fig. 5.4.1. Time Diagrams of Voltages at Input and Output of Recirculator at $m = 0.8$ and $M = 5$.

$$h_s(t) = \sum_{k=0}^{\infty} m^k h_s(t - kT),$$

where $h_4(t) = 1(t) - 1(t - \tau)$ is the pulse characteristic of an optimum filter for a square-wave pulse, then, because of (1.7.1), the autocorrelation function of noise at its output has the form shown in Fig. 5.4.2, b.

19



19

Fig. 5.4.2. Pulse characteristic of combination of optimum filter for pulse and recirculator at $m = 0.8$ (a) and correlation function of output noise (b).

The maximum values of this function are observed at moments of time that are multiples of the repetition quase-period T and vary by the law

19

$$R_s(kT) = \frac{a\tau}{1-m^2} m^{|k|}. \quad (5.4.3)$$

Specifically, at $k = 0$, we find the output of this noise

$$\sigma_s^2 = \frac{a\tau}{1-m^2}. \quad (5.4.4)$$

The noise storage coefficient is then

$$Q_1 = \frac{\sigma_5^2}{\sigma_4^2} = \frac{1}{1-m^2}. \quad (5.4.5)$$

Since the voltage at the output of the entire system is equal to the difference of the voltage taken from the output of the adder and the voltage at the output of the delay device by time NT:

$$u_7(t) = u_5(t) - u_6(t) = u_5(t) - u_5(t-NT),$$

then the noise at the output of the entire system has the output

$$\sigma_7^2 = m_1[u_7^2(t)] = 2\sigma_5^2 - 2R(NT) = 2 \frac{\sigma_5^2}{1-m^2} (1-m^N).$$

Accordingly, the noise output is transferred by a combination of delay device by time NT and subtraction device with coefficient

$$Q_1 = \frac{\sigma_7^2}{\sigma_5^2} = 2(1-m^N).$$

This coefficient is less than one, i.e., the noise is attenuated in power, while the signal/noise ratio accordingly increases if $m^N > 0.5$, i.e., if the number of pulses in the sequence satisfies the inequality

$$N < N_0 = \frac{\ln 0.5}{\ln m} \approx \frac{0.7}{1-m}. \quad (5.4.6)$$

Accordingly, the use of the combination of subtraction device and delay device by time NT has meaning only with a comparatively small number of pulses in the sequence or with a feedback coefficient of the circulator sufficiently close to one. Thus, for example, at $N = 20$ the feedback coefficient should be greater than 0.97, which is difficult to achieve in practice.

19

Thus, the use of a combination of delay device (by time NT) and subtraction device in the optimum filter for sequences of a greater number of pulsed signals is usually unfeasible.

This conclusion is very important, especially in practice. The fact is that a delay device by time NT whose value can reach a fraction of a second is practically impossible to accomplish in the form

of an ultrasonic line with sufficiently broad bandpass and moderate attenuation (at least at the given stage of equipment development).

Using (5.4.2) and (5.4.4), we find the ratio of the square of the peak signal and noise output at the output of the recirculator:

$$q_s^2 = \frac{V_1^2}{a} \frac{1+m}{1-m} (1-m^N)^2.$$

Accordingly, the use of a recirculator permits one to achieve a gain in output signal/noise ratio

$$B = \frac{q_s^2}{q_n^2} = \frac{1+m}{1-m} (1-m^N)^2. \quad (5.4.7)$$

With constant value of m , the gain increases with an increase of the number of pulses at first rapidly then more slowly and then essentially remains unchanged (Fig. 5.4.3). The latter is explained by the fact that the signal ceases to be accumulated at $m^N \ll 1$.

Let us call the number N_a at which the gain comprises 0.95 of the maximum possible at given value of m , reached at $N = \infty$, the active number of stored pulses. It follows from this definition that

$$N_a = \frac{\ln 20}{-\ln m} \approx \frac{3}{1-m}. \quad (5.4.8)$$

With a constant number of pulses, the gain increases with an increase of the feedback coefficient and then, passing through maximum at some value of $m = m_0$, drops sharply (Fig. 5.4.4). This is explained by the fact that the signal is fed to the input (and accordingly is stored) during N periods while noise is fed to the input during an infinitely large number of periods. Therefore, the output signal power initially increases more rapidly with an increase of m and then more slowly than noise output. At $m = 1$ the noise output increases without limit while the signal output increases only N^2 times.

Investigating (5.4.7) for the maximum value with respect to m , we find an equation for the optimum feedback coefficient:

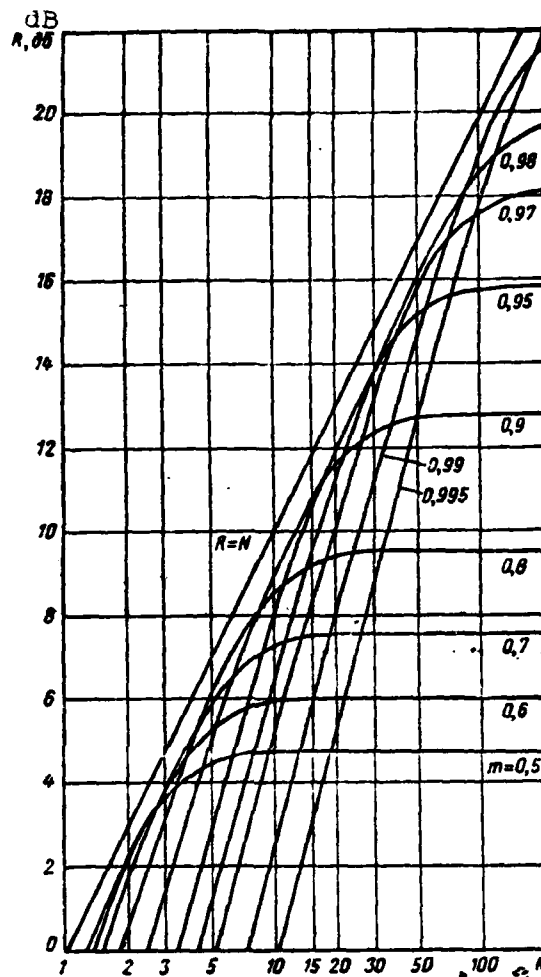


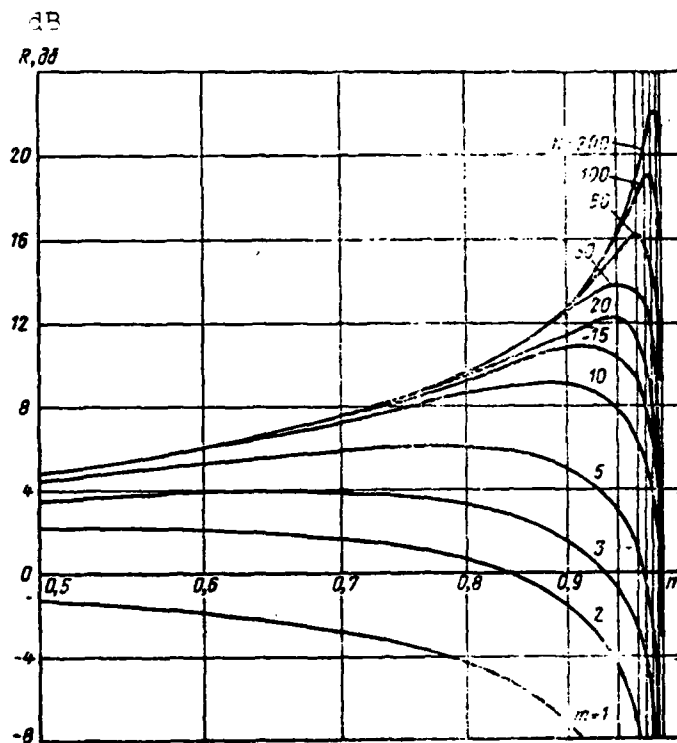
Fig. 5.4.3. Gain as function of N.

$$m_0^{-N} - N \left(\frac{1}{m_0} - m_0 \right) = 1.$$

For the practically important case of large value of N, its root is [121]

$$m_0 = \exp \left(- \frac{1.27}{N} \right) \approx 1 - \frac{1.27}{N}. \quad (5.4.9)$$

The error of calculating the optimum feedback coefficient by this formula is reduced with an increase of N and comprises a fraction of a percent at N = 10. Therefore, $m_0 \approx 0.98$ at N = 50 and $m_0 \approx 0.99$ at N = 100.



201

Fig. 5.4.4. Gain as function of m .

It follows from (5.4.9) and (5.4.7) that the maximum possible gain is

202

$$R_{\text{max}} \approx 0.8N. \quad (5.4.10)$$

Since, as shown in the previous section, an optimum filter for the envelope of a square-wave sequence has the gain N , then a recirculator with optimum feedback coefficient permits one to achieve a signal/noise ratio only a decibel less.

However, to achieve the maximum possible gain in the case of sequences consisting of a large number of pulses, one must increase the feedback coefficient to values very close to one.

In practice this causes difficulties since self-excitation of the circulator occurs with the slightest increase of the feedback coefficient due to instability of the parameters.

To avoid the indicated difficulties when receiving sequences of a large number of pulsed signals and in this case to achieve a further

increase of signal/noise ratio, one can use several rather than one recirculator. This possibility will be considered in the next section.

And now let us explain the conclusions achieved above by the special method on the possibility of replacing an optimum filter by a circulator for the envelope of a square-wave sequence of pulsed signals. The recirculator has the transfer function

$$K(\omega) = \frac{1}{1 - me^{-j\omega T}}$$

and the amplitude-frequency characteristic

$$K(\omega) = \frac{1}{\sqrt{1 - 2m \cos \omega T + m^2}}$$

which is a comb characteristic (see Fig. 5.4.5, plotted for $m = 0.9$). 203

At frequencies that are a multiple of the repetition rate, this characteristic reaches maximum values

$$K_{\max} = K(n\Omega) = \frac{1}{1 - m} \text{ at } n = 0, 1, 2, \dots,$$

and at frequencies of $\omega = (n + \frac{1}{2})\Omega$, it reaches minimum values of

$$K_{\min} = \frac{1}{1 + m}.$$

Thus, the considered device is a comb filter.

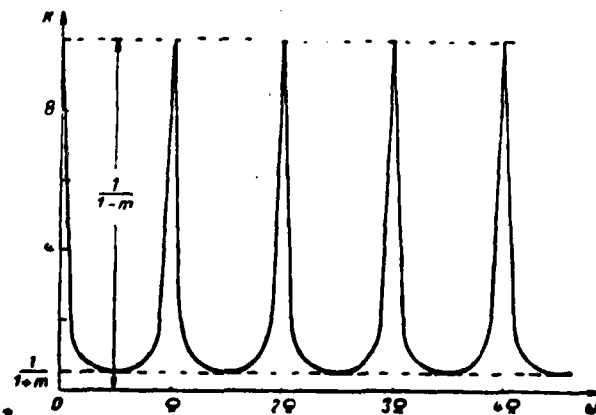


Fig. 5.4.5. Frequency characteristic of recirculator.

If a sequence of pulsed signals and white noise is fed to its input, only those spectral components which have frequencies close to the signal repetition rate are transmitted to its output with large coefficient. They include the most intensive components of the signal spectrum. The remaining signal components and also most spectral components of noise are transmitted to the output with attenuation.

Because of this, the signal/noise ratio at the output of a comb filter is considerably greater than that at the input. The essence of separation of periodic or quasi-periodic signals from a noisy background by means of comb filters is also included in this.

20

2. System With Two Identical Recirculators

Let us consider the operation of a system consisting of an optimum filter for a single pulsed signal (OFOS) and two identical recirculators (Fig. 5.4.6).

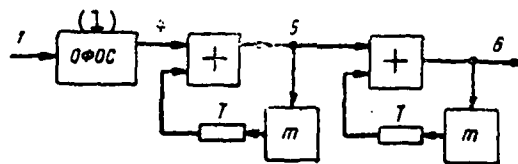


Fig. 5.4.6. Block diagram of double system.
Key: (1) Optimum filter for single pulsed signal

The voltage amplitude of the k -th pulse of a signal at the input of the second recirculator is described by (5.4.1). Therefore, the voltage amplitude of this pulse at the output at $1 \leq k \leq N$ is

$$V_s(k) = v_s[(k-1)T + \tau] = \sum_{l=0}^{k-1} m^l V_s(k-l) = \\ = \frac{V_{1s}}{(1-m)^2} \{1 - m^k [1 - m^k(1-m)]\},$$

and at $k \geq N$ is

$$V_s(k) = \sum_{n=1}^k m^{k-n} V_s(n-1) = \frac{V_{1s}}{(1-m)^2} m^{k-N} \times \\ \times \{1 - m^N - (1-m)[k(1-m^N) - N]\}.$$

Having investigated the last expression for the maximum value with respect to k , we find

$$k_0 = E \left(\frac{N}{1-m^N} - \frac{1}{1-m} - \frac{1}{\ln m} \right) \approx E \left(\frac{N}{1-m^N} - 0,5 \right).$$

The peak value of the output signal is

20

$$\begin{aligned} V_{\text{out}} = V_s(k_0) &\approx \frac{V_1 \tau}{(1-m)^2} m^{k_0-N} \{1 - m^N - (1-m) \times \\ &\times [k_0(1-m^N) - N]\} \approx \frac{V_1 \tau}{(1-m)^2} \frac{3-m}{2} (1-m^N) m^{k_0-N}. \end{aligned} \quad (5.4.11)$$

In the case frequently encountered in practice when $Nm^N < 1$, $k_0 \approx N$ and

$$V_{\text{out}} \approx V_1 \tau / (1-m)^2, \quad (5.4.12)$$

the peak value of the signal at the output is observed at the moment of the end of the last signal at the input. The coefficient of signal storage by the second recirculator comprises $g_2 \approx (1-m)^{-1}$ and coincides with a similar coefficient for the first recirculator.

Output noise $u_s(t) = \sum_{k=0}^{\infty} m^k u_s(t-kT)$ has the output

$$\begin{aligned} \sigma_s^2 = m_1 [u_s^2(t)] &= \sum_{k=0}^{\infty} \sum_{l=0}^{\infty} m^{k+l} m_1 [u_s(t-kT) u_s(t-lT)] = \\ &= \sum_{k=0}^{\infty} \sum_{l=0}^{\infty} m^{k+l} R_s[(k-l)T], \end{aligned}$$

where $R_s(t)$ is the autocorrelation function of noise at the output of the first recirculator.

Using expression (5.4.3) for this function, we find

$$\sigma_s^2 = \sum_{k=0}^{\infty} \sum_{l=0}^{\infty} m^{k+l} \frac{\sigma_1^2}{1-m^2} m^{k-l} = \sigma_1^2 (1+m^2)/(1-m^2)^2. \quad (5.4.13)$$

Accordingly, the coefficient of noise storage by two recirculators is

$$Q_2 = (1+m^2)/(1-m^2)^2, \quad (5.4.14)$$

and by the second recirculator is

$$Q' = Q_2/Q_1 = (1+m^2)/(1-m^2)^2. \quad (5.4.15)$$

AD-A115 395

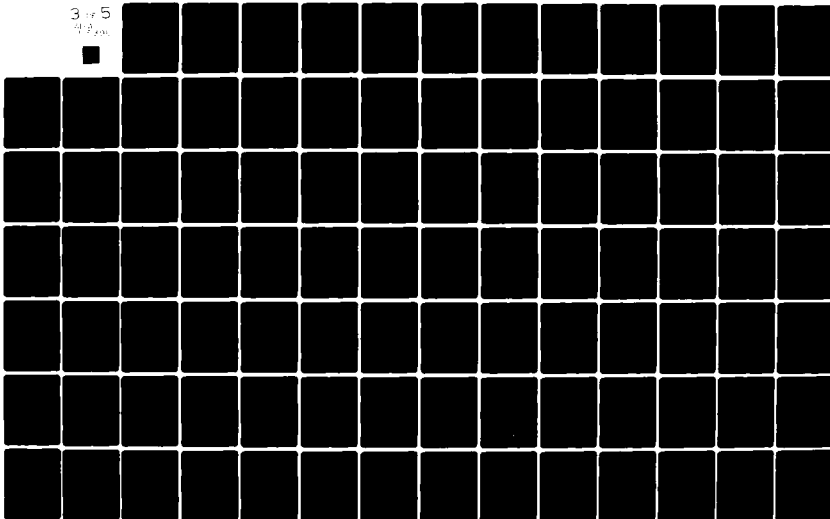
FOREIGN TECHNOLOGY DIV WRIGHT-PATTERSON AFB OH
OPTIMUM FILTERS AND PULSED SIGNAL STORAGE DEVICES (U)
MAY 82 Y S LEZIN
FTD-ID(RS)T-0182-81

F/6 9/5

UNCLASSIFIED

NL

3 of 5
4/8/80



The ratio of the coefficients of noise storage by the second and first recirculators

206

$$\lambda = Q'/Q_1 = (1+m^2)/(1-m^2) \quad (5.4.16)$$

is appreciably greater than one, comprising 9.53 at $m = 0.9$.

Thus, noise is stored in the second recirculator by a completely different law than in the first recirculator, increasing in this case in power a considerably greater number of times. This is explained by the fact that the uncorrelated values of noise are added in the first recirculator, due to which their outputs are added, whereas the instantaneous values of noise separated by an interval that is a multiple of the delay time in the recirculator have a stronger correlation after passage through the first recirculator and are therefore stored in the second recirculator by a law close to the law of gain of a signal which is stored by voltage rather than by power.

The signal/noise ratio at the output of the system comprises

$$q_6^2 = \frac{V_n^2}{\sigma_6^2} \approx \frac{V_1^2}{a} \frac{(1+m)^2}{(1-m)(1+m^2)}, \quad (5.4.17)$$

and the gain in signal/noise ratio is

$$B_2 = \frac{q_6^2}{q_4^2} = \frac{(1+m)^2}{(1-m)(1+m^2)}. \quad (5.4.18)$$

The additional gain due to the second recirculator

$$R = B_1/B_2 = 2 - (1-m)^2/(1+m^2)$$

essentially does not differ from two recirculators at $0.8 \leq m \leq 1$.

Thus, the use of a second recirculator permits one to achieve a gain in signal/noise ratio no more than two in power. The reason for such a small gain compared to (5.4.7) is included in strong correlation of noise at the output of the first recirculator.

Comparison of (5.4.18) and (5.4.7) shows that the use of a second recirculator permits one to achieve a gain of the same value as in a system with a single recirculator whose feedback coefficient is

considerably closer to one. Thus, for example, two recirculators with $m = 0.9$ provide the same gain as one recirculator with $m = 0.95$.

20

Thus, difficulties in realization of recirculators, related to providing a stable feedback coefficient sufficiently close to one required to achieve a large gain in signal/noise ratio, can be overcome by series connection of two or several recirculators.

3. System with n Identical Recirculators (Multiple System)

It was established above that if the number of N stored pulsed signals is so great that

$$m^N \ll 1, \quad (5.4.19)$$

then the coefficient of signal storage by one recirculator comprises $g_1 = (1 - m)^{-1}$. Therefore, the coefficient of signal storage by n recirculators

$$g_n \approx g_1^n \approx (1 - m)^{-n}. \quad (5.4.20)$$

Let white noise with the following intensity and limited in band-pass act on the input

$$\left. \begin{aligned} F_0(\omega) &= 2a & \text{at } 0 < \omega < 2\pi\Delta F, \\ F_0(\omega) &= 0 & \text{at } \omega > 2\pi\Delta F. \end{aligned} \right\}$$

Since the square of the modulus of the transfer function of n recirculators is

$$K_n^2(\omega) = (1 - 2m \cos \omega T + m^2)^{-n},$$

then the noise output is

208

$$\begin{aligned} \sigma_n^2 &= \frac{1}{2\pi} \int_0^\infty F_0(\omega) K_n^2(\omega) d\omega = \frac{a}{\pi} \int_0^{2\pi\Delta F} \frac{d\omega}{(1 - 2m \cos \omega T + m^2)^n} = \\ &= \frac{a}{\pi T} \int_0^{2\pi\Delta FT} \frac{dx}{(1 - 2m \cos x + m^2)^n} = \\ &= \frac{a}{\pi T} \left[\sum_{k=1}^{E(2\Delta FT)} \int_{(k-1)\pi}^{k\pi} \frac{dx}{(1 - 2m \cos x + m^2)^n} + \right. \\ &\quad \left. + \int_{E(2\Delta FT)\pi}^{2\pi\Delta FT} \frac{dx}{(1 - 2m \cos x + m^2)^n} \right] = \frac{a}{\pi T} [E(2\Delta FT) \times \end{aligned}$$

$$\times \int_0^{\pi} \frac{dx}{(1-2m \cos x + m^2)^n} + \int_0^{\pi R(2\Delta F T)} \frac{dx}{(1-2m \cos x + m^2)^n}]$$

and due to the fact that usually $2\Delta F T \gg 1$,

$$\sigma_n^2 \approx 2a\Delta F \frac{1}{\pi} \int_0^{\pi} \frac{dx}{(1-2m \cos x + m^2)^n}.$$

Using formula 3.616.2 of [92] and taking into account that the output of input noise is $\sigma_0^2 = 2a\Delta F$, we find the noise storage coefficient

$$Q_n = \frac{\sigma_n^2}{\sigma_0^2} = \frac{1}{(1-m^2)^n} \sum_{k=0}^{n-1} \frac{(n-1+k)!}{(k!)^2 (n-1-k)!} \left(\frac{m^2}{1-m^2} \right)^k. \quad (5.4.21)$$

It follows from (5.4.20) and (5.4.21) that a multiple system provides the gain [122]

$$B_n = \frac{q_n^2}{Q_n} = (1+m)^n \left/ \sum_{k=0}^{n-1} \frac{(n-1+k)!}{(k!)^2 (n-1-k)!} \left(\frac{m^2}{1+m} \right)^k \right. \quad (5.4.22)$$

Consideration of the dependence of this gain on n , shown by the solid curves in Fig. 5.4.7, shows that the gain increases as n increases and as m approaches 1, reaching very large values.

209

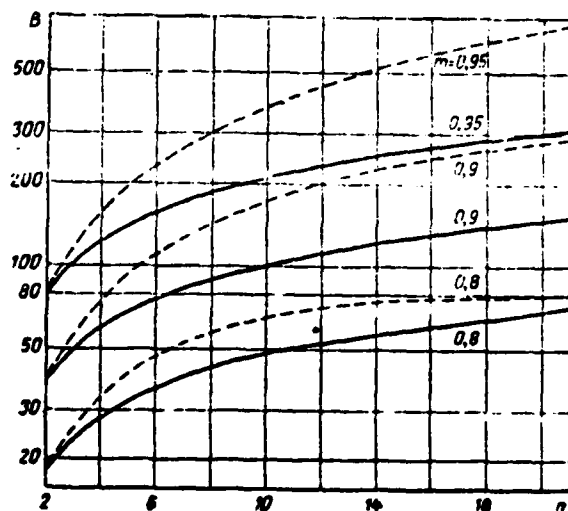


Fig. 5.4.7. Gain in multiple and two-stage systems as function of relative total delay time.

4. Two-Stage System

It was shown in item 2 that the use of a second recirculator identical to the first permits one to achieve a comparatively slight gain in signal/noise ratio. This is explained by the fact that the noise at the output of the first recirculator has strong correlation. The harmful effect of this correlation can be attenuated by increasing the delay time in the feedback circuit of the second recirculator M times [123] (Fig. 5.4.8), where M is an integer. In this case the second recirculator, unlike the first, will accumulate the sequences of signals, each of which contains M pulses, rather than the received pulsed signals. Thus, in this case the received pulsed signals will be stored in two stages. Therefore, the system is also called a two-stage system. If m_1 and m_2 are the feedback coefficients of these recirculators, then the k -th pulsed signal at the output of the first recirculator (i.e., at the input of the second recirculator) has, according to (5.4.1) the amplitude

210

$$V_s(k) = V_1 \tau \frac{1 - m_1^k}{1 - m_1} \quad \text{at } 1 \leq k \leq N.$$

In like fashion the lM -th pulsed signal at the output of the second recirculator has the amplitude

$$\begin{aligned} V_s(lM) &= \sum_{q=1}^l m_2^{l-q} V_s(qM) = \frac{V_1 \tau}{1 - m_1} \sum_{q=1}^l m_2^{l-q} (1 - m_1^{qM}) = \\ &= \frac{V_1 \tau}{1 - m_1} \left(\frac{1 - m_2^l}{1 - m_2} - m_1^{lM} \frac{z^l - 1}{z - 1} \right) \quad \text{at } 1 \leq l \leq L, \end{aligned}$$

where $z = m_2/m_1^M$ and $L = N/M$ is the number of sequences stored in the second recirculator.

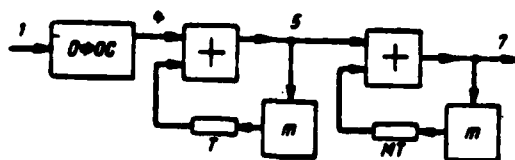


Fig. 5.4.8. Block diagram of two-stage system.
Key: (1) Optimum filter for single pulsed signal.

The peak value of the stored signal, as shown by calculations is observed at the end of the signal at the input of the system being considered. Its value is

$$V_{\text{max}} = V_z(N) = \frac{V_{1z}}{1-m_1} \left(\frac{1-m_2^L}{1-m_2} - m_1^N \frac{z^L-1}{z-1} \right).$$

Since usually $z > 2$ and L is on the order of 10, then $z^L \gg 1$ and

$$V_z \approx \frac{V_{1z}}{1-m_1} \left(\frac{1-m_2^L}{1-m_2} - \frac{m_2^L}{z-1} \right).$$

Accordingly, the signal is stored by the analyzed system with the coefficient

21.

$$g = \frac{V_z}{V_{1z}} = \frac{1}{(1-m_1)(1-m_2)} \left(1 - m_2^L \frac{z-m_2}{z-1} \right).$$

By analogy with the expression for the power at the output of two identical recirculators (see item 2), the power at the output of the considered system is

$$\sigma_z^2 = \sum_{k=0}^{\infty} \sum_{l=0}^{\infty} m_2^{k+l} R_s[(k-l)MT].$$

Substituting autocorrelation function (5.4.3) of noise at the output of the first recirculator into this expression and adding the double row, we find

$$\sigma_z^2 = \frac{\sigma_1^2}{(1-m_1^2)(1-m_2^2)} \frac{1+m_1^M m_2}{1-m_1^M m_2}.$$

Accordingly, the coefficient of noise stored by the system comprises

$$Q = \frac{\sigma_z^2}{\sigma_1^2} = \frac{1+m_1^M m_2}{(1-m_1^2)(1-m_2^2)(1-m_1^M m_2)}.$$

while the power gain in signal/noise ratio is

$$B_s = \frac{g^2}{Q} = \frac{1+m_1}{1-m_1} \frac{1+m_2}{1-m_2} \frac{1-m_1^M m_2}{1+m_1^M m_2} \times \left(1 - m_2^L \frac{z-m_2}{z-1} \right)^2. \quad (5.4.23)$$

Having assumed that $M = 1$ and accordingly that $L = N$, we find the gain provided by two recirculators with identical delays

$$B_2 = \frac{1+m_1}{1-m_1} \frac{1+m_2}{1-m_2} \frac{1-m_1 m_2}{1+m_1 m_2} \left(1 - m_2^N \frac{z-m_2}{z-1} \right)^2 \approx \frac{1+m_1}{1-m_1} \frac{1+m_2}{1-m_2} \frac{1-m_1 m_2}{1+m_1 m_2}.$$

Thus, the additional gain determined by an M-fold increase of delay time in the feedback circuit of the second recirculator comprises 21:

$$R = \frac{B_2}{B_1} = \frac{1+m_1 m_2}{1-m_1 m_2} \frac{1-m_1^M m_2}{1+m_1^M m_2} \left(1 - m_2^L \frac{z-m_2}{z-1} \right)^2.$$

Specifically, if M and L are selected as large as $m_1^M \ll 1$ and $m_2^L \ll 1$, then the additional gain is

$$R \approx (1+m_1 m_2) / (1-m_1 m_2)$$

and comprises 4.56, 9.54 and 19.5, respectively, at $m_1 = m_2 = 0.8, 0.9$ and 0.95.

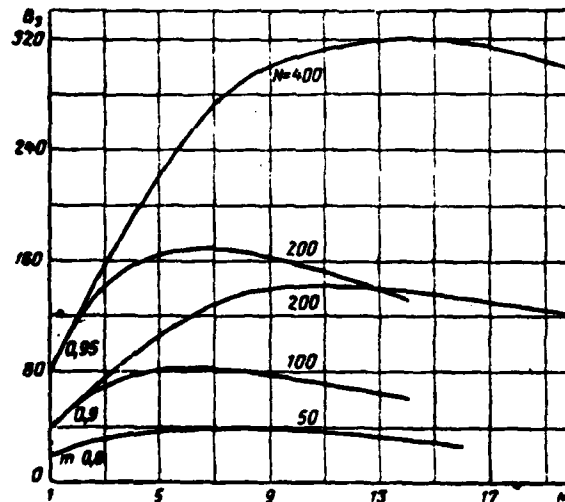


Fig. 5.4.9. Dependence of gain in two-stage system on M.

Consideration of the dependence of gain (5.4.23) on M (Fig. 5.4.9) shows that the gain initially increases sharply with an increase of M and then increases more slowly, reaching a very sloping maximum, after which it decreases smoothly. This is explained by the fact that there is a sharp decrease of the noise storage coefficient with an increase of M, beginning at one, due to the decrease of the correlation

coefficient of the noise components stored in the second recirculator, 21. whereas the signal storage coefficient varies insignificantly due to the reduction in the number of L accumulated sequences, due to which there is a rapid increase of the gain. The decrease of the noise storage coefficient slows down with a further increase of M and the drop of the signal storage coefficient increases, which initially slows down the increase of the gain and then leads to a decrease of it.

The optimum value of M [124] at which the gain is maximum is

$$M_{\text{opt}} \approx (0,6 \div 0,7) m(1-m)N. \quad (5.4.24)$$

Accordingly, very high efficiency of a system with two recirculators having different delays is achieved with a large number of stored pulsed signals due to an appreciable increase of the delay time in the second recirculator.

Let us compare two systems for the extent of the gain, one of which consists of n identical recirculators and the second of which consists of two recirculators with delays by T and $(n-1)T$, respectively [122]. Both systems have identical length of the total delay in their feedback circuits. This condition has an important practical meaning since design of delay devices causes the greatest difficulties when implementing these systems and these difficulties increase with an increase of delay time.

Having assumed in (5.4.23) that $m_1 = m_2 = m$ and $M = n-1$ and assuming that $m^L \ll 1$, we find

$$B_1 \approx [(1+m)/(1-m)]^2 (1-m^n)/(1+m^n). \quad (5.4.25)$$

The dependence of this gain on n , represented by the dashed curves in Fig. 5.4.7 have basically the same nature as the dependence of gain (5.4.22) for a multiple system, but at $2 \leq n \leq 21$ are located above the latter, which also indicates the greater efficiency of two-stage systems compared to multiple systems.

Consideration of this dependence shows that at $10 \leq n \leq 21$ a two-stage system with $m = 0.9$ is equivalent to a multiple system with $m = 214 = 0.95$. The bottom dashed curve in Fig. 5.4.7, which characterizes

gain (5.4.25) at $m = 0.8$, clearly reflects the fact that in the case of any value of m distinct from 1 the increase of gain (5.4.25) slows down and approaches its own maximum value with a significant increase of n

$$B_{3M} = \{(1+m)/(1-m)\}^2,$$

equal to the square of the gain of a single recirculator. A further increase of the gain is possible only by converting to a three-stage system.

It follows from (5.4.25) and (5.4.22) that a two-stage system provides an additional gain compared to a multiple system

$$R(m, n) = \frac{1}{(1+m^n)(1+m)^{n-1}} \frac{1-m^n}{1-m} \times \sum_{k=0}^{n-1} \frac{(n-1+k)!(1-m)^{n-1-k}}{(k!)^2(n-1-k)!} \left(\frac{m^2}{1+m}\right)^k. \quad (5.4.26)$$

Specifically, at $m = 1$

$$R(1, n) = \lim_{m \rightarrow 1} R(m, n) = \frac{n}{2^{n-1}} \frac{(2n-2)!}{[(n-1)!]^2} \approx 0.564 \left(\sqrt{n-1} + \frac{1}{\sqrt{n-1}} \right) \left[1 - \frac{1}{8(n-1)} \right].$$

Consideration of the dependence of this gain on n (Fig. 5.4.10) shows that in the case of $m = 0.8$ the gain initially increases with an increase of n and then decreases after reaching a maximum at $n = 9$. This is explained by the noted slowing of the increase of the gain of a two-stage system with a significant increase of n and should occur at any value of $m < 1$. However, at large value of m , the additional gain reaches a maximum with large value of n .

At $0.9 \leq m \leq 1$, the additional gain increases monotonically as n increases to 21. In this case its value for any value of n is higher, the closer m is to 1. At $0.9 \leq m \leq 1$ and $9 \leq n \leq 21$ the gain is in the range from 1.7 to 2.6.

Thus, compared to a multiple system, a two-stage system is more efficient and is therefore easier to realize.

215

The high efficiency of a two-stage system is explained not only by an increase of the length of the total delay in the feedback circuits but by the efficient design of this system as well.

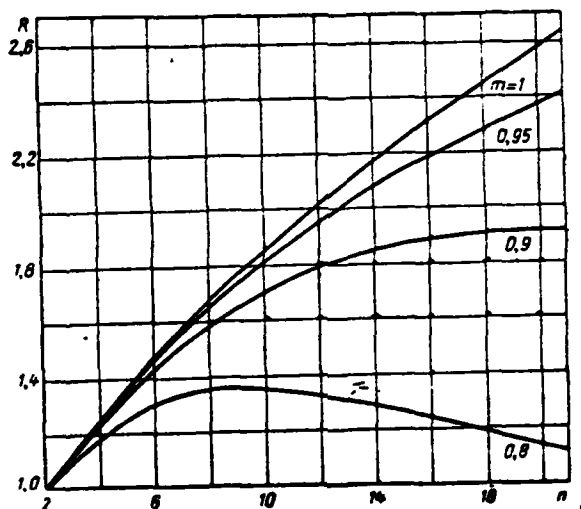


Fig. 5.4.10. Additional gain in two-stage system compared to multiple system as function of relative length of delay.

Thus, the following systems may be sufficiently effective practical approximations of an optimum filter for sequences of pulsed signals:

- a) a system with a single recirculator if the number of N stored pulsed signals does not exceed the actual number (5.4.8) of pulses (let us call this system a single storage device);
- b) a system with two identical recirculators (a double storage device) if N comprises from one to two active numbers;
- c) a two-stage system (two-stage storage device if N is double the active number.

The storage systems enumerated above are analyzed in detail in the second part of the book with regard to nonuniform frequency characteristics of the feedback circuits (and primarily of the delay devices) of recirculators, the nonoptimum nature of the prestorage filter and detector and so on.

Part 2

21

PULSED SIGNAL STORAGE DEVICES

CHAPTER VI

THRESHOLD SIGNALS WITH COHERENT STORAGE OF PULSED SIGNAL SEQUENCES

219

6.1. PRELIMINARY REMARKS

1. Concept of Threshold Signal

A signal of such energy (output or amplitude), the probability of correct detection of which at a given noise level and established probability of a false alarm is equal to a previously defined value (for example $D = 0.9$ or $D = 0.5$ [125]), is called a threshold or minimum distinguishable signal. In other words, a threshold signal is a minimum signal in absolute value which is still detected with given probability on a background of given noise level which causes a false alarm with fixed probability.

The ratio of threshold signal to noise level is called the threshold signal/noise ratio. Its value is determined both by the properties of the signal being received and by the method of processing it, determined by the structure of the radio receiver and the parameters of its components.

The threshold ratio specifically depends on whether the parameters of this signal (amplitude, initial phase, frequency, length and repetition quasi-period) are previously known or not, whether this signal is subject to fluctuations and what the law of these fluctuations is and so on. The design of the receiver may also be varied as a function of the signal properties.

The signals in the given and following chapters are considered in the form of a pulse sequence with previously known repetition quasi-period and the receivers for detecting them are also considered. The purpose of this consideration is to establish the structure of practically acceptable receivers in determination of threshold signal/noise ratios.

22

2. Concept of Coherent and Noncoherent Storage

The radar signal being received is a radio pulse sequence. If the initial phases of these radio pulses are identical or vary from pulse to pulse by some known law (see section 5.2), then this sequence is called coherent. If the initial phases of the radio pulses of the sequence vary by random (or some previously unknown) law, this sequence is noncoherent.

If the determinant nature of phase ratios of the pulses of a coherent sequence is used in reception, this reception is called coherent. If reception is processing only the amplitude values of the oscillation being received, then it is noncoherent (amplitude). Since the information contained in the phase of the oscillation being received will not be used in this case, the threshold signals will be somewhat greater than those during coherent reception.

Reception of a noncoherent sequence of radio pulse signals can be only noncoherent.

As established above, optimum processing of the radio pulse sequence being received includes its intraperiod filtration and storage of individual periods. Storage of individual periods of the sequence being received, which utilizes the coherent nature of its radio pulses manifested in the determinant nature of the phase relations of these radio pulses, is called coherent. It can be fulfilled on a radio frequency and specifically in an optimum filter for the envelope of a radio pulse sequence or in devices that are practical approximations of this filter, as which a recirculator or comb filter can be used in the form of a combination of a large number of oscillating circuits and so on. However, to reduce the requirements on the stability of

22

the components of this filter or storage device (see section 5.2), coherent storage is usually carried out on a video frequency after coherent detection of the coherent radio pulse sequence being received, which converts it to a video pulse sequence.

In this case a coherent (synchronous) detector [41-43] controlled by a reference oscillation whose frequency coincides with the frequency of the signal being received, is used in the receiver. If the signal being received is known with accuracy up to the phase, then the phase of the reference oscillation should coincide with the signal phase.

A coherent detector is a linear component. Therefore, a coherent receiver is a linear system. Because of this, coherent storage on a radio frequency, i.e., up to a coherent detector, is completely equivalent to storage after a coherent detector. The latter is best accomplished by a video frequency optimum filter for the envelope of the received sequence of pulsed signals.

Storage (by periods) of the oscillation being received in which only amplitude information is used and phase information is lost is called noncoherent. It is accomplished after noncoherent (amplitude) detection of the radio pulse sequence being received.

Threshold signals during coherent storage are considered in the given chapter and those with noncoherent storage are considered in chapter 10.

6.2. Coherent Storage of Completely Known Sequences of Pulsed Signals

1. Structure of Radio Receiver

A completely known sequence of pulsed signals can be regarded as a completely known single signal of rather complex shape determined by the shape of the given sequence.

As follows from Chapter 1, an optimum detector of a completely known signal $v(t) = V(t)\cos(\omega_0 t + \phi)$ on a background of normal white noise $n(t)$ consists of cross-correlation and threshold devices (Fig. 6.2.1, a).

A radio-frequency filter optimum to a given signal can be used as a device that calculates the cross-correlation function between the signal and the oscillation being received $x(t) = v(t) + n(t)$. The given signal is obviously completely equivalent to the combination of a coherent detector with reference oscillation $\cos(\omega_0 t + \phi)$ and a video frequency filter optimum to the envelope of the signal $V(t)$ (Fig. 6.2.1, b).

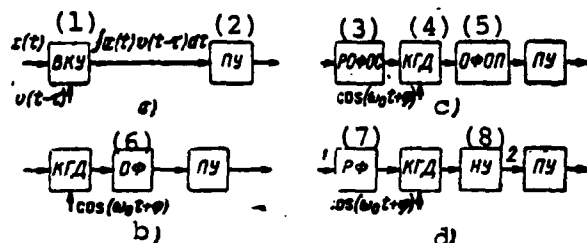


Fig. 6.2.1. Block diagrams of receivers for coherent storage of completely known signals.
 Key: (1) Cross-correlation device; (2) Threshold device; (3) Radio-frequency optimum filter for single pulsed signal; (4) Coherent detector; (5) Video frequency optimum filter for envelope of sequence of pulsed signals; (6) Optimum filter; (7) Radio-frequency filter; (8) Video frequency storage device.

In the considered case of detecting a completely known sequence of radio pulse signals, the video frequency filter should be optimum for a corresponding sequence of video pulse signals. It consists of a filter optimum to a single video pulse signal of the sequence and of a video frequency filter optimum to the envelope of this sequence. The first of these filters can be replaced by a filter completely equivalent to it and optimum to a single radio pulse signal of the sequence being received and placed in front of a coherent detector (Fig. 6.2.1, c).

In a receiver which is a practical approximation of an optimum receiver, a radio-frequency optimum filter is replaced by a simpler filter, while the video frequency optimum filter for the envelope of the sequence is replaced by a storage device (Fig. 6.2.1, d).

A receiver which accomplishes coherent storage of a completely known sequence of pulsed signals (Fig. 6.2.1) consists of linear components (with the exception of the threshold device). Therefore, the signal and noise pass through the receiver to the input of the threshold device completely independently of each other. In this case the noise at the output of the linear part of the receiver is distributed by the same Gauss law as at the input (see item 1, section 2.2).

Because of this, relations (1.2.12) and (1.2.9) are valid for the given case. Accordingly, correct detection and a false alarm are characterized, respectively, by the following probabilities

$$D = \frac{1}{2} \left[1 + \Phi \left(\frac{q_2}{\sqrt{2}} - l \right) \right] \quad (6.2.1)$$

and

$$F = \frac{1}{2} [1 - \Phi(l)],$$

where q_2 is the ratio of the peak signal to the effective value of noise at the input of the threshold device.

Being given the probability level of a false alarm, let us determine from the last expression the relative threshold

$$l = \arg \Phi(1 - 2F),$$

where $\arg \Phi(y) = x$ is a function inverse to $y = \Phi(x)$. Having substituted this value into (6.2.1), we find the detection characteristic

$$D = \frac{1}{2} \left\{ 1 + \Phi \left[\frac{q_2}{\sqrt{2}} - \arg \Phi(1 - 2F) \right] \right\}. \quad (6.2.2)$$

The detection characteristics calculated by this formula using the tables of the probability integral [126, 127] are presented in Fig. 6.2.2.

Having established the probability levels of detection and a false alarm, let us determine from (6.2.2) the corresponding threshold signal/noise ratio:

$$q_{ss} = \sqrt{2} \arg \Phi(2D - 1) + \sqrt{2} \arg \Phi(1 - 2F).$$

Specifically, at $D = 0.5$, in view of the fact that $\arg \phi(0) = 0$,

2

$$q_{\text{th}} = \sqrt{2} \arg \Phi(1 - 2F),$$

and at $D = 0.9$

$$q_{\text{th}} = 1,282 + \sqrt{2} \arg \Phi(1 - 2F).$$

The values of the threshold signal/noise ratios calculated by these formulas are reduced in Table 6.2.1.

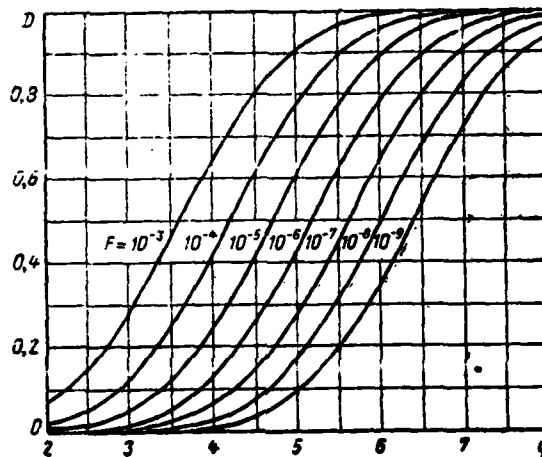


Fig. 6.2.2. Detection characteristics of completely known sequences of signals.

Let us note that the square of the threshold signal/noise ratio is equal to the duplicate distinguishability (visibility) factor of the receiver [128].

Table 6.2.1.

D	F								
	10^{-1}	10^{-2}	10^{-3}	10^{-4}	10^{-5}	10^{-6}	10^{-7}	10^{-8}	10^{-9}
0.5	1,282	2,321	3,090	3,719	4,265	4,753	5,199	5,612	5,998
0.9	2,564	3,603	4,372	5,000	5,546	6,035	6,481	6,894	7,280

To calculate the sensitivity of the receiver, let us determine the threshold energy of the input signal. For this purpose let us replace the radio-frequency filter (Fig 6.2.1, d) by a video frequency filter equivalent to it. Let the use of the storage device together

22

with this filter permit us to achieve a gain in signal/noise ratio B compared to an optimum filter for a single pulsed signal (its value is calculated for coherent cases in the three following chapters).

According to the definition of this gain and relation (1.2.11)

$$B = \frac{q_{2n}^2}{\frac{E_{10n}}{a}} = \frac{aq_{2n}^2}{E_{10n}}, \quad (6.2.3)$$

where E_{10n} is the total threshold energy of a single pulsed signal of the sequence.

Specifically, if the shape of this pulsed signal is square-wave,

$$E_{10n} = \frac{1}{2} V_{1n}^2 \tau = P_{1n} \tau, \quad (6.2.4)$$

where V_1 is amplitude and P_1 is signal output.

Accordingly, the signal has threshold energy

$$E_{10n} = \frac{aq_{2n}^2}{B}, \quad (6.2.5)$$

threshold output

$$P_{1n} = \frac{aq_{2n}^2}{B\tau} \quad (6.2.6)$$

and threshold amplitude

$$V_{1n} = \sqrt{\frac{2a}{B\tau}} q_{2n}. \quad (6.2.7)$$

Since noise has the intensity

$$a = \frac{1}{2} kTn,$$

where k is a Boltzmann constant equal to 1.38×10^{-23} J/deg, T is the absolute ambient temperature and n is the noise coefficient of the receiver, then

$$E_{10n} = \frac{kTnq_{2n}^2}{2B} \quad (6.2.8)$$

$$P_{1n} = \frac{kTnq_{2n}^2}{2B\tau} \quad (6.2.9)$$

and

$$V_{1n} = \sqrt{\frac{kTn}{B\tau}} q_{2n} \quad (6.2.10)$$

Relations (6.2.8)-(6.2.10) describe receiver sensitivity quantitatively. It follows from these relations that receiver sensitivity is higher, the greater gain the storage device provides in signal/noise ratio.

In the case of optimum reception of a square-wave sequence of N radio pulse signals, $B = N$, due to which the maximum possible (potential) sensitivity of the receiver is characterized by the values

$$P_{1max} = \frac{kTnq_{2n}^2}{2N\tau} \quad (6.2.11)$$

and

$$V_{1max} = \sqrt{\frac{kTn}{N\tau}} q_{2n} \quad (6.2.12)$$

6.3. Coherent Storage of Sequences of Pulsed Signals With Unknown Initial Phase

1. Structure of Receiver

The initial phase of the pulsed signals of a sequence is usually unknown since the precise distance from the radar station to the object is unknown.

A block diagram of an optimum receiver (Fig. 1.2.6), in which two cross-correlation devices controlled by two quadrature oscillations are used, is constructed in item 2, section 1.2 for a signal with unknown random phase. A combination of a coherent detector and video frequency optimum filter for the envelope of the signal being received may be used as the cross-correlation device. If a coherent sequence of

pulsed signals is being received, then as shown in section 5.1, an optimum filter consists of one for a single pulsed signal (OFOS) and one for the envelope of this sequence (OFOP). The optimum filter for a single signal can be replaced by a radio-frequency optimum filter for a single pulsed signal (ROFOS), having placed it in front of the coherent detector.

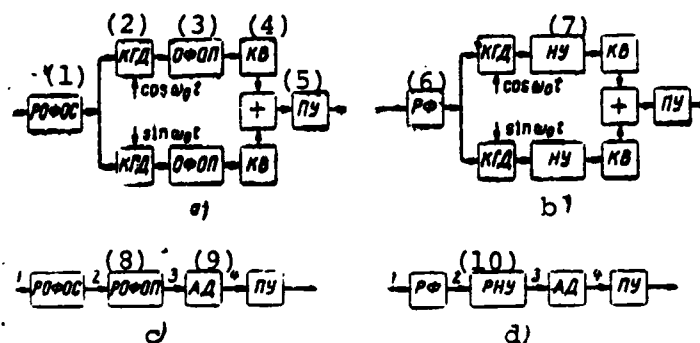


Fig. 6.3.1. Block diagrams of receivers for coherent storage of signals with unknown initial phase.

Key: (1) Radio-frequency optimum filter for single pulsed signal; (2) Coherent detector; (3) Video frequency optimum filter for envelope of pulsed signal sequence; (4) Square-law generator; (5) Threshold device; (6) Radio-frequency filter; (7) Video frequency storage device; (8) Radio-frequency optimum filter for envelope of pulsed signal sequence; (9) Amplitude detector; (10) Radio-frequency storage device.

Thus, an optimum receiver for a coherent sequence of pulsed signals with unknown initial phase consists of an ROFOS, two coherent detectors controlled by square-law oscillations of the carrier frequency, two OFOP, two square-law generators, an adder and a threshold device (Fig. 6.3.1, a).

If a nonideal storage device NU is used in this receiver instead of an OFOP and a radio-frequency filter RF is used instead of an ROFOS, the receiver (Fig. 6.3.1, b) will be nonoptimum, but will accomplish coherent storage of sequences of pulsed signals with unknown initial phase.

As was shown in section 1.6, a two-channel receiver (Fig. 6.3.1, a) is completely equivalent to a single-channel receiver with amplitude detector (Fig. 6.3.1, c). In similar fashion the receiver (Fig. 6.3.1, b) is equivalent to the receiver (Fig. 6.3.1, d). Pulsed signals are

stored in receivers (Fig. 6.3.1, c and d) before the detector, i.e., on the radio frequency, which is very difficult to accomplish (see section 5.2). Therefore, they are not used in practice and are introduced to simplify calculation of the threshold signals.

2. Calculation of Detection Characteristics and Threshold Signals

The voltage at the output of an amplitude detector (Fig. 6.3.1, c and d), which we shall regard as linear to be specific and which has normalized characteristic $u_4 = U_3$, where U_3 is the voltage amplitude at its input, is distributed by the same law as this amplitude. Accordingly, the indicated voltage is distributed upon reception of noise alone by Rayleigh law:

$$W(u_4) = \frac{u_4}{\sigma_3^2} \exp\left(-\frac{u_4^2}{2\sigma_3^2}\right) \cdot l(u_4), \quad (6.3.1)$$

and upon reception of a signal-noise mixture by Rayleigh-Rice law (generalized Rayleigh law) [20, 129]:

$$W(u_4) = \frac{u_4}{\sigma_3^2} \exp\left(-\frac{u_4^2 + V_3^2}{2\sigma_3^2}\right) I_0\left(\frac{u_4 V_3}{\sigma_3^2}\right) l(u_4),$$

where V_3 is the signal amplitude at the detector input, σ_3^2 is the noise output (dispersion) at the indicated input and $I_0(x)$ is a modified (video-altered) zero-order Bessel function of first kind [25].

Because of this, the probability of a false alarm is

$$F = \int_{U_0}^{\infty} \frac{u_4}{\sigma_3^2} \exp\left(-\frac{u_4^2}{2\sigma_3^2}\right) du_4 = e^{-\eta}, \quad (6.3.3)$$

where $\eta = \frac{U_0^2}{2\sigma_3^2}$, and the probability of detection is

$$\begin{aligned} D &= \int_{U_0}^{\infty} \frac{u_4}{\sigma_3^2} \exp\left(-\frac{u_4^2 + V_3^2}{2\sigma_3^2}\right) I_0\left(\frac{u_4 V_3}{\sigma_3^2}\right) du_4 = \\ &= \int_{\frac{U_0}{\sqrt{2}}}^{\infty} x \exp\left(-\frac{x^2 + q_3^2}{2}\right) I_0(q_3 x) dx, \end{aligned} \quad (6.3.4)$$

where $q_3 = V_3/\sigma_3$ is the signal/noise ratio.

It follows from (6.3.3) that:

$$l = \sqrt{\ln \frac{1}{\gamma}}. \quad (6.3.5)$$

The probability of detection (6.3.4) can be calculated by means of the tables [130] of the probability integral of Rayleigh-Rice distribution:

$$Q(u, v) = \int_u^\infty p \exp\left(-\frac{v^2 + s^2}{2}\right) I_0(vs) dp.$$

However, since not only the detection characteristics but threshold signals as well must be calculated, determination of which is related to the need to carry out cumbersome and exhaustive calculations when using the indicated tables, the method of approximate calculation of the detection characteristics and threshold signals is outlined below.

V. I. Senimovich [131] showed that the following asymptotic formula is valid

$$\int_z^\infty x \exp\left(-\frac{x^2 + s^2}{2}\right) I_0(sx) dx = \frac{1}{\sqrt{2\pi}} \int_{u-\eta}^\infty e^{-\frac{x^2}{2}} dx,$$

where

$$u = z - s \text{ and } \eta = \frac{1}{2s} - \frac{u}{(2s)^2} + \frac{1}{3} \frac{u^2 + 0.5}{(2s)^3} + O\left(\frac{1}{s^4}\right).$$

Because of this, (6.3.4) assumes the form

$$D = \frac{1}{2} [1 - \Phi(y)], \quad (6.3.6)$$

where

230

$$y = \frac{1}{\sqrt{2}} \left(u - \frac{1}{2q_1} + \frac{u}{2q_2} - \frac{u^2 + 0.5}{6q_3} \right). \quad (6.3.7)$$

and

$$u = \sqrt{2}l - q_1 = \sqrt{2 \ln \frac{1}{\gamma}} - q_1. \quad (6.3.8)$$

The detection characteristics calculated by these formulas are plotted in Fig. 6.3.2.

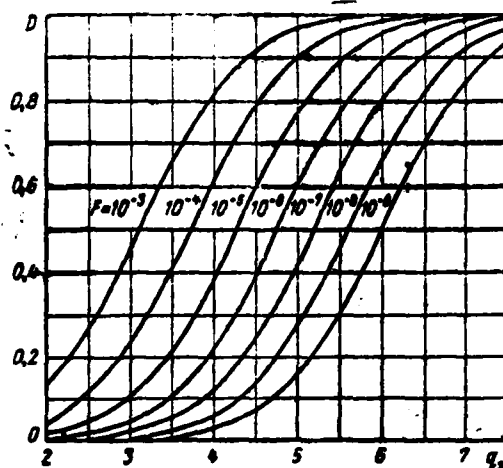


Fig. 6.3.2. Detection characteristics of sequences of signals with unknown initial phases.

Being given the probabilities of detection and a false alarm, one can calculate the value of the threshold signal/noise ratios. Substituting the value $y = -\arg\phi(2D - 1)$ into (6.3.7) and also using (6.3.8), we find a fourth-power equation with respect to q_3 . Since solution of the latter is complicated, we first find the first approximation q_{31} . To do this, it is sufficient to use only two terms on the right side of (6.3.7), which leads to the quadratic equation

$$q_{31}^2 - \sqrt{2}(1-y)q_{31} + 0.5 = 0, \quad (6.3.9)$$

solution of which is as follows:

23

$$q_{31} = \frac{1-y + \sqrt{(1-y)^2 - 1}}{\sqrt{2}}.$$

To find the next approximation q_{32} one should utilize the fact that correction $\Delta q_3 = q_{32} - q_{31}$ is very small compared to the first approximation.

Then, using (6.3.7) and (6.3.9), it is easy to show that

$$\frac{\Delta q_3}{q_{31}} \approx \frac{(2l+5y)\sqrt{2}q_{31} - 4l^2 + 1.5}{12q_{31}^4}.$$

It was established by calculation that this relative correction comprises tenths of a percent at $D = 0.9$. Its value decreases as the probability level of a false alarm decreases. This is explained by the increase in the value of the threshold signal/noise ratio, which leads to a relative decrease of the older terms of the right side of expression (6.3.7).

At $D = 0.5$, the correction is so small that it does not affect the third sign. This is explained by the fact that in the given case $y = 0$, due to which the value of u is small and the role of the last two terms in expression (6.3.7) is insignificant.

Using the threshold signal/noise ratios calculated in this manner (Table 6.3.1), the results of the previous chapter and formulas (6.2.5)-(6.2.12), it is easy to calculate the sensitivity of a receiver that accomplishes coherent storage of a sequence of pulsed signals with unknown initial phase. The only difference from the calculation made in section 6.2 is in the different values of the threshold signal/noise ratios.

Table 6.3.1.

D	P						
	10^{-6}	10^{-5}	10^{-4}	10^{-3}	10^{-2}	10^{-1}	10^{-0}
0.5	3.58	4.17	4.69	5.16	5.59	5.99	6.36
0.9	4.88	5.47	5.99	6.45	6.88	7.28	7.65

Let us calculate the gain in receiver sensitivity with coherent storage of a sequence of pulsed signals with unknown initial phase compared to coherent storage of a completely known sequence. In this case let us use the data of Tables 6.2.1 and 6.3.1. The power gain decreases with a decrease of the probability level of a false alarm and at $D = 0.9$ is somewhat less than at $D = 0.5$ (Fig. 6.3.3). This is explained by the fact that the threshold signal/noise ratios increase with an increase of the level of detection probability and a decrease of the false alarm probability. In this case generalized Rayleigh law (6.3.2) approximates the normal probability distribution [20], which is observed at the input of the threshold device of the

receiver for coherent storage of a completely known sequence of pulsed signals. Because of this, the difference between the threshold signals becomes even less.

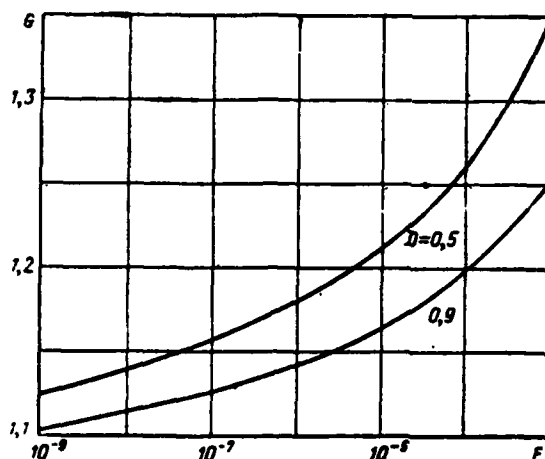


Fig. 6.3.3. Gain due to the fact that initial phase of signals is unknown as function of false alarm probability.

The latter can be explained differently by the fact that signal suppression by noise in the amplitude detector is attenuated with an increase of signal/noise ratio, due to which the threshold signals in a receiver with this detector (Fig. 6.3.1, c and d) hardly differ from the threshold signals in a receiver with coherent detector (Fig. 6.2.1, c and d).

233

However, the power gain of threshold signals is not great in the most unfavorable case. This is explained by the fact that coherent storage of pulsed signals is accomplished in both cases.

6.4. Coherent Storage of Sequences of Pulsed Signals Fluctuating in Unison

1. Types of Signal Fluctuations

The radar signals being received are the result of reflection of emitted signals from targets of one or another nature. In most cases these targets have a very complex structure. Moreover, if their overall dimensions are greater than wavelength, the signal being received

can be regarded as the sum of the large number of oscillations reflected by the individual elements of the target. The latter, being added in random phases, also determine the random nature of the signal being received, which is manifested in fluctuations of its level.

If the received signal is the sum of a large number of independent elementary reflected signals approximately identical in intensity, then, in view of the central limiting theorem of probability theory [20, 132], the signal being received has the statistical properties of normal noise. Accordingly, the instantaneous values of the reflected signal are distributed by normal law, phase is distributed by uniform law and amplitude is distributed by Rayleigh law (6.3.1), where $\sigma_3^2 = n^2$ is the mean output (variance) of the signal.

Subsequently, it is important to note that due to this, the probability distribution of the square of the ratio of the fluctuating signal to noise is exponential:

$$W(q^2) = \frac{1}{2\rho^2} \exp\left(-\frac{q^2}{2\rho^2}\right), \quad (6.4.1) \quad 23$$

where $\rho = n/\sigma$ is the ratio of the effective values of signal and noise.

The reflected pulsed signals contained in the sequence can fluctuate differently. They can be completely (or rigidly) correlated, partially correlated and independent of each other [133, 134].

In the first case pulsed signals, although they fluctuate by random law, they assume the same amplitude value identical for all signals of a square-wave sequence. Examples of two realizations of a sequence of pulsed signals fluctuating in this manner are presented in Fig. 6.4.1, a and b. These fluctuations are called harmonious and the sequence of pulsed signals is said to fluctuate in unison.

The direct opposite of harmonious fluctuations are independent fluctuations. In this case the reflected signals in some repetition periods are completely independent (Fig. 6.4.1, c) and fluctuate by random law similar to normal noise. Therefore, these signals are called noise-like or independently fluctuating signals.

235

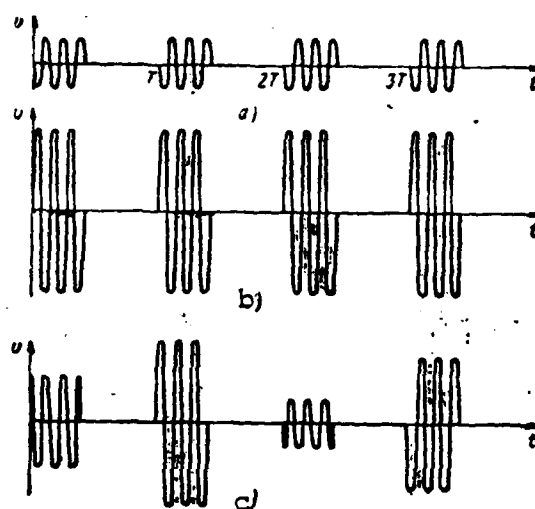


Fig. 6.4.1. Sequence of fluctuating signals.

The case of partially (incompletely) correlated fluctuating signals occupies the intermediate position between the two considered cases.

23

Harmonious fluctuations of signals are naturally observed when the mutual arrangement of the elements remains unchanged during irradiation of the target. Accordingly, harmonious fluctuations are slow fluctuations. Independent fluctuations occur when the mutual arrangement of the elements of the irradiated target vary strongly during the repetition period of the signal. Therefore, these fluctuations are sometimes called rapid fluctuations. They occur on very short waves, at low repetition rate and with rapid banks of the irradiated target.

2. Structure of Radio Receiver

A coherent sequence of signals fluctuating in unison occupies the intermediate position between a regular, completely known sequence of pulsed signals and a sequence of signals fluctuating independently from pulse to pulse.

The considered sequence is essentially a regular sequence of pulsed signals with unknown initial phase and relative amplitude. Since the shape of this sequence is usually known, knowledge of the amplitude

and the initial phase of one of the radio pulses (for example, of the first) of this sequence transforms it to a completely known sequence of pulsed signals.

Therefore, this sequence of pulsed signals may be regarded as a single radio pulse signal of very complex shape with unknown amplitude and initial phase. The latter considerably facilitates design of receivers for coherent storage of the indicated sequence.

23

It was shown in item 2, section 1.2 that an optimum receiver for a signal with unknown, unmeasured initial phase and amplitude has the same structure as in this case when only the initial phase of the signal is unknown. Due to this, receivers designed for coherent storage of a sequence of signals fluctuating in unison fully conform to receivers for coherent storage of a sequence of pulsed signals with unknown initial phase (Fig. 6.3.1).

3. Calculation of Detection Characteristics and Threshold Signals

Since the signal at both the receiver input (Fig. 6.3.1, b) and at the input of the amplitude detector has random amplitude and random initial phase, it is similar to noise in its statistical properties with Rayleigh distribution of amplitudes and uniform distribution of initial phases.

Since the signal and noise are statistically mutually independent and Gaussian at the detector input, their outputs are added. Therefore, the instantaneous value of the voltage of the signal/noise mixture at the output of a linear amplitude detector with normalized characteristic* is distributed by Rayleigh law:

$$W(u_4) = \frac{u_4}{\sigma_3^2 + \eta_3^2} \exp \left[-\frac{u_4^2}{2(\sigma_3^2 + \eta_3^2)} \right] \cdot I(u_4).$$

*The normalized characteristic of a linear amplitude detector has the form

$$u_4 = U_3,$$

where u_4 is the instantaneous value of output voltage and U_3 is the voltage amplitude at the input.

where σ_3^2 is the output (variance) of the signal at the detector input.

Because of this, the probability of a false alarm is

23

$$F = \int_{t_0}^{\infty} \frac{u_1}{\sigma_3} \exp \left[-\frac{u_1^2}{2\sigma_3^2} \right] du_1 = e^{-\rho}, \quad (6.4.2)$$

and the probability of detection is

$$D = \int_{t_0}^{\infty} \frac{u_1}{\sigma_3 + \eta_3} \exp \left[-\frac{u_1^2}{2(\sigma_3^2 + \eta_3^2)} \right] du_1 = \exp \left(-\frac{\rho^2}{1 + \rho^2} \right), \quad (6.4.3)$$

where $\rho = \frac{\eta_1}{\sigma_3}$ is the signal/noise ratio at the detector input.

It follows from the last two equalities that

$$D = F^{\frac{1}{1+\rho^2}}. \quad (6.4.4)$$

The characteristic feature of the detection characteristics calculated by this formula (Fig. 6.4.2) consists in the fact that the detection probability increases at first rapidly with an increase of signal/noise ratio and this increase slows down after values of $D = 0.5-0.6$ are reached and then becomes very slow.

This type of detection characteristic is typical during reception of fluctuating signals and is explained by the fact that the Rayleigh probability distribution of a signal/noise mixture at the detector output has comparatively long "tails."

Let us determine from (6.4.4) the threshold signal/noise ratio:

$$\rho_{th} = \sqrt{\frac{\ln F}{\ln D} - 1}. \quad (6.4.5)$$

Consideration of Table 6.4.1 with the values of threshold signal/noise ratios shows that the threshold ratios at $D = 0.9$ are 2.6-2.7 times greater than those at $D = 0.5$. This is the result of a special type of detection characteristic.

Table 6.4.1.

23

D	F						
	10^{-3}	10^{-4}	10^{-5}	10^{-6}	10^{-7}	10^{-8}	10^{-9}
0,5	2,99	3,51	3,95	4,35	4,72	5,06	5,38
0,9	8,03	9,28	10,59	11,39	12,31	13,17	13,99

Using these threshold ratios, formulas (6.2.5)-(6.2.12) and the results of the following chapters, it is easy to calculate the sensitivity of a receiver for coherent storage of signals fluctuating in unison.

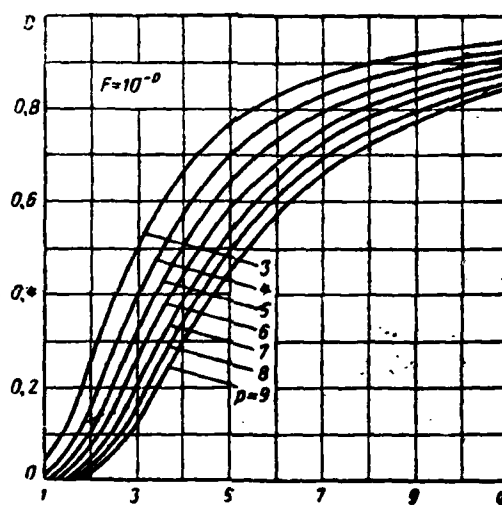


Fig. 6.4.2. Detection characteristics of sequences of signals fluctuating in unison.

6.5. Coherent Storage of Pulsed Signals with Unknown Doppler Frequency Shift

1. A Multichannel System

Coherent storage of pulsed signals can be accomplished comparatively easily if their carrier frequency is previously known. In radar this corresponds to reception of signals reflected from fixed targets. However, the targets that are of greatest interest to radar (missiles, aircraft and so on) are most frequently moving. The signals reflected from these targets, due to the Doppler phenomenon, have a carrier frequency ω_{0n} differing by Doppler frequency Ω from the carrier frequency ω_0 of the sounding pulses:

23

$$\omega_{\text{ref}} = \omega_0 + \Omega \approx \omega_0 \left(1 + \frac{2v_r}{c} \right), \quad (6.5.1)$$

where v_r is the radial speed of the target with respect to the radar system and c is the speed of radio wave propagation.

If radial speed were previously known, it would be sufficient to shift the frequency of the reference oscillations in the receivers (Fig. 6.2.1, d and 6.3.1, b) by the Doppler frequency for coherent storage of signals reflected from this target.

However, the radial speed of a target must usually be determined during (or after) its detection. Therefore, the Doppler frequency is previously unknown.

To accomplish coherent storage of signals from moving targets, there are three possibilities which are considered below.

The first includes design of a multichannel receiver. Each channel corresponds to one of the comparatively narrow sections of the spectrum of anticipated Doppler frequencies. The combination of all its channels completely overlaps the spectrum of expected Doppler frequencies. The k -th channel of this receiver is made according to a block diagram (Fig. 6.5.1) that differs from the receiver (Fig. 6.3.1, b) by the presence of a Doppler frequency generator (GChD) and a mixer Sm of the emitted frequency ω_0 and Doppler frequency Ω . A phase-reversing circuit (FV) changes the phase of one of the reference oscillations by 90° .

The Doppler frequency for a given channel is selected by a fixed frequency:

$$\Omega_k = \Omega_{\text{min}} + \left(k + \frac{1}{2} \right) \Delta\Omega,$$

where $\Delta\Omega = \frac{\Omega_{\text{max}} - \Omega_{\text{min}}}{M}$ is the width of the bandpass of each channel, Ω_{max} and Ω_{min} are the maximum and minimum expected Doppler frequencies, respectively, M is the number of channels and k is an integer lying in the range from 0 to $M - 1$. 240

The latter expression is valid on the assumption that the reference oscillations of adjacent channels differ in frequency by the same value $\Delta\Omega$.

The greater the number of channels and the narrower their bandpass is, the more precisely coherent storage of signals impinging in the given receiver channels is accomplished.

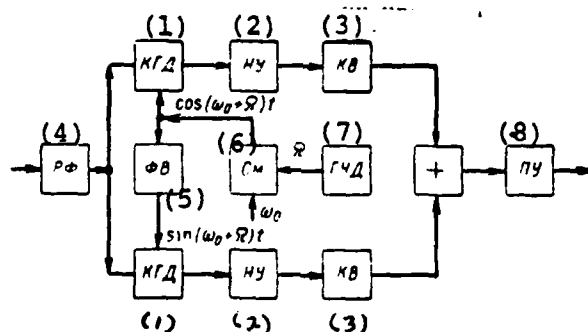


Fig. 6.5.1. Block diagram of receiver for coherent storage of signals reflected from moving targets. Key: (1) Coherent detector; (2) Video frequency storage device; (3) Square-law generator; (4) Radio-frequency filter; (5) Phase-shifting circuit; (6) Mixer; (7) Doppler frequency generator; (8) Threshold device.

Let us estimate the required number of receiver channels. If the frequency of the signal being stored in the k -th channel differs by value ΔF from the median frequency of this channel, then this leads to the fact that the pulse amplitude at the output of a coherent detector will vary during storage. Let the initial phase of the signal being received be equal to zero at the beginning of storage and let the pulse amplitude at the output of the coherent detector be V_H . The signal received at the output of the coherent detector at the end of storage will have the amplitude $V_k = V_H \cos 2\pi \Delta f t_H$, where t_H is the signal storage time. If the decrease of pulse amplitude at the output of a coherent detector by a factor of $\sqrt{2}$ is regarded as permissible, then $\cos 2\pi \Delta f t_H \leq \frac{1}{\sqrt{2}}$, hence, it follows that $|\Delta f| t_H \leq \frac{1}{8}$.

The maximum absolute value of the frequency difference Δf is equal to half the width of the channel bandpass $\Delta F/2 = \Delta\Omega/4\pi$. Therefore,

$$\Delta Ft_H = 0.25. \quad (6.5.2)$$

The signal storage time cannot be greater than the time of its existence (this time is usually limited by the time during which the target moves at constant radial velocity).

Specifically, if a sequence of N pulsed signals with repetition quasi-period T is received, we have $t_H \leq NT$. Only the active number of pulsed signals N_a is stored with exponential-weight storage (see (5.4.8)) and

$$t_H \leq N_a T. \quad (6.5.3)$$

We will subsequently keep this case in mind. If it is required to convert to the case of ideal storage, it is sufficient to assume that $N_a = N$.

According to (6.5.2) and (6.5.3), the required number of channels is

$$M = \frac{F_{\text{max}} - F_{\text{min}}}{\Delta F} = 4N_a T (F_{\text{max}} - F_{\text{min}}).$$

If the targets subject to detection can both come closer and move away with identical range of velocities, due to which $F_{\text{min}} = -F_{\text{max}}$, then

$$M = 8N_a T F_{\text{max}} = \frac{16N_a v_{r\text{max}} T}{\lambda},$$

where λ is wavelength.

If we take as an example $v_{r\text{max}} = 300$ m/s, $T = 1$ ms, $\lambda = 1$ meter and $N_a = 20$, then we have $M = 96$ channels.

If the wavelength is shortened, the active number of pulses being stored and the length of the repetition period of the system is increased and the range of velocities of the targets being detected is broadened, the number of receiver channels required for coherent storage of signals increases even further.

Thus, the number of channels of a receiver that accomplishes coherent storage of signals from rapidly moving targets reaches many tens and even hundreds.* In this case the feasibility of realizing this receiver may be doubtful.

242

2. Single-Channel Systems

The second possibility of coherent storage of signals from moving targets consists in searching for the target by radial velocity and is realized by a receiver (Fig. 6.5.1) in which the GChD [Doppler frequency generator] is retuned over the entire range of expected Doppler frequencies.

The described receiver requires rather long time to retune the GChD for detection of the signals and to store these signals.** Therefore, it cannot be used for tactical concepts in systems for detection of rapidly moving targets.

Finally, let us consider the third possibility of coherent storage of signals from moving targets. It is realized by means of a single-channel system in which the pulsed signals with different Doppler frequency shifts are stored simultaneously and coherently. Its basic component is the recirculator (Fig. 6.5.2).

* Some decrease of the volume of the equipment is possible when using sequential (two-stage) detection of signals [135]. In this case preliminary detection of signals is carried out with high probability of a false alarm and rough determination of their frequency during the first stage by using a set of a small number of comparatively wideband filters that encompass the entire spectrum of the expected Doppler frequencies. During the second stage, the sections of the spectrum in which the presence of signals is assumed from the results of the first stage are analyzed carefully by means of a small comb of narrowband filters.

** The method of sequential (multistage) search has been suggested to significantly reduce the signal detection time [136, 137]. In this case a search is made for the signal in several stages (in two stages in the simplest case). During the first stage, the signal is detected with high probability of a false alarm by rapid retuning of a comparatively wideband filter over the entire spectrum of anticipated Doppler frequencies. In this case its frequency is estimated roughly. During the next stage this section of the spectrum in which the presence of a signal is suspected from the results of the first stage is subjected to more careful analysis by retuning a sufficiently narrowband filter and to determine the presence of this signal with low probability of a false alarm.

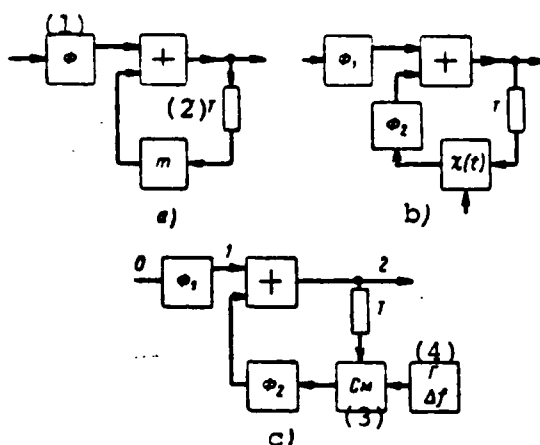


Fig. 6.5.2. Block diagrams of recirculators—coherent signal storage devices.
Key: (1) Filter; (2) Flip-flop; (3) Mixer; (4) High-frequency generator.

Let us explain its operating principle on the simplest example when a sinusoidal oscillation $u_1(t) = U \cos \omega t$, whose frequency we assume to be initially known, is fed to the input. The oscillation $u_3(t) = m U \cos \omega(t - T)$ is fed to the second input of the adder (Fig. 6.5.2, a) as a result of circulation through the feedback circuit. It will be in phase with oscillation $u_1(t)$ only if $\omega = \frac{2\pi}{T} n$, where n is an integer. The oscillation $u_2(t) = (1 + m) U \cos \omega t$ is formed at the output after cophasal addition of the two oscillations in the adder. The amplitude of the output voltage will be $1 + m + m^2$ times greater than that of the input voltage in the case of two-stage circulation, it will increase $\frac{1 + m^{k+1}}{1 - m}$ times in the case of k circulations and so on.

If $m = 1$ is fulfilled, then the amplitude of the output oscillation will increase $k + 1$ times as a result of k circulations. Coherent storage of the input oscillation is also included in this.

The oscillations of the other frequency $\omega \neq 2\pi n/T$ will not be added to the phase shifts equal to ωT , $2\omega T$, $3\omega T$ and so on. These phase shifts can be compensated for by placing a phase shifter by angle

$\chi(\omega T) = 2\pi R \left(\frac{\omega T}{2\pi} \right)$ (Fig. 6.5.2, b) in the feedback circuit of the recirculator.

If the frequency of the input oscillation is previously unknown, its coherent storage can be achieved by changing the angle of rotation of the phase of the phase shifter by the law

$$\chi(t) = \frac{2\pi}{T} t, \quad (6.5.4)$$

which is equivalent to shifting the frequency of the circulating oscillation by the value $\Delta\omega = \frac{d\chi}{dt} = \frac{2\pi}{T}$ (Fig. 6.5.2, c). In this case the angle of rotation of phase varies smoothly during the signal delay time T in the feedback circuit and assumes all possible values from zero (at $t = 0$) to π (at $t = T/2$) and further to 2π (at $t = T$). Because of this, regardless of what the value of frequency of the oscillation being stored is, the phases of the oscillations to be stored will coincide at one of the moments of time during length T , which also determines their coherent storage.

Coherent storage occurs at the moment of time during which the phase rotation angle (6.5.4) coincides with accuracy up to integer 2π with the phase delay angle of the oscillation occurring due to its delay by time T in the feedback circuit. Therefore, the condition for coherent storage in this case is as follows:

$$\Delta\omega t = \omega T - 2\pi n_1,$$

where n_1 is an integer.

Accordingly, coherent storage of the frequency oscillation ω occurs at moments of time

$$t = \frac{1}{\Delta\omega} (\omega T - 2\pi n_1). \quad (6.5.5)$$

Thus, the frequency of the input oscillation is linearly related to the moment the maximum output oscillation is reached. By measuring this moment of time, one can measure the frequency of the input oscillation. Single-channel spectrum analyzers for simultaneous analysis are also based on this principle [138-140]. 24

If radio pulses of length τ_0 with repetition period T and with unknown frequency ω rather than continuous harmonic oscillations are fed

to the input of the recirculator, then for coherent storage of them one must change the phase of the phase shifter of the recirculator by the law

$$\chi(t) = \frac{2\pi}{\tau_0} t \quad (6.5.6)$$

or shift the frequency of the circulating pulses by the value

$$\Delta\omega = \frac{2\pi}{\tau_0} \quad (6.5.7)$$

In this case the phase rotation angle of the radio pulse to be stored varies smoothly during its duration in the range whose width is equal to 2π . Because of this, regardless of the value of the carrier frequency of the radio pulses to be stored, their phases coincide at one of the moments of time during their duration. This also leads to coherent storage of them. In this case the moments of coherent storage, according to (6.5.5), carry information about the frequency of the radio pulses to be stored.

When receiving radar signals reflected from moving targets, their frequency is described by (6.5.1), due to which condition (6.5.5) assumes the form

$$t(\Omega) = \frac{1}{\Delta\omega} (\omega_0 T + \Omega T - 2\pi n_1) = \frac{1}{\Delta\omega} (\Omega T + 2\pi n_2), \quad (6.5.8)$$

where n_2 is an integer. It was assumed in this case that the repetition period is a multiple of the period $T_0 = 2\pi/\omega_0$ of the carrier oscillation. Specifically, when receiving a signal from a fixed target ($\Omega = 0$),

$$t(0) = \frac{2\pi n_2}{\Delta\omega} = n_2 \tau_0 \quad (6.5.9)$$

Accordingly, coherent storage of signals reflected from a fixed target, regardless of the moment of their arrival, always occurs at moments that are a multiple of the duration of the pulses being received.

This is easy to understand if one takes into account that the delay of these pulses by T changes their phase by a value that is a

multiple of 2π and their coherent storage may occur only at those moments of times during which the phase shift (6.5.6) is a multiple of 2π . By setting this value equal to (6.5.6), we find (6.5.9).

It follows from (6.5.8) and (6.5.9) that the time shift of the maximum output signal determined by coherent storage, due to the Doppler frequency shift of the input signal

$$\Delta t = t(\Omega) - t(0) = \frac{7\Omega}{\Delta\omega} \quad (6.5.10)$$

is proportional to the value of this shift.

Let us consider coherent storage of a sequence of N pulsed signals with unknown Doppler frequency shift

$$v_0(t) = \sum_{k=0}^{N-1} V_0(t - kT) \cos(\omega t + \alpha),$$

where $V_0(t - kT)$ is the law of amplitude variation of the k -th pulse in the sequence, ω is described by expression (6.5.1) and α is the initial phase.

Let us assume that the Doppler frequency is much less than the spectral width of the pulsed signal: $|\Omega| \ll 2\pi/\tau_0$, where τ_0 is the length of this signal. This condition is easily transformed to the following condition: $|v_r|\tau_0 \ll 0.5\lambda_0$, i.e., variation of the distance between the radar station and the target during the length of the pulse being received is much less than half the wavelength. This condition is usually fulfilled in practice, with the exception of cases of very fast targets, superlong pulses and very short wavelengths.

After passing through the prestorage filter F_1 (Fig. 6.5.2, c), the sequence of pulsed signals assumes the form

$$v_1(t) = \sum_{k=0}^{N-1} V_1(t - kT) \cos(\omega t + \alpha).$$

The voltage at the output of the recirculator is the sum of the voltage at its input and of the voltages determined by one, two and so on circulations of the input voltage. During circulation the oscillations are delayed each time by time T , the frequency is shifted by $\Delta\omega$ and are

filtered by means of filter F_2 . Let us assume in the first approximation that a signal pulse having carrier frequencies $\omega + \Delta\omega$, $\omega + 2\Delta\omega$, ..., $\omega + (N - 1)\Delta\omega$, respectively, during the first $N-1$ circulations is transmitted by filter F_2 without any distortions and that there is the carrier frequency $\omega + N\Delta\omega$ during the N -th circulation, which lies outside the bandpass of filter F_2 and is completely filtered by it. Accordingly, the bandpass of the feedback circuit of the recirculator is approximately $N - 1$ times greater in the considered case than in an ordinary recirculator.

The output voltage during the $(k + 1)$ -th period ($kT < t < (k + 1)T$) is the sum of the following voltages:

- a) existing at the input during the same time,
- b) being fed to the input one period earlier (i.e., during the k -th period) and subjected to one circulation through the feedback circuit,
- c) being fed to the input during the $(k-1)$ -th period and making two circulations and so on (Fig. 6.5.3, a).

Due to the assumption made above about the band of filter F_2 , the number of these terms is equal to $k + 1$ at $0 \leq k \leq N - 1$ and $2N - k - 1$ at $N \leq k \leq 2(N - 1)$, since only N pulsed signals are fed to the input of the recirculator and each of them circulates through the feedback circuit only $N - 1$ times.

It is easy to ascertain that with single circulation of oscillation $V_1(t)\cos(\omega t + \alpha)$, the following oscillation is formed

$$\begin{aligned} V_1(t-T)\cos[(\omega(t-T) + \alpha + \Delta\omega)] = \\ = V_1(t-T)\cos[(\omega + \Delta\omega)t - \omega T + \alpha]. \end{aligned}$$

with double circulation,

$$V_1(t-2T)\cos[(\omega + 2\Delta\omega)t - 2\omega T - \Delta\omega T + \alpha].$$

with triple circulation,

$$V_1(t-mT)\cos\left[(\omega + m\Delta\omega)t - m\omega T - \frac{m(m-1)}{2}\Delta\omega T + \alpha\right].$$

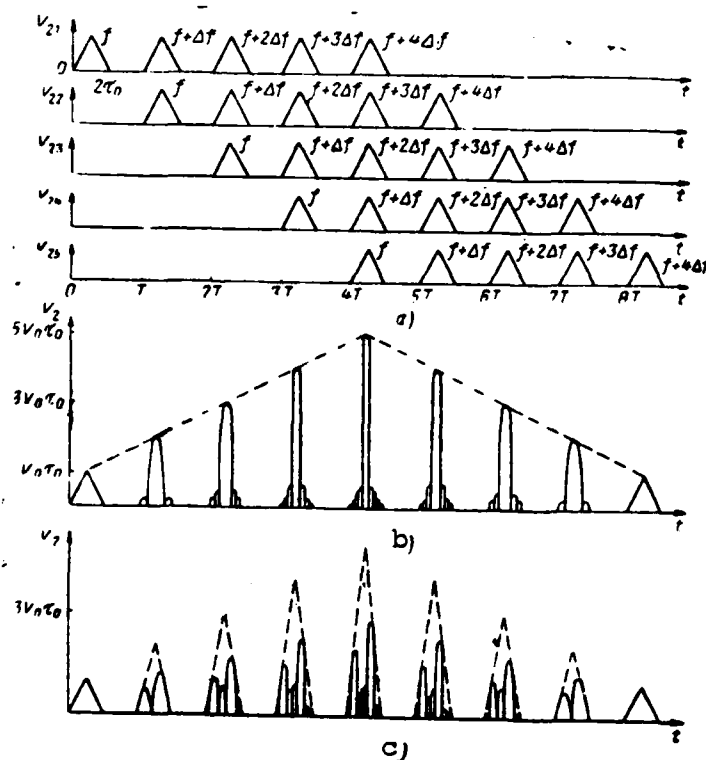


Fig. 6.5.3. Time variation of amplitudes of recirculator responses to i -th pulse ($i = 1-5$) of input oscillation (a) and amplitudes of their sum in the absence (b) and presence (c) of Doppler frequency shift.

with m -tuple circulation,

$$V_1(t - 3T) \cos[(\omega + 3\Delta\omega)t - 3\omega T - 3\Delta\omega T + \alpha].$$

Because of this, the voltage at the output of the recirculator (Fig. 6.5.3, b and c) is

$$v_2(t) = \sum_{k=0}^{N-1} V_1(t - kT) \sum_{m=0}^k \cos[(\omega + m\Delta\omega)t - m\omega T - \frac{m(m-1)}{2} \Delta\omega T + \alpha] + \sum_{k=N}^{2(N-1)} V_1(t - kT) \times \sum_{m=k-N+1}^{N-1} \cos[(\omega + m\Delta\omega)t - m\omega T - \frac{m(m-1)}{2} \Delta\omega T + \alpha].$$

For correct operation of the circuit, the following condition must be fulfilled

$$\Delta\omega T = 2\pi n,$$

$$(6.5.11)$$

where n is an integer.

Therefore, the previous equality assumes the form

$$v_1(t) = \operatorname{Re} \left\{ \left[\sum_{k=0}^{N-1} V_1(t-kT) \sum_{m=0}^k e^{jm(\Delta\omega t - \omega T)} + \sum_{k=N}^{2(N-1)} V_1(t-kT) \sum_{m=k-N+1}^{N-1} e^{jm(\Delta\omega t - \omega T)} \right] e^{j(\omega t + \alpha)} \right\}.$$

Adding these geometric progressions, we find

$$\begin{aligned} v_1(t) = & \sum_{k=0}^{N-1} V_1(t-kT) \frac{\sin \frac{k+1}{2} (\Delta\omega t - \omega T)}{\sin \frac{1}{2} (\Delta\omega t - \omega T)} \times \\ & \times \cos \left[\left(\omega + \frac{k}{2} \Delta\omega \right) t - \frac{k}{2} \omega T + \alpha \right] + \\ & + \sum_{k=N}^{2(N-1)} V_1(t-kT) \frac{\sin \frac{2N-k-1}{2} (\Delta\omega t - \omega T)}{\sin \frac{1}{2} (\Delta\omega t - \omega T)} \times \\ & \times \cos \left[\left(\omega + \frac{k}{2} \Delta\omega \right) t - \frac{k}{2} \omega T + \alpha \right]. \end{aligned}$$

Thus, the output voltage is a sequence of $2N - 1$ pulses and the k -th pulse ($0 < k \leq N - 1$) of this sequence has the amplitude

$$V_{1k}(t) = V_1(t-kT) \left| \frac{\sin \frac{k+1}{2} (\Delta\omega t - \omega T)}{\sin \frac{1}{2} (\Delta\omega t - \omega T)} \right|, \quad (6.5.12)$$

which is the product of the amplitude of the k -th pulse at the input and of the absolute value of an ideal comb function (see (5.1.5)) repeated with period $2\pi/\Delta\omega = \tau_0$ equal to the length of the pulsed signals being received. The latter reaches maximum values equal to $k + 1$ at $\Delta\omega t - \omega T = 2\pi n_3$, where n_3 is an integer, i.e., at moments of time that satisfy the condition $t = kT + (n_3 + F_{\pi} T) \tau_0$, where n_4 is an integer and $0 < n_4 < T/\tau_0$. These maximum values are repeated with a period equal to the length of the pulsed signals being received.

Let us assume that these signals have square-law shape and arrive at one of the moments of time lagging behind the beginning of the $(k + 1)$ -th period by the time that is a multiple of integer

τ_0 *, so that their amplitude varies by the law

$$\left. \begin{aligned} V_0(t) &= V_0 & \text{at } kT + n_s \tau_0 < t < kT + (n_s + 1) \tau_0, \\ V_0(t) &= 0 & \text{at other values of } t, \end{aligned} \right\}$$

where k and n_s are integers (and $0 < k < N-1$ and $0 < n_s < \frac{T}{\tau_0}$).

If the prestorage filter F_1 is optimum for these radio pulses with carrier frequency ω , then due to its small frequency difference with respect to the frequency of the signals being received, the amplitude at its output will vary by essentially the same triangular law as in the absence of a frequency difference:

$$\left. \begin{aligned} V_1(t-kT) &= V_0(t-kT-n_s \tau_0) \\ &\quad \text{at } kT + n_s \tau_0 < t \leq kT + (n_s + 1) \tau_0, \\ V_1(t-kT) &= V_0[kT + (n_s + 2) \tau_0 - t] \\ &\quad \text{at } kT + (n_s + 1) \tau_0 < t < kT + (n_s + 2) \tau_0, \\ V_1(t-kT) &= 0 \\ &\quad \text{at other values of } t. \end{aligned} \right\}$$

Because of this, amplitude (6.5.12) of the output pulse reaches maximum values at those moments of time which correspond to the maximums of the absolute value of an ideal comb function lying in the range of the pulse length at the input of the recirculator.

At $F_d = 0$, this maximum is the only one and is observed at the moment $t = kT + (n_s + 1) \tau_0$, coinciding with the mid-point of the pulse at the input of the recirculator, and has the value

251

$$V_{2m}(k) = (k+1) V_0 \tau_0. \quad (6.5.13)$$

If there is a Doppler frequency shift, the amplitude of the k -th output pulse has two maximum values at the following moments of time

$$\left. \begin{aligned} &\text{and} \quad \left. \begin{aligned} t_1 &= kT + (n_s + TF_d) \tau_0 \\ t_2 &= kT + (n_s + 1 + TF_d) \tau_0 \end{aligned} \right\} \text{at } F_d > 0 \\ &\text{or} \\ &\text{and} \quad \left. \begin{aligned} t_1 &= kT + (n_s + 1 + TF_d) \tau_0 \\ t_2 &= kT + (n_s + 2 + TF_d) \tau_0 \end{aligned} \right\} \text{at } F_d < 0. \end{aligned} \right\}$$

*The more general case is considered below.

The values of these maximums are as follows:

$$\left. \begin{array}{l} \text{and} \\ \text{at} \\ \text{and} \end{array} \right\} \begin{array}{l} V_{2M1}(k) = (k+1)V_0\tau_0TF_d \\ V_{2M2}(k) = (k+1)V_0\tau_0(1-TF_d) \\ V_{2M1}(k) = (k+1)V_0\tau_0(1-T|F_d|) \\ V_{2M2}(k) = (k+1)V_0\tau_0T|F_d| \end{array} \left\{ \begin{array}{l} \text{at } F_d > 0 \\ \text{at } F_d < 0. \end{array} \right.$$

The highest of them is that which is closer to moment $kT + \tau_0$ of the maximum input pulse, i.e., the first maximum if $F/2 < F_d < F$ or $-(F/2) < F_d < 0$ and the first maximum if $0 < F_d < F/2$ or $-F < F_d < -(F/2)$.

According to the property of an ideal comb function, each of the maximums of the k -th output pulse has the length (from the first zeros)

$$\left. \begin{array}{l} \tau_1(k) = \frac{2\tau_0}{k+1} \quad \text{at } 0 < k < N-1 \\ \text{and} \\ \tau_1(k) = \frac{2\tau_0}{2N-k-1} \quad \text{at } N < k < 2(N-1), \end{array} \right\} \quad (6.5.14)$$

i.e., it is $(k+1)$ and $(2N-k-1)$ times less, respectively, than the pulse length at the input of the recirculator (Fig. 6.5.3, b and c). Specifically, at $k = N-1$ the pulse has the maximum possible amplitude

$$\left. \begin{array}{l} V_1(N) = NV_0\tau_0(1-|F_d|T) \quad \text{at } -\frac{F}{2} < F_d < \frac{F}{2} \\ \text{and} \\ V_1(N) = NV_0\tau_0F_dT \quad \text{at } \frac{F}{2} < |F_d| < F \end{array} \right\} \quad (6.5.15)$$

and minimum length

$$\tau_1 = \frac{2\tau_0}{N}. \quad (6.5.16)$$

If there is no Doppler frequency shift ($F_d = 0$), formula (6.5.15) coincides with (5.3.1) that describes the peak value of the signal at the output of an optimum filter for a sequence of N pulsed signals.

It follows from (6.5.15) that the relative decrease of the peak value of the output signal due to the Doppler frequency shift varies by piecewise-linear law:

$$\left. \begin{aligned} \frac{V_2(N)}{V_{2m}(N)} &= 1 - |F_d|T & \text{at } 0 \leq |F_d| \leq \frac{F}{2}, \\ \frac{V_2(N)}{V_{2m}(N)} &= |F_d|T & \text{at } \frac{F}{2} \leq |F_d| \leq F \end{aligned} \right\} \quad (6.5.17)$$

and in the most unfavorable case ($|F_d|T = 0.5$) comprises 0.5 (i.e., 6 dB). Assuming that the Doppler shift is random and that it has uniform probability distribution in the range $(-F, F)$, we find that the average decrease of amplitude is 0.75 (i.e., 2.5 dB). This decrease can be made even less by increasing n times the shift frequency $\Delta\omega$ in the feedback circuit. In this case $2n$ maximum values following at time intervals τ_0/n rather than two maximum values are observed during pulse length $2\tau_0$. One of them lies near the greatest maximum of the output signal in the absence of a Doppler shift and hardly differs from it in value. However, this requires broadening of the bandpass of the feedback circuit of the recirculator n -fold, which cannot be accomplished in practice due to the absence of sufficiently wideband delay lines.

The noise in the considered system (Fig. 6.5.2, c) is stored by the same law as in an ordinary coherent pulsed signal storage device with known frequency or in an optimum filter for a sequence of these signals (see item 2, section 5.3). This is explained by the fact that due to the assumption of the small Doppler shift compared to the spectral width of the signals being received, the prestorage optimum filter for a single pulse with unshifted carrier frequency accomplishes essentially optimum intraperiod processing of the received signals having just as small a Doppler shift of the carrier frequency [15]. Linear phase modulation (or frequency modulation) of noise during each repetition period, which occurs during circulation through the feedback circuit, does not alter their random nature and accordingly the law of their storage. Therefore, the noise output at the output of the considered system is the same as at the output of an optimum filter for a sequence of pulsed signals (see (5.3.5)).

Consequently, the loss in the signal/noise ratio in respect to power, conditioned by the Doppler shift of frequency, is equal to the square of a lessening of signal amplitude (6.5.17) and in the worst case comprises 6 dB, and on the average 2.5 dB.

The case when the arrival time of pulsed signals is known and coincides with the moment of passage through zero or a value that is a multiple of 2π of phase shift (6.5.6) created in the feedback circuit

by a phase shifter was considered above. This assumption usually does not occur. In this case the amplitude of the output pulse even with unshifted carrier frequency (Fig. 6.5.4, b) may vary due to noncoincidence of the moment of the maximum input signal with the moment of passage of a value that is a multiple of 2π (Fig. 6.5.4, a) through phase (6.5.6).

In the case of a Doppler frequency shift of the output pulse, it may increase to the maximum possible value and it may also decrease (Fig. 6.5.4, c). In this case the maximum and mean values of losses have the same values as before.

Thus, both the range to the target (with accuracy up to the interval corresponding to the pulse length τ_0 and its speed (by the shift of this maximum with respect to the moment that is a multiple of the indicated length)* can be determined by the position of the maximum output signal. These signal parameters can be measured on a scope with brightness mark, linear horizontal scanning with repetition period of the system and linear vertical scanning with period equal to signal length. One can use a two-scale scope with circular scanning for this purpose. The harmonic oscillation of the shifting frequency $\Delta\omega$ should be used to create rapid scanning and the harmonic oscillation found by dividing the frequency of the first oscillation and having a period equal to the repetition period of the system should be used to create slow scanning. The scope with fast scanning is used to measure speed and the one with slow scanning is used to measure range. To increase the accuracy of the latter, one can make the range indicator two-scale.

We note that due to the fact that usually $\Delta\omega \ll \omega_0$, then it is practically difficult to convert the frequency in the feedback circuit of the recirculator by the diagram shown in Fig. 6.5.2, c. Therefore, double frequency conversion is employed (Fig. 6.5.5). The frequency of the first heterodyne f_1 is selected from the condition of good filtra-

* We note that the radial velocity of the target is determined clearly only with clear measurement of the Doppler frequency shift, which is possible in the given circuit only at $|F_d| < F$ [154].

tion of undesirable combination frequencies on the intermediate frequency $f - f_1$. The frequency of the second heterodyne differs from that of the first by the value of the required signal frequency shift. The difference frequency is determined after the first conversion and the total frequency is determined after the second: $f - f_1 + f_2 = f - f_1 + (f_1 + \Delta f) = f + \Delta f$. The APCh [intermediate-frequency amplitude] of one of the heterodynes is used to maintain equality (6.5.11), required for correct operation of the circuit.

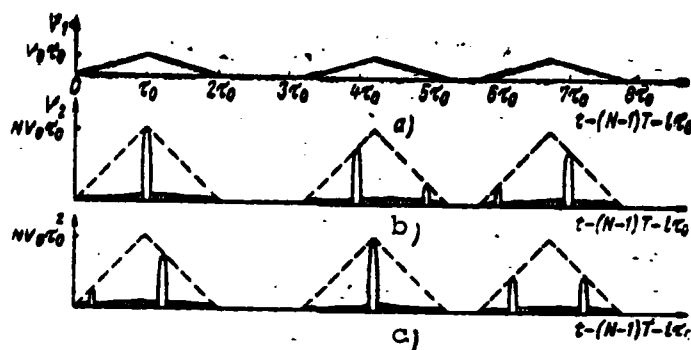


Fig. 6.5.4. Time variation of pulse amplitudes at input (a) and output with and without Doppler frequency shift (b— $F_D = 0$; c— $F_D = 0.25 F$). Here i is an arbitrary integer ($0 \leq i < T/T_0 - 8$).

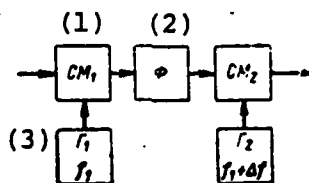


Fig. 6.5.5. Block diagram of frequency shift device by value f .

Key: (1) Frequency mixer; (2) Filter; (3) High-frequency generator.

In conclusion let us again emphasize that realization of this system requires considerable broadening of the bandpass of the recirculator delay line, which may be difficult in some cases and may require the use of a multichannel system. If the indicated difficulty can be overcome, then the considered single-channel circuit should be preferable to a system with large number of channels.

A COHERENT SINGLE-STAGE STORAGE DEVICE

7.1. CHARACTERISTICS OF STORAGE DEVICE

It is shown in item 1, section 5.4 that the simplest practical approximation of an optimum filter for a sequence of video pulse signals is the combination of a prestorage filter and recirculator. The advantage provided by this combination is calculated in the same section in the case when an optimum filter for a single pulsed signal is used as the prestorage filter while the feedback circuit of the recirculator has broad bandpass without limit. The latter assumption is usually not fulfilled in practice. Moreover, the radio-frequency part of the coherent receiver that includes a coherent detector and that has good selectivity is in front of signal storage. Because of this, the use of an additional prestorage optimum filter for a single pulsed signal is not feasible.

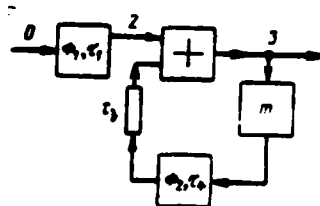


Fig. 7.1.1. Block diagram of single storage device.

Key: (1) Filter

In this regard let us consider a single storage device (Fig. 7.1.1) in the form of a combination of a prestorage filter F_1 and a recirculator whose feedback circuit consists of an attenuator with transfer coefficient m , delay device by time t_3 and filter F_2 that takes into account the nonuniform frequency characteristic of the feedback circuit (and mainly of the delay device). This storage device is an integral part of a coherent receiver (Fig. 6.2.1, d or Fig. 6.3.1, b).

25

The purpose of this consideration is to determine the gain of signal/noise ratio provided by this storage device compared to an optimum filter for a single signal. This permits one to calculate the value of the threshold signals upon storage by means of a single coherent storage device using the relations found in the previous chapter.

Let us assume that frequency filters F_1 and F_2 have bell-shaped frequency and linear phase characteristics, i.e., they have the transfer function

$$K_{1,2}(\omega) = \exp \left(-\frac{1}{8\pi c^2} \omega^2 \tau_{1,2}^2 - j\omega t_{1,2} \right), \quad (7.1.1)$$

where $\tau_{1,2}$ is the length of the pulsed responses of these filters, $t_{1,2}$ is the delay time of the oscillations in them, $c^2 = \frac{2}{\pi} \ln \frac{1}{d}$; and d is the level of reading the response time of the filter and of its bandpass (and signal length below).

To simplify notation of the subsequent expressions, let us disregard the delay of oscillations during their passage through filter F_1 , i.e., let us assume that $t_1 = 0$. The permissibility of this is obvious. With the exception of section 7.5, in which the more general case is considered, the delay time of oscillations in the recirculator feedback circuit is equal to the repetition quasi-period of pulsed signals, i.e., $t_3 + t_4 = T$.

Let us assume that the signal is a square-wave sequence of bell-shaped video pulses.

Let us judge the validity of the assumptions made above.

The validity of a bell approximation for the frequency characteristic of prestorage filter F_1 raises no doubts since this filter modulates the radio-frequency part of the coherent receiver preceding the storage device, which is usually multicircuit, due to which its frequency characteristic is very close to bell-shaped. 258

Bell approximation of the frequency characteristic is less precise, but acceptable for the filter in the feedback circuit since the oscillations are usually delayed by radio frequency and are accompanied by considerable attenuation (see item 1, section 11.1). Therefore, four or five selective amplifiers [141], whose resulting frequency characteristic can approximately be regarded as bell, is used in the indicated circuit. This is also indicated by experimental data.

Bell approximation of the shape of real pulsed signals is no less precise than approximation by square-wave pulses, especially in the case of their short length. The fact that a bell pulse is theoretically extended in time from $-\infty$ to ∞ is not significant since it is assumed that the stored sequence of pulsed signals has a very high on-off time ratio.

With regard to the square-wave shape of the envelope of the sequence of pulsed signals, the shape of this sequence can be selected as simpler due to the noncritical structure of the optimum filter to changes in the shape of the video signal (item 2, section 2.4) and the congruence of the optimum filter for a video signal and pulse sequence with envelope of the same shape (item 3, section 5.1). Other shapes of the envelope of the sequence can easily be recalculated to an equivalent square-wave shape.

The above assumptions on the form of the frequency characteristics of filters and the shape of the pulsed signals considerably simplify investigation of the storage of pulsed signals since in this case it becomes possible to make use of the fact that bell pulses, passing through filters with bell frequency characteristics, do not change their shape [142.]

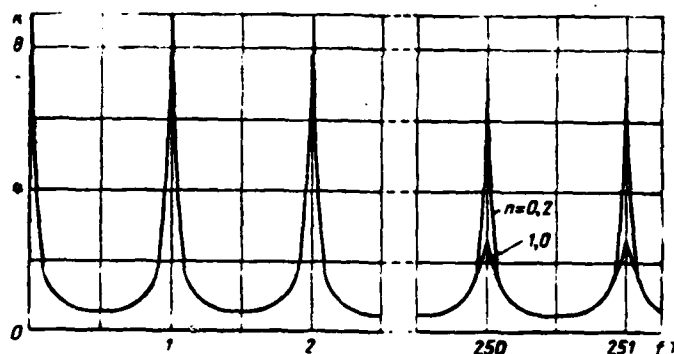


Fig. 7.1.2. Amplitude-frequency characteristic of single storage device.

The considered storage device obviously has the transfer function [143] 258

$$\bar{K}(\omega) = \frac{K_1(\omega)}{1 - mK_2(\omega)e^{-j\omega T}} = \frac{K_1(\omega)}{1 - mK_2(\omega)e^{-j\omega T}} \quad (7.1.2)$$

and the amplitude-frequency characteristic 259

$$K(\omega) = \frac{K_1(\omega)}{\sqrt{1 - 2mK_2(\omega)\cos\omega T + m^2K_2^2(\omega)}}, \quad (7.1.3)$$

which is a comb characteristic (Fig. 7.1.2) and reaches maximum values at frequencies of $\omega = l\Omega$ that are multiples of the repetition rate $\Omega = 2\pi/T$ (Fig. 7.1.3)

$$\begin{aligned} K_{\max}(l) &= K(l\Omega) = \frac{K_1(l\Omega)}{1 - mK_2(l\Omega)} = \\ &= \frac{\exp\left[-\frac{1}{8\pi}\left(\frac{l\Omega\tau_1}{c}\right)^2\right]}{1 - m \exp\left[-\frac{1}{8\pi}\left(\frac{l\Omega\tau_2}{c}\right)^2\right]}, \end{aligned} \quad (7.1.4)$$

and reaches minimum values on frequencies of $\omega = (l + 0.5)\Omega$

$$K_{\min}(l) = K\left[\left(l + \frac{1}{2}\right)\Omega\right] = \frac{K_1\left[\left(l + \frac{1}{2}\right)\Omega\right]}{1 - mK_2\left[\left(l + \frac{1}{2}\right)\Omega\right]}.$$

Let us determine the bandpass $\delta\Omega_1$ of the l -th spike of the comb characteristic (7.1.3) at the level of $1/\sqrt{2}$. Assuming that the bandpasses of filters F_1 and F_2 are considerably broader than that of the 260

spike, due to which

$$K_{1,2} \left(l\Omega + \frac{\delta\Omega_l}{2} \right) \approx K_{1,2}(l\Omega),$$

we determined from the condition

$$K \left(l\Omega + \frac{\delta\Omega_l}{2} \right) = \frac{1}{\sqrt{2}} K(l\Omega)$$

the relative bandpass of the 1-th spike (Fig. 7.1.4):

261

$$\frac{\delta F(l)}{F} = \frac{\delta\Omega_l}{\Omega} = \frac{1}{\pi} \arccos \left\{ 1 - \frac{[1 - mK_2(l\Omega)]^2}{2mK_2(l\Omega)} \right\}, \quad (7.1.5)$$

which makes sense only at $0.172 < mK_2(l\Omega) < 1$. Specifically, if $m_3 = mK_2(l\Omega)$ is sufficiently close to 1, then using formulas

$$\cos x \approx 1 - \frac{x^2}{2} \quad \text{and} \quad \sqrt{m_3} \approx \frac{1 + m_3}{2},$$

it is easy to find from (7.1.5)

262

$$\frac{\delta F(l)}{F} \approx \frac{2}{\pi} \frac{1 - mK_2(l\Omega)}{1 + mK_2(l\Omega)}. \quad (7.1.6)$$

At $mK_2(l\Omega) = 0.5, 0.7$ and 0.8 , this formula yields errors of 7.8, 3 and 0.7 percent, respectively.

Substituting $\omega = l\Omega + \nu$, where $|\nu| < \Delta\Omega_1$, into (7.1.3) and using (7.1.4), (7.1.6) and $\cos T \approx 1 - 1/2(\nu T)^2$, we find

$$\frac{K(\Omega l + \nu)}{K(\Omega l)} \approx \frac{1}{\sqrt{1 + \left(\frac{2\nu}{\Delta\Omega_1} \right)^2}} \quad (7.1.7)$$

Accordingly, the amplitude-frequency characteristic of the storage device (Fig. 7.1.5, curve 1) coincides at small frequency differences with respect to the nearest maximum to the amplitude-frequency characteristic of a resonance circuit with the same bandpass.

It follows from (7.1.4)-(7.1.6) that filter F_1 affects only the maximum value of the comb characteristic of the storage device, while filter F_2 affects both the value of these maximums and the bandpass of its spikes.

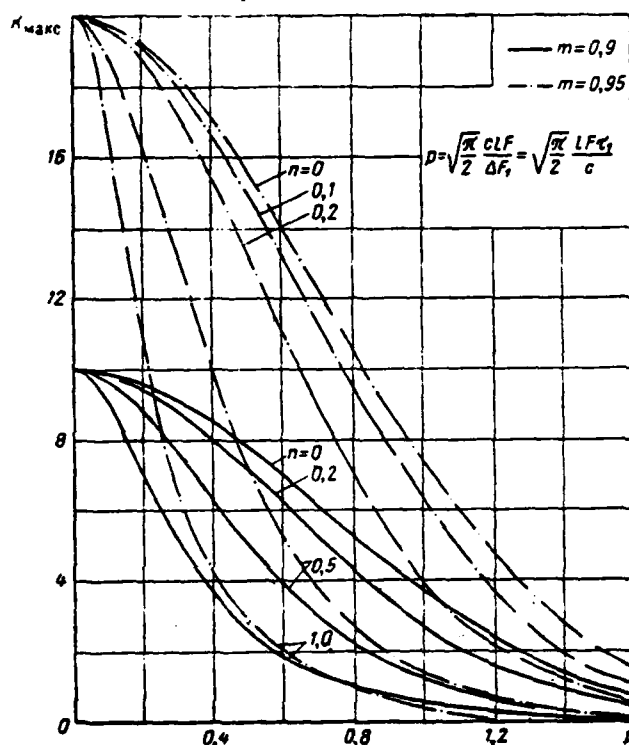


Fig. 7.1.3. Upper envelopes of amplitude-frequency characteristic of single storage device.

It is easy to see that the components of the storage device perform the following linear operations on the signal: 263

1) the convolution operation C_p , i.e., the operation of the effect of a filter with response time τ_p on a pulse $v(t, \tau)$ of length τ :

$$C_p v(t, \tau) = v\left(t, \sqrt{\tau^2 + \tau_p^2}\right), \quad (7.1.8)$$

where

$$v(t, \tau) = \frac{1}{\tau} \exp\left[-2\pi\tau^2\left(\frac{t}{\tau}\right)^2\right], \quad (7.1.9)$$

2) delay operation by time T :

$$\Gamma v(t) = v(t-T), \quad (7.1.10)$$

3) attenuation operation by a factor of m :

$$\Lambda v(t) = mv(t). \quad (7.1.11)$$

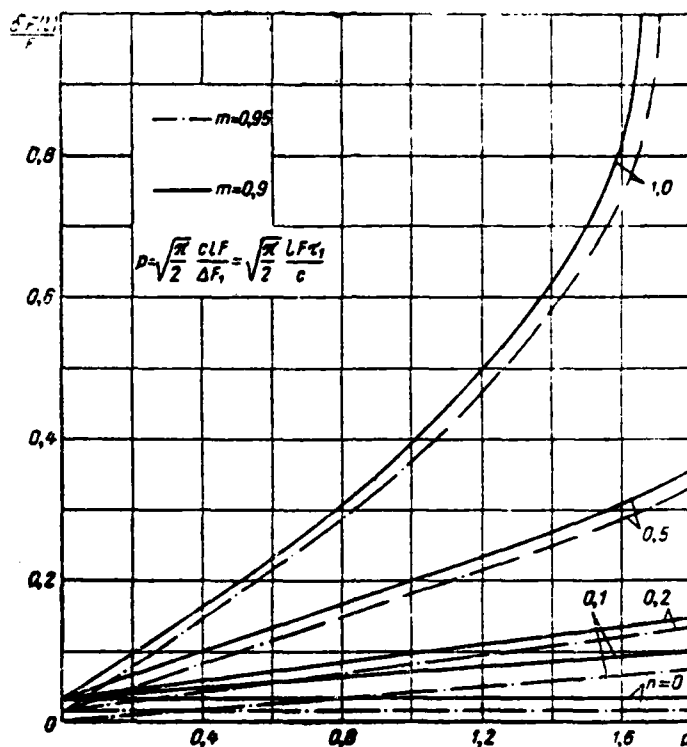


Fig. 7.1.4. Dependence of relative bandpass of 1-th spike of amplitude-frequency characteristic on parameter p .

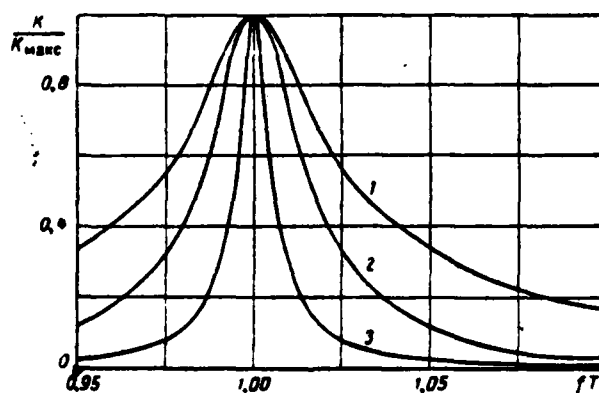


Fig. 7.1.5. Shape of spikes of amplitude-frequency characteristics of single (1), double (2) and two-stage storage devices at $M = 5$ (3).

Because of this, the pulse characteristic of the storage device, 263
i.e., its response to a single pulse $\delta(t) = \sqrt{2} cv(t, 0)$, is

$$\begin{aligned}
 h_1(t) &= C_1 \sum_{k=0}^{\infty} A^k C_1^k \Gamma^k \sqrt{2} c v(t, 0) = \\
 &= \sqrt{2} c \sum_{k=0}^{\infty} m^k v(t - kT, \sqrt{\tau_1^2 + k\tau_4^2}).
 \end{aligned}
 \tag{7.1.12}$$

Thus, the pulse characteristic of the storage device consists of an infinitely large number of bell-shaped pulses and the k -th pulse reaches a maximum at moment $t = kT$ and has the amplitude (Fig. 7.1.6, a)

$$\begin{aligned}
 H_1(kT) &= \sqrt{2} c m^k v(0, \sqrt{\tau_1^2 + k\tau_4^2}) = \\
 &= \frac{\sqrt{2} c m^k}{\tau_1 \sqrt{1 + kn^2}}
 \end{aligned}
 \tag{7.1.13}$$

and length (Fig. 7.1.6, b)

$$\tau_2(k) = \sqrt{\tau_1^2 + k\tau_4^2} = \tau_1 (1 + kn^2)^{1/2}, \tag{7.1.14}$$

where $n = \frac{\tau_4}{\tau_1} = \frac{\Delta F_1}{\Delta F_2}$ is the ratio of the bandpass of the prestorage filter and the feedback circuit of the recirculator. 264

Thus, the restriction of the bandpass of the recirculator feedback circuit leads to a more rapid than exponential decrease of the maximum pulse characteristic of the storage device and to the fact that the lengths of its pulse components increase with an increase of the ordinal number of these pulses.

7.2. Signal Storage

265

It follows from the foregoing that if a square-wave sequence of N bell pulsed signals of amplitude V_0 and length τ_0 act on the input of the system:

$$v_0(t) = V_0 \tau_0 \sum_{i=0}^{N-1} v(t + iT, \tau_0)$$

we find at the output of the prestorage filter

$$v_1(t) = C_1 v_0(t) = V_0 \tau_0 \sum_{i=0}^{N-1} v(t + iT, \sqrt{\tau_0^2 + \tau_1^2}).$$

and at the output of the storage system

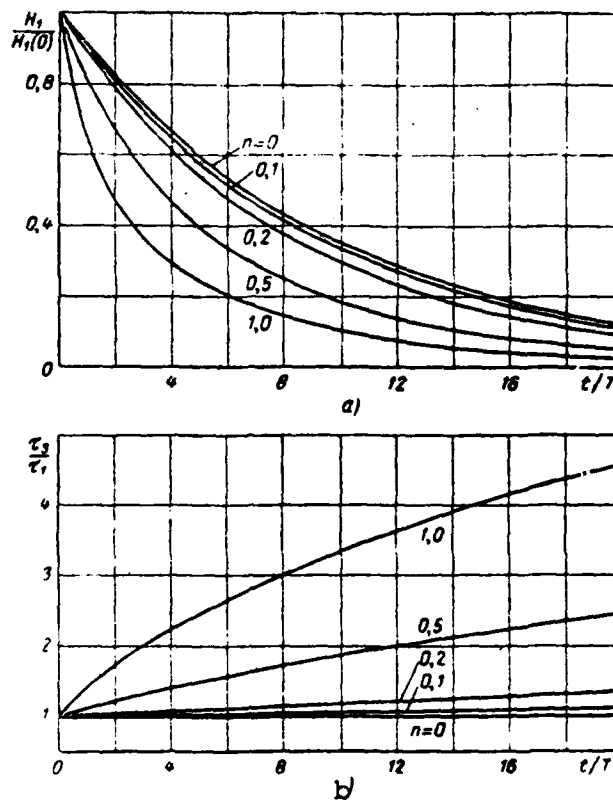


Fig. 7.1.6. Time variation of envelope (a) and pulse length (b) of pulse characteristic of storage device.

$$\begin{aligned}
 v_s(t) &= \sum_{k=0}^{\infty} \Lambda^k C_k^k \Gamma^k v_s(t) = \\
 &= V_s \tau_s \sum_{k=0}^{\infty} m^k \sum_{l=0}^{N-1} v(t + [l-k]T, \sqrt{\tau_0^2 + \tau_1^2 + k\tau_4^2}).
 \end{aligned} \quad (7.2.1)$$

The peak value of the stored signal is obviously observed at $t = 0$:

$$V_s = v_s(0) = V_s \tau_s \sum_{k=0}^{\infty} m^k \sum_{l=0}^{N-1} v([l-k]T, \sqrt{\tau_0^2 + \tau_1^2 + k\tau_4^2}).$$

Due to the high on-off time ratio of the stored pulse signals and the very short response times of the filters compared to the repetition quasi-period:

$$\tau_0 \ll T; \quad \tau_1 \ll T; \quad \tau_4 \ll T, \quad (7.2.2)$$

the last expression is simplified considerably:

$$V_3 \approx V_0 \tau_0 \sum_{k=0}^{N-1} m^k v(0, \sqrt{\tau_0^2 + \tau_1^2 + k\tau_1^2}) =$$

$$= V_0 \tau_0 \sum_{k=0}^{N-1} \frac{m^k}{\sqrt{\tau_0^2 + \tau_1^2 + k\tau_1^2}}. \quad (7.2.3)$$

Accordingly, the signal transfer coefficient of the system being analyzed comprises 26

$$g_1 = \frac{V_3}{V_0} = \gamma \sum_{k=0}^{N-1} \frac{m^k}{\sqrt{1 + \gamma^2 + k\gamma^2}}, \quad (7.2.4)$$

where $\gamma = \frac{\tau_0}{\tau_1} = \frac{1}{c^2} \Delta F_1 \tau_0$ is a coefficient proportional to the product of the bandpass of the prestorage filter by the length of the input pulse (the prestorage filter is optimum to this pulse at $\gamma = 1$).

The signal transfer coefficient can essentially be calculated rather accurately by formula (7.2.4) using a digital computer at large value of N and value of n distinct from zero. Therefore, it is of interest to find a simpler, although approximate expression for g_1 . To do this, let us use the Euler formula [144] that permits us to reduce calculation of the sum to calculation of the integral. In the considered case

$$g_1 = \frac{\gamma}{n} \sum_{k=0}^{N-1} \frac{m^k}{\sqrt{\frac{1+\gamma^2}{n^2} + k}} \approx \frac{\gamma}{n} \left(\int_0^{N-1} \frac{e^{-\ln \frac{1}{m} x} dx}{\sqrt{\frac{1+\gamma^2}{n^2} + x}} + \right.$$

$$\left. + \frac{1}{2} \frac{1}{\sqrt{\frac{1+\gamma^2}{n^2}}} + \frac{1}{2} \frac{m^{N-1}}{\sqrt{\frac{1+\gamma^2}{n^2} + N-1}} \right) =$$

$$= \gamma \left[\frac{1}{n} \int_0^\infty \frac{e^{-\ln \frac{1}{m} x} dx}{\sqrt{\frac{1+\gamma^2}{n^2} + x}} - \frac{m^{N-1}}{n} \int_0^\infty \frac{e^{-\ln \frac{1}{m} y}}{\sqrt{\frac{1+\gamma^2}{n^2} + N-1+y}} dy + \right.$$

$$\left. + \frac{1}{2\sqrt{1+\gamma^2}} + \frac{m^{N-1}}{2\sqrt{1+\gamma^2 + (N-1)\gamma^2}} \right].$$

Using formula (3.362.2) from [92] twice, we find

267

$$\begin{aligned}
g_1 \approx & \frac{\gamma}{n} \sqrt{\frac{\pi}{\ln \frac{1}{m}}} m^{-\frac{1+\gamma^2}{n^2}} \times \\
& \times \left[\Phi \left(\sqrt{\left(\frac{1+\gamma^2}{n^2} + N - 1 \right) \ln \frac{1}{m}} \right) - \right. \\
& \left. - \Phi \left(\sqrt{\frac{1+\gamma^2}{n^2} \ln \frac{1}{m}} \right) \right] + \frac{\gamma}{2} \left(\frac{1}{\sqrt{1+\gamma^2}} + \right. \\
& \left. + \frac{m^{N-1}}{\sqrt{1+\gamma^2 + (N-1)n^2}} \right).
\end{aligned} \tag{7.2.5}$$

In the case when $(1+\gamma^2) \ln \frac{1}{m} \approx (1+\gamma^2)(1-m) \geq 9n^2$, there is the possibility of using the following asymptotic expression for the probability integral [25]:

$$\Phi(z) \approx 1 - \frac{e^{-z^2}}{\sqrt{\pi} z} \left(1 - \frac{1}{2z^2} \right),$$

and of simplifying the formula found above:

$$\begin{aligned}
g_1 \approx & \frac{\gamma}{\sqrt{1+\gamma^2}} \left[\frac{1}{\ln \frac{1}{m}} \left(1 - \frac{n^2}{2(1+\gamma^2) \ln \frac{1}{m}} \right) + 0.5 \right] - \\
& - \frac{\gamma m^{N-1}}{\sqrt{1+\gamma^2 + n^2(N-1)}} \times \\
& \times \left[\frac{1}{\ln \frac{1}{m}} \left(1 - \frac{n^2}{2[(1+\gamma^2 + n^2(N-1)) \ln \frac{1}{m}] \right)^{-0.5}} \right].
\end{aligned} \tag{7.2.6}$$

The error of these formulas is less, the closer m is to 1, the lower n is and the larger N and γ are. In most cases of interest, this error does not exceed several percent.

Consideration of the dependence of the signal transfer coefficient (7.2.4), calculated on the BESM-2 computer, on the number of stored pulses (Fig. 7.2.1) shows that the signal transfer coefficient increases with an increase of the number of stored pulses. This increase is more intensive, the closer the feedback coefficient to one, the wider the band of the feedback circuit and the wider the bandpass of the prestorage filter. 268

With unrestricted broadening of the bandpass of the feedback circuit, the signal transfer coefficient approaches the function 269

$$g_1(n=0) = \frac{\gamma}{\sqrt{1+\gamma^2}} \frac{1-m^N}{1-m}. \tag{7.2.7}$$

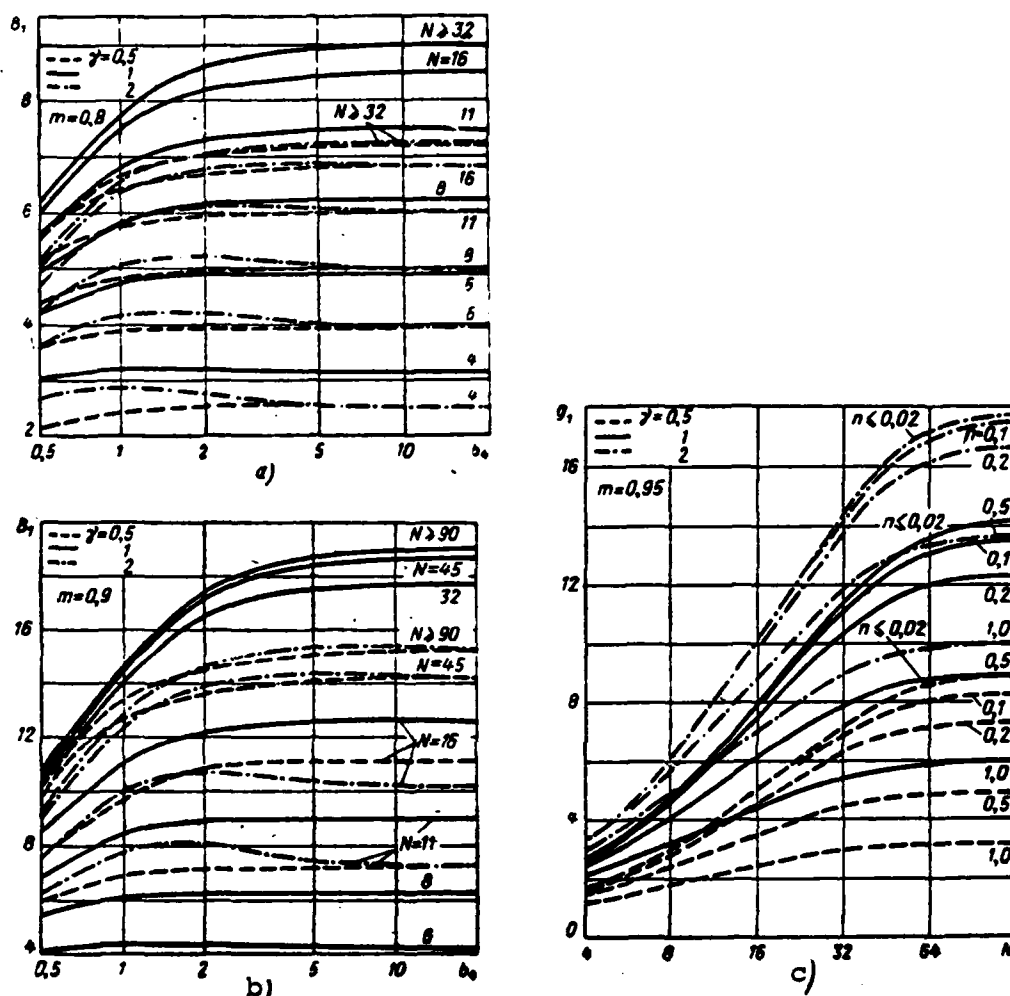


Fig. 7.2.1. Dependence of signal transfer coefficient by single storage device on N at different values of n .

which differs only by the multiplier from expression (5.4.2) found as a result of investigating the storage of pulsed signals in an idealized recirculator (i.e., one having unlimited broad bandpass of the feedback circuit).

The multiplier $\gamma(1 + \gamma^2)^{-1/2}$ in (7.2.7) is obviously the transfer coefficient of the signal by the prestorage filter. Therefore, the storage coefficient of the signal by the recirculator comprises

$$d_1 = g_1 \frac{\gamma(1 + \gamma^2)^{-1/2}}{\gamma} = \gamma(1 + \gamma^2)^{-1/2} \sum_{k=0}^{N-1} \frac{m^k}{\gamma(1 + \gamma^2 + k\gamma^2)}.$$

Analysis of the results of calculation with condition (5.4.19) shows that the bandpass of the recirculator feedback circuit, required to find the signal transfer coefficient differing by less than 5% of the value of this coefficient in an idealized system, is considerably less (by a factor of 5-13) than the value calculated for the case of uncompensated additional signal delay time in the feedback circuit when the stored pulse signals are added to the time shift, which reduces the efficiency of storage [7, 143].

Thus, compensation of the additional signal delay time in the recirculator feedback circuit permits a sharp reduction of requirements on the width of the bandpass of the indicated circuit and thus simplification of the storage device.

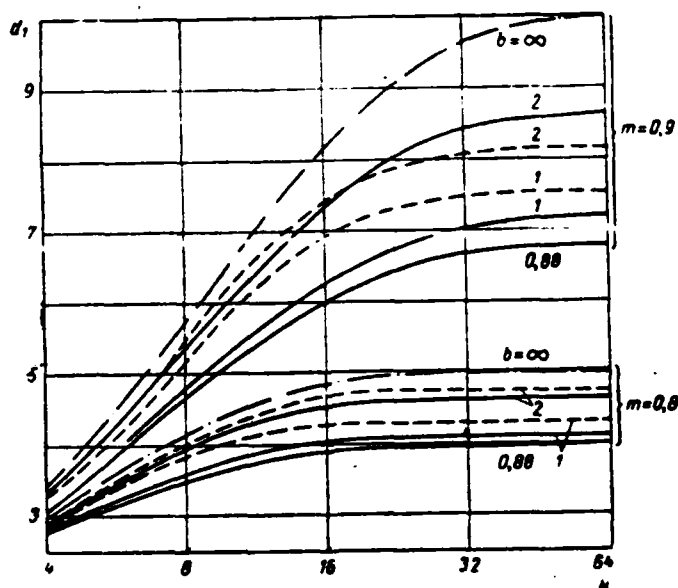


Fig. 7.2.2. Dependence of coefficient of signal storage by recirculator.

The dependence of the coefficient of signal storage by the recirculator on N at different approximations of the frequency characteristics of filters F_1 and F_2 and the shape of pulsed signals is plotted in Fig. 7.2.2. The solid curves correspond to the case of bell approximation of filter characteristics and the shape of pulsed signals considered above at $N = 1$, $\gamma = 2$ and $d = 0.5$. The dashed curves are related to the case when the pulsed signals are square-shaped, the

filters are identical low-frequency RC-filters and the effective delay time of pulsed signals is compensated during storage [145]. The dash-dot curves correspond to the hypothesis that the filters have square-law frequency characteristics with bandpasses of ΔF_1 and ΔF_4 (where $\Delta F_1 \leq \Delta F_4$). This case is obviously equivalent to storage in an ideal recirculator having broad bandpass without restriction ($b = \Delta F_4 \tau_0 = \infty$).

Comparison of these functions shows that they are identical and hardly differ with different approximations of the filter characteristics and signal shape.

7.3. Storage of Noise

Substituting (7.1.12) into (7.1.2), we find the output of stored noise

$$\sigma_3^2 = 2ac^2 \int_{-\infty}^{\infty} \left[\sum_{k=0}^{\infty} m^{2k} v(t - kT, \sqrt{\tau_1^2 + k\tau_4^2}) \right]^2 dt.$$

In view of (7.2.2), individual pulses of the pulse characteristic essentially do not overlap. Therefore,

$$\begin{aligned} \sigma_3^2 &\approx 2ac^2 \int_{-\infty}^{\infty} \sum_{k=0}^{\infty} m^{2k} v^2(t - kT, \sqrt{\tau_1^2 + k\tau_4^2}) dt = \\ &= 2ac^2 \sum_{k=0}^{\infty} \frac{m^{2k}}{\tau_1^2 + k\tau_4^2} \int_{-\infty}^{\infty} \exp \left[-4\pi c^2 \frac{t^2}{\tau_1^2 + k\tau_4^2} \right] dt. \end{aligned}$$

Using formula (3.321.3) from [92], we find

272

$$\sigma_3^2 = \frac{ac}{\tau_1} \sum_{k=0}^{\infty} \frac{m^{2k}}{\sqrt{1 + k\tau_4^2}}. \quad (7.3.1)$$

Having assumed that $m = 0$, we determine the noise output at the output of the prestorage filter:

$$\sigma_2^2 = \frac{ac}{\tau_1}.$$

Consequently, the noise storage coefficient comprises

$$Q_1 = \frac{\sigma_3^2}{\sigma_2^2} = \sum_{k=0}^{\infty} \frac{m^{2k}}{\sqrt{1 + k\tau_4^2}}. \quad (7.3.2)$$

We find this result by the spectral method [146-147]. If white noise with intensity (1.2.4) is fed to the input, the noise at the output has the energy spectrum

$$F_s(\omega) = 2aK^2(\omega) = \frac{2aK_1^2(\omega)}{1 - 2mK_s(\omega) \cos \omega T + m^2 K_2^2(\omega)}$$

and output

$$\begin{aligned} \sigma_s^2 &= \frac{1}{2\pi} \int_0^\infty F_s(\omega) d\omega = \\ &= \frac{a}{\pi} \int_0^\infty \frac{K_1^2(\omega)}{1 - 2mK_s(\omega) \cos \omega T + m^2 K_2^2(\omega)} d\omega. \end{aligned} \quad (7.3.3)$$

Calculation of this integral causes great difficulties in the general case. However, it can be calculated approximately by the method of slowly variable coefficients [146]. The bases for using this method are inequalities (7.2.2).

Let us divide the integration interval in (7.3.3) into individual sections, each of which corresponds to the period of variation of a rapidly oscillating multiplier $\cos \omega T$: 273

$$\begin{aligned} \sigma_s^2 &= \frac{a}{\pi} \sum_{i=0}^\infty \int_{i\Omega}^{(i+1)\Omega} \frac{K_1^2(\omega) d\omega}{1 - 2mK_s(\omega) \cos \omega T + m^2 K_2^2(\omega)} = \\ &= \frac{a}{\pi} \sum_{i=0}^\infty \int_0^\Omega \frac{K_1^2(i\Omega + x) dx}{1 - 2mK_s(i\Omega + x) \cos x + m^2 K_2^2(i\Omega + x)}. \end{aligned}$$

On the basis of (7.2.2) at $0 < x \leq \Omega$, we have

$$K_1(i\Omega + x) \approx K_1(i\Omega) \text{ и } K_2(i\Omega + x) \approx K_2(i\Omega),$$

in view of which

$$\sigma_s^2 \approx \frac{2a}{\pi T} \sum_{i=0}^\infty K_1^2(i\Omega) \int_0^\Omega \frac{dy}{1 - 2mK_s(i\Omega) \cos y + m^2 K_2^2(i\Omega)}.$$

Using formula (3.613.2) from [92], we find

$$\begin{aligned} \sigma_s^2 &\approx \frac{a}{\pi} \Omega \sum_{i=0}^\infty \frac{K_1^2(i\Omega)}{1 - m^2 K_2^2(i\Omega)} = \\ &= \frac{a}{\pi} \sum_{i=0}^\infty \frac{K_1^2(i\Omega)}{1 - m^2 K_2^2(i\Omega)} \Delta(i\Omega). \end{aligned}$$

Since the value of the i -th period of the function $\cos \omega T$, in view of (7.2.2), is very small compared to the bandpass of the system and accordingly compared to the width of the output noise spectrum, then the latter sum can be approximately replaced by the integral

$$\sigma_3^2 \approx \frac{a}{\pi} \int_0^\infty \frac{K_1^2(\omega) d\omega}{1 - m^2 K_2^2(\omega)} = \frac{1}{2\pi} \int_0^\infty 2a \frac{K_1^2(\omega) d\omega}{1 - m^2 K_2^2(\omega)}. \quad (7.3.4)$$

The integral expression $2a \frac{K_1^2(\omega)}{1 - m^2 K_2^2(\omega)}$ can be interpreted as the energy spectrum of stored noise averaged by the period of the oscillating multiplier $\cos \omega T$.

Having substituted the expressions for the amplitude-frequency characteristics of filters into (7.3.4)

274

$$K_{1,2}(\omega) = \exp\left(-\frac{\omega^2 \tau_{1,2}^2}{8\pi c^2}\right),$$

which ensue from (7.1.1), we find

$$\sigma_3^2 \approx \frac{a}{\pi} \int_0^\infty \frac{\exp\left(-\frac{1}{4\pi c^2} \tau_1^2 \omega^2\right) d\omega}{1 - m^2 \exp\left(-\frac{1}{4\pi c^2} \tau_2^2 \omega^2\right)}$$

and after changing the variable integration by the law $z = \exp\left(-\frac{\tau_2^2 \omega^2}{4\pi c^2}\right)$, we will have

$$\sigma_3^2 \approx \frac{ac}{\sqrt{\pi} \tau_1} \int_0^1 \frac{1}{1 - m^2 z^{n^2}} \frac{dz}{\sqrt{\ln(1/z)}}.$$

Since $m^2 z^{n^2} < 1$, then

$$\frac{1}{1 - m^2 z^{n^2}} = \sum_{k=0}^\infty (m^2 z^{n^2})^k$$

and

$$\sigma_3^2 \approx \frac{ac}{\sqrt{\pi} \tau_1} \int_0^1 \sum_{k=0}^\infty m^{2k} \frac{z^{kn^2} dz}{\sqrt{\ln(1/z)}}.$$

Changing the order of integration and summation and using formula (4.269.4) from [92], we again find (7.3.1).

To avoid the need to use a digital computer to calculate (7.3.2), let us use the Euler formula [144] and formula (3.362.2) from [92] and let us find the approximate expression:

$$Q_1 \approx \frac{1}{n} \sqrt{\frac{\pi}{2 \ln(1/m)}} m^{-\frac{1}{n^2}} \left[1 - \Phi\left(\frac{1}{n} \sqrt{2 \ln \frac{1}{m}}\right) \right] + 0.5, \quad (7.3.5)$$

whose accuracy is higher, the closer m is to 1 and the smaller n is. It yields an error of approximately 10% at $n = 1$ and $m = 0.9$.

If $n^2 < 0.22 \ln \frac{1}{m} \approx 0.22(1-m)$, then (7.3.5) is simplified even further:

$$Q_1 \approx \frac{1}{2 \ln(1/m)} \left(1 - \frac{n^2}{4 \ln(1/m)} \right) + 0.5. \quad (7.3.6)$$

In this case the error is only 3.6% even in the case of $m = 0.8$ and $n = 0.2$.

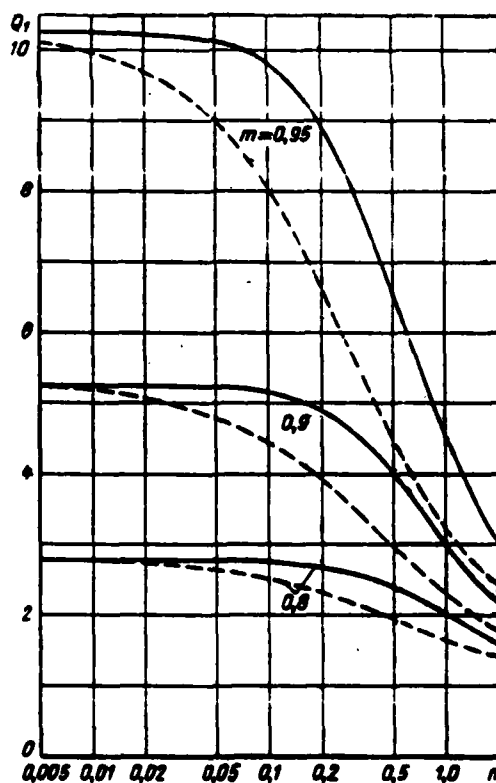


Fig. 7.3.1. Noise storage coefficient in single storage device as function of n at different values of m .

Consideration of the dependence of the noise storage coefficient on n (the solid curves in Fig. 7.3.1) shows that the noise storage coefficient decreases sharply with an increase of the ratio of the pre-storage filter bandpass and the recirculator feedback circuit, especially if the feedback coefficient of the recirculator is close to one. Therefore, if the bandpass of the prestorage filter is constant, the noise output at the output is less, the narrower the bandpass of the feedback circuit and the less this feedback coefficient. 276

The dependence of the noise storage coefficient on n in a storage device in which filters F_1 and F_2 are low-frequency RC-filters with bandpasses of ΔF_1 and ΔF_2 (at the level of $1/\sqrt{2}$) [7, 146], are shown in the same figure by the dashed lines. Consideration of them shows that the noise storage coefficient in the case of RC-filters depends more strongly on n . This is explained by the lesser square-wave nature of the amplitude-frequency characteristics of these filters.

7.4. Gain in Signal/Noise Ratio

Let us characterize the efficiency of the storage device quantitatively by the gain in the signal/noise ratio with respect to the power which it provides compared to an optimum filter for a single pulsed signal of the sequence being received [148-150].

Since the indicated ratio comprises the following at the output of an optimum filter for a single signal

$$q_{20}^2 = \frac{V_2^2(\tau_1 = \tau_0)}{\sigma_2^2(\tau_1 = \tau_0)} = \frac{V_0^2}{2 \frac{ac}{\tau_0}},$$

and at the output of the storage device

$$q_{\text{max}}^2 = \frac{V_{\text{max}}^2}{\sigma_{\text{max}}^2} = \frac{V_0^2 g^2}{\frac{ac}{\tau_1} Q},$$

where g and Q are the signal transfer coefficient and the noise storage coefficient, respectively, by this storage device, then the given storage device provides a gain in output signal/noise ratio compared to an optimum filter for a single pulse signal. 277

$$B = \frac{q_{\text{max}}^2}{q_{20}^2} = \frac{2g^2}{\gamma Q}. \quad (7.4.1)$$

To calculate the power losses in the signal/noise ratio provided by a storage device compared to an optimum filter for a sequence of pulsed signals, it is sufficient to separate the number of N pulsed signals in this (square-wave) sequence into gain (7.4.1):

$$G = \frac{N}{B} = \frac{N\gamma Q}{2g^2}.$$

Consideration of the dependence of the gain calculated by formulas (7.2.4), (7.3.2) and (7.4.1) and provided by a single storage device on N (Fig. 7.4.1) shows that the gain initially increases slowly as N increases at given value of n , then increases rapidly and then increases more and more slowly approaching some maximum value. If m approaches one and n decreases, the value of the gain increases and reaches a maximum at a large value of N .

If n is sufficiently small, i.e., if the feedback circuit is sufficiently wideband and $\gamma = 1$, formula (5.4.7), which describes the gain provided by an idealized storage device, follows from (7.2.4), (7.3.2) and (7.4.1).

It is also obvious from comparison of the curves presented in Fig. 7.4.1 that a storage device with small value of m provides a large gain with small number of N and the gain is greater in a storage device with large value of m at large value of N . This indicates that an optimum value of m , whose value approaches 1 as N increases, corresponds to each value of N . An explanation of this is given in item 1, section 5.4.

It follows from consideration of the dependence of the gain on the dimensionless bandpass $b_4 = \Delta F_{\text{eq}} = \frac{0.44\gamma}{n}$ of the feedback circuit (Fig. 7.4.2) read at the $d = 0.5$ level that the gain is always greater at any values of b_4 and N in the case when the prestorage filter is optimum to a single pulsed signal ($\gamma = 1$).

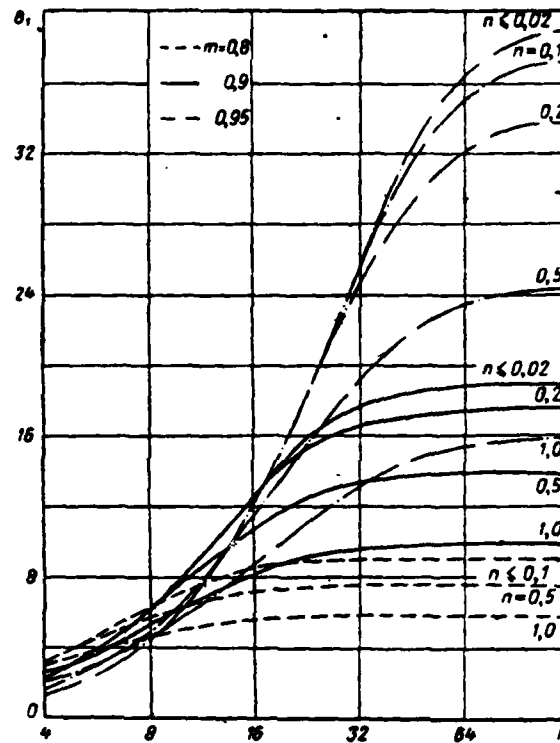


Fig. 7.4.1. Dependence of gain on number of pulses for single storage device.

The gain increases monotonically at $\gamma = 0.5$ and 1 with comparatively large value of N with broadening of the feedback circuit bandpass, while it initially increases at $\gamma = 2$ and then decreases slowly after reaching some maximum, approaching the same maximum value as at $\gamma = 0.5$. This maximum is expressed more strongly, the closer m is to one and the smaller N is.

The presence of this maximum is explained by the fact that the bandpass of the prestorage filter is twice as large at $\gamma = 2$ than that which is required for optimum intraperiod filtration. This excess bandpass partially compensates for the insufficient bandpass of the feedback circuit, which also determines the increase of the gain. With further broadening of the feedback circuit bandpass due to the excessively broad bandpass of the prestorage filter, the noise storage coefficient increases more rapidly than the square of the signal transfer coefficient, which also leads to some decrease of the gain.

With an increase of b_4 , the gain may be decreased at small value of N due to the more rapid increase of the noise storage coefficient compared to an increase of the square of the signal transfer coefficient.

It also follows from the curves shown in Fig. 7.4.2 that the feedback circuit bandpass required to provide a gain which exceeds 90% of the maximum possible at given value of N can be approximately calculated by the following formula at $\gamma = 1$

$$b_4 \geq b_{41} 10^{\alpha_1 (1-m^N)}, \quad (7.4.2)$$

in which b_{41} and α_1 are functions of m . Their values and also the minimum values of the required bandpass with condition (5.4.19), i.e., at very large value of N , are placed in Table 7.4.1.

Table 7.4.1.

m	0.8	0.9	0.95
b_{41}	0.302	0.355	0.525
α_1	0.61	0.70	0.70
b_{4min}	1.2	1.8	2.6

It follows from (7.4.2) that the requirements on the width of the feedback circuit bandpass increase as the number of stored pulse signals increases and as m approaches one, quite agrees with simple physical concepts.

It is important to know that the required bandpass of the feedback circuit is considerably less in the considered case than upon storage of square-wave video pulses by a storage device with low-frequency RC filters and in the absence of compensation for the signal delay in filter F_2 [7]. This is explained by the fact that first, the product of the length by the width of the spectrum is appreciably less in a bell pulse than in a square-wave pulse [151] and second, which is the main thing, the bandpass of this filter must be broadened sharply to maintain high efficiency of the storage device in the absence of compensation for the signal delay in filter F_2 in order to reduce this delay.

281

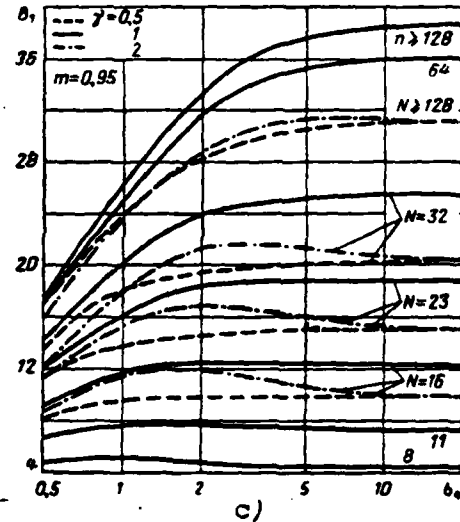
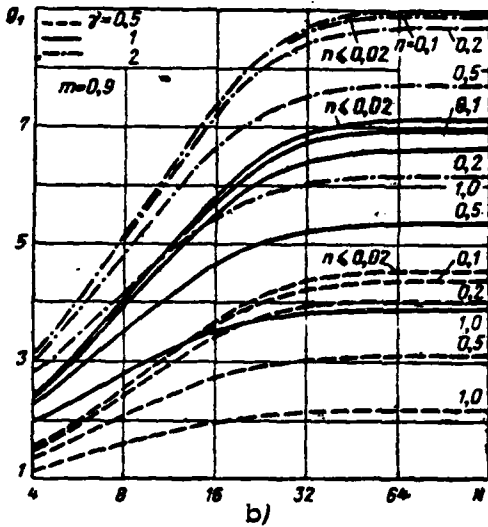
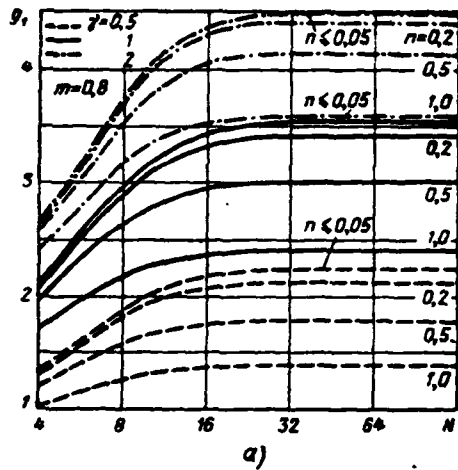


Fig. 7.4.2. Dependence of gain on bandpass for single storage device.

Accordingly, compensation for the additional delay time of the signal in the recirculator feedback circuit permits considerable reduction of the requirement on the width of the bandpass of this circuit and thus considerable simplification of the design and circuitry of the storage device.

28.

It also follows from consideration of Fig. 7.4.2 that, if the prestorage filter is optimum to a single pulse signal ($\gamma = 1$), the gain is 20-25% higher than in the cases of a doubly increased ($\gamma = 2$) and a one-half decrease ($\gamma = 0.5$) bandpass.

282

Thus, the width of the prestorage filter bandpass slightly affects the gain in signal/noise ratio.

Thus, the possibility of increasing the output signal/noise ratio 8, 17 and 35 times by a coherent single storage device with $m = 0.8$, 0.9 and 0.95 and with relative bandpass of $b_4 = 1.2$, 1.8 and 2.6 is shown above. The possibility of realizing these storage devices raises no doubts and has been confirmed experimentally [141, 152 and so on].

7.5. Requirements on Accuracy of Maintaining Equality of Delay Time in Recirculator Feedback Circuit and of Repetition Quasi-Period of Pulsed Signals

It is further noted (see item 1, section 11.1) that special measures are usually implemented in an analog storage device aimed at the delay time T_3 of the oscillations in the recirculator feedback circuit coinciding with the length of the repetition quasi-period of the pulsed signals. Despite this, due to variation of temperature and other destabilizing factors during operation of storage devices, the delay time may differ from the length of the repetition quasi-period by some value Δ , which we call the error time:

$$\Delta = T_3 - T.$$

In this case the storage of pulsed signals will be less efficient.

Let us determine the degree of decrease of the signal transfer coefficient of the storage device due to inequality of delay time and repetition quasi-period and let us formulate the requirements on the possible value of the error time.

In the considered case operation (7.1.10) has the form

$$\Gamma v(t) = v(t - T_3) = v(t - T - \Delta),$$

due to which formula (7.2.1) will be as follows:

2

$$v_1(t) = V_0 \tau_0 \sum_{k=0}^{\infty} m^k \sum_{l=0}^{N-1} v(t + [l - k]T - k\Delta, \sqrt{\tau_0^2 + \tau_1^2 + k\tau_2^2}).$$

Specifically, at moment $t = t_1$, where $0 < |t_1| < \tau_0/2$ and $\text{sign } t_1 = \text{sign } \Delta$, we have

$$v_3(t_1) = V_0 \tau_0 \sum_{k=0}^{\infty} m^k \sum_{l=0}^{N-1} v(t_1 + [l-k]T - k\Delta, \sqrt{\tau_0^2 + \tau_1^2 + k\tau_k^2}).$$

The latter expression, due to (7.2.2), is simplified

$$v_3(t_1) \approx V_0 \tau_0 \sum_{k=0}^{N-1} m^k v(t_1 - k\Delta, \sqrt{\tau_0^2 + \tau_1^2 + k\tau_k^2}).$$

The signal reaches a peak value of $V_3 = v_3(t_{\text{ONT}})$ at some value of $t_1 = t_{\text{ONT}}$. The signal transfer coefficient then comprises

$$g_1(\alpha, \delta) = \frac{V_3}{V_0} = \gamma \sum_{k=0}^{N-1} \frac{m^k}{\gamma \sqrt{1 + \gamma^2 + k n^2}} \exp \left[-\frac{2\pi c^2 \gamma (\alpha - \delta k)^2}{1 + \gamma^2 + k n^2} \right], \quad (7.5.1)$$

where $\alpha = \frac{t_{\text{ONT}}}{\tau_0}$ and $\delta = \frac{\Delta}{\tau_0}$. Specifically, (7.5.1) changes to (7.2.4) in the absence of an error and at zero moment of time.

The transfer coefficient decreases (Fig. 7.5.1) as the error time increases and it decreases more strongly, the smaller the value of n and the larger the value of γ . This is very simple to explain physically. The larger the value of n , i.e., the narrower the bandpass of the recirculator feedback circuit, the more strongly the pulsed signal is extended in time during recirculation through this circuit. Its time shift due to error then affects the value of the stored signal less.

284

The larger the value of γ , the shorter the length of the pulsed signals at the output of the prestorage filter and the stronger the time error in the effect of storage of these signals is felt.

The values of the permissible time errors, corresponding to a decrease of the signal transfer coefficient by 5%, were calculated on the Minsk-1 digital computer for different parameters of the storage device and number of stored pulses (Fig. 7.5.2). These values decrease as n decreases, γ and N increase and as m approaches one. The latter is

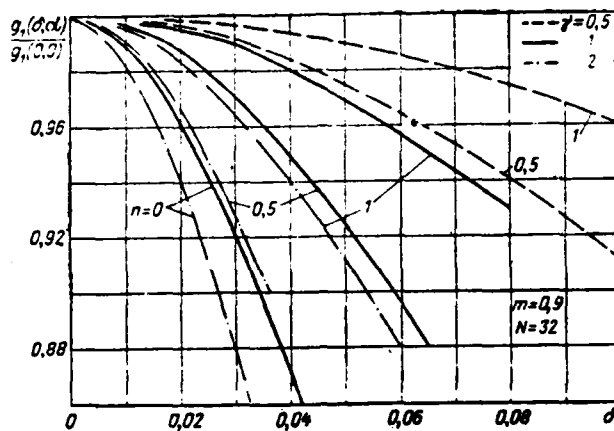


Fig. 7.5.1. Transfer coefficient of signal by single storage device as a function of relative error time.

explained by an increase of the active number of stored pulse signals (see (5.4.8)).

Thus, delay time and repetition quasi-period errors whose value has the order of several hundredths of a fraction of the length of the pulsed signal and is strongly dependent on the parameters of the storage device and the number N are permissible during storage of pulsed signals in a single-stage storage device with $m = 0.9$ and 0.95 .

These requirements on the accuracy of maintaining the equality of the delay time and of the repetition quasi-period, although they are rather rigid, they are still easy to fulfill. It is sufficient to refer to the long-known fact that the error time that comprises no more than $5 \cdot 10^{-3}$ of the pulse length [153-155] is assumed permissible in coherent-pulsed systems for selection of moving targets.

286

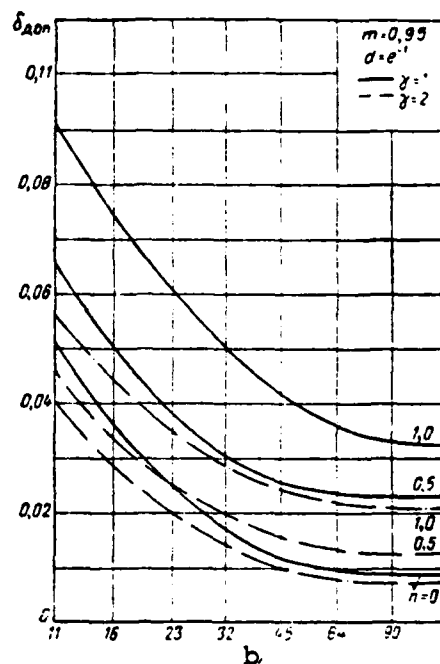
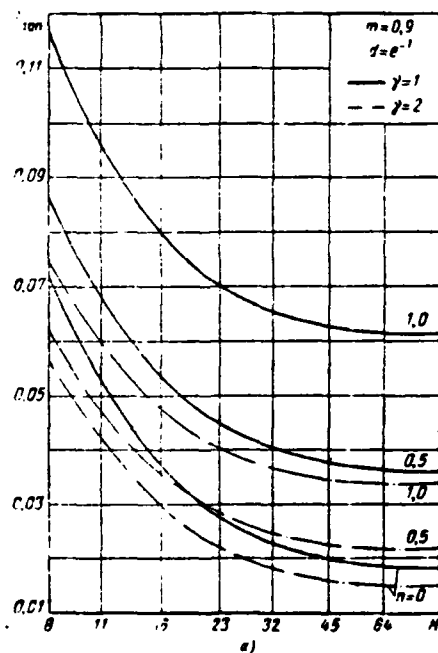


Fig. 7.5.2. Dependence of permissible time errors on N at $m = 0.9$ (a) and $m = 0.95$ (b).

A COHERENT DOUBLE STORAGE DEVICE

8.1. CHARACTERISTICS OF STORAGE DEVICE

Since the coherent single storage device considered in the previous chapter permits one to achieve a slight gain in signal/noise ratio at a value of m given from concepts of retaining stability (see section 11.2), it is of interest to analyze a coherent double storage device (Fig. 8.1.1) in which two series-connected recirculators with delays by the repetition quasi-period are used [156, 157].

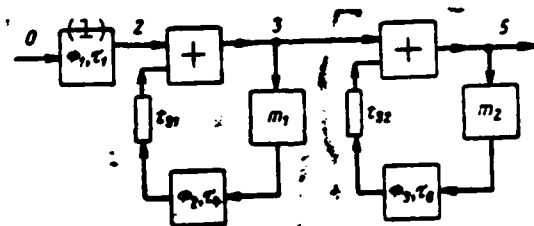


Fig. 8.1.1. Block diagram of double storage device.

Key: (1) Filter.

It has the transfer function

$$K(\omega) = \frac{K_1(\omega)}{[1 - m_1 K_1(\omega) e^{j\omega \tau_{21}}][1 - m_2 K_1(\omega) e^{j\omega \tau_{22}}]} = \frac{K_1(\omega)}{[1 - m_1 K_1(\omega) e^{j\omega T}][1 - m_2 K_1(\omega) e^{j\omega T}]} \quad (8.1.1)$$

$$K(\omega) = \frac{K_1(\omega)}{\sqrt{[1 - 2m_1 K_2(\omega) \cos \omega T + m_1^2 K_2^2(\omega)]} \times \sqrt{[1 - 2m_2 K_3(\omega) \cos \omega T + m_2^2 K_3^2(\omega)]}} \quad (8.1.2)$$

where $\bar{K}_1(\omega)$ and $\bar{K}_2(\omega)$ are described by expression (7.1.1) and $\bar{K}_3(\omega)$ differs in the general case from $\bar{K}_2(\omega)$ only by the response and delay times. Recirculators can usually be assumed identical, i.e., $\bar{K}_3(\omega) = \bar{K}_2(\omega)$, $m_2 = m_1 = m$, due to which

$$\bar{K}(\omega) = \frac{K_1(\omega)}{[1 - m K_2(\omega) e^{j\omega T}]^2} \quad (8.1.3)$$

and

$$K(\omega) = \frac{K_1(\omega)}{[1 - 2m K_2(\omega) \cos \omega T + m^2 K_2^2(\omega)]}. \quad (8.1.4)$$

The amplitude-frequency characteristic (8.1.4) of the considered storage device, as in the case of a single storage device (Fig. 7.1.1), is a comb characteristic and reaches maximum values at frequencies that are a multiple of the repetition rate

$$K_{\max}(\Omega) = K(\Omega) = \frac{K_1(\Omega)}{[1 - m K_2(\Omega)]^2}, \quad (8.1.5)$$

and minimum values at frequencies $\omega = (1 + 0.5)\Omega$

$$K_{\min}(\Omega) = K\left[\left(1 + \frac{1}{2}\right)\Omega\right] = \frac{K_1\left[\left(1 + \frac{1}{2}\right)\Omega\right]}{\left\{1 + m K_2\left[\left(1 + \frac{1}{2}\right)\Omega\right]\right\}^2}.$$

The shape of the spike of this characteristic is shown by curve 2 in Fig. 7.1.5. It coincides with the amplitude-frequency characteristic of a two-stage tuned amplifier with small frequency differences with respect to the nearest maximum. Therefore, the bandpass of the mentioned spike at the level of $1/\sqrt{2}$ comprises [55]

$$\delta F_1(l) = (2^{1/2} - 1)^{1/2} \delta F_1(l) = 0.644 \delta F_1(l).$$

where $\delta F_1(l)$ is the bandpass (7.1.5) of the l -th spike of the characteristic of a single storage device.

Having narrower bandpasses of the amplitude-frequency characteristic, a double storage device can store a greater number of pulsed signals.

In the general case its pulse characteristic is

$$\begin{aligned}
 h_2(t) &= \sum_{l=0}^{\infty} \Lambda_2^l C_6^l \Gamma^l h_1(t) = \sqrt{2}c \sum_{l=0}^{\infty} \Lambda_2^l C_6^l \Gamma^l \times \\
 &\quad \times \sum_{k=0}^{\infty} m_1^k v(t - kT, \sqrt{\tau_1^2 + k\tau_4^2}) = \\
 &= \sqrt{2}c \sum_{l=0}^{\infty} m_2^l \sum_{k=0}^{\infty} m_1^k v(t - [k+l]T, \sqrt{\tau_1^2 + k\tau_4^2 + l\tau_6^2}) = \\
 &= \sqrt{2}c \sum_{k=0}^{\infty} m_2^k \sum_{l=0}^k \left(\frac{m_1}{m_2}\right)^l v(t - kT, \sqrt{\tau_1^2 + l\tau_4^2 + (k-l)\tau_6^2}),
 \end{aligned} \tag{8.1.6}$$

where Λ_2 is an attenuation operation by a factor of m_2

Specifically, if the recirculators are identical: $m_2 = m_1 = m$ and $\tau_6 = \tau_4$, then

$$h_2(t) = \sqrt{2}c \sum_{k=0}^{\infty} (k+1)m^k v(t - kT, \sqrt{\tau_1^2 + k\tau_4^2}). \tag{8.1.7}$$

Thus, the pulse characteristic of a double storage device consists of an infinitely large number of pulses of the same length of (7.1.14) following with repetition quasi-period T , which as in the case of a single storage device, and of amplitude (Fig. 8.1.2)

$$H_2(kT) = \frac{\sqrt{2}c(k+1)m^k}{\tau_1(1 + kn^2)^{1/2}}, \tag{8.1.8}$$

that exceeds $(k+1)$ -fold the amplitude (7.1.13) of the k -th pulse in the case of a single storage device. Therefore, the pulse amplitude of the pulse characteristic of a double storage device decreases appreciably more slowly as k increases than in the case of a single storage device (Fig. 7.1.6, a). The latter also indicates the capability of storing a greater number of pulsed signals by means of this storage device.

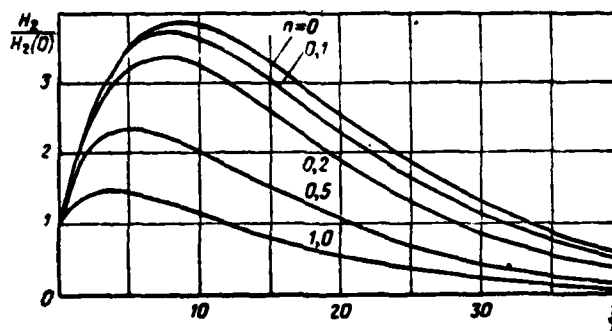


Fig. 8.1.2. Envelopes of pulse characteristic of double storage device.

8.2. Signal Storage

The signal voltage at the input of the second recirculator is described by expression (7.2.1). Since the second recirculator operates by the same algorithm as the first, then by analogy with (7.2.1) in the general case when the recirculators are different,

$$v_s(t) = \sum_{i=0}^{\infty} A_2^i C_0^i \Gamma^i v_s(t) = V_0 \tau_0 \sum_{i=0}^{\infty} m_2^i \sum_{k=0}^{\infty} m_1^k \times \\ \times \sum_{l=0}^{N-1} v(t + [l - k - i]T, \sqrt{\tau_0^2 + \tau_1^2 + k\tau_4^2 + i\tau_6^2}).$$

Specifically, at moment $t = xT$, where x is an integer,

$$v_s(xT) = V_0 \tau_0 \sum_{i=0}^{\infty} m_2^i \sum_{k=0}^{\infty} m_1^k \sum_{l=0}^{N-1} v([x + l - k - i]T, \sqrt{\tau_0^2 + \tau_1^2 + k\tau_4^2 + i\tau_6^2}).$$

Because of (7.2.2), it is sufficient to consider only the terms in this expression corresponding to the equality $x + l - k - i = 0$, due to which

$$v_s(xT) \approx V_0 \tau_0 \sum_{i=x}^{N+x-1} \sum_{l=0}^i m_2^l m_1^{i-l} \times \\ \times u(0, \sqrt{\tau_0^2 + \tau_1^2 + (l-i)\tau_4^2 + i\tau_6^2}) = \\ = V_0 \gamma \sum_{i=x}^{N+x-1} m_1^i \sum_{l=0}^i \frac{(m_2/m_1)^l}{\sqrt{1 + \gamma^2 + (l-i)n_1^2 + in_2^2}}, \quad (8.2.1)$$

where $n_1 = \tau_4/\tau_1$ and $n_2 = \tau_6/\tau_1$.

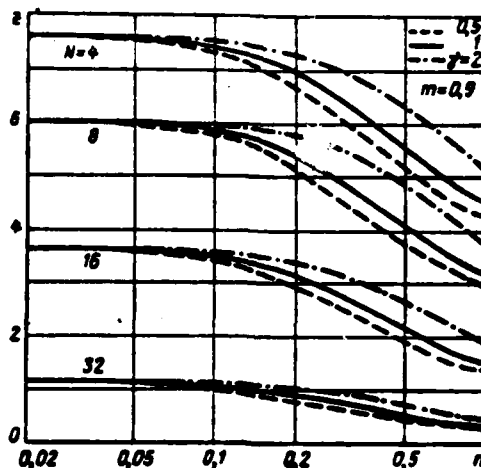


Fig. 8.2.1. Dependence of solutions of equation (8.2.3) on n .

At $m_2 = 0$ when there is no second recirculator, we find an expression that coincides with (7.2.3) at $x = 0$ and $n_1 = n$. In the case of identical recirculators, $m_2 = m_1 = m$ and $n_2 = n_1 = n$,

$$v_s(xT) = V_0 \gamma \sum_{l=x}^{N+x-1} \frac{(l+1)m^l}{V1 + \gamma^2 + ln^2}, \quad (8.2.2)$$

which coincides at $n = 0$ with the expressions found for an idealized storage device in [143, 158].

293

The peak value of the signal at the output of a double storage device can be observed somewhat later at $t = yT$, where y is an integer, rather than at moment $t = 0$, corresponding to the mid-point of the last pulse of the sequence to be stored at the input. It can be determined either from the condition

$$\left. \frac{\partial v_s(xT)}{\partial x} \right|_{x=y} = 0,$$

which is very difficult, or by analysis of the difference

$$v_s(xT) - v_s([x-1]T) = V_0 \gamma m^{x-1} \times \left\{ \frac{(N+x)m^N}{V1 + \gamma^2 + (N+x-1)n^2} - \frac{x}{V1 + \gamma^2 + (x-1)n^2} \right\}.$$

It follows from this expression that the desired number y is the entire

part $E(z)$ of solution z of the equation

$$\left(1 + \frac{N}{z}\right)^2 m^{2N} = 1 + \frac{Nn^2}{1 + \gamma^2 + (z-1)n^2}. \quad (8.2.3)$$

29:
29:

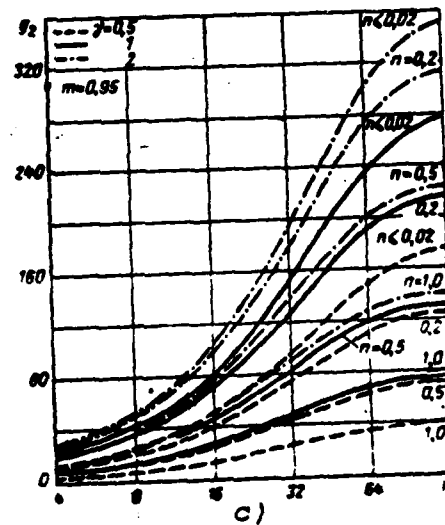
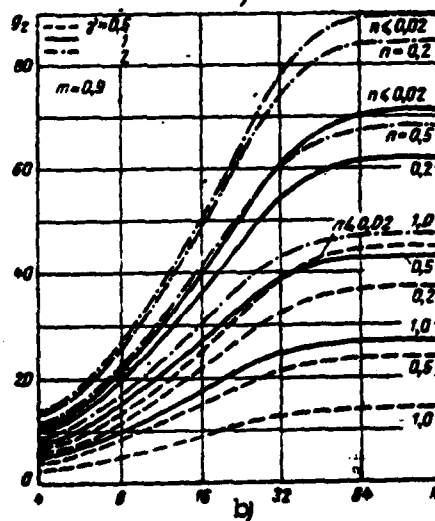
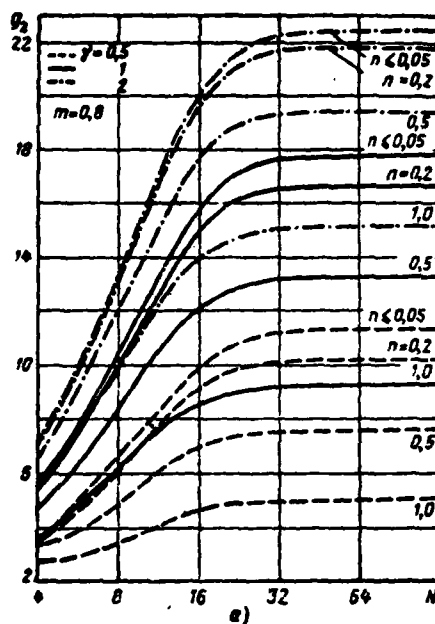


Fig. 8.2.2. Transfer coefficient of signal by double storage device as function of number of pulses.

Consideration of the solutions of this equation (Fig. 8.2.1) calculated on the Minsk-1 computer shows that a shift of the peak value of the stored signal is observed only with a comparatively small number of stored pulse signals. Its value is higher, the lower the value of N and n , the closer m is to one and the higher the value of γ .

This conclusion becomes obvious if one takes into account that when m approaches 1, γ increases and n decreases, the considered storage device approaches closer and closer to an idealized device, i.e., one consisting of recirculators with feedback coefficient equal to one and with unlimited broad bandpass of the feedback circuit. After the end of the signal at the input of the storage device, the signal amplitude at the input of the second recirculator remains constant, due to which the signal is stored without limit at its output to an infinitely high level, which is observed with infinitely long delay of the relative moment of the end of the signal at the input.

Naturally, a real storage device with fixed parameters is closer to an idealized device, the lower the value of N .

An increase of the shift of the peak value of the stored signal with an increase of γ is explained by the fact that the wideband nature of the recirculator feedback circuit increases in the case of fixed value of n , which brings the considered system close to an idealized system.

It follows from (8.3.2) that at $n = 0$ the shift of the peak value is observed (i.e., $y = E(z) \geq 1$) only provided $(N + 1)m^N \geq 1$, which coincides with the value found in item 2, section 5.4.

The peak value of the stored signal is calculated by formula (8.2.2) at $x = y$, while the signal transfer coefficient is

$$g_s = \frac{v_s(yT)}{V_s} = \gamma \sum_{l=y}^{N+y-1} \frac{(l+1)m^l}{\sqrt{1+\gamma^2+ln^2}} \quad (8.2.4)$$

The dependence of the signal transfer coefficient on N (Fig. 8.2.2) calculated on the Minsk-1 computer has the same nature as for a single storage device (Fig. 7.2.1). However, the values of the signal transfer coefficients in a double storage device are appreciably higher with the same values of parameters, which is quite natural.

Analysis of the results of calculation also shows that the bandpass of the feedback circuits must be broadened approximately one and a half times compared to the case of a single storage device to achieve a signal transfer coefficient distinct from a similar coefficient by less than 5% in an idealized storage device.

8.3. Storage of Noise

By substituting (8.1.7) into (1.7.2), using (7.2.2), changing the order of integration and adding and calculating the integral, as in derivation of (7.3.1), we find

$$\sigma_s^2 = \frac{ac}{v_1} \sum_{k=0}^{\infty} \frac{(k+1)^2 m^{2k}}{V \sqrt{1+kn^2}}. \quad (8.3.1)$$

Consequently, the coefficient of noise storage by a double storage device is

$$Q_s = \sum_{k=0}^{\infty} (k+1)^2 m^{2k} / V \sqrt{1+kn^2}. \quad (8.3.2)$$

The dependence of the coefficient of noise storage by a double storage device on the bandpass ratio n (Fig. 8.3.1) has the same nature as in a single storage device (Fig. 7.3.1), but the value of these coefficients is considerably higher.

It follows from (8.3.2) and (7.3.2) that the coefficient of noise storage by a second recirculator comprises

$$Q' = \frac{Q_s}{Q_1} \sum_{k=0}^{\infty} \frac{(k+1)^2 m^{2k}}{V \sqrt{1+kn^2}} \left/ \sum_{k=0}^{\infty} \frac{m^{2k}}{V \sqrt{1+kn}} \right. \quad (8.3.3)$$

Comparison of the dependence of this coefficient on n (Fig. 8.3.2) to similar functions (Fig. 7.4.1) for a single storage device (i.e., for the first recirculator) shows that the second recirculator stores the noise a considerably greater number of times than the first. Thus, for example, at $m = 0.9$ and $n = 0.1$ the noise output is increased by the first recirculator 5.16-fold and by the second 48.2-fold, i.e., almost 10 times greater. This is explained by the strong correlation of noise at the output of the first recirculator (see item 2, section 5.4).

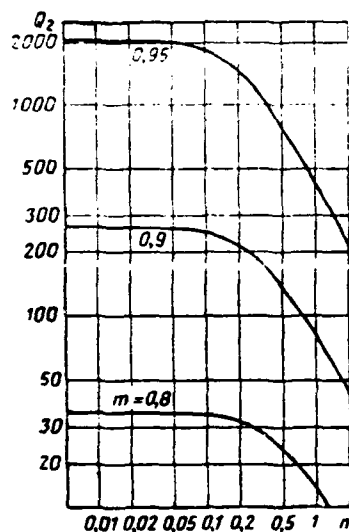


Fig. 8.3.1. Dependence of coefficient of noise storage by double storage device on n .

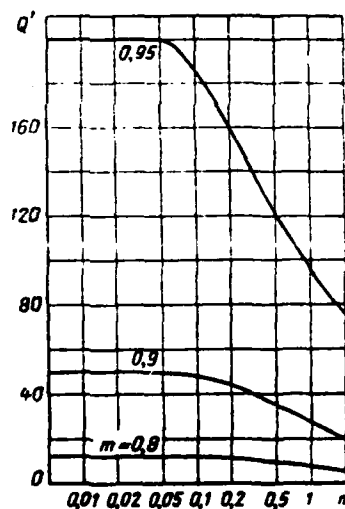


Fig. 8.3.2. Dependence of coefficient of noise storage by second recirculator on n .

8.4. Gain in Signal/Noise Ratio

The dependence of the gain calculated by formulas (7.4.1), (8.2.4) and (8.3.2) provided by a double storage device on N (Fig. 8.4.1) has the same nature as in the case of a single storage device (Fig. 7.4.1). The main difference of these functions is that the maximum value of the gain in the case of a double storage device is reached at a higher value of N .

Comparison of these functions for single and double storage devices shows that two recirculators with $m = 0.8$ are equivalent to a single recirculator with $m = 0.9$, while two recirculators with $m = 0.9$ are equivalent to a single recirculator with $m = 0.95$ (see item 2, section 5.4). This permits one to get around the difficulties of finding the values of m close to 1 by using the second recirculator.

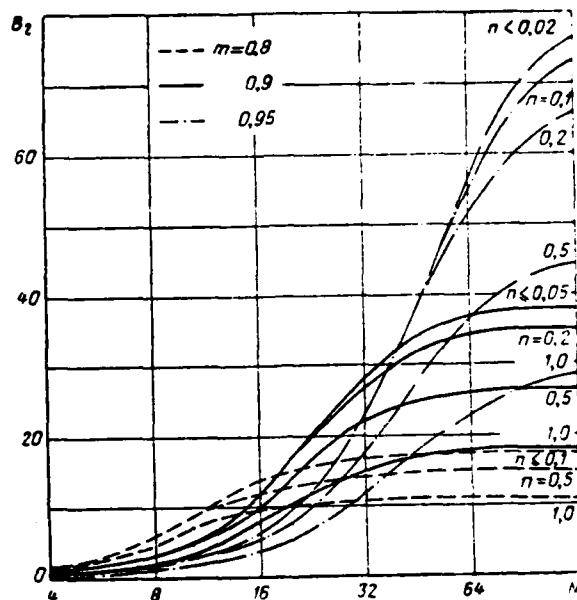


Fig. 8.4.1. Gain of Double Storage Device as Function of Number of Pulses.

Consideration of the dependence of the gain when using a double storage device on the dimensionless bandpass of the recirculator feedback circuit calculated at the 0.5 level (Fig. 8.4.2) shows that the gain increases monotonically as b_4 increases at $\gamma = 0.5$ and 1 and at comparatively large value of N . If $\gamma = 2$, then the gain initially increases as b_4 increases, and then decreases after reaching a certain maximum, approaching the same maximum value as at $\gamma = 0.5$. As in the case of a system with a single recirculator, this maximum is expressed more strongly, the less the value of N and the closer m approaches 1, while its presence is explained by partial compensation of the insufficient bandpass of the feedback circuits by the excess bandpass of the pre-storage filter. In this case the gain can even somewhat exceed that at $\gamma = 1$.

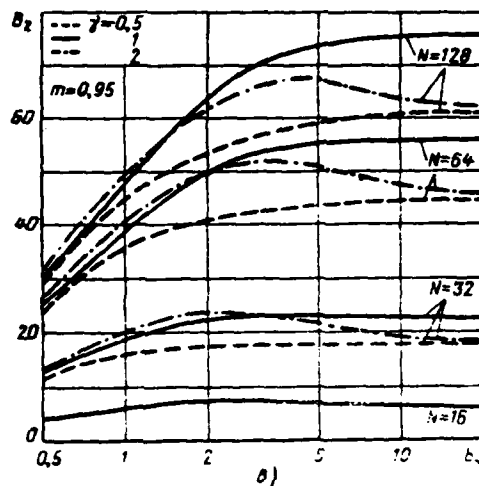
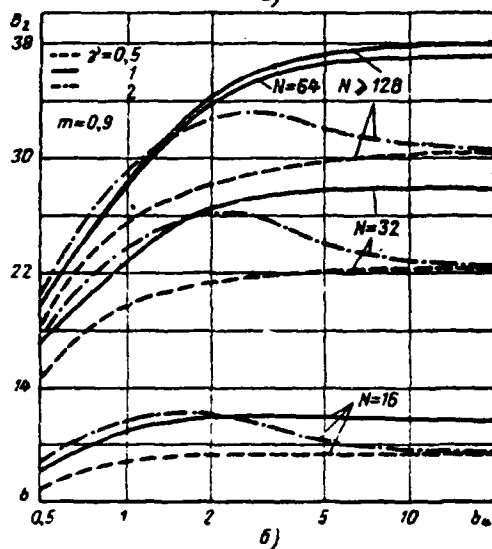
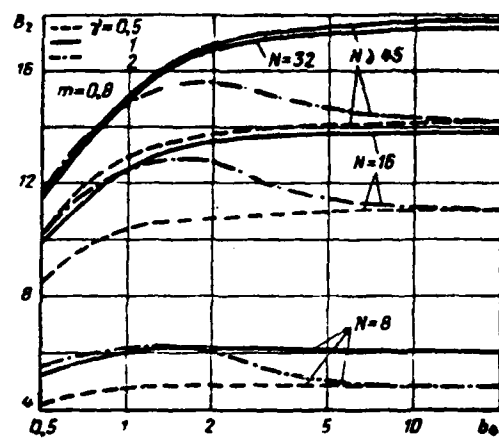


Fig. 8.4.2. Gain of double storage device as function of feedback circuit bandpass.

At small values of N , the gain at $\gamma = 1$ is considerably less dependent on the feedback circuit bandpass as in the case of a single storage device. 299

It follows from Fig. 8.4.2 that the feedback circuit bandpass of the recirculators required to achieve a gain whose value is not less than 90% of the maximum possible at $\gamma = 1$ with given value of N (i.e., in an idealized storage device) can be calculated by the formula

$$b_0 \geq b_{0\max} \cdot 10^{m(1-\gamma)}, \quad (8.4.1)$$

which differs from formula (7.4.2) only by the values of coefficients b_{42} and α_2 (Table 8.4.1).

Thus, as in the case of a single storage device, the requirements on the bandpass of the recirculator feedback circuits of a double storage device increase as N increases and as m approaches 1.

Table 8.4.1.

m	0,8	0,9	0,95
b_{41}	0,335	0,610	0,990
α_2	0,60	0,51	0,42

As in a single storage device, the required bandpass in the considered storage device is considerably lower than during storage with compensation for the signal delay time in filter Φ_2 [7].

Consideration of the functions shown in Fig. 8.4.2 shows that the gain varies by no more than 25% upon variation of γ from 0.5 to 1 and then to 2. This indicates the weak critical nature of the gain to variation of the bandpass of the prestorage filter near the optimum value.

8.5. Additional Gain Due to Use of Second Recirculator

The additional gain caused by using a second recirculator increases to values on the order of two with an increase of N (Fig. 8.5.1). If the value is higher, the broader the bandpass of the prestorage filter.

An additional gain is observed only if the number of stored pulsed signals comprises no less than 50-60% of the active number (5.4.8), if the following condition is fulfilled

$$N \geq (1,5-1,8)/(1-m). \quad (8.5.1)$$

The number of stored pulsed signals is equal to the active number if N exceeds 1.4-1.6. At $\gamma = 0.5$, the additional gain increases with an increase of bandpass b_4 (Fig. 8.5.1).

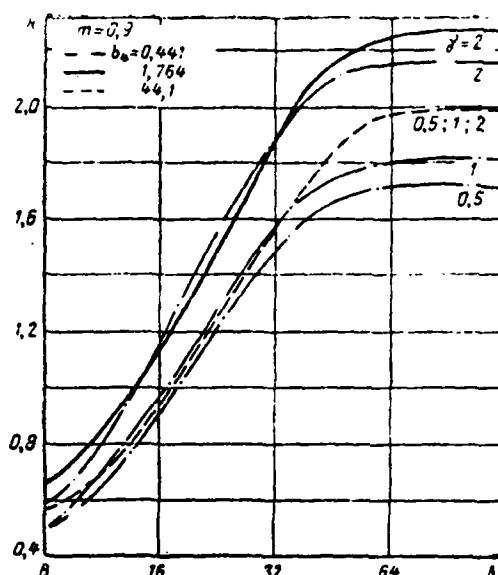


Fig. 8.5.1. Dependence of additional gain on number of pulses.

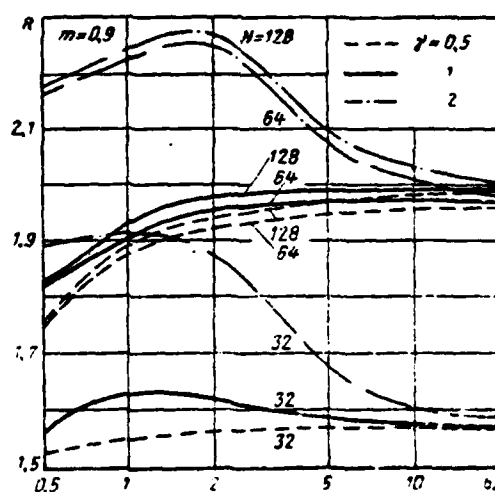


Fig. 8.5.2. Dependence of additional gain on feedback circuit bandpass

This same nature of dependence is also observed at $\gamma = 1$ if the number of stored pulsed signals is greater than the active number. With an active number of stored pulses and at $\gamma = 1$ and also at any value of N and at $\gamma = 2$, the additional gain initially increases with an increase of b_0 and then decreases. This is also explained by partial compensation of the insufficient bandpasses of the feedback circuit by the excess bandpass of the prestorage filter.

Thus, the use of a second recirculator identical to the first permits one to additionally increase the signal/noise ratio approximately twofold with sufficiently large number of stored pulsed signals. The comparatively low value of the additional gain is explained by the high correlation of noise at the input of the second recirculator, which was already noted above. Attenuation of the harmful effect of noise correlation, which leads to a sharp increase of the additional gain, is achieved in a two-stage storage device. The next chapter is also devoted to consideration of it.

COHERENT TWO-STAGE STORAGE DEVICE

9.1. CHARACTERISTICS OF STORAGE DEVICE

With two-stage storage (see item 4, section 5.4), the delay time of oscillations in the feedback circuit of the second recirculator is integer M times greater than the repetition quasi-period of pulsed signals [123-124]. Because of this, a two-stage storage device (Fig. 9.1.1) differs from a double storage device (Fig. 8.1.1) only by the fact that a delay device by time $t_{33} = MT - t_6$ rather than a delay device by time $t_{32} = T - t_6$, as in a double storage device, is used in the second recirculator of a two-stage storage device.

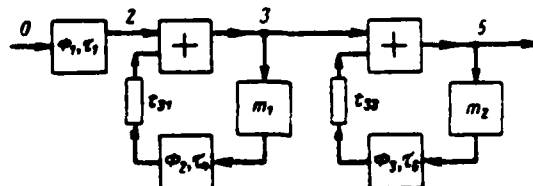


Fig. 9.1.1. Block diagram of two-stage storage device.
Key: (1) Filter.

The considered storage device has the transfer function

$$\begin{aligned}
 K(\omega) &= \frac{K_1(\omega)}{[1 - m_1 K_1(\omega) e^{j\omega t_{31}}] [1 - m_2 K_1(\omega) e^{j\omega t_{32}}]} = \\
 &= \frac{K_1(\omega)}{[1 - m_1 K_1(\omega) e^{j\omega T}] [1 - m_1 K_1(\omega) e^{j\omega MT}]}
 \end{aligned} \tag{9.1.1}$$

$$K(\omega) = \frac{K_1(\omega)}{\sqrt{1 - 2m_1 K_2(\omega) \cos \omega T + m_1^2 K_2^2(\omega)}} \times \frac{1}{\sqrt{1 - 2m_2 K_3(\omega) \cos \omega MT + m_2^2 K_3^2(\omega)}} \quad (9.1.2)$$

Accordingly, the amplitude-frequency characteristic of a two-stage storage device is the product of the amplitude-frequency characteristics of a single storage device (7.1.3) and of a second recirculator with delay by time MT . Both these characteristics are comb type, however, in the case of a single storage device the spikes of this characteristic follow with the repetition rate of pulsed signals and have bandpass (7.1.5), while in the case of the second recirculator with delay by MT , the spikes of the characteristic follow with rate which is M times less than the repetition rate of pulsed signals and have a lower bandpass by a factor of M because of this. As a result of remultiplication of these two characteristics, a comb characteristic of a two-stage storage device whose spikes (see, for example, curve 3 in Fig. 7.1.5) are located at frequencies that are a multiple of the signal repetition rate and have considerably narrower bandpasses than in the case of a single storage device, is formed.

Using (9.1.2) at $m_1 = m_2$ and $K_3(\omega) = K_2(\omega)$, one can show that the bandpass of the spike of the amplitude-frequency characteristic of a two-stage storage device is less by approximately a factor of $\sqrt{1 + M^2}$ at $M \geq 3$ than in the case of a single storage device:

$$\delta F_1 \approx \frac{\delta F_1}{\sqrt{1 + M^2}} \approx \frac{\delta F}{M}. \quad (9.1.3)$$

Having an appreciably smaller bandpass of the spikes of the amplitude-frequency characteristic, a two-stage storage device can store a considerably greater number of pulsed signals.

Denoting by Π the delay operation by time MT : $\Pi u(t) = \Gamma^M u(t) = u(t - MT)$, and using (7.1.8), (7.1.11) and (7.1.12), we find the pulse characteristic of a two-stage storage device

$$h_1(t) = \sum_{i=0}^{\infty} A_2^i C_6^i \Pi^i h_1(t) = \sqrt{2}c \sum_{i=0}^{\infty} m_2^i \times \\ \times \sum_{k=0}^{\infty} m_1^k v(t - [k + iM]T, \sqrt{\tau_1^2 + k\tau_4^2 + i\tau_6^2}).$$

This expression can be represented differently as:

$$h_1(t) = \sqrt{2}c \sum_{i=0}^{\infty} m_1^i \times \\ \times \sum_{l=0}^{E(l/M)} z^l v(t - lT, \sqrt{\tau_1^2 + (l - iM)\tau_4^2 + i\tau_6^2}). \quad (9.1.4)$$

where $z = m_2/m_1^M$.

It follows from (7.1.4) that the l -th pulse of the pulse characteristic is in the general case the sum of $\left[E\left(\frac{l}{M}\right) + 1\right]$ bell pulse with different lengths and amplitudes. However, in the special, but very similar case when

$$\tau_6 = M^{1/2}\tau_4 \quad \text{or} \quad n_6 = M^{1/2}n_4 = M^{1/2}n_1, \quad (9.1.5)$$

i.e., the bandpass of the recirculator feedback circuit with M -times greater delay is \sqrt{M} times less than the bandpass of the other recirculator, expression (9.1.4) is simplified:

$$h_1(t) = \sqrt{2}c \sum_{l=0}^{\infty} m_1^l \frac{z^{E(l/M)+1} - 1}{z - 1} v(t - lT, \tau_1 \sqrt{1 + ln^2}). \quad (9.1.6)$$

Comparing (9.1.6) to (7.1.12) and (8.1.7), we conclude that the pulse characteristics of a two-stage (with condition (9.1.5)), single and double storage devices differ only by the law of amplitude variation of their individual pulses. Specifically, in a two-stage storage device for which condition (9.1.5) is fulfilled, this law is as follows:

$$H_1(kT) = \frac{\sqrt{2}c}{\tau_1} \frac{m_1^k}{\sqrt{1 + kn^2}} \frac{z^{\left(\frac{k}{M}\right) + 1} - 1}{z - 1}. \quad (9.1.7)$$

It is plotted for $n = 0$, $m_1 = m_2 = 0.9$ and $M = 10$ in Fig. 9.1.2, a. The 306 dashed curve in this figure reproduces the upper envelope of the function $H_{3\text{max}}(kT)$. The pulse characteristic of this storage device is plotted in Fig. 9.1.2, b. Consideration of these functions shows the intermittent amplitude variation of the pulse characteristic of a two-stage storage device. This is explained by the fact that the feedback in the second recirculator (Fig. 9.1.1) operates with a delay M times greater than that in the first recirculator.

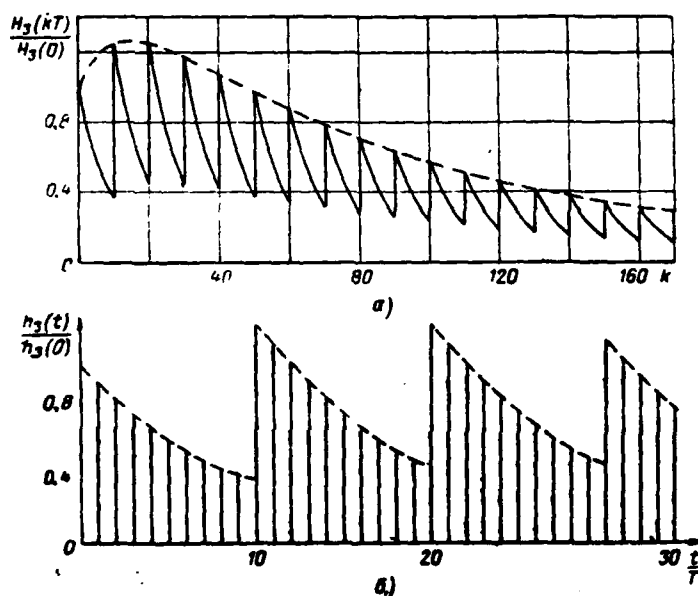


Fig. 9.1.2. Envelope of pulse characteristic (a) and pulse characteristic (b) of two-stage storage device.

The upper envelopes of the amplitudes of the pulse characteristic of a two-stage storage device at different values of M are plotted in Fig. 9.1.3. The case of $M = \infty$ corresponds to a single storage device while $M = 1$ corresponds to a double storage device. It is easy to see that the upper envelopes of the amplitudes of the pulse characteristic of a two-stage storage device decrease in time considerably more slowly than in a double and especially in a single storage device. Using (9.1.7) for $n = 0$ and $m_2 = m_1 = m$, it is easy to show that this decrease occurs in a two-stage storage device at comparatively large values of t according to the law

$$H_{\text{max}}(t) \approx H_1(0) \frac{z}{z-1} m^{\frac{t}{MT}}, \quad (9.1.8)$$

whereas it occurs for a single storage device as

$$H_1(t) = H_1(0) m^{\frac{t}{T}},$$

and for a double storage device

$$H_2(t) = H_1(0) \left(1 + \frac{t}{T}\right) m^{\frac{t}{T}}.$$

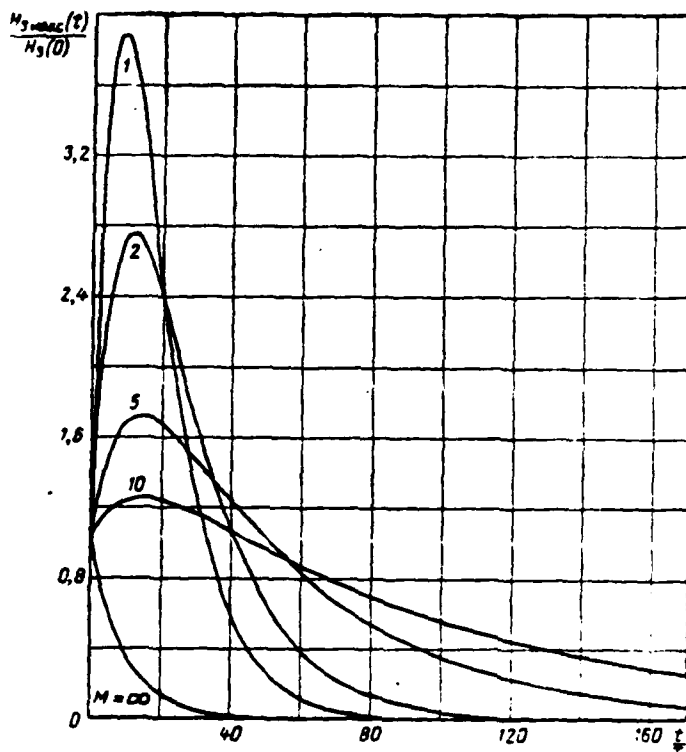


Fig. 9.1.3. Upper envelopes of pulse characteristic of two-stage storage device.

Thus, as the rate of the amplitude envelope of the pulse characteristic decreases, a two-stage storage device with feedback coefficient m is equivalent to a single storage device with feedback coefficient $m^{1/M}$. This indicates the capability of storing a considerably greater number of pulsed signals with a two-stage storage device than when using a single and even a double storage device.

9.2. Signal Storage

Voltage (7.2.1) acts on the input of the second recirculator during

storage of a pulsed signal sequence. Therefore, by analogy with (7.2.1) at the output of the storage device

$$v_s(t) = \sum_{l=0}^{\infty} A_2^l C_0^l \Pi^l v_s(t) = V_0 \tau_0 \sum_{l=0}^{\infty} m_2^l \sum_{k=0}^{\infty} m_1^k \times \\ \times \sum_{i=0}^{N-1} v(t + [l - k - iM]T, \sqrt{\tau_0^2 + \tau_1^2 + k\tau_1^2 + i\tau_0^2}).$$

At $t = 0$, the output voltage of the signal reaches a peak value

$$V_s = V_0 \tau_0 \sum_{l=0}^{\infty} m_2^l \sum_{k=0}^{\infty} m_1^k \times \\ \times \sum_{i=0}^{N-1} v([l - k - iM]T, \sqrt{\tau_0^2 + \tau_1^2 + k\tau_1^2 + i\tau_0^2}).$$

Because of (7.2.2), this expression is simplified:

$$V_s \approx V_0 \tau_0 \sum_{l=0}^{z \left(\frac{N-1}{M} \right)} m_2^l \sum_{k=0}^{N-iM-1} \frac{m_1^k}{\sqrt{1 + \tau^2 + kn_1^2 + in_2^2}}.$$

Consequently, the coefficient of signal transfer by a two-stage storage device is

309

$$g_s(N) = \gamma \sum_{l=0}^{z \left(\frac{N-1}{M} \right)} m_2^l \sum_{k=0}^{N-iM-1} \frac{m_1^k}{\sqrt{1 + \tau^2 + kn_1^2 + in_2^2}}. \quad (9.2.1)$$

Specifically, if the number of N stored pulsed signals is a multiple of M , i.e., $N = ML$, where L is also an integer, then

$$g_s(ML) = \gamma \sum_{l=0}^{L-1} m_2^l \sum_{k=0}^{(L-1)M-1} \frac{m_1^k}{\sqrt{1 + \tau^2 + kn_1^2 + in_2^2}}. \quad (9.2.2)$$

At $M = 1$ when a two-stage storage device degenerates into a double storage device, we find an expression which differs only by the constant multiplier from expression (8.2.1) at $z = 0$, which describes the signal amplitude at the output of a double storage device.

In the case of infinitely broad bandpasses of the recirculator feedback circuits, i.e., $n_1 = n_2 = 0$, (9.2.2) leads to the form that

differs only by the constant multiplier from the expression found in item 4, section 5.4.

If the feedback coefficients and bandpasses of the recirculator feedback circuits are identical ($m_1 = m_2 = m$ and $n_1 = n_2 = n$), then (9.2.2) assumes the form

$$g_s(ML) = \gamma \sum_{i=0}^{L-1} \sum_{k=0}^{(L-i)M-1} \frac{m^{k+i}}{\sqrt{1 + \gamma^2 + (k+i)n^2}}. \quad (9.2.3)$$

Specifically, with optimum bandpass of the prestorage filter

$$g_s(ML) = \sum_{i=0}^{L-1} \sum_{k=0}^{(L-i)M-1} \frac{m^{k+i}}{\sqrt{2 + (k+i)n^2}}. \quad (9.2.4)$$

The bandpasses of the feedback circuits will also be different due to the difference of the delay devices in these recirculator circuits. Apparently, a device with long delay time will have a smaller bandpass. 310 Specifically, with condition (9.1.5), $m_1 = m_2 = m$ and $\gamma = 1$, we have

$$g_s(ML) = \sum_{i=0}^L \sum_{k=0}^{(L-i)M-1} \frac{m^{k+i}}{\sqrt{2 + (i+Ml)n^2}}. \quad (9.2.5)$$

Consideration of the signal transfer coefficients from M (Fig. 9.2.1) calculated by this formula on the BESM-2 computer shows that the signal transfer coefficient decreases with an increase of the delay time in the second recirculator feedback circuit. The extent of this decrease is higher, the higher the value of n , the closer m is to 1 and the lower the value of N .

This is explained in the following manner. According to (9.1.5), n_2 also increases with an increase of M , i.e., the bandpass of the second recirculator feedback circuit is constricted. However, since n is sufficiently small, this does not lead to a significant constriction of the stored signal spectrum and therefore causes no strong attenuation of its peak value. There is sharp attenuation of the high-frequency components of the signal with larger value of n during circulation of the signal, which also determines the intensive decrease of its peak value.

The number of L subsequences stored in the second recirculator decreases with an increase of M in the case of fixed value of $N = ML$. Then similar to condition (5.4.19) of the practical independence of output voltage of the number of stored pulses, the inequality

$$m^L \ll 1 \quad (9.2.6)$$

becomes ever weaker and then ceases to be fulfilled. This also leads to a decrease of the coefficient of signal storage by the second recirculator and consequently to a decrease of the coefficient of signal transfer by the storage device. This is naturally observed at lower value of M , the closer m is to 1 and the lower the value of N .

The increase of losses in signal transfer caused by a decrease of N is especially high at small values of n and is insignificant at large values of n . This is explained by the fact that an increase of n is equivalent to a decrease of the feedback coefficient to a value at which inequality (9.2.6) remains sufficiently strong even at a lower value of N , due to which there is almost no increase of losses. 312

9.3. Storage of Noise

Substituting (9.1.4) into (1.7.2) and disregarding the effect of mutual overlap of these pulses due to the high on-off time ratio of pulses of the pulse characteristic, we find

$$\begin{aligned} \sigma_s^2 \approx & 2ac^2 \sum_{l=0}^{\infty} m_1^{2l} \sum_{i=0}^{\infty} z^i \sum_{k=0}^{\infty} z^k \times \\ & \times \int_{-\infty}^{\infty} v(t, \sqrt{\tau_1^2 + (l-iM)\tau_1^2 + i\tau_0^2}) \times \\ & \times v(t, \sqrt{\tau_1^2 + (l-kM)\tau_1^2 + k\tau_0^2}) dt. \end{aligned}$$

Since according to (7.1.9),

$$\int_{-\infty}^{\infty} v(t, \tau_0) v(t, \tau_0) dt = \frac{1}{\sqrt{2\pi} \sqrt{\tau_0^2 + \tau_1^2}},$$

the output of stored noise is

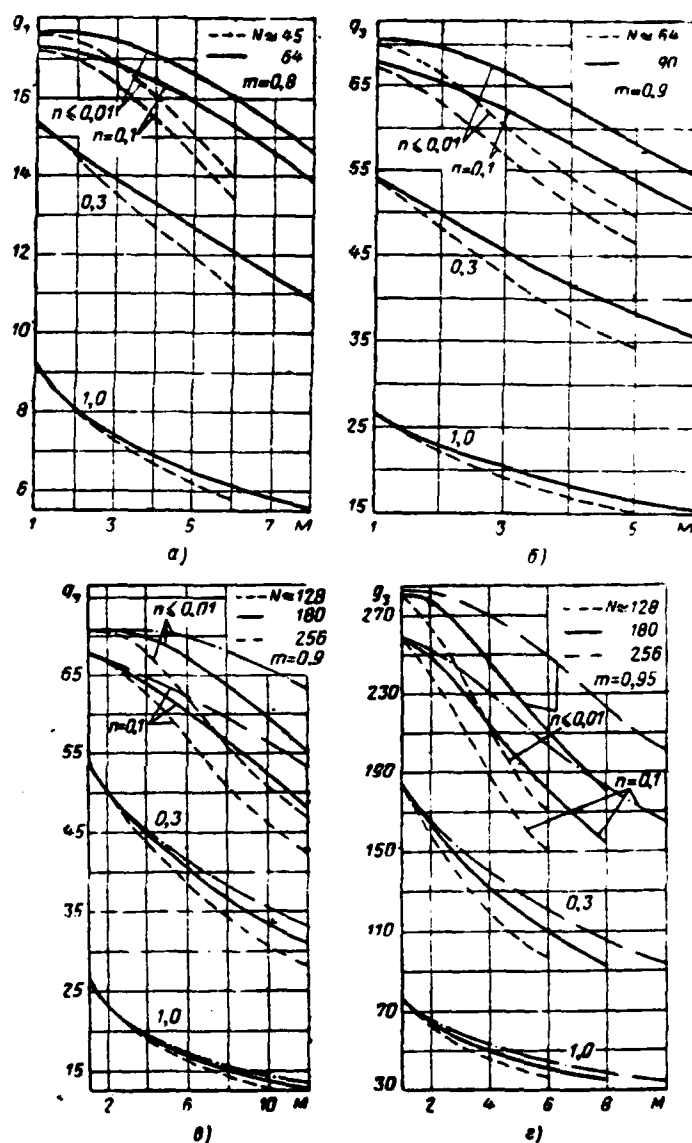


Fig. 9.2.1. Dependence of coefficient of signal transfer by two-stage storage device on M .

$$\begin{aligned}
 q_s^2 = & \frac{ac}{\epsilon} \sum_{l=0}^{\infty} m_1^{2l} \sum_{k=0}^{R(l/M)} z^k \times \\
 & \times \sum_{h=0}^{R(l/M)} \frac{z^h}{\sqrt{1 + \left[l - (l+k) \frac{M}{2} \right] n_1^2 + \frac{l+k}{2} n_2^2}}.
 \end{aligned}
 \tag{9.3.1}$$

while the coefficient of noise storage is

$$Q_s = \sum_{l=0}^{\infty} m_1^{2l} \sum_{i=0}^{E(l/M)} z^i \times \quad (9.3.2)$$

$$\times \sum_{k=0}^{E(l/M)} \frac{z^k}{\sqrt{1 + \left[l - (i+k) \frac{M}{2} \right] n_1^2 + \frac{i+k}{2} n_2^2}}.$$

Specifically, if $m_2 = 0$, i.e., there is no second recirculator, (9.3.2) 313 degenerates into (7.3.2). In the idealized case of infinitely broad bandpasses of the feedback circuits ($n_1 = n_2 = 0$), we find from (9.3.2) after very laborious transformations the expression derived in item 4, section 5.4. Having selected the value of M in it as large as possible so that $m_1^M \ll 1$, we will have

$$Q'_s = \frac{1}{(1 - m_1^2)(1 - m_2^2)}.$$

It follows from this expression that the coefficients of noise storage by the first and second recirculator, respectively, comprise

$$Q_s = \frac{1}{1 - m_1^2} \quad \text{and} \quad Q'_s = \frac{1}{1 - m_2^2},$$

i.e., noise is stored in the second recirculator by the same law as in the first. This is natural since the inequality presented above is the noncorrelation condition of the noise components stored by the second recirculator.

If the feedback coefficients and bandpasses of the recirculators are identical, then

$$Q_s = \sum_{l=0}^{\infty} m_1^{2l} \sum_{i=0}^{E(l/M)} \sum_{k=0}^{E(l/M)} \frac{z^{i+k}}{\sqrt{1 + \left[l - (i+k) \frac{M-1}{2} \right] n^2}}. \quad (9.3.3)$$

At $M = 1$ this formula degenerates to (8.3.2).

It is easy to ascertain that

$$\sum_{i=0}^R z^i \sum_{j=0}^R \theta_{i+j} z^j = \sum_{i=0}^R (i+1) \theta_i z^i + \sum_{i=R+1}^{2R} (2R+1+i) \theta_i z^i,$$

where θ_p is coefficients dependent only on ordinal number p .

Therefore, (9.3.3) can also be represented in the following form:

31

$$Q_s = \sum_{k=0}^{M-1} \frac{m^{2k}}{\sqrt{1+kn^2}} +$$

$$+ \sum_{k=M}^{\infty} m^{2k} \left\{ \sum_{l=0}^{E\left(\frac{l}{M}\right)} \frac{(l+1) z^l}{\sqrt{1 + \left[k - \frac{l}{2}(M-1)\right] n^2}} +$$

$$+ \sum_{l=E\left(\frac{k}{M}\right)}^{2E\left(\frac{k}{M}\right)} \frac{\left[2E\left(\frac{k}{M}\right) + 1 - l\right] z^l}{\sqrt{1 + \left[k - \frac{l}{2}(M-1)\right] n^2}} \right\}. \quad (9.3.4)$$

With identical feedback coefficients and bandpasses that satisfy condition (9.1.5), from expression (9.3.2) follows

$$Q_s = \frac{1}{(1-m^{M-1})} \sum_{l=0}^{\infty} \frac{\left[m^{l-(M-1)E\left(\frac{l}{M}\right)} - m^{l+M-1} \right]^2}{\sqrt{1+ln^2}} =$$

$$= \frac{1}{(1-m^{M-1})^2} \sum_{l=0}^{\infty} \frac{\left[m^{E\left(\frac{l}{M}\right) + MR\left(\frac{l}{M}\right)} - m^{l+M-1} \right]^2}{\sqrt{1+ln^2}}, \quad (9.3.5)$$

where $R(x)$ is the fractional part of integer x .

The dependence of the noise storage coefficients on M , calculated by the last formula on the BESM-2 computer (Fig. 9.3.1), has identical nature: the noise storage coefficient (and accordingly its output power) decrease in the first approximation by exponential law as M increases. This decrease is especially sharp with an increase of M from 1 to 2 and 3. In this case the noise storage coefficient is attenuated by a factor of approximately 1.5 and 2-2.5.

The noise storage coefficient decreases even more slowly with a further increase M . This is explained by the fact that the degree of correlation attenuation decreases more and more upon transition from

AD-A115 395

FOREIGN TECHNOLOGY DIV WRIGHT-PATTERSON AFB OH
OPTIMUM FILTERS AND PULSED SIGNAL STORAGE DEVICES, (U)
MAY 82 Y S LEZIN
FTD-ID(RS)T-0182-81

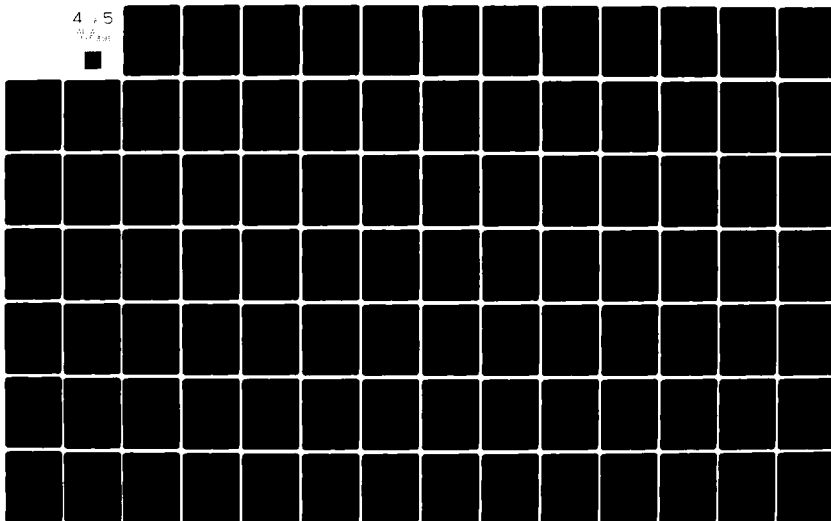
F/G 9/5

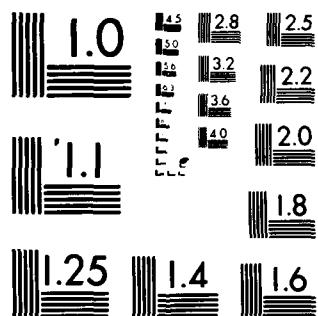
UNCLASSIFIED

NL

4 5

7.6.81





MICROCOPY RESOLUTION TEST CHART

NATIONAL BUREAU OF STANDARDS-1963-A

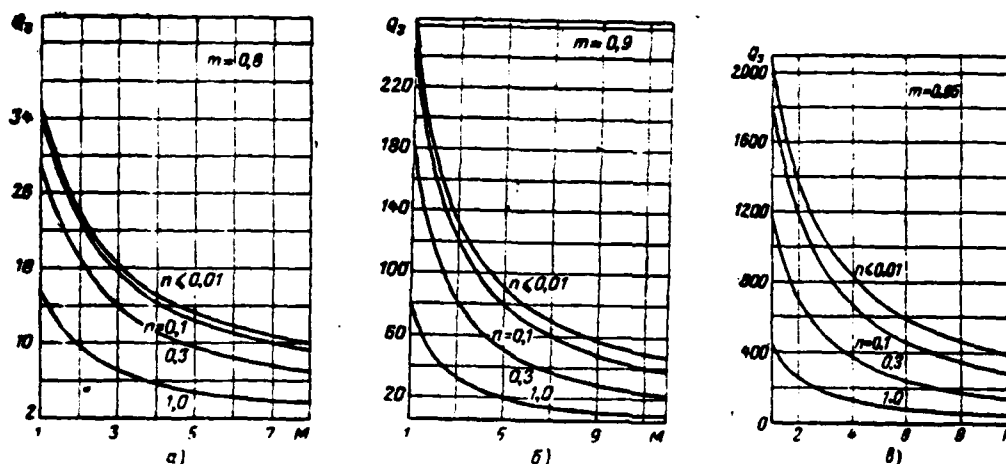


Fig. 9.3.1. Coefficient of noise storage by two-stage storage device as function of M .

$M = 1$ to $M = 2$ and 3 after sharp attenuation of the correlation coefficients of the noise stored in the second recirculator.

316

The noise storage coefficient decreases even more strongly as M increases, the larger the value of n and the closer M is to 1.

There is a sharp constriction of the bandpass of the second recirculator feedback circuit $\Delta F_s = n^{-1} M_1^{-1/2} \Delta F_1$, with an increase of n and M , which causes strong attenuation of the high-frequency components of noise at the output. Therefore, the noise storage coefficient is attenuated even more strongly with an increase of M , the higher the value of n .

The effect of the feedback coefficient on the attenuation of the noise storage coefficient is explained by the fact that the correlation coefficient of the noise stored in the second recirculator and whose value is attenuated more sharply with an increase of M , causing stronger attenuation of the stored noise output, is also higher with a larger value of m .

The main conclusion is that the noise power at the output of a two-stage storage device can be sharply attenuated by increasing the delay time several-fold in the feedback circuit of the second recirculator. Attenuation of the output power of noise more than half is achieved at comparatively small values of M , on the order of 3, when the second recirculator is not very strongly complicated and can be realized in some cases.

9.4. Gain in Signal/Noise Ratio

The gain provided by a two-stage storage device was calculated by formulas (7.4.1), (9.2.5) and (9.3.5) for the case of (9.1.5) with optimum bandpass of the prestorage filter. Consideration of the dependence of this gain on M (Fig. 9.4.1) shows that the gain initially increases with an increase of M and then decreases after reaching some maximum at optimum value of (5.4.25). The course of these functions is explained in item 4, section 5.4.

The maximum gain increases with an increase of N , upon approach of m to 1 and with a decrease of n . These results are obvious.

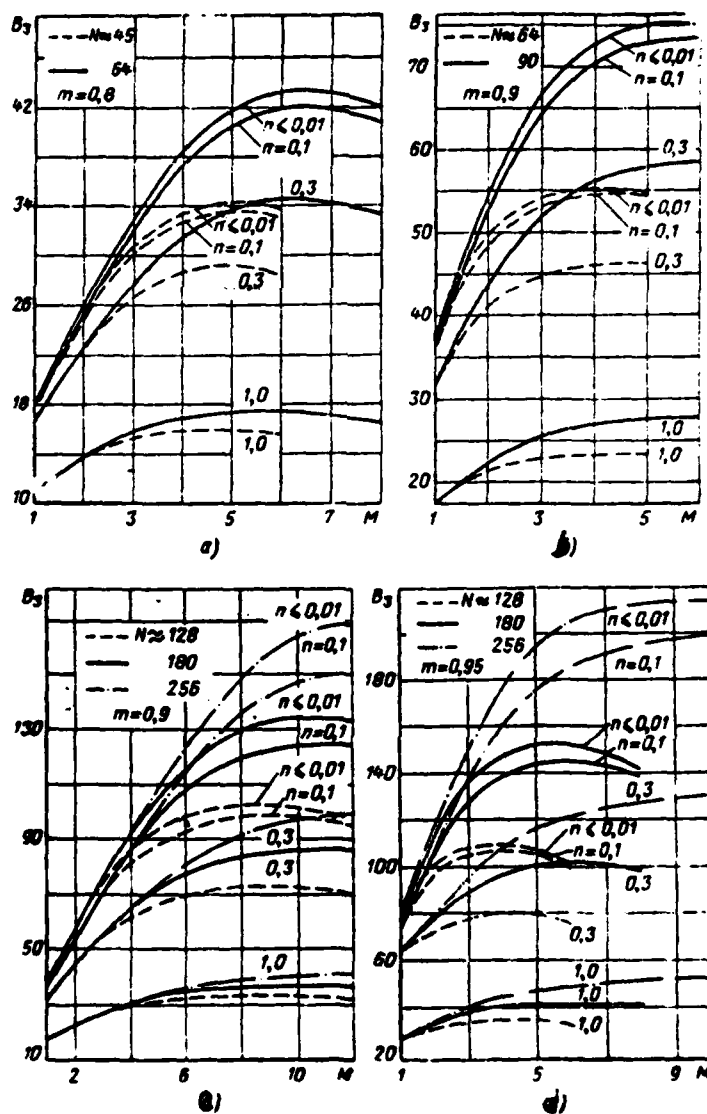


Fig. 9.4.1. Dependence of gain of two-stage storage device on M .

The ratio of the maximum gain to the number of stored pulsed signals 31 comprises 0.68-0.76, 0.66-0.86 and 0.81-0.85, respectively, at $m = 0.8$, 0.9 and 0.95 with sufficiently small value of $n \leq 0.01$. This ratio decreases as N increases.

Thus, replacement of optimum filtration by sequences of a larger number of pulsed signals by their two-stage storage using sufficiently wideband recirculators leads to comparatively small losses in the threshold signal, on the order of 1 dB.

The extent of these losses is decreased as m approaches 1. In this case the delay time in the feedback circuit of the second recirculator also decreases in view of (5.4.25), which simplifies its realization.

Additional losses appear with an increase of n , i.e., with a decrease of the bandpasses of the recirculator feedback circuits $b_4 = \Delta F_4 \tau_0 = \frac{0.441}{n}$ and $b_5 = \Delta F_5 \tau_0 = \frac{0.441}{n} M^{-1/2}$. However, their value is low at $n = 0.1$ and comprises a fraction of a decibel. These losses increase as N increases. The losses increase to 1-2 dB at $n = 0.3$. The losses increase to values on the order of tens of decibels at $n = 1$, i.e., the efficiency of a two-stage storage device drops sharply.

The additional gain caused by an increase of the delay time in the feedback circuit of the second recirculator from a value equal to the repetition quasi-period of the stored pulsed signals to an optimum value $M_{\text{OPT}} T$ increases with an increase of N and with a decrease of n .

The additional power gain comprises approximately 1.5, 2, 2.5 and 3.5, respectively (i.e., approximately 1.8, 3, 4 and 5.5 dB) at small values of n (less than 0.1) and with number of stored pulsed signals exceeding the active number (5.4.8), 2, 3, 4 and 6 times. The additional gain increases with a further increase of N . If n increases to 0.3, then the additional gain decreases by a value comprising a fraction of a decibel with small value of N and approximately 1 dB with large value of N .

A further increase of n to 1 reduces the additional gain to 1-3 dB. The value of this gain also increases with an increase of N .

Thus, two-stage storage is rather effective if the number of stored pulsed signals is no less than three times their active number, while the bandpass of the first recirculator feedback circuit is three times broader than that of the optimum prestorage filter. 31

However, the ratio of the indicated bandpasses should be on the order of 10 so that the losses are low compared to an idealized two-stage storage device. In this case the nature of the dependence of the bandpass of the second recirculator feedback circuit on M , which can differ from (9.1.5) in practice, will have a slight effect on the value of the gain obtained.

Since the number of signal recirculations through the feedback circuit of the second recirculator is less with two-stage storage than in the case of double storage, the bandpass of this circuit can be correspondingly reduced.

Accordingly, two-stage storage requires comparatively moderate width of the bandpass of the second recirculator feedback circuit, the main component of which is the delay device.

This recirculator should provide delay by time $M_{\text{OPT}}T$, which can be difficult, with sufficiently broad bandpass. If this delay device cannot be made, it may be feasible to reduce M from the optimum value (5.4.24) to 3. An additional gain on the order of 2 can then be achieved at $n \leq 0.1$ and at large value of N compared to a double storage device.

Consequently, the very complicated and important problem of efficient storage of sequences of a large number of pulsed signals can be solved by using a two-stage storage device consisting of two recirculators with sufficiently wideband feedback, delayed by the length of one and several repetition quasi-periods of pulsed signals, respectively.

NONCOHERENT EXPONENTIAL-WEIGHT STORAGE DEVICE

10.1. PRELIMINARY REMARKS

1. Advantages and Disadvantages of Noncoherent Storage

If pulsed signals are stored after a noncoherent (amplitude) detector (Fig. 10.1.1, a), it is called noncoherent storage (see section 6.1). It is the only one possible if the sequence of pulsed signals being received is not coherent.

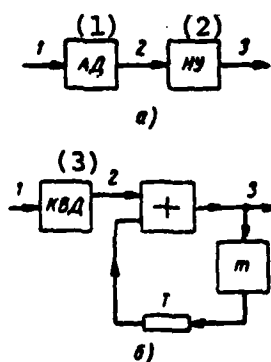


Fig. 10.1.1. Block diagrams of noncoherent storage devices.

Key: (1) Amplitude detector; (2) Video frequency storage device; (3) Square-law detector.

However, even when receiving coherent sequences of pulsed signals, noncoherent storage can be feasible since first, it permits a

considerable increase of receiver sensitivity (compared to the case when storage is not used) and second, unlike coherent storage, it does not require complication of the receiver determined by the need to design it on a circuit with very large number of channels or with very wideband delay line in the recirculator feedback circuit (see section 6.5). It is further shown that the loss in receiver sensitivity is comparatively low when coherent storage is replaced by noncoherent storage.

Yet another disadvantage is inherent to noncoherent storage. It includes the fact that only the information written in the amplitude of the signals being received is used during noncoherent storage and the information included in the phase (frequency) of these signals is completely lost. Because of this information about the speed of a target that caused signal reflection is lost.

2. Characteristics of Noncoherent Storage Devices with Exponential Weight Function

The significant feature of a noncoherent storage device is the presence of an amplitude detector, which is a typically nonlinear component.

Nonlinear components (for example, square-law generators) are also used during coherent storage of signals with unknown initial phase. However, the signal is fed to them only after storage, i.e., when its level will be higher. Nonlinear conversion of the signal-noise mixture occurs in noncoherent storage even before storage when the signal is weak compared to noise. Suppression of the signal by noise is observed in this case [129]. The lower sensitivity of a receiver with noncoherent storage is also explained by this.

Due to its nonlinearity, an amplitude detector causes a change of the distribution laws of random voltages, which are usually Gaussian at its input.

Thus, if an instantaneous voltage of a mixture of a pulsed signal of amplitude V and Gaussian noise of output σ^2 acts on the input of a

detector which we subsequently assume is square-law with normalized characteristic

$$u_2 = U_1^2 \quad (10.1.1)$$

(here u_2 is the instantaneous value of output voltage and U_1 is the voltage amplitude at the input) distributed according to the normal law, then according to [20, 129] the output voltage has the following probability distribution:

$$W(u_2) = \frac{1}{2\sigma^2} \exp\left(-\frac{u_2 + V^2}{2\sigma^2}\right) I_0\left(\frac{V\sqrt{u_2}}{\sigma^2}\right) \cdot 1(u_2). \quad (10.1.2)$$

When using a linear detector, the instantaneous voltage of the signal-noise mixture is distributed by generalized Rayleigh law (6.3.2).

Thus, random voltages which are distributed by a law differing from normal act on the input of a storage device following an amplitude detector of any type. The distribution law of these voltages varies upon their transmission through a storage device which is a linear system. It is very difficult to determine it since there are presently no engineering methods of calculating the distribution laws of voltages at the output of a linear system when random voltages distributed by other than normal law are acting on its input.

True, there is one special case at which the distribution function at the output of a linear system can be calculated comparatively simply and rather precisely. This is the effect of random voltage on a linear system whose bandpass is considerably less than the spectral width of the input voltage. The random voltage is normalized with this condition at the output of a linear system [15, 20, 159].

A similar tendency toward normalization is also observed in a storage device whose voltage output is equal to the sum of input voltage samples. This is explained by the fact that if the number of terms is sufficiently high and their distribution laws are identical, then in view of the central limiting theorem of probability theory, the sum of these terms is distributed by approximately normal law [15, 20].

The indicated normalization of voltage at the output of the storage device can be explained differently. The frequency characteristic

of the storage device is a comb type with sufficiently narrow transmission bands (see item 1, section 5.4). Therefore, if random voltages having broad spectrum act on this system, the distribution of the output voltage becomes close to normal.

323

In most papers known to us on noncoherent storage [10-13, 160-161] this phenomenon of normalization of random voltages at the output of the storage device is also used. However, it is assumed in all these papers (and in other papers [134, 162*]) that the storage device is ideal in the sense that the voltage at its output is the sum of a large number of input voltage samples:

$$u_s(t) = \sum_{k=1}^N u_s(t - kT).$$

But most real storage devices (a recirculator, RC-commutator, comb filter, storage tube and so on) add the input voltages with exponential weight function (EVF)

$$u_s(t) = \sum_{k=0}^{\infty} m^k u_s(t - kT) = \sum_{k=0}^{\infty} m^k u_{sk}. \quad (10.1.3)$$

Such a storage device has the pulse characteristic

$$h(t) = \sum_{k=0}^{\infty} \delta(t - kT) m^k = \sum_{k=0}^{\infty} \delta(t - kT) e^{-kt}, \quad (10.1.4)$$

where $t = \frac{1}{T} \ln \frac{1}{m}$ is the coefficient of the exponential weight function and m is the weight multiplier.

The normalized envelope of this pulse characteristic at $t > 0$ is the exponent $e^{-\xi t}$. Because of this, the indicated device is naturally called a storage device with exponential weight function. It is an approximation of a real storage device with delayed feedback. Unlike

324

* With the exception of Ye. G. Trubitsyn's paper [163].

feedback circuit contains no frequency filter (Fig. 10.1.1, b) is studied in the given chapter for significant simplification of analysis.

The results obtained in this case are valid if the bandpass of the storage device feedback circuit is much broader than that of the pre-storage (and predetector in this case) filter since condition 7.4.2 is fulfilled. The method of accounting for the final bandpass of a storage device is outlined in item 4, section 10.6.

Due to the exponential nature of storage law (10.1.3), the distribution laws of different terms of output voltage have different parameters. Therefore, the numerical characteristics of these terms (for example, the mean values and outputs) may differ strongly. If the received oscillation is a steady random process, i.e., if its distribution laws do not vary in time, the mean values of the terms of output voltage vary by the law m^k with an increase of their ordinal number k and they vary by the law m^{2k} with an increase of output. Specifically, at $m = 0.9$, even the 10th term has a mean value less by approximately a factor of 2.9 and output less by a factor of approximately 8.2 than the zero term. At $m = 0.8$, the indicated characteristics of the 10th term are less by a factor of 9.3 and 84, respectively, than that of the zero term.

Accordingly, the conditions of the central limiting theorem of probability theory are not fulfilled in the considered case at $m = 0.8-0.95$ and normalization of the output voltage is comparatively weak.

This also determines the difficulty of determining the distribution laws of random voltages at the output of noncoherent storage devices with exponential weight function. And the threshold signals cannot be calculated without a knowledge of these laws.

The distribution laws of the voltages of a signal-noise mixture at the output of the considered device are further determined by the approximate method.

10.2. Random Voltage Distribution at Output of Square-Law Storage Device With Exponential Weight Function and Frequency of False Alarms

325

A square-law storage device is understood as a combination of a square-law detector and recirculator (Fig. 10.1.1, b). Selection of the detector as square-law is explained by the fact that the analytical expressions of the statistical characteristics of random voltages are simpler for this detector. This simplifies the analysis. The results found in this case are approximately valid for devices with different type detectors as well [160, 164, 165].

We note that due to the first of conditions (7.2.2), the terms of the sum (10.1.3) are essentially mutually independent. The samples of input voltage u_{2k} contained in this sum are distributed by law (10.1.2).

If for brevity of notation we write $y = \frac{u_1}{2\sigma^2}$, $x_k = \frac{u_{2k}}{2\sigma^2}$ and $q = V/\sigma$ and if the number of terms of sum (10.1.3) is taken as finite and equal to N , then instead of (10.1.2) and (10.1.3) we find

$$W(x_k) = \exp\left(-x_k - \frac{q^2}{2}\right) I_0(q\sqrt{2x_k}) \quad (10.2.1)$$

and

$$y = \sum_{k=0}^{N-1} m^k x_k. \quad (10.2.2)$$

The random value x_k has the characteristic function [20]

$$\begin{aligned} \Phi(v) &= \int_{-\infty}^{+\infty} W(x_k) e^{jvx_k} dx_k = \\ &= \int_0^{\infty} e^{-\frac{q^2}{2} - x_k(1-jv)} I_0(q\sqrt{2x_k}) dx_k. \end{aligned}$$

Changing the variable by law $|x_k^2 = z$ and using formula (6.631.4) from [92] with regard to the fact that $I_0(y) = J_0(jy)$, we find

$$\Phi(v) = (1 - jv)^{-1} \exp\left(\frac{q^2}{2} \frac{jv}{1 - jv}\right). \quad (10.2.3)$$

Both distribution (10.2.1) and the characteristic function (10.2.3) are identical for all values of x_k . 326

Based on the known property of the characteristic function, the k-th term of sum (10.2.2) has the characteristic function

$$\theta_k(v) = \theta(m^k v) = (1 - jm^k v)^{-1} \exp\left(\frac{q^2}{2} \frac{jm^k v}{1 - jm^k v}\right).$$

Due to the mutual independence of the terms of this sum, its characteristic function is equal to the product of the characteristic functions of the terms [20]:

$$\theta(v) = \prod_{k=0}^{N-1} \theta_k(v) = \prod_{k=0}^{N-1} \left[(1 - jm^k v)^{-1} \exp\left(\frac{q^2}{2} \frac{jm^k v}{1 - jm^k v}\right) \right].$$

The probability distribution density of sum (10.2.2) is determined by using an inverse Fourier transform:

$$\begin{aligned} W(y) &= \frac{1}{2\pi} \int_{-\infty}^{+\infty} \theta(v) e^{-jyv} dv = \\ &= \frac{1}{2\pi} \int_{-\infty}^{+\infty} \left\{ \prod_{k=0}^{N-1} \left[(1 - jm^k v)^{-1} \times \right. \right. \\ &\quad \left. \left. \times \exp\left(\frac{q^2}{2} \frac{jm^k v}{1 - jm^k v}\right) \right] \right\} e^{-jyv} dv. \end{aligned} \quad (10.2.4)$$

Calculation of this integral in the general case causes difficulties which have not yet been overcome. Therefore, let us limit ourselves to the case of the absence of a signal ($q = 0$). The probability density of the output sum is then

$$W(y) = \frac{1}{2\pi} \int_{-\infty}^{+\infty} \frac{1}{B(v)} e^{-jyv} dv,$$

where $B(v) = \sum_{k=0}^{N-1} (1 - jm^k v)$ is a polynomial of N-th power with respect to v.

Since its roots are prime:

$$v_k = -jm^{-k}, \quad (10.2.5)$$

then, as is known [166],

$$W(y) = \sum_{k=0}^{N-1} \frac{1}{B'(v_k)} e^{-v_k y},$$

where $B'(v_k)$ is the derivative of $B(v)$ with respect to v at value of $v = v_k$.

Therefore, after transformations with regard to (10.2.5), we find

$$W(y) = \sum_{k=0}^{N-1} \frac{m^{-k} \exp(-y m^{-k})}{\prod'_{n=0}^{N-1} (1 - m^{n-k})} l(y),$$

where the prime of the product denotes omission of a multiplier with $n = k$. If we return to the initial variable $u_3 = 2\sigma^2 y$, then

$$W(u_3) = \frac{1}{2\sigma^2} \sum_{k=0}^{N-1} \frac{m^{-k} \exp\left(-\frac{u_3}{2\sigma^2 m^k}\right)}{\prod'_{n=0}^{N-1} (1 - m^{n-k})} l(u_3).$$

Specifically, with a finite number of terms and also with condition (5.4.19), which is frequently fulfilled in real storage devices, we have [167]

$$W(u_3) = \frac{1}{2\sigma^2} \sum_{k=0}^{\infty} \frac{m^{-k}}{\prod'_{n=0}^{\infty} (1 - m^{n-k})} e^{-\frac{u_3}{2\sigma^2 m^k}} l(u_3). \quad (10.2.6)$$

One can show [7, 168] that this series converges uniformly. Because of this, let us integrate it term by term with respect to u_3 to determine the integral distribution function of the output noise, as a result of which we find at $U > 0$

$$\begin{aligned} P(U) = \text{Bep}(u_3 > U) &= \int_0^{\infty} W(u_3) du_3 = \\ &= \sum_{k=0}^{\infty} \left[\prod'_{n=1}^{\infty} (1 - m^{n-k}) \right]^{-1} e^{-\frac{U}{2\sigma^2 m^k}}. \end{aligned} \quad (10.2.7)$$

Then the probability of a false alarm comprises at $U_0 > 0$

328

$$F = P(U_0) = \sum_{k=0}^{\infty} \exp\left(-\frac{l}{m^k}\right) / \prod_{n=0}^{\infty} \left(1 - \frac{m^n}{m^k}\right), \quad (10.2.8)$$

where $l = U_0/2\sigma^2$ is the relative threshold level.

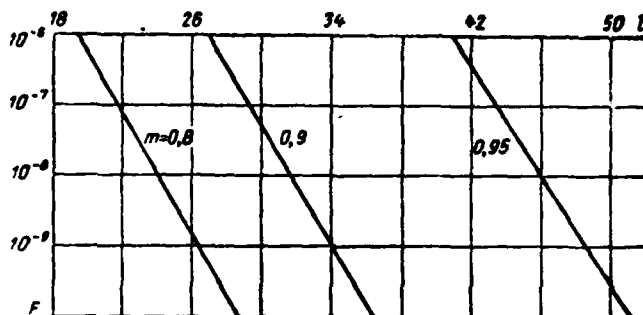


Fig. 10.2.1. Dependence of probability of false alarm on relative threshold.

Calculations by this formula are related to the need to fulfill some rather cumbersome and precise calculations. The results of calculating the dependence of the threshold level on the probability of a false alarm, carried out on a BESM-2 computer, are presented in Fig. 10.2.1.

If one proceeds from approximation of the distribution of output noise by normal law, then, as shown in section 10.3,

$$F \approx \frac{1}{2} \left[1 - \Phi \left(\frac{U_0 - \frac{2\sigma^2}{1-m}}{\sqrt{2 \frac{(2\sigma^2)^2}{1-m^2}}} \right) \right], \quad (10.2.9)$$

hence,

$$l_1 = \frac{1}{1-m} \left[1 + \sqrt{2 \frac{1-m}{1+m}} \arg \Phi(1-2F) \right]. \quad (10.2.10)$$

If the distribution law of output noise is approximated by "chi-square" equivalent distribution (see section 10.3), then

329

$$F \approx P \left[\frac{U_0(1+m)}{\sigma^2}; 2 \frac{1+m}{1-m} \right], \quad (10.2.11)$$

where

$$P(\chi^2, n) = \frac{1}{2^{\frac{n-2}{2}} \Gamma(\frac{n}{2})} \int_0^\infty x^{n-1} e^{-\frac{x^2}{2}} dx \quad (10.2.12)$$

is the integral "chi-square" distribution function [169]. The roots $l_2 = U_0/2\sigma^2$ of equation (10.2.11) are determined from tables [170].

Consideration of Table 10.2.1 with the results of calculating the relative threshold by strict formula (10.2.8) and by approximate formulas (10.2.10) and (10.2.11) shows that approximation of the output noise distribution by both normal law and by "chi-square" law lead to impermissibly large errors in determination of the response threshold. The value of these errors decreases as m approaches 1, which is explained by the increased normalization of output noise.

Table 10.2.1.

P	10^{-3}			10^{-4}		
	l	l_1	l_2	l	l_1	l_2
0.8	19.5	12.9	17.2	26.4	15.0	22.1
0.9	26.9	20.9	24.9	34.1	23.7	30.4
0.95	40.8	35.2	39.1	48.7	39.2	45.5

The errors are somewhat less with "chi-square" approximation than with normal approximation. Therefore, when making rough, approximate calculations one can approximate the output noise distribution by "chi-square" law. Unfortunately, the calculating errors increase with respect to the threshold as the probability level of a false alarm decreases.

The frequency of false alarms rather than the probability of a false alarm is frequently used when designing parameter detection and measurement systems. In this regard let us calculate the indicated frequency at the output of the considered storage device (Fig. 10.1.1, b).

The frequency of false alarms obviously coincides with the mean number of noise blips at the output level per unit time, which is written in the given case by the formula

$$v(U_0) = \int_0^{\infty} \dot{n}_3 W(U_0, \dot{n}_3) d\dot{n}_3,$$

where $W(n_3, \dot{n}_3)$ is the joint probability density of noise voltage n_3 at the output of the storage device and its rate of variation \dot{n}_3 .

Determination of this density is very complicated. Therefore, let us calculate the frequency of false alarms as the quotient from division of the probability of a false alarm by the average length of the noise blip:

$$v = \frac{r}{m_1(\tau)}. \quad (10.2.13)$$

Let us use the fact that the probability of a false alarm for the given case is precisely calculated while the average length of the noise blip is slightly dependent on the nature of noise distribution and therefore this noise can be calculated approximately by a normal process whose blips at a sufficiently high level (compared to the noise level) U_0 have the mean length

$$m_1(\tau) = \frac{\sqrt{2\pi} \sigma_3}{f_3(U_0 - m_{13})}, \quad (10.2.14)$$

where σ_3 and m_{13} are the effective and mean values of noise, respectively,

$$f_3 = \frac{\int_0^{\infty} \omega^2 F_3(\omega) d\omega}{\int_0^{\infty} F_3(\omega) d\omega} \quad (10.2.15)$$

is the mean square of noise frequency and $F_3(\omega)$ is its energy spectrum.

Formula (10.2.14) is a generalization of the well-known formula (see, for example, (10.78) in [20]) for the case of a normal process with zero mean value.

331

Accordingly, in the considered case

$$v \approx \frac{f_3(U_0 - m_{13}) F}{\sqrt{2\pi} \sigma_3}. \quad (10.2.16)$$

Specifically, if the linear part of the receiver is equivalent to a filter with bell-shaped amplitude-frequency characteristic

$$K(\omega) = K(\omega_0) \exp[-\alpha(\omega - \omega_0)^2], \quad (10.2.17)$$

where $\alpha = 0.0351/\Delta F^2$, ΔF is the bandpass at level $1/\sqrt{2}$, then the noise at the input of a square-law detector when white noise with energy spectrum (1.2.4) is acting on the input has the energy spectrum

$$F_1(\omega) = 2\alpha K^2(\omega_0) \exp[-2\alpha(\omega - \omega_0)^2],$$

at the output of this detector [213]

$$F_2(\omega) = F_2(0) \exp[-\alpha\omega^2],$$

and at the output of an analog storage device it is

$$F_3(\omega) = \frac{F_2(0) \exp[-\alpha\omega^2]}{1 - 2m \cos \omega T + m^2}.$$

The last energy spectrum is a comb type with repetition quasi-period $2\pi F = 2\pi/T$ and width $2\pi\Delta F$ at level $1/\sqrt{2}$. Since usually $\Delta FT \gg 1$, then as shown in section 7.3, this spectrum can be averaged by the period of the oscillating multiplier $\cos \omega T$ when calculating the integrals in (10.2.15). Then

$$\beta_3^2 \approx \frac{\frac{1}{1-m^2} \int_0^\infty \omega^2 F_2(\omega) d\omega}{\frac{1}{1-m^2} \int_0^\infty F_2(\omega) d\omega} = \beta_2^2.$$

Consequently, the mean square values of the noise frequencies at the output and input of an analog storage device essentially coincide.

332

Specifically, for the case of (10.2.17), $\beta_3 \approx \beta_2 = 3.79\Delta F$. Substituting this expression into (10.2.16) and also the relations

$$m_{12} = \frac{2\sigma^2}{1-m^2} \quad \text{and} \quad \sigma_1^2 = \frac{(2\sigma^2)^2}{1-m^2},$$

which follow from formula (10.3.9) derived below, we find

$$v = 1.51\Delta F \left(\sqrt{1-m^2} - \sqrt{\frac{1+m}{1-m}} F \right). \quad (10.2.18)$$

where l is selected by the given probability of a false alarm by means of graphs (Fig. 10.2.1). For example, if $F = 10^{-6}$, $m = 0.9$ and $\Delta F = 1$ MHz, then $\nu = 11.1$ Hz.

The frequency of false alarms were calculated for the case of quadratic storage of noise at $N = 20$ and $m = 1$ by this formula and by the explicit formula presented in [15] to estimate the accuracy of the approximate formula (10.2.16). The results of these calculations for $F = 10^{-6}$ and 10^{-9} differed by 5.3 and 18%, respectively. One can show that this error in the value of the frequency of false alarms can cause an error in determination of threshold level whose value is less than 1%.

Thus, the outlined method* of calculating the frequency of false alarms with noncoherent storage provides accuracy quite acceptable for practice.

10.3. Storage of Sequences of Nonfluctuating Pulsed Signals

1. Distribution Cumulants of Nonfluctuating Signal-Noise Mixture at Output of Storage Device

Since integral (10.2.4) that describes the probability density of the voltage of a nonfluctuating signal-noise mixture at the output of a noncoherent storage device with exponential weight function has not yet been calculated, an attempt is made below to calculate approximately the indicated probability distribution. To do this, the numerical characteristics of the output voltage are first determined. 333

The numerical characteristics of the random values which are more frequently used are the moments of distribution of different orders [15, 20]—mean value, standard deviation and so on. However, other numerical characteristics—cumulants—or distribution semi-invariants, or more convenient when making the calculations [20, 132].

By definition, the derivative of the same order of logarithm of a characteristic function at point $\nu = 0$ divided by j^k is called a k -th order cumulant:

* This method was proposed by M. M. Leshchinskiy.

$$\begin{aligned} \kappa_k &= j^{-k} \left[\frac{d^k}{dv^k} \ln \theta(v) \right]_{v=0} = \\ &= j^{-k} \left\{ \frac{d^k}{dv^k} \left[\ln \int_{-\infty}^{\infty} W(x) e^{jvx} dx \right] \right\}. \end{aligned} \quad (10.3.1)$$

Hence follows two important properties of a cumulant [132]:

1) A cumulant of any k -order of the product of random value x by constant a is equal to the product of the k -th power of a constant by the cumulant of a random value, i.e.,

$$\kappa_k(ax) = a^k \kappa_k(x). \quad (10.3.2)$$

2) A cumulant of any order of the sum of independent random values is equal to the sum of cumulants of the same order of these values, i.e.,

$$\kappa_k \left(\sum_{n=1}^N x_n \right) = \sum_{n=1}^N \kappa_k(x_n). \quad (10.3.3)$$

The latter property, called a composition rule [132], is valid for moments only for the first three orders. The advantage of cumulants is included in this.

Let us determine the distribution cumulants of voltage at the input of a recirculator, i.e., at the output of a square-law detector (Fig. 10.1.1, b). To do this, let us first calculate the characteristic function of this voltage. Using (10.2.3) that describes the characteristic function of the value $x = u_2/2\sigma^2$, we find

$$\theta(v) = (1 - j2\sigma^2 v)^{-1} \exp \left(\frac{q^2}{2} \frac{j2\sigma^2 v}{1 - j2\sigma^2 v} \right).$$

Its natural logarithm or the cumulant function

$$\psi(v) = \ln \theta(v) = \frac{q^2}{2} \frac{j2\sigma^2 v}{1 - j2\sigma^2 v} - \ln(1 - j2\sigma^2 v)$$

has an n -th order derivative:

$$\psi^{(n)}(v) = (2j\sigma^2)^n (n-1)! (1 - j2\sigma^2 v)^{-n} \left(1 + \frac{nq^2}{2} \frac{j2\sigma^2 v}{1 - j2\sigma^2 v} \right).$$

Dividing this expression by j^n and assuming that $v = 0$, we determine the n -th order cumulant of voltage at the input of a storage device:

$$\kappa_{n1} = (n-1)! (2\sigma^2)^n \left(1 + n \frac{q^2}{2}\right). \quad (10.3.4)$$

Let us then determine the cumulants of voltage distribution at the output κ_{n2} . Since the terms of the sum (10.1.3) are mutually independent, then because of the composition rule (10.3.3)

$$\kappa_{n2} = \sum_{k=0}^{\infty} \kappa_n^{(k)},$$

where $\kappa_n^{(k)}$ is an n -th order cumulant of the k -th term.

According to (10.3.2), the latter is related to a cumulant of the same order of input voltage at moment $t - kT$ of the following function:

$$\kappa_n^{(k)} = m^{kn} \kappa_{n1}.$$

Because of this, the n -th order cumulant of output voltage is

$$\kappa_{n2} = \sum_{k=0}^{\infty} m^{kn} \kappa_{n1}^{(k)}. \quad (10.3.5)$$

Accordingly, the cumulant of any order of voltage at the output of a storage device with exponential weight function is related by a simple function to cumulants of the same order of voltage at the input of this device. 335

The derived expression is very general and valid in any case. It is easy to generalize for storage devices with other weight functions.

In the special case of receiving a square-wave sequence of N non-fluctuating pulsed signals on a continuous noise background, the first N discrete values of input voltage will be a signal-noise mixture while the remaining ones will be noise.

Let us denote by κ_{n2}^i and κ_{n2}^n the n -th order cumulants of input voltage during the action of a signal-noise mixture and noise alone, respectively. Then

$$x_{n3} = x'_{n3} \frac{1 - m^{nN}}{1 - m^n} + x''_{n3} \frac{m^{nN}}{1 - m^n} \quad (10.3.6)$$

If the number of pulses is high or the value of the weight multiplier is small, so that

$$m^{nN} \ll 1 \text{ and } x''_{n3} m^{nN} \ll x'_{n3}, \text{ then } x_{n3} \approx x'_{n3} / (1 - m^n).$$

When receiving a continuous noise oscillation

$$x_{n3} = x''_{n3} / (1 - m^n). \quad (10.3.7)$$

In the case of quadratic storage with exponential weight function and Gaussian noise at the input, according to (10.3.4), formulas (10.3.6) and (10.3.7) assume the form

$$x_{n3} = (n-1)! \frac{(2q^2)^n}{1 - m^n} \left[1 + n \frac{q^2}{2} (1 - m^{nN}) \right] \quad (10.3.8)$$

and

$$x_{n3} = (n-1)! \frac{(2q^2)^n}{1 - m^n}. \quad (10.3.9)$$

It follows from (10.3.8) that the output voltage has the asymmetry coefficient

$$k = \frac{x_{33}}{x_{23}^{3/2}} = 2 \frac{(1+m)(1-m^2)^{1/2}}{1+m+m^2} \frac{1 + \frac{3}{2} q^2 (1 - m^{3N})}{[1 + q^2 (1 - m^{2N})]^{3/2}} \quad (10.3.10)$$

and the excess coefficient

33

$$\gamma = \frac{x_{43}}{x_{23}^2} = 6 \frac{1 - m^2}{1 + m^2} \frac{1 + 2q^2 (1 - m^{4N})}{[1 + q^2 (1 - m^{2N})]^2}. \quad (10.3.11)$$

These formulas are valid both in the presence of a signal and in its absence ($q = 0$).

Consideration of the dependence of the asymmetry and excess coefficients on signal/noise ratio (see Fig. 10.3.1) shows that the noise distribution has such large asymmetry and excess that it cannot even be approximately considered normal. This coincides with the conclusion made previously (see section 10.2).

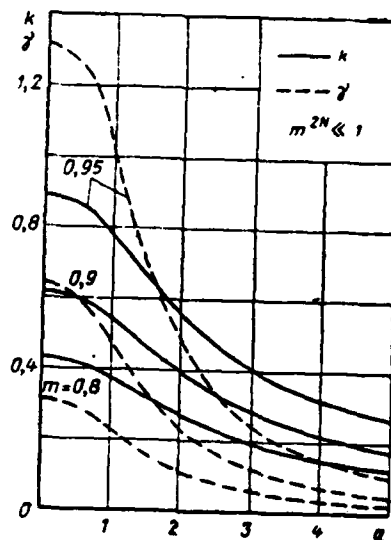


Fig. 10.3.1. Asymmetry and excess coefficients as functions of signal/noise ratio.

If the signal/noise ratio increases, both asymmetry and the excess decrease (asymmetry somewhat more slowly than excess). A decrease of these coefficients indicates the approach of the distribution of signal-noise mixture to normal law with an increase of the weight multiplier and with an increase of the signal/noise ratio. The latter is explained 337 by the fact that the distribution (10.1.2) of the signal-noise mixture at the input of the recirculator varies significantly from exponential law at $q = 0$ to a law close to normal at large value of q as the signal/noise ratio increases. However, even at $m = 0.95$ and $q = 2$ the output voltage distribution can only be assumed approximately normal.

The question arises of how to use the voltage cumulants determined above at the output of a noncoherent storage device with exponential weight function for approximate, but rather precise calculation of the distribution law of this voltage. This problem is also considered below.

2. Expansion of Probability Distribution Function of Output Voltage to Edgeworth and Laguerre Series

Asymptotic expansion of the distribution function of a random value, based on normal distribution, is accomplished by an Edgeworth series [132].

For the probability density of voltage u it has the form

$$W(u) = \frac{1}{\sqrt{x_2}} \left[\varphi(x) - \frac{k}{6} \varphi^{(3)}(x) + \frac{\gamma}{24} \varphi^{(4)}(x) + \frac{k^2}{72} \varphi^{(6)}(x) - \frac{x_3}{120x_2^{5/2}} \varphi^{(5)}(x) - \frac{k\gamma}{144} \varphi^{(7)}(x) - \frac{k^3}{1296} \varphi^{(9)}(x) + \dots \right],$$

where

$$x = \frac{u - x_1}{\sqrt{x_2}}; \quad \varphi(x) = \frac{1}{\sqrt{2\pi}} \exp\left(-\frac{x^2}{2}\right); \quad \varphi^{(n)}(x) = \frac{d^n}{dx^n} \varphi(x);$$

and x_n is the n -order cumulant of voltage u .

This series converges more rapidly, the closer the investigated process is to normal, i.e., the less the asymmetry and excess coefficients and so on. At $k = \gamma = 0$ and $x_5 = \dots = 0$, the probability distribution is normal

$$W(u) = \frac{1}{\sqrt{2\pi x_2}} \exp\left[-\frac{(u - x_1)^2}{2x_2}\right]. \quad (10.3.13)$$

Relation (10.2.9) also follows from (10.3.9) and (10.3.13).

By integrating (10.3.12) with respect to u from U to ∞ , we find an Edgeworth series for the integral distribution function: 338

$$P(U) = \frac{1}{2} \left[1 - \Phi\left(\frac{y}{\sqrt{2}}\right) \right] + \frac{k}{6} \varphi^{(3)}(y) - \frac{\gamma}{24} \varphi^{(4)}(y) - \frac{k^2}{72} \varphi^{(6)}(y) + \dots, \quad (10.3.14)$$

where $y = \frac{U - x_1}{\sqrt{x_2}}$.

The remainder term of the Edgeworth series is on the order of the first discarded term. The tables of [126, 171, 172] should be used when calculating the distribution functions using an Edgeworth series.

Edgeworth series can be used to calculate the distribution functions only if the distribution is close to normal. The criterion of this proximity is the smallness of the asymmetry and excess coefficients and also the coefficients $x_3/x_2^{3/2}$ and so on. These coefficients can obviously be regarded as small if their absolute value is less than 0.1. In this case it is usually sufficient to take into account no more than four terms of this series.

If there is no proximity of the considered and normal distributions, the Edgeworth series converges so slowly that calculations are possible only by using a digital computer.

If the probability distribution differs strongly from normal and has great asymmetry, for example, due to the probability density of negative values of random voltage being equal to zero, which is specifically observed after a square-law detector and an insufficiently efficient recirculator or a different filter, then expansion of the distribution functions into a series by functions of the Laguerre orthogonal system may yield better results [173-175].

$$W(u) = \frac{x_1}{x_2} x^a e^{-x} \sum_{k=0}^{\infty} g_k L_k^a(x), \quad (10.3.15)$$

where

$$L_k^a(x) = \frac{1}{k!} e^x x^{-a} \frac{d^k}{dx^k} (x^{a+k} e^{-x}) \quad (10.3.16)$$

is a generalized k-th order Laguerre polynomial [25]:

33:

$$\begin{aligned} a &= \frac{x_1^2}{x_2} - 1; \quad x = \frac{x_1}{x_2} u; \quad g_0 = \frac{1}{\Gamma\left(\frac{x_1^2}{x_2}\right)}; \quad g_1 = g_2 = 0; \\ g_3 &= \frac{\frac{x_1^2}{x_2}}{x_2 \Gamma\left(\frac{x_1^2}{x_2} + 3\right)} \left(2 - \frac{x_1 x_3}{x_2^2}\right); \\ g_4 &= \frac{3x_1^2}{x_2 \Gamma\left(\frac{x_1^2}{x_2} + 4\right)} \left(6 - 4 \frac{x_1 x_3}{x_2^2} + \frac{x_1^2 x_4}{3x_2^3}\right); \\ g_5 &= \frac{24x_1^2}{x_2 \Gamma\left(\frac{x_1^2}{x_2} + 5\right)} \left(6 - 5 \frac{x_1 x_3}{x_2^2} + \frac{5}{6} \frac{x_1^2 x_4}{x_2^3} - \frac{x_1^3 x_5}{24x_2^5}\right); \\ g_6 &= \frac{40x_1^2}{x_2 \Gamma\left(\frac{x_1^2}{x_2} + 6\right)} \left[\left(30 + \frac{x_1^2}{x_2}\right) \left(1 - \frac{x_1 x_3}{x_2^2}\right) + \frac{x_1^4 x_3^2}{4x_2^5} + \right. \\ &\quad \left. + \frac{15}{2} \frac{x_1^2 x_4}{x_2^3} - \frac{3}{4} \frac{x_1^3 x_5}{x_2^4} + \frac{x_1^4 x_6}{40x_2^5} \right] \text{ and so on,} \end{aligned}$$

and $\Gamma(x)$ is a gamma-function.

Consequently, the coefficients of this expansion, like those of the Edgeworth series, are expressed by distribution cumulants of random voltage u .

Integrating (10.3.15) with respect to u within the limits from U to ∞ , we find a Laguerre expansion for the integral distribution function

$$P(U) = P\left(2 \frac{x_1}{x_2} U; 2 \frac{x_1^2}{x_2}\right) - \left(\frac{x_1}{x_2} U\right)^{a+1} e^{-\frac{x_1}{x_2} U} \sum_{k=1}^{\infty} \frac{g_k}{k} L_{k-1}^{a+1}\left(\frac{x_1}{x_2} U\right), \quad (10.3.17)$$

where the "chi-square" integral distribution function $P(\chi^2, n)$ is characterized by (10.2.12).

The Laguerre series (10.3.15) and (10.3.17) can be used to calculate the probability densities and distribution functions in the case when the distribution of the considered random value is close to "chi-square" distribution. The criterion of this proximity is the smallness of the expansion coefficients g_3, g_4, g_5 and so on. In this case calculation carried out by using only the zero term of these series alone yields satisfactory accuracy in most cases. 340

If the storage device were ideal, i.e., if it added N blips of the received oscillation with weight equal to one and if it were preceded by a square-law detector, the voltage of the stored noise would be precisely distributed by "chi-square with $2N$ degrees of freedom" law [11, 13, 133]. Actually, in this case, according to (10.3.4) and (10.3.5):

$$\begin{aligned} x_{n2} &= Nx_{n2} = N(n-1)!(2\sigma^2)^n; \\ a+1 &= \frac{x_{12}^2}{x_{22}} = N; \quad \frac{x_{12}}{x_{22}} = \frac{1}{2\sigma^2}; \quad g_3 = g_4 = \dots = 0 \end{aligned}$$

and

$$P(U) = P\left(\frac{U}{\sigma^2}; 2N\right).$$

If the samples (storage) are added by law (10.1.3), where $m = 0.8-0.95$ and if the number of samples is infinitely large, one can assume that the output noise is also distributed by approximately "chi-square" law. Then from (10.3.9) and (10.3.17) follows

$$P(U) \approx P \left[\frac{U(1+m)}{\sigma^2}; 2 \frac{1+m}{1-m} \right],$$

which coincides with (10.2.11) at $U = U_0$ and $P(U_0) = F$.

It is shown in section 10.2 that the assumption made above about the nature of output noise distribution is rather cumbersome, although acceptable for approximate calculations.

3. Threshold Signals in Absence of Fluctuations

The probability of detection with exponential weight storage of nonfluctuating signals can be calculated by using the first four terms of an Edgeworth series:

$$D = P(U_0) \approx \frac{1}{2} \left[1 - \Phi \left(\frac{x}{\sqrt{2}} \right) \right] + \frac{k_3}{6} \varphi^{(3)}(x) - \frac{\gamma_3}{24} \varphi^{(4)}(x) - \frac{k_3^2}{72} \varphi^{(6)}(x), \quad (10.3.18)$$

where $x = \frac{U_0 - x_{11}}{\sqrt{x_{11}}}$, and x_{n3} , k_3 and γ_3 are calculated by formulas (10.3.8), (10.3.10) and (10.3.11).

Being given U_0 , based on the level of the probability of a false alarm and the value of the weight multiplier of the recirculator, the signal/noise ratio and the number of pulses in the sequence, one can calculate the cumulants of the first four orders, the asymmetry and excess coefficients and then the probability of detection.

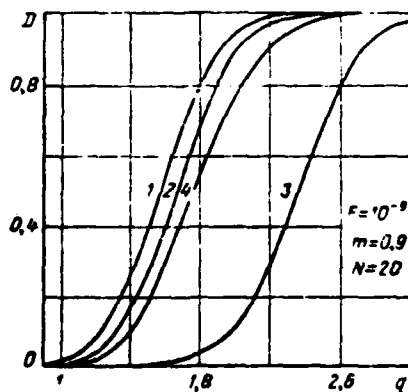


Fig. 10.3.2. Characteristics of detecting nonfluctuating signals.

The detection characteristic with noncoherent storage of nonfluctuating signals, calculated by formula (10.3.18), is shown by curve 3 as an example in Fig. 10.3.2. The detection characteristics with coherent exponential weight storage of a completely known (curve 1) and known with the exception of the initial phase (curve 2) sequence of nonfluctuating signals are plotted in the same figure for comparison. All these characteristics have the same form.

Curve 4 in the same figure reproduces the detection characteristic with noncoherent exponential weight storage of nonfluctuating signals plotted with approximation of the instantaneous voltages of noise and signal/noise mixture by normal distribution law at the output of a noncoherent exponential weight storage device. Comparison of curves 3 and 4 shows the unsatisfactory nature of normal approximation of the distribution laws of random voltages at the output of a noncoherent exponential weight storage device. 342

The threshold signals can be calculated by the following method. Let us ascertain the level of detection probability and let us determine the first approximation of the signal/noise ratio corresponding to it q_0 from the relation

$$D = \frac{1}{2} \left[1 - \Phi \left(\frac{U_0 - x_{11}}{\sqrt{2x_{11}}} \right) \right],$$

which, using (10.3.8), is transformed to the form

$$\begin{aligned} q_0^2(1 - m^N) - 2[l(1 - m) - 1] = \\ = \sqrt{8 \frac{1 - m}{1 + m}} z [1 + q_0^2(1 - m^{2N})]^{1/2}, \end{aligned}$$

where $z = \arg \Phi(2D - 1)$. Specifically, $z = 0$ at $D = 0.5$ and $z = 0.9062$ at $D = 0.9$.

The derived equation is biquadratic in the general case ($z \neq 0$) with respect to q_0 . Its solution at $D = 0.9$ is as follows:

$$q_0 = \frac{1}{\sqrt{1 - m^N}} \left\{ 2[l(1 - m) - 1] + 6.768 \frac{1 - m}{1 + m} (1 + m^N) + \right.$$

$$+ 2,563 \sqrt{\frac{1-m}{1+m}} \times \\ \times \sqrt{1 + 4[l(1-m)-1](1+m^N) + 6,768 \frac{1-m}{1+m} (1+m^N)}^{1/2}. \quad (10.3.19)$$

At $D = 0.5$, due to the fact that $z = 0$, the first approximation is considerably simpler:

$$q_0 = \left\{ \frac{2[l(1-m)-1]}{1-m^N} \right\}^{1/2}. \quad (10.3.20)$$

To refine the result obtained, let us assume that correction Δq is small compared to the first approximation. Representing (10.3.18) by the function $D(q) = D(q_0 + \Delta q)$ and expanding the latter into a Taylor series, we find

$$D = D(q_0 + \Delta q) \approx D(q_0) + \left. \frac{dD}{dq} \right|_{q=q_0} \cdot \Delta q = D(q_0) + D'(q_0) \Delta q.$$

Since $D(q_0)$ is the result of substituting q_0 into (10.3.18), in which the first term of this expression approaches D and the sum of the next three terms assumes some value ΔD , then $D = D + \Delta D + D'(q_0) \Delta q$, hence,

$$\Delta q \approx -\frac{\Delta D}{D'(q_0)} \approx -\frac{\Delta D}{D'_0(q_0)},$$

where

$$D_0 = \frac{1}{2} \left[\left(1 - \Phi \frac{x}{\sqrt{2}} \right) \right] = \frac{1}{\sqrt{\pi}} \int_{\frac{U_0 - x_{12}}{\sqrt{2}x_{23}}}^{\infty} e^{-t^2} dt.$$

By differentiating the last integral with respect to the parameter, we find

$$D'_0 = \frac{1}{\sqrt{2\pi}} \exp \left[-\left(\frac{U_0 - x_{12}}{\sqrt{2}x_{23}} \right)^2 \right] \left[\frac{1}{2} \frac{U_0 - x_{12}}{x_{23}^{3/2}} \frac{dx_{23}}{dq} + \frac{1}{x_{23}^{1/2}} \frac{dx_{12}}{dq} \right].$$

Specifically, $U_0 = x_{12}$ and $D'_0 = (2\pi x_{12})^{-1/2} x'_{12}$ at $D = 0.5$ and $D'_0 = 0.1755 x_{12}^{-1/2} [x'_{12} - 0.6407 x_{12}^{-1/2} x'_{12}]$ at $D = 0.9$.

Because of (10.3.8) and the previous formulas, we have at $D = 0.5$

$$\Delta q \approx 0,3348 \frac{1-m^2}{1+m+m^2} \frac{1 + \frac{3}{2} q_0^2 (1-m^{2N})}{q_0 (1-m^N) [1 + q_0^2 (1-m^{2N})]}, \quad (10.3.21)$$

and at $D = 0.9$ we have

$$\Delta q \approx - \frac{\sqrt{\frac{1-m}{1+m}} [1 + q_0^2 (1 - 0,1755 q_0 (1-m^N) \{ 1 - 1,2814 (1+m^N) \sqrt{\frac{1-m}{1+m}} \times - m^{2N} \})^{1/2} \Delta D]}{\times [1 + q_0^2 (1-m^{2N})]^{-1/2}}, \quad (10.3.22)$$

where

$$\begin{aligned} \Delta D = & 0,05634 \frac{(1+m)(1-m^2)^{1/2}}{1+m+m^2} \frac{1 + \frac{3}{2} q_0^2 (1-m^{2N})}{[1 + q_0^2 (1-m^{2N})]^{3/2}} + \\ & + 0,07637 \frac{1-m^2}{1+m^2} \frac{1 + 2q_0^2 (1-m^{4N})}{[1 + q_0^2 (1-m^{2N})]^2} - \\ & - 0,03589 \frac{(1+m)^2 (1-m^2)}{1+m+m^2} \frac{[1 + \frac{3}{2} q_0^2 (1-m^{2N})]^2}{[1 + q_0^2 (1-m^{2N})]^3}. \end{aligned} \quad (10.3.23)$$

The greater simplicity of the expression for correction at $D = 0.5$ is explained by the fact that $x = 0$ and $\phi^{(3)}(0) = 0$ in this case. Therefore, it is sufficient to take into account only the first two terms of the Edgeworth series when calculating the detection probability since its remainder term is on the order of the third term, which is equal to zero in the given case. Expression (10.3.21) is also more precise since the segment of function $D(q)$ corresponding to it can be assumed linear with greater accuracy than the segment adjacent to $D = 0.9$.

Calculations show that the relative value of the correction at $m \geq 0.8$ and $N \geq 4$ does not exceed 1.35%. The value of this correction decreases as m approaches 1 and as N increases.

Consideration of the dependence of threshold signal/noise ratios on N (Fig. 10.3.3)* shows that the threshold ratio decreases as the number

* The following notations were used in this figure and also in the

of pulses increases until m^N becomes negligible. The threshold ratios are lower with sufficiently large number of pulses, the greater the probability of a false alarm and the closer m is to 1. The level of detection probability is hardly dependent on the threshold ratio: the latter are only 10-20% higher at $D = 0.9$ than at $D = 0.5$.

345

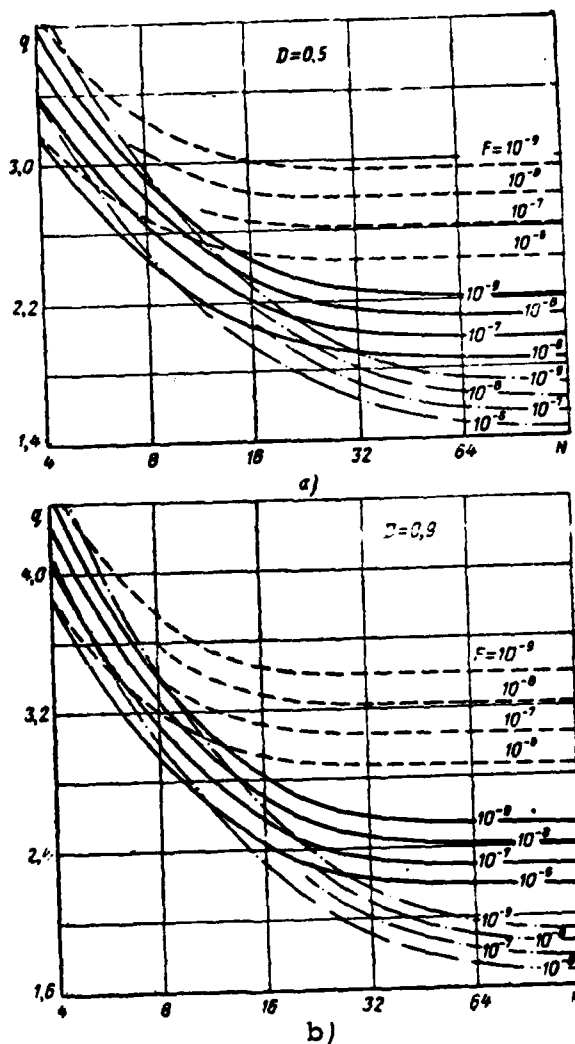


Fig. 10.3.3. Dependence of threshold ratios on number of stored nonfluctuating signals.

subsequent figures (Figs. 10.3.4, 10.3.5, 10.4.2-10.4.4, 10.5.1 and 10.5.2): curves corresponding to $m = 0.8$ are denoted by dashed curves, those for $m = 0.9$ are denoted by solid curves and those for $m = 0.95$ are denoted by dash-dot curves.

344

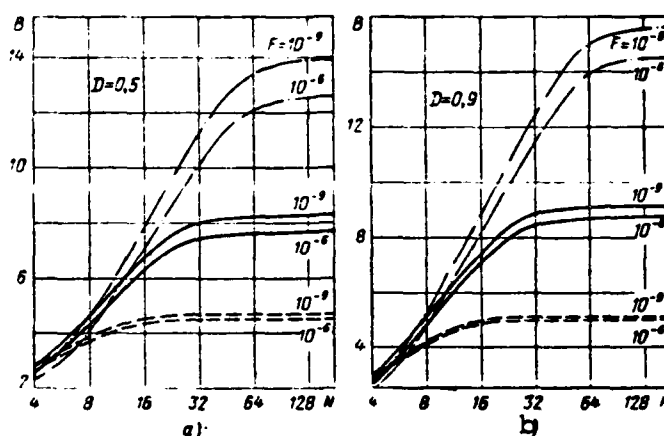


Fig. 10.3.4. Effect of storing nonfluctuating signals as function of their number.

The dependence of the storage effect on the number of pulses are shown in Fig. 10.3.4.* The storage effect is understood as the power gain of threshold signals due to the use of only the square-law detector of the storage device with exponential weight function. The storage effect is higher, the greater the number of pulses in the sequence to be stored and the closer m is to 1. The storage effect is hardly dependent on the probability levels of a false alarm on correct detection.

If the number of pulses is sufficiently high, the value of the storage effect is approximately 4.5-5 at $m = 0.8$, 8-9 and $m = 0.9$ and 13-15 at $m = 0.95$.

Accordingly, the use of a storage device with exponential weight function after a noncoherent detector permits one to achieve a greater power gain of threshold signals, which indicates the feasibility of this use.

The dependence of the power loss of threshold signals upon replacement of coherent exponential weight storage of signals with unknown

*See note on p. 310.

initial phase by noncoherent storage is shown in Fig. 10.3.5.* This loss increases as the number of pulses, the weight multiplier and the probability level of a false alarm increase and as the probability level of detection decreases. The latter is explained by the fact that in this case the threshold signal/noise ratio decreases and because of this signal suppression by noise in the amplitude detector increases [129].

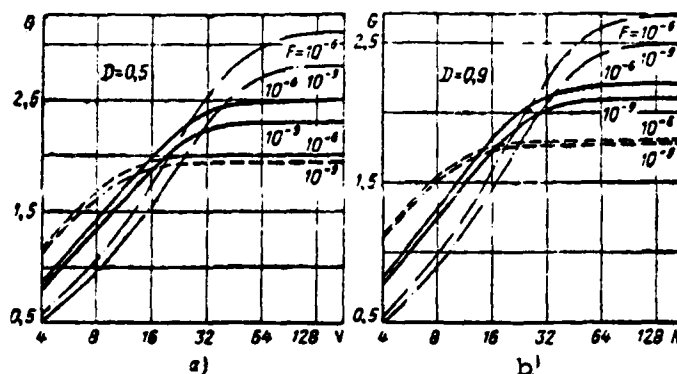


Fig. 10.3.5. Loss during noncoherent storage of non-fluctuating signals as function of their number.

10.4. Storage of Sequences of Pulse Signals Fluctuating in Unison

1. Distribution Cumulants of Stored Mixture of Signals and Noise Fluctuating in Unison

The detection characteristics of signals fluctuating in unison are usually calculated in the following manner [12, 13, 133]. The expression for the detection probability of a nonfluctuating signal of specific amplitude V is taken. It is also assumed valid with a fluctuating signal, having used the given value of amplitude, but characterizes the conditional probability of detection. Having averaged it statistically for all possible values of amplitude, we find the desired detection probability.

348

This procedure can also be used essentially in the given case by averaging (10.3.18) for all possible signal/noise ratios with regard to (6.4.1):

* See note on p. 310.

$$D = \int_0^{\infty} D(q^2) \frac{1}{2q^2} \exp\left(-\frac{q^2}{2q^2}\right) dq^2.$$

However, it is very difficult to calculate this integral since the conditional probability $D(q^2)$ is a very complex function. Moreover, since expression (10.3.18) is approximate, it is difficult to provide an estimate of the error of this calculation beforehand.

Determination of the numerical characteristics of distribution of a mixture of a fluctuating signal and noise at the output of a storage device and using them to calculate the distribution functions and then the detection characteristics are simpler.

Expression (10.3.8) is also valid with harmonious fluctuations of a signal. It characterizes the conditional distribution cumulant of output voltage $\kappa_{n3}(q^2)$. To determine the unconditional cumulant κ_{n3} , statistical averaging must be carried out with regard to (6.4.1). However, direct averaging of an n -th order conditional cumulant leads to the correct result only at $n = 1$, i.e., one can average directly only a first-order cumulant coinciding with the mean value m_{13} .

Direct statistical averaging is possible only for the initial moments of any order. Actually, by definition [20], the n -th order initial moment of voltage u , provided that the square of the signal/noise ratio q^2 is observed, is

$$m_n(q^2) = \int_{-\infty}^{+\infty} u^n W(u/q^2) du = \frac{\int_{-\infty}^{+\infty} u^n W_2(u, q^2) du}{W_1(q^2)},$$

hence, it follows that:

$$m_n(q^2) W_1(q^2) = \int_{-\infty}^{+\infty} u^n W_2(u, q^2) du.$$

Therefore, the total (unconditional) moment of any order n

$$m_n = \int_{-\infty}^{+\infty} \int_{-\infty}^{+\infty} u^n W_2(u, q^2) du dq^2 = \int_{-\infty}^{+\infty} m_n(q^2) W_1(q^2) dq^2 \quad (10.4.1)$$

is the result of direct statistical averaging of the conditional initial moment of the same order.

In similar fashion, the n -th order conditional central moment (at $n \geq 2$) is, by definition

$$M_n(q^2) = \int_{-\infty}^{+\infty} [u - m_1(q^2)]^n W(u/q^2) du = \\ = \frac{\int_{-\infty}^{+\infty} [u - m_1(q^2)]^n W_2(u, q^2) du}{W_1(q^2)},$$

hence,

$$\int_{-\infty}^{+\infty} M_n(q^2) W_1(q^2) dq^2 = \int_{-\infty}^{+\infty} dq^2 \int_{-\infty}^{+\infty} [u - m_1(q^2)]^n W_2(u, q^2) du.$$

The last expression differs from that for the complete (unconditional) central moment

$$M_n = \int_{-\infty}^{+\infty} dq^2 \int_{-\infty}^{+\infty} (u - m_1)^n W_2(u, q^2) du,$$

where m_1 is the first-order total moment.

This also proves the statement made above on the possibility of direct statistical averaging of only the initial moments of any order.

By directly averaging the first-order conditional cumulant (moment) (10.3.8), we will have

$$\kappa_{11} = \frac{2\sigma^2}{1-m} [1 + p^2(1-m^N)]. \quad (10.4.2)$$

Changing from conditional cumulants (10.3.8) to conditional initial moments by means of known relations [20, 132], averaging them with regard to (6.4.1) and again changing from the total initial moments to total cumulants, we find

3

$$\begin{aligned}
\chi_{21} &= \left(\frac{2\rho^2}{1-m} \right)^2 \left\{ \rho^4 (1-m^N)^2 + \right. \\
&\quad \left. + \frac{1-m}{1+m} [1 + 2\rho^4 (1-m^N)] \right\}, \\
\chi_{33} &= 2 \left(\frac{2\rho^2}{1-m} \right)^3 \left\{ \rho^4 (1-m^N)^3 + \right. \\
&\quad + 3 \frac{1-m}{1+m} \rho^4 (1-m^N) (1-m^{2N}) + \\
&\quad \left. + \frac{(1-m)^2}{1+m+m^2} [1 + 3\rho^4 (1-m^{3N})] \right\}, \\
\chi_{44} &= 6 \left(\frac{2\rho^2}{1-m} \right)^4 \left\{ \rho^4 (1-m^N)^4 + \right. \\
&\quad + 4 \frac{(1-m)}{1+m} \rho^4 (1-m^N)^2 (1-m^{2N}) + \\
&\quad + 4 \frac{(1-m)^2}{1+m+m^2} \rho^4 (1-m^N) (1-m^{3N}) + \\
&\quad + 2 \left(\frac{1-m}{1+m} \right)^2 \rho^4 (1-m^{2N})^2 + \\
&\quad \left. + \frac{(1-m)^3}{(1+m)(1+m^2)} [1 + 4\rho^4 (1-m^{4N})] \right\}.
\end{aligned} \tag{10.4.3}$$

These formulas are valid at any values of m and N . In the considered case of $0.8 \leq m < 1$ they assume the following approximate form:

$$\chi_{nn} \approx (n-1)! \left(2\rho^2 \frac{1-m^N}{1-m} \right)^n \text{ at } n = 2, 3 \text{ and } 4 \tag{10.44}$$

2. Distribution of Stored Mixture of Signals and Noise Fluctuating in Unison

It follows from (10.4.4) that the distribution of a mixture of signals and noise fluctuating in unison at the output of a noncoherent storage device has asymmetry $k \approx 2$ and excess $\gamma \approx 6$ (calculation by explicit formulas (10.4.3) for the most unfavorable case of $m = 0.8$, $N = 4$ and $\rho^2 = 7.21$ yields $k = 1.9877$ and $\gamma = 5.943$. The latter differ from approximate values by -0.615 and -0.95% , respectively).

35

Since the asymmetry and excess coefficients are so high, the use of an Edgeworth series to calculate the detection characteristics and threshold signals is essentially impossible due to its slow convergence.

It follows from (10.1.2) and (10.3.4) that the noise at the output of a square-law detector has exponential distribution with cumulants of any order n

$$\kappa_{n2} = (n-1)!(2\sigma^2)^n \quad (10.4.5)$$

and the asymmetry and excess coefficients are equal to 2 and 6, respectively. This leads to the idea that the distribution of a stored mixture of signals and noise fluctuating in unison and unstored noise are similar. This is explained in the following manner. Because of the total correlation of signals fluctuating in unison, they are stored by the same laws as are regular signals. However, the result of their storage remains random and the nature of its distribution is the same as that of unstored noise.

Comparing (10.4.2) and (10.4.4) to (10.4.5), we conclude that the second-, third- and fourth-order cumulants both of the stored mixture and of unstored noise are expressed by similar formulas, while the formulas for first-order cumulants differ somewhat. Therefore, unlike unstored noise, distribution of which is exponential (see (10.1.2) at $V = 0$), the stored mixture of signals and noise fluctuating in unison should have exponential distribution shifted along the voltage axis

$$W(u_s) = \frac{1}{2\sigma_s^2} \exp\left(-\frac{u_s - V_0}{2\sigma_s^2}\right) I(u_s - V_0),$$

where σ_s^2 and V_0 are constants which are subject to determination. One can show that this distribution has the cumulants

$$\kappa_{1s} = V_0 + 2\sigma_s^2 \text{ and } \kappa_{ns} = (n-1)!(2\sigma_s^2)^n \text{ at } n > 1.$$

It follows from the expressions for the first- and second-order cumulants that $2\sigma_s^2 = \kappa_{2s}$ and $V_0 = \kappa_{1s} - \kappa_{2s}^{1/2}$.

35

Thus, a stored mixture of signals and noise fluctuating in unison is distributed with probability density

$$W(u_s) = \frac{1}{\kappa_{2s}^{1/2}} \exp\left(-\frac{u_s - \kappa_{1s}}{\kappa_{2s}^{1/2}} - 1\right) I(u_s - \kappa_{1s} + \kappa_{2s}^{1/2})$$

and at $U > \kappa_{1s} - \kappa_{2s}^{1/2}$ has integral distribution function

$$P(U) = \int_U^\infty W(u_s) du_s = \exp\left(-\frac{U - \kappa_{1s}}{\kappa_{2s}^{1/2}} - 1\right). \quad (10.4.6)$$

To ascertain the validity of the assumptions made above, let us calculate by two different methods the probability of excess stored mixture of a level equal to a first-order cumulant. It follows from (10.4.6) that $P(x_{13}) = e^{-1} = 0.36788$ and calculating (10.3.14) using an Edgeworth series, we find

$$P(x_{13}) = \frac{1}{2} [1 - \Phi(0)] + \frac{1}{6} k_3 \varphi^{(3)}(0) \approx \\ \approx 0.5 - \frac{1}{6} \cdot 2 \cdot 0.39894 = 0.36702.$$

Therefore, distribution (10.4.6), although it is approximate, it is quite suitable for calculations of threshold signals. In this case their accuracy at $D = 0.5$ is apparently higher than at $D = 0.9$.

3. Threshold Signals During Harmonious Fluctuations

According to (10.4.6), the detection probability during noncoherent exponential weight storage of signals fluctuating in unison comprises (see curve 2 in Fig. 10.4.1)

$$D = \exp\left(-\frac{U_0 - x_{13}}{x_{23}^{1/2}} - 1\right). \quad (10.4.7)$$

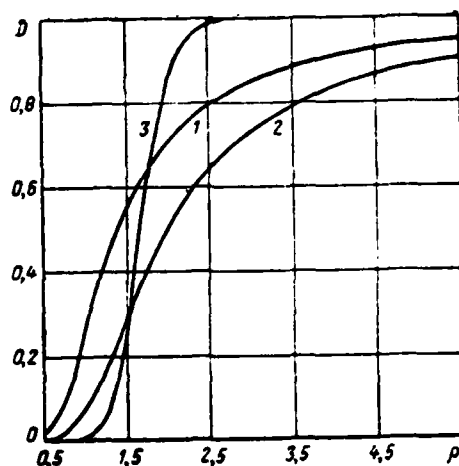


Fig. 10.4.1. Detection characteristics of fluctuating signals (1 and 2—coherent and noncoherent storage of signals fluctuating in unison, respectively; 3—noncoherent storage of independently fluctuating signals).

It follows from (10.4.2), (10.4.4) and (10.4.7) that

$$\rho^s = \frac{l(1-m) - 1 + \left(1 - \ln \frac{1}{D}\right)(1+m^N) \frac{1-m}{1+m}}{(1-m^N) \ln \frac{1}{D}} \quad (10.4.8)$$

or for rough calculations

$$\rho^s \approx [l(1-m) - 1] / \left[(1-m^N) \ln \frac{1}{D} \right]. \quad (10.4.9)$$

The dependence of the threshold ratios on N , calculated by formula (10.4.8) (Fig. 10.4.2*) have essentially the same character as during storage of nonfluctuating signals. The main difference is included in the fact that the threshold ratios at $D = 0.9$ are 2.6-2.7-fold greater than at $D = 0.5$. As in the case of coherent storage (see section 6.4), this is the result of signal fluctuations.

The dependence of the storage effect of signals fluctuating in unison (Fig. 10.4.3*) on the number of stored pulsed signals hardly differs from similar functions in the absence of fluctuations (Fig. 10.3.4). True, the storage effect is somewhat less in the case of harmonious fluctuations.

355

The dependence of the power loss upon replacement of coherent storage by noncoherent on the number of pulses (Fig. 10.4.4*) has the same nature as during storage of nonfluctuating signals. With harmonious fluctuations, although the loss is somewhat greater, it is still comparatively small and does not exceed 3 at $m \leq 0.95$.

356

10.5. Storage of Sequences of Independently Fluctuating Pulsed Signals

1. Distribution Cumulants of Stored Mixture of Independently Fluctuating Signals and Noise

Independently fluctuating (from pulse to pulse) pulsed signals are similar in their properties to noise (see section 6.4). Because of this, a mixture of a fluctuating signal and noise at the output of a

* See note on p. 310.

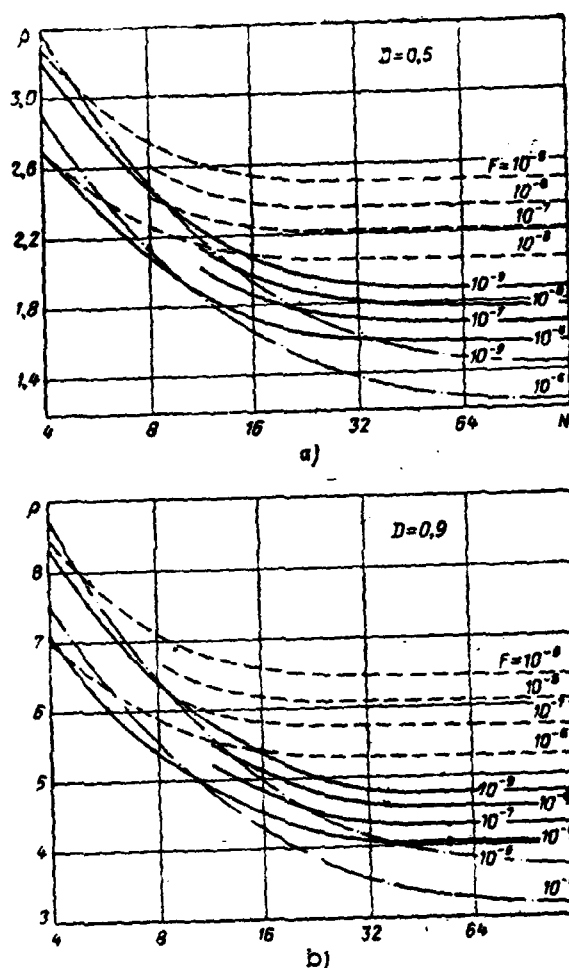


Fig. 10.4.2. Dependence of threshold ratios on number of stored signals fluctuating in unison

square-law detector is distributed, like noise alone, by exponential law:

356

$$W(u_2) = \frac{1}{2(\sigma^2 + \eta^2)} \exp \left[-\frac{u_2}{2(\sigma^2 + \eta^2)} \right] 1(u_2).$$

The only difference is that the role of output σ^2 at the input of the detector is played by the sum of signal η^2 and noise outputs. Therefore, according to (10.4.5), the voltage of a mixture of independently fluctuating signal and noise at the output of a detector has an n -order cumulant

$$\kappa_{n2} = (n-1) [2(\sigma^2 + \eta^2)]^n. \quad (10.5.1)$$

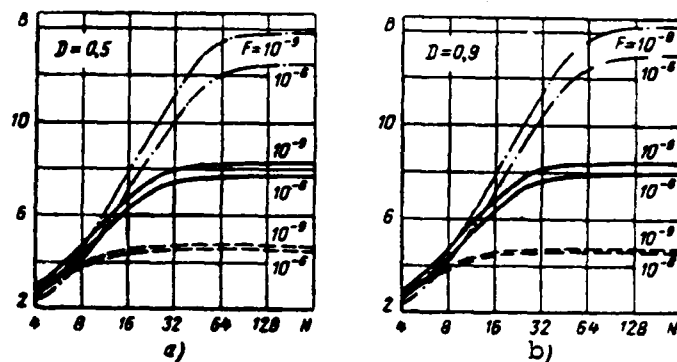


Fig. 10.4.3. Storage effect of signals fluctuating in unison as function of their number.

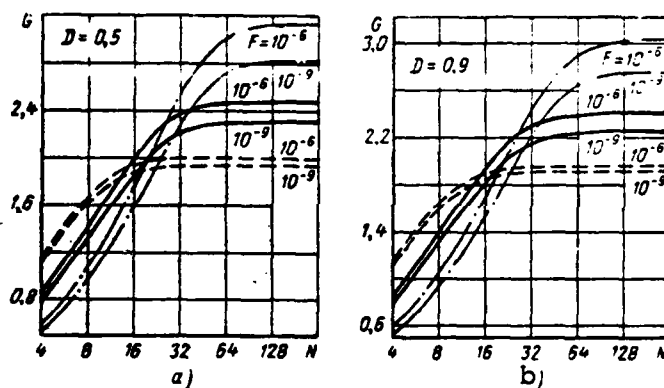


Fig. 10.4.4. Loss during noncoherent storage of signals fluctuating in unison as function of their number.

This expression can be found more strictly by statistical averaging of the conditional initial moments of distribution with regard to (6.4.1) calculated by means of (10.4.5) and subsequent conversion from the derived total initial moments to cumulants. 356

Because of (10.3.9) and (10.5.1), the stored mixture has the cumulants

$$\kappa_{ns} = (n-1)! \frac{(2\sigma^2)^n}{1-m^n} [(1+p^n)(1-m^{nN}) + m^{nN}]. \quad (10.5.2)$$

2. Threshold Signals With Independent Fluctuations

The asymmetry and excess coefficients of a stored mixture of independently fluctuating signals and noise, calculated by using (10.5.2), 357

hardly differ from similar coefficients for stored noise (Fig. 10.3.1) and have comparatively large value. However, expansion of the integral distribution function into Edgeworth series (10.3.14) in the middle part of this function (at $P(U) > 0.3$) converges so rapidly that the calculations of both the detection characteristics and of the threshold signals are possible (although very laborious) even without using a digital computer.

Thus, the detection probability is calculated by formulas (10.3.18) and (10.5.2). An example of the detection characteristic calculated in this manner is curve 3 in Fig. 10.4.1.

The threshold ratios with independent fluctuations can be calculated by the same method as in the absence of fluctuations. In this case the threshold ratio ρ is calculated as the sum of the first approximation and the correction:

$$\rho = \rho + \Delta\rho, \quad (10.5.3)$$

where at $D = 0.5$

$$\rho_0^2 = \frac{l(1-m)-1}{1-m^N} \quad (10.5.4)$$

and

$$\Delta\rho = 0.167 \frac{1-m^2}{1+m+m^2} \frac{(1+\rho_0^2)^2 (1-m^{3N}) + m^{3N}}{(1+\rho_0^2)^2 (1-m^{2N}) + m^{2N}}, \quad (10.5.5)$$

and at $D = 0.9$

$$\begin{aligned} \rho_0^2 = & \frac{l(1-m)-1 + 1.642 \frac{1-m}{1+m} (1-m^N) +}{\left(1 - 1.642 \frac{1-m}{1+m} \times \right.} \\ & \left. + \left\{ \left[l(1-m)-1 + 1.642 \frac{1-m}{1+m} (1-m^N) \right]^2 - \right. \right. \\ & \left. \left. \times \frac{1+m^N}{1-m^N} \right) \times \right.} \quad (10.5.6) \\ & \left. - \left(1 - 1.642 \frac{1-m}{1+m} \frac{1+m^N}{1-m^N} \right) \left\{ \left[l(1-m)-1 \right]^2 - 1.642 \frac{1-m}{1+m} \right\}^{1/2} \right. \\ & \left. \times (1-m^N) \right. \end{aligned}$$

$$\Delta\rho = - \frac{\sqrt{\frac{1-m}{1+m}} [(1+\rho_0^2)(1-m^{2N}) + m^{2N}]^{1/2} \times}{0.351\rho_0(1-m^N) \times} \times \Delta D \times \left\{ 1 - \frac{1.2814}{\sqrt{\frac{1+m}{1-m}}} \frac{(1+\rho_0^2)(1+m^N)}{[(1+\rho_0^2)(1-m^{2N}) + m^{2N}]^{1/2}} \right\} \quad (10.5.7)$$

$$\begin{aligned} \Delta D &= 0.05634 \frac{(1+m)(1-m^2)^{1/2}}{1+m+m^2} \times \\ &\times \frac{(1+\rho_0^2)(1-m^{3N}) + m^{3N}}{[(1+\rho_0^2)(1-m^{2N}) + m^{2N}]^{3/2}} + 0.07637 \frac{1-m^2}{1+m^2} \times \\ &\times \frac{(1+\rho_0^2)(1-m^{4N}) + m^{4N}}{[(1+\rho_0^2)(1-m^{2N}) + m^{2N}]^2} - 0.03589 \frac{(1+m)^2(1-m^2)}{(1+m+m^2)^2} \times \\ &\times \frac{[(1+\rho_0^2)(1-m^{3N}) + m^{3N}]^2}{[(1+\rho_0^2)(1-m^{2N}) + m^{2N}]^2}. \end{aligned} \quad (10.5.8)$$

The dependence of threshold ratios on N (Fig. 10.5.1*) calculated by these formulas has the same nature as in the absence of fluctuations (Fig. 10.3.3) and with harmonious fluctuations (Fig. 10.4.2). True, unlike the case of harmonious fluctuations, threshold ratios differ by only 20-30% at $D = 0.5$ and $D = 0.9$. This is the result of greater normalization of the distribution of the stored mixture.

The dependence of the storage effect of noise-like signals on the number of pulses (Fig. 10.5.2*) have approximately the same nature as in other, previously considered cases (Figs. 10.3.4 and 10.4.3).

However, there is yet another significant difference included in the higher value of the storage effect in the considered case both at $D = 0.5$ and especially at $D = 0.9$. This is explained by the fact that the distribution of a mixture of independently fluctuating signals and noise varies very strongly from asymmetrical exponential distribution to distribution close to normal as a result of storage. Because of this, the storage effect at $D = 0.5$ as the square of the ratio of the median**distribution is greater than in the absence of fluctuations

361

* See note on p. 310.

** The value corresponding to probability 0.5 is called the median distribution of a random value [176].

and during harmonious fluctuations when the nature of the distribution does not vary as a result of storage.

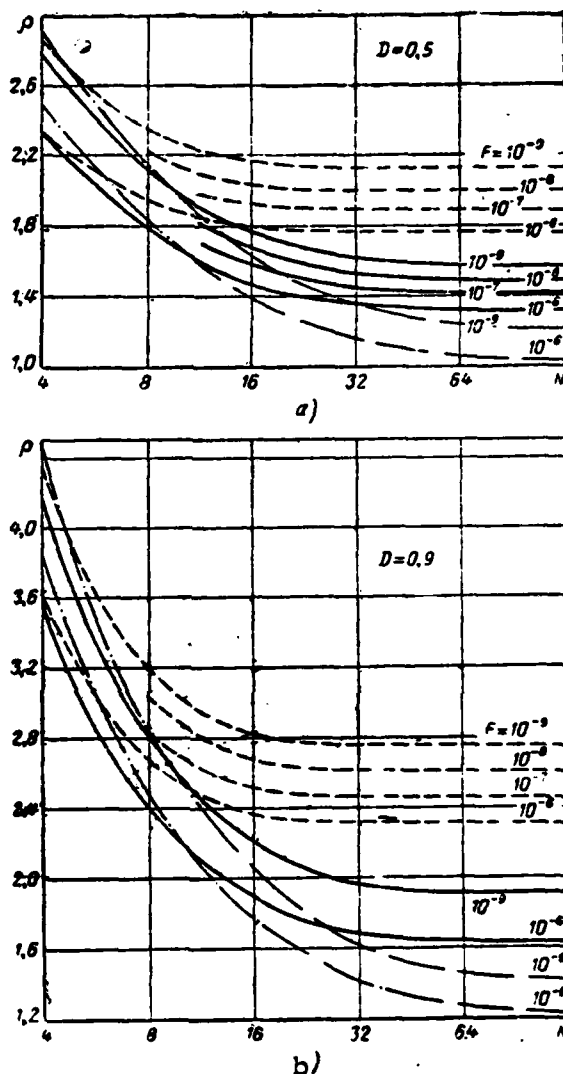


Fig. 10.5.1. Dependence of threshold ratios on number of independently fluctuating signals.

The very great effect of storage at $D = 0.9$ and of independent fluctuations is also explained by significant variation in the nature of distribution of the signal-noise mixture as a result of storage. At $D = 0.9$ the storage effect is equal to the square of the ratio of 90% voltage distribution quantiles of a stored and unstored mixture (90% quantile is a random value which corresponds to 90% probability [176]). Prior to storage, the signal-noise mixture is distributed by exponential law, the square of the 90% quantile of which is greater than the square

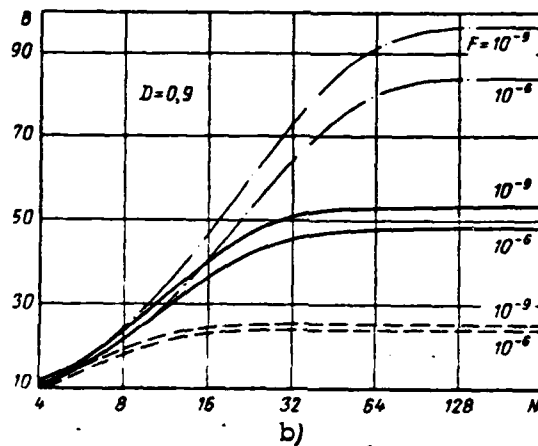
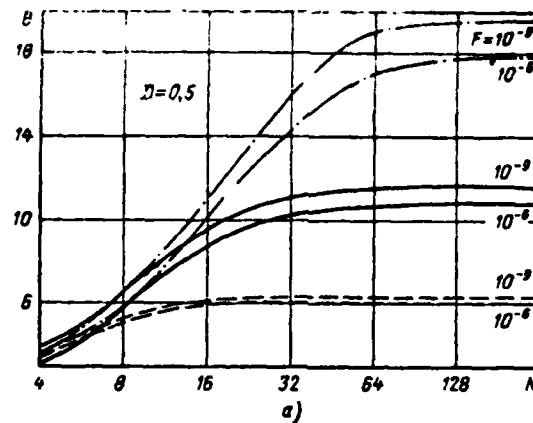


Fig. 10.5.2. Effect of storage of independently fluctuating signals as function of their number.

of the median by a factor of 6.6. After storage, the indicated mixture 361 is distributed by approximately normal law in which the squares of the 90% quantile and median differ by a factor of 1.5. Therefore, the effect of storage at $D = 0.9$ is approximately $(6.6/1.5) = 4.4$ times greater than at $D = 0.5$.

The latter is in good agreement with the calculated values of the storage effect (see Fig. 10.5.2).

Thus, noncoherent storage is especially effective during detection of independently fluctuating pulsed signals with high degree of probability. It permits one to achieve a 25-90-fold gain in receiver sensitivity at $m = 0.8-0.95$.

This is not surprising since the considered system is essentially

an approximation of an optimum detector of independently fluctuating pulsed signals [10-13, 177].

It is also essential to note that the storage effect of independently fluctuating signals with weight multiplier $0.8 \leq m < 1$ may exceed the number of stored pulses by a factor of 1.5-2 (Fig. 10.5.2, b) at $D = 0.9$ (and generally upon detection with high probability). Consequently, a sequence of several pulses separated in time and frequency by those values so that their fluctuations are mutually independent upon reception can be transmitted instead of studying a single pulse of greater energy in the case of its fluctuation during reception. The energy of this sequence can be less by a factor of 1.5-2 than that of a single pulse, while receiver sensitivity will be the same. 362

A similar situation is also observed with ideal (unweighted) storage of independently fluctuating signals [12, 13].

10.6. Some Generalizations

1. Storage of Nonsquare-Law Sequences of Pulsed Signals

Noncoherent exponential weight storage of square-wave sequences of pulsed signals, i.e., those having identical amplitudes, was considered above. However, in some cases (for example, during reception of radar signals in the circular scanning mode), the sequence of pulsed signals has a nonsquare-wave envelope. The method outlined above for calculating the threshold signals may also be applied to this case. The probability of a false alarm does not depend in this case on the shape of the envelope of the sequence and is calculated by formula (10.2.8). The cumulants of the output voltage of the signal-noise mixture in the absence of fluctuations are calculated by the more general formula (10.3.5) rather than by formula (10.3.6), which permits one to take into account the nonsquare-law nature of the envelope of the sequence. The expressions found in this manner for these cumulants are substituted into formula (10.3.18), which permits one to calculate both the detection characteristics and the threshold signals. If the minimum threshold signal in the case of a square-wave sequence always corresponds to the last pulsed signal of the sequence, then the minimum

threshold signal with nonsquare-wave envelope is observed at a different moment of time [121]. The latter can be determined by investigating (10.3.18) for the extreme value.

The threshold signal/noise ratios with quadratic exponential weight storage of sequences of pulsed signals whose envelope has triangular, cosine and square-wave shape (curves 1, 2 and 3, respectively) with identical maximum amplitude are shown as an example [178] in Fig. 10.6.1. 1. Consideration of them shows that variation of the shape of the envelope of the sequence from triangular to cosine and then to square-wave with the same number of pulses leads to a decrease of the threshold ratios. This is explained by an increase of the energy of the pulsed signal sequence.

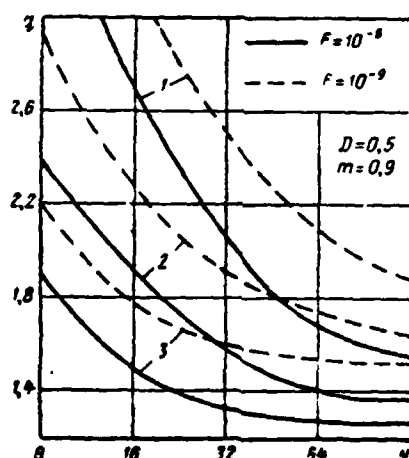


Fig. 10.6.1. Dependence of threshold ratios on N for different sequences.

A real sequence of pulsed signals can be replaced by an equivalent square-wave sequence with amplitude equal to the maximum amplitude of a real sequence when calculating threshold signals. The number of pulses of this equivalent sequence can be calculated by the formulas presented in [178].

2. Noncoherent Double Storage Device

364

To further reduce the threshold signals after a noncoherent single storage device (Fig. 10.1.1, b), one can connect an additional

recirculator. In this case a noncoherent double storage device will be formed (Fig. 10.6.2, a).

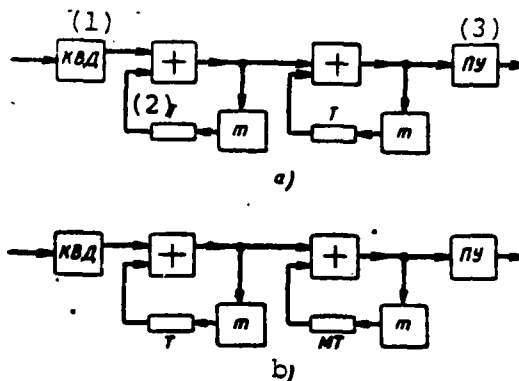


Fig. 10.6.2. Noncoherent double (a) and two-stage (b) storage devices.

Key: (1) Square-law detector; (2) Flip-flop; (3) Threshold device.

Unlike equation (10.1.3), which establishes the relationship between the voltages at the input and output of the first recirculator, the voltage at the output of the second recirculator is

$$u_2(t) = \sum_{k=0}^{\infty} (k+1) m^k u_1(t-kT). \quad (10.6.1)$$

The last expression is easily found by convoluting the input voltage $u_1(t)$ with pulse characteristic of two recirculators

$$h_2(t) = \sum_{k=0}^{\infty} (k+1) m^k \delta(t-kT).$$

Equations (10.1.3) and (10.6.1) shows that the law of double storage differs from the law of single storage by the presence of an additional multiplier $k+1$ with weight multiplier m^k . Therefore, the expression for the probability of a false alarm with quadratic double storage can be found directly from formula (10.2.8), having replaced m^k in it by $(k+1)m^k$, as a result of which

$$F = \sum_{k=0}^{\infty} \exp \left[-\frac{l}{(k+1)m^k} \right] / \prod_{n=0}^{\infty} \left[1 - \frac{(n+1)m^n}{(k+1)m^k} \right]. \quad (10.6.2)$$

This formula, like the results outlined below, was found by M. M. Leshchinskiy [179, 180].

The dependence of the probability of a false alarm on the relative threshold is plotted in Fig. 10.6.3.

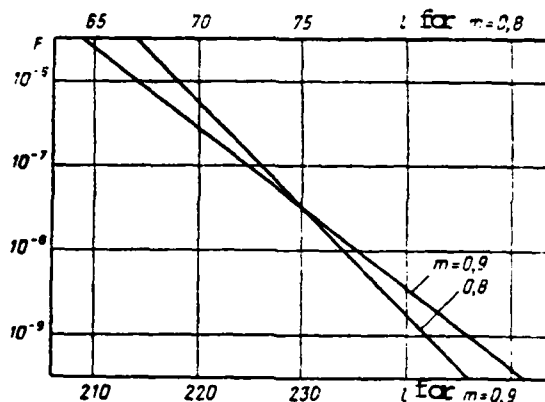


Fig. 10.6.3. Probability of false alarm as function of relative threshold with double storage.

Since the n -order cumulant of output voltage by analogy with (10.3.5) is in the given case

$$\kappa_{n4} = \sum_{k=0}^{\infty} (k+1)^n m^{kn} \chi_{n2}^{(k)}, \quad (10.6.3)$$

then according to (10.3.4), with double storage of a square-wave sequence of N pulsed signals, unlike (10.3.8)

$$\kappa_{n4} = (2\sigma^2)^n (n-1)! \left[\sum_{k=0}^{\infty} (k+1)^n m^{kn} + \frac{nq^2}{2} \sum_{k=0}^{N-1} (k+1)^n m^{kn} \right]. \quad (10.6.4)$$

The threshold signal/noise ratios (Fig. 10.6.4, a and b) and the storage effect (Fig. 10.6.5, a and b) were calculated by formulas (10.3.18) and (10.6.4). Comparison of the curves plotted on these figures and in Figs. 10.3.3 and 10.3.4 indicates that a double storage device with $m = 0.8$ permits one to achieve the same storage effect (gain) both in the noncoherent and coherent case (see section 8.4) as a single storage device with $m = 0.9$, while a double storage device with $m = 0.9$ is equivalent in this sense to a single storage device with $m = 0.95$. The use of a second recirculator in a noncoherent storage device permits one to achieve an additional power gain from 1.4 to 1.8. The value of this gain is somewhat less than with coherent storage. This is explained by the nonlinear nature of the amplitude (square-law) detector.

36

36

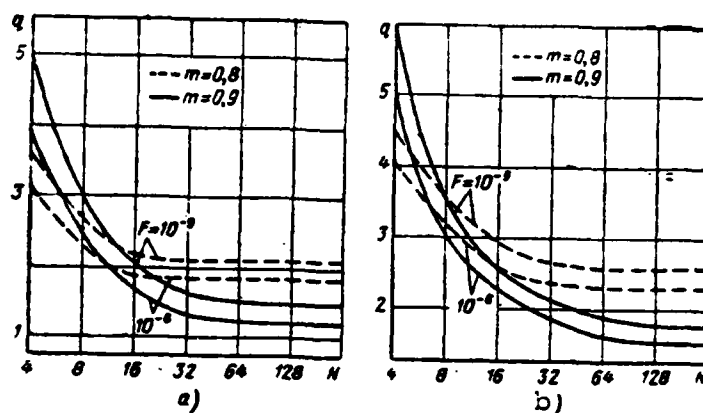


Fig. 10.6.4. Dependence of threshold ratios on N with double storage.

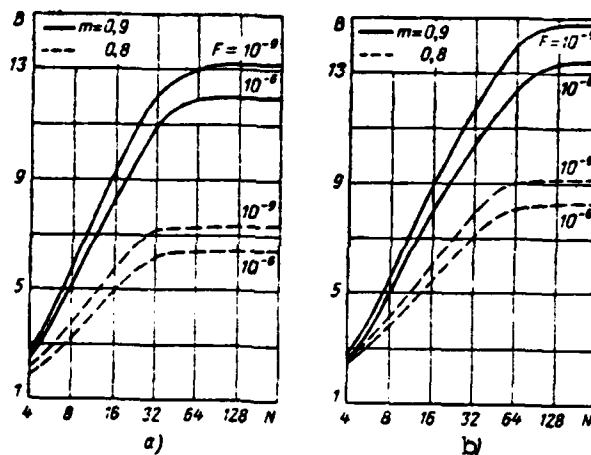


Fig. 10.6.5. Storage effect as function of N with double storage.

3. Noncoherent Two-Stage Storage Device

3

The considered storage device (Fig. 10.6.2, b) differs from a noncoherent double storage device (Fig. 10.6.2, a) only by the fact that the delay time in the feedback circuit of its second recirculator is M times greater than the repetition quasi-period of the pulsed signals.

Since according to (9.1.6) the pulse characteristic of series connection of two idealized recirculators (i.e., with unlimited bandpass of the feedback circuit) with delays by T and MT

$$h(t) = \sum_{k=0}^{\infty} m^k \frac{z^{E(k/M)+1} - 1}{z - 1} \delta(t - kT),$$

where $z = m^{1-M}$, due to which the voltage at the output is

$$u_s(t) = \sum_{k=0}^{\infty} m^k \frac{z^{E(k/M)+1} - 1}{z - 1} u_s(t - kT),$$

then by analogy with noncoherent single and double storage devices [see (10.2.8), (10.6.2), (10.3.8) and (10.6.4)] the probability of a false alarm in the considered storage device is

$$F = \frac{\sum_{k=0}^{\infty} \exp\left[-\frac{I_0^2(z-1)}{m^k [z^{E(k/M)+1} - 1]}\right]}{\prod_{n=0}^{\infty} \left\{1 - \frac{m^n [z^{E(n/M)+1} - 1]}{m^k [z^{E(k/M)+1} - 1]}\right\}}. \quad (10.6.5)$$

and the n -order cumulant of output voltage of a mixture of nonfluctuating signal and noise is 36

$$\begin{aligned} \kappa_{ns} = (2\sigma^2)(n-1)! & \left\{ \sum_{k=0}^{\infty} \left[m^k \frac{z^{E(k/M)+1} - 1}{z - 1} \right]^n + \right. \\ & \left. + \frac{n\sigma^2}{2} \sum_{k=0}^{N-1} \left[m^k \frac{z^{E(k/M)+1} - 1}{z - 1} \right]^n \right\}. \end{aligned} \quad (10.6.6)$$

Using these expressions and formula (10.3.8) by the method outlined above, one can calculate the threshold signals and the storage effect with noncoherent two-stage storage. In this case the results are expected that indicate the possibility of using a noncoherent two-stage storage device to store a rather large number of pulsed signals (on the order of hundreds) with losses slightly exceeding those with ideal (i.e., unweighted) noncoherent storage.

4. Method of Accounting for Final Bandpass of Recirculator With Noncoherent Storage

The different noncoherent storage devices were considered above on the assumption that the feedback circuit of the recirculator has unrestricted wide bandpass. This assumption is valid if this bandpass is much wider than the spectrum of the pulsed signals being stored and

accordingly is wider than the bandpass of the prestorage and predetector filter F_1 that simulates the linear part of the receiver.

The assumption indicated above was made only to simplify the calculations. The problem of threshold signals when using different noncoherent storage devices can also be solved with a final bandpass of the feedback circuit of the recirculators used in them. The method of calculating the threshold signals for the case of noncoherent single storage device is outlined below (Fig. 10.6.6, a).

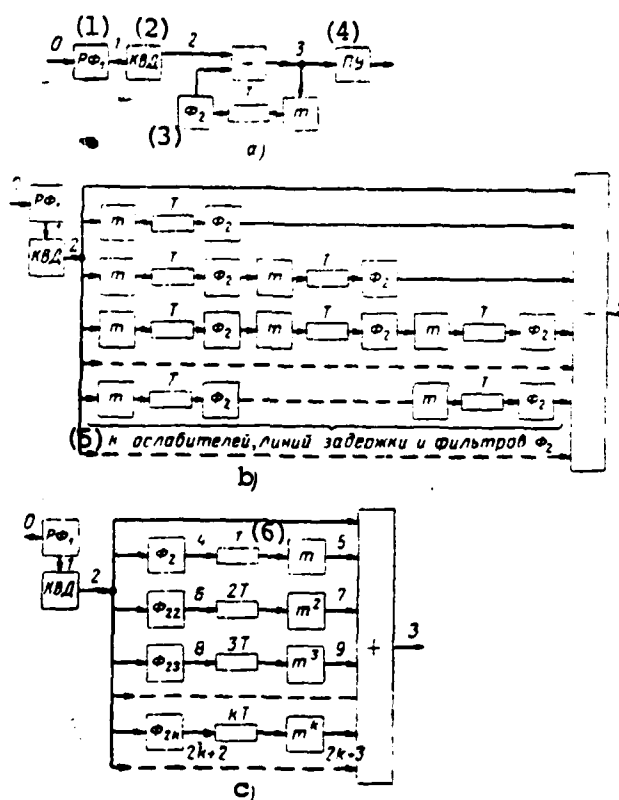


Fig. 10.6.6. Equivalent block-diagrams of noncoherent single storage device.

Key: (1) Radio-frequency filter; (2) Square-law detector; (3) Filter; (4) Threshold device; (5) To attenuators, delay lines and filters F_2 ; (6) Flip-flop

It is easy to ascertain that the block diagram of this storage device can be represented in the form of an equivalent block diagram (Fig. 10.6.6, b) with addition of the output voltages of an infinitely large number of parallel channels. In this case the k -th channel

(where $k = 0-\infty$) consists of series-connection of k attenuators, filters F_2 and delay devices by time T . Obviously the k attenuators with transfer coefficient m are equivalent to a single attenuator with transfer coefficient m^k , the k delay devices by T are equivalent to a single delay device by time kT and the k filters F_2 are equivalent to some filter F_{2k} . Specifically, if filter F_2 has a bell frequency characteristic

37

$$K_s(\omega) = \exp \left[-\ln \frac{1}{d} (\omega/2\pi\Delta F_s)^2 \right],$$

where ΔF_2 is its bandpass at level d , then filter F_{2k} will also have bell frequency characteristic with bandpass $\Delta F_{2k} = k^{-1/2} \cdot \Delta F_2$.

Because of this, the equivalent circuit (Fig. 10.6.6, b) can be represented in the form shown in Fig. 10.6.6, c. In this case the output voltage of the storage device is

$$u_s(t) = u_2(t) + \sum_{k=1}^{\infty} u_{2k+1}(t) = \sum_{k=0}^{\infty} m^k u_2(t - kT).$$

Since these terms are mutually independent due to (7.2.2), the n -order cumulant of output voltage is

$$\kappa_{n_s} = \sum_{k=0}^{\infty} m^{kn} \kappa_n(2k+2),$$

where $\kappa_n(2k+2)$ is the n -order cumulant of voltage at point $(2k+2)$ of the equivalent circuit at moment $t - kT$. This voltage is the output voltage for a typical radio engineering link consisting of a filter F_1 , square-law detector and filter F_{2k} . Any order cumulants of this voltage can be calculated by the method developed by Emerson [181]. The values of these cumulants for the special case, but one important for practice, when filters F_1 and F_2 have bell characteristics, are presented in [20].

The probability of a false alarm, the relative threshold level, detection characteristics and threshold signals can be calculated by the known cumulants of output voltage according to the method outlined in sections 10.2 and 10.3. Unfortunately, these calculations are related to very cumbersome calculations.

PROBLEMS OF PRACTICAL REALIZATION OF ANALOG PULSED SIGNAL STORAGE DEVICES

11.1. CHARACTERISTICS OF DELAY DEVICES USED IN ANALOG STORAGE DEVICES

1. Types of Delay Devices Used

The main component of any analog storage device is the delay device by time on the order of several milliseconds, equal to or a multiple of the repetition period of the pulsed signals of the radio engineering system. For effective storage of these signals, the bandpass of this device, as shown in section 7.4., should be at least double the value inverse to their length. Accordingly, the delay device of a microsecond pulsed signal storage device should have a bandpass on the order of 2 MHz.

Ultrasonic delay lines (UZLZ) are usually employed as delay devices with delay time on the order of several milliseconds and with bandpass on the order of several megahertz. The main advantage is in the long delay time per unit length, which is explained by the comparatively low propagation velocity of ultrasound in the conducting medium (on the order of 1.5-6 m/ms). Both liquid and solid materials are used as the conducting medium. The parameters that characterize the main physical properties of the materials most frequently used as the acoustic line are presented in Table 11.1.1 [154].

A liquid acoustic line usually fills a steel pipe on the ends of which are mounted in a special armature piezoquartz converters of electric to ultrasonic oscillations and ultrasonic to electric oscillations (Fig. 11.1.1, a). The quartz comes into contact with the liquid on both sides. To eliminate multiple reflections from the ends of the tube, the walls are tapered at an angle of 45° . 372

Table 11.1.1

Acoustic Line Material	Velocity, m/ms	Attenuation, dB/m	Temperature Velocity Coefficient at 20°C
Mercury	1.43-1.5	8.3	$-2 \cdot 10^{-4}$
Fused Quartz	3.76	0.68	$5 \cdot 10^{-6} - 2.3 \cdot 10^{-2}$
Glass	4.5-5.6	22.8	$-5.8 \cdot 10^{-5}$
Magnesium Alloys	5.6-5.8	10-20	—
Steel	4.7-6.1	9-44	$4 \cdot 10^{-4}$
Aluminum	5.1-6.4	11.8	$-2 \cdot 10^{-4}$

To reduce overall dimensions, solid delay lines (LZ) are made in the form of notched rods (Fig. 11.1.1, b) or multisided plates (Fig. 11.1.1, c), in which the delayed signals undergo multiple reflections. Quartz transducers are glued to the surface of the rod.

The frequency characteristics of the delay line are determined mainly by the characteristics of the quartz transducers. The latter have sharply marked resonance properties at frequencies determined by the thickness of the quartz plate and having the order of tens of megahertz. Therefore, ultrasonic delay lines usually delay radio pulses whose resonance frequency coincides with that of the quartz transducers. If the video pulses must be delayed by using ultrasonic delay lines, then these pulses are fed to a balanced modulator BM for modulation of the oscillation being fed from the carrier frequency generator G (on the order of 15-20 MHz) and the radio pulses formed in this manner are fed to the ultrasonic delay line, where they are delayed by the necessary time and are then amplified (to compensate for attenuation during passage through the ultrasonic delay line) and are detected by a synchronous detector SD (Fig. 11.1.2).

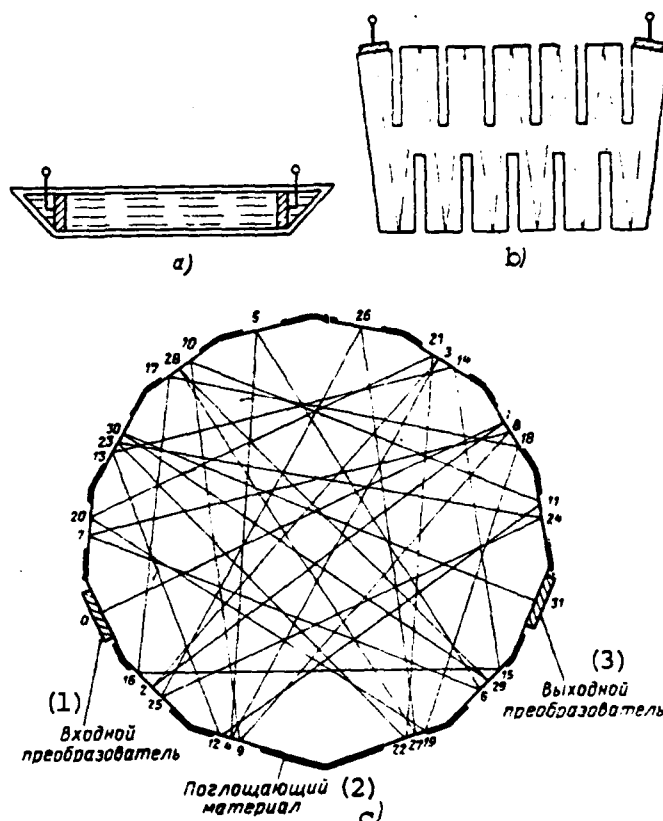


Fig.11.1.1. Ultrasonic delay lines.

Key: (1) Input transducer; (2) Absorbing material;
(3) Output transducer.

Signal attenuation in the ultrasonic delay line comprises a value 372
on the order of 50-70 dB, of which approximately 35-40 dB are losses
in the transducers. If barium titanate ceramics are used instead of a 373
crystalline piezoquartz plate as the transducers, these losses are re-
duced to 10 dB. However, the bandpass is reduced somewhat in this
case [154].

To eliminate the dependence of the delay time on the ambient tem-
perature, the delay line is placed in a thermostat, usually a multi-
layered one, which permits the temperature to be held in the range of
 $\pm 0.01^\circ\text{C}$ with variation of ambient temperature by $\pm 50^\circ\text{C}$ [68]. In or- 374
der that the delay of the pulsed signal in the line be sufficiently
accurately equal to the repetition period of the pulsed system T , this
system is started from a synchronizer with the same delay line [154-155].
Both delay lines are placed alongside each other in the same thermostat.

In this case equality of the delay line and repetition period can be achieved with accuracy on the order of a thousandth of a percent.

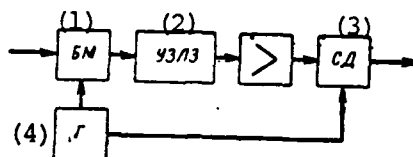


Fig. 11.1.2. Block diagram of delay device.
Key: (1) Balanced modulator; (2) Ultrasonic delay line; (3) Synchronous detector; (4) High-frequency generator.

Despite a number of advantages of mercury ultrasonic delay lines (low level of various reflections, low attenuation and so on), they have not been used recently due to the inconvenience of operating them (mercury is toxic, requires periodic purification, is sensitive to vibrations and so on). Therefore, magnesium and quartz ultrasonic delay lines are most frequently employed. They are comparatively inexpensive, simple to manufacture, small in dimensions, tolerate strong vibrations and impacts well and do not require serious maintenance.

As an example, let us present the parameters of a fused quartz ultrasonic delay line: delay time is 1 ms, resonance frequency is 15 MHz, bandpass (at level $1/\sqrt{2}$) is 6 MHz, attenuation is 45 dB, dynamic range (signal level with respect to level of all spurious reflections) is 40 dB, the "three-cycle echo" level is 50 dB, weight is 500 grams, volume is 410 cm^3 , operating temperature is -55 to $+100^\circ\text{C}$ and the temperature velocity coefficient is 10^{-4} . It has the shape of a pentadecahedron (Fig. 11.1.1, c) and the signals in it are reflected 30 times from different edges of the plate.

A magnesium ultrasonic delay line, the technique of manufacture of which is simpler, has somewhat worse parameters (attenuation up to 50-70 dB and so on) and therefore the cost is lower.

Pulses can also be delayed by magnetic recording of them and subsequent reading at the necessary moment of time [117, 182] and also by recording on cathode-ray tubes with charge storage (storage tubes) and

reading the recorded charge pattern. These problems are outlined in detail in [182-185] and others.

The signal delay (storage) time in these devices is equal to the time interval between the moments of writing and reading and can be made as long as desired. This also includes the main advantage of these delay devices.

However, magnetic recording on tape, drum or disk is integrated with mechanical movement of the magnetic carrier with respect to the recording and reading heads. The speed of this movement should be maintained with very high accuracy, which is difficult in practice. Creation of electron beam scanning voltages that provide rather precise recording of signals to the corresponding spot of the cathode-ray tube screen and subsequent reading of the "tracks" of these signals also causes great difficulties.

Moreover, specific distortions occur when recording to magnetic material and to the screen of a cathode-ray tube with charge storage—extension of the recorded pulse in length [186], clogging (seeding) adjacent sections of the screen by secondary electrons [182, 186, 187] and so on. In this case the resolution of the pulse systems deteriorates and the noise level increases.

These features should also be taken into account when solving the problem of the feasibility of using magnetic and cathode-ray delay devices in optimum filters and pulse signal storage devices.

Despite the noted disadvantages, cathode-ray tubes with charge storage (storage tubes) are used both in pulsed signal storage devices and especially in moving target selection systems.

Nevertheless, the best qualitative indicators of these systems provide delay devices in the form of ultrasonic delay lines.

2. Spurious Reflections in Ultrasonic Delay Lines

376

The greatest difficulties in realization of analog storage devices are caused by the presence of spurious reflections or false signals, which are caused by passage of the signal being delayed over paths different from the main (calculated) path. Therefore, when feeding a rather short pulse to the input of a real ultrasonic delay line, several tens of false pulses with different amplitudes and delays appear at its output in addition to the pulse delayed by the required time T . As an example, the results of measurements for one of the real ultrasonic quartz delay lines are shown in Table 11.1.2 [152]. The pulse delayed by 669 μ s is the useful signal, while the remaining pulses are spurious reflections. The strongest of them is the so-called "trircular echo," having a delay three times greater than that of the main signal and attenuation of 55 dB. It is caused by double reflection from the output and input transducers of the delay line. All the other spurious reflections have greater attenuation—from 66 to 80 dB—and lower delay, beginning at 48 μ s. The sum of all the spurious signals is 45 dB less than the signal. The parameters of these spurious reflections usually have an irregular nature [152, 188]. Therefore, it is feasible to estimate these parameters statistically. The mean-square value of the amplitude of spurious reflections of this ultrasonic delay line comprises -53 dB compared to the main signal.

Table 11.1.2

Delay Time, μ s	48	141	143	176	237	331	376	425	473	525	570	572	661
Attenuation, dB	70	80	80	72	74	80	75	78	66	78	78	76	74
Delay Time, μ s	669	673	676	763	765	859	860	954	—	—	—	—	2007
Attenuation, dB	0	71	74	74	77	74	71	69	68	72	77	78	55

Due to their random nature, spurious reflections, being added to internal and external noise, make it difficult to separate the signal. However, their harmful effect is not limited to this. It is shown below how spurious reflections limit the upper bound of the stable feedback coefficient of a storage device (recirculator), thus reducing its efficiency, and sharply reducing its dynamic range.

Therefore, a reduction of the level and number of spurious reflections is one of the main problems solved in design of ultrasonic delay lines.

To reduce the amplitude of spurious reflections, corrugation of the side walls of the acoustic line and painting of the walls are employed to create an absorbing layer. To eliminate spurious reflections by eliminating the corresponding side paths of ultrasonic wave propagation, special notches or kerfs are made in the acoustic line (Fig. 11.1.1, b). The spurious signals, which are the sum of several signals reflected twice from different pairs of opposite surfaces, can be attenuated by partial compensation of their components, achieved by alternate shifting of the reflecting surfaces by a value equal to one-fourth the wavelength. Spurious reflections with multiple delays are attenuated by special cylindrical holes drilled in the acoustic line perpendicular to the direction of wave propagation and having a diameter on the order of several wavelengths. These methods are outlined in detail in [188]. Other useful recommendations to reduce spurious reflections are presented in survey [68].

11.2. Elimination of Self-Excitation of Analog Storage Device

1. Stability of Storage Device With Regard to Spurious Reflections

The spurious reflections in the ultrasonic delay line of a storage device can cause self-excitation of it. Therefore, let us consider the condition of stability of a storage device with the presence of auxiliary channels that cause spurious reflections in the ultrasonic delay line. This storage device (Fig. 11.2.1) is essentially a feedback amplifier and its stability can be judged by using the Niquist criterion [28]: if the end of the vector of the complex feedback coefficient $\bar{K}(\omega)$ of the amplifier (storage device), describing a closed curve on a complex plane, does not encompass the point $(+1, 0)$ upon variation of frequency ω from 0 to ∞ , then this device is stable. 378

Let us first consider the case of multiple spurious reflections in which $T_k = kT$, where k is an integer. The complex feedback coefficient is then

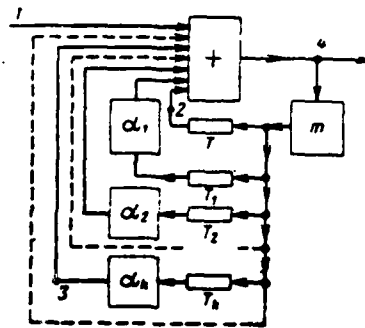


Fig. 11.2.1. Block diagram of integrating device with regard to auxiliary delay channels.

$$K(\omega) = m \left(e^{j\omega T} + \sum_{k=1}^n \alpha_k e^{j\omega k T} \right), \quad (11.2.1)$$

where α_k is the additional attenuation coefficient of the k -th spurious reflection. Since usually $\sum_{k=1}^n \alpha_k \ll 1$, the first vector that describes the feedback coefficient of the main channel plays the main role in (11.2.1). It describes a circle of radius m upon variation of frequency. This vector is directed horizontally toward point $(1, 0)$ at frequencies $\omega = l\Omega = l \frac{2\pi}{T}$ that are a multiple of repetition rate. All the vectors that characterize the feedback coefficients of the auxiliary channels on these 37 frequencies will have the same direction (Fig. 11.2.2, a). Therefore, the total feedback coefficient is equal to the arithmetic sum of the feedback coefficients of individual channels:

$$K_l(l\Omega) = m \left(1 + \sum_{k=1}^n \alpha_k \right).$$

while the end of the total vector will lie to the left of point $(1, 0)$ only provided that

$$m \left(1 + \sum_{k=1}^n \alpha_k \right) < 1. \quad (11.2.2)$$

This is a necessary and sufficient condition of storage device stability in the case of multiple spurious reflections.

Let us show that this condition is also valid in the case of non-multiple spurious reflections, when

$$\bar{K}(\omega) = m \left(e^{j\omega T} + \sum_{k=1}^n a_k e^{j\omega T_k} \right), \quad (11.2.3)$$

where T_k is a nonmultiple of T and usually $0 < T < 3T$.

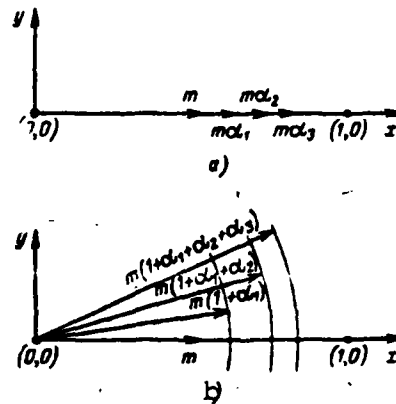


Fig. 11.2.2. Vector diagrams for feedback coefficients of storage devices.

And the first vector r plays the main role in this vector sum in the given case. It is directed horizontally at frequencies $l\Omega$ that are a multiple of the repetition rate. In this case the vector of the feedback coefficient of the k -th auxiliary channel will be directed at an angle $l\Omega T_k$. Since the bandpass of the storage device is approximately 1,000 times greater than the repetition rate, then l can assume any whole value up to 1,000. Since T_k essentially lies in the range $0.3T$, then the angle of rotation of the k -th vector can assume any value in practice in the range (0.2π) .

Obviously, the end of the sum of two vectors having length m and $m\alpha_1$ and arbitrary phases always lies within a circle with radius $m(1 + \alpha_1)$; the end of the sum of three vectors m , $m\alpha_1$ and $m\alpha_2$ long and with arbitrary phases lies within a circle of radius $m(1 + \alpha_1 + \alpha_2)$ and so on (Fig. 11.2.2, b). Therefore, the end of the total vector (11.2.3) always lies within a circle of radius $m \left(1 + \sum_{k=1}^n \alpha_k \right)$.

This circle will not encompass the point $(1, 0)$ only if its radius is less than 1, i.e., if condition (11.2.2) is fulfilled.

Accordingly, it is necessary and sufficient that the feedback circuit of the main channel satisfy the following condition for stability

$$m < 1 / \left(1 + \sum_{k=1}^n a_k \right). \quad (11.2.4)$$

Thus, the presence of spurious reflections limits the upper value of the feedback coefficient of the storage device and thus the gain provided by the storage device during storage of a sufficiently large number of pulsed signals. Actually, it follows from (11.2.4) that the maximum stable feedback coefficient (through the main channel) is

$$m_{\text{max}} = \frac{1 - \epsilon}{1 + \sum_{k=1}^n a_k}$$

and at

$$\sum_{k=1}^n a_k < 1$$

$$m_{\text{max}} \approx 1 - \epsilon - \sum_{k=1}^n a_k,$$

38

where ϵ is a sufficiently small positive value selected from the condition of maintaining stability with instability of the storage device parameters (for example, $\epsilon = 0.01$).

Then according to (5.4.7) with sufficiently large number of stored pulses when $m_{\text{max}}^N \ll 1$, the maximum possible gain of a coherent storage device is

$$B_{\text{max}} \approx \frac{1 + m_{\text{max}}}{1 - m_{\text{max}}} = \frac{2(1 - \epsilon)}{\sum_{k=1}^n a_k + \epsilon} + 1. \quad (11.2.5)$$

Specifically, if the levels of all spurious reflections are identical, i.e., $a_k = a$ for $k = 0-n$, then

$$B_{\text{max}} \approx \frac{2(1 - \epsilon)}{na + \epsilon} + 1.$$

Having assumed, for example, that $\epsilon = 0.01$, we find B_{max} equal to 8.93, 20.8 and 100, respectively, at $a = 0.01$ and $n = 24$, $a = 0.01$ and $n = 9$ and $a = 0.001$ and $n = 10$.

Thus, spurious reflections sharply reduce the efficiency (gain) of the storage device. This reduction is greater, the greater the number and the higher the relative level.

Therefore, to ensure high efficiency of an analog storage device, it can be made on the basis of an ultrasonic delay line in which the minimum values are the number and especially the level of spurious reflections. Unfortunately, the ultrasonic delay lines manufactured at present have comparatively high level of spurious reflections that reach values on the order of 0.03-0.1 in some cases. In this regard the problem of designing efficient analog storage devices based on ultrasonic delay lines with comparatively large spurious reflections is very important. This problem is similar to a known degree to that of designing a highly reliable system of insufficiently reliable components. Some methods of solving the indicated problem are considered below in section 11.5.

38:

2. Eliminating Self-Excitation of Storage Device Due to Instability of Its Components

The instability of the transfer coefficients of the storage device components can disrupt its normal operation and lead to self-excitation. Even a slight increase of the amplification factor of one of the amplifiers that compensate for signal attenuation in an ultrasonic delay line can disrupt the condition of stability (11.2.4) and cause self-excitation. A decrease of the transfer coefficient of one of the components of the storage device may lead to a sharp decrease of gain, i.e., to a reduction of its efficiency. Thus, for example, if this decreases causes variation of m from 0.95 to 0.9, i.e., by only 5.8 percent, the maximum gain decreases from 39 to 19, i.e., more than one-half.

To eliminate the possibility of both self-excitation and a decrease of the efficiency of the storage device, automatic regulation of its feedback coefficient is employed. One of the possible block diagrams of a storage device with this regulation is shown in Fig. 11.2.3 [139, 189]. Its operation is based on comparison of amplitude V_1 of the un-stored auxiliary video pulse to the amplitude of the stored pulse V_2 attenuated $(1 - m_0)$ times, where m_0 is the calculated value of the

feedback coefficient of the storage device. These amplitudes are identical during normal operation. Deviation of m from the calculated value changes the value of the stored signal, due to which the equality of amplitudes is disrupted. In this case a voltage which is integrated and used to control the value of the coefficient of the intermediate-frequency amplifier is generated at the output of the subtraction device. The time constant of this regulation is on the order of $10T$.

38.

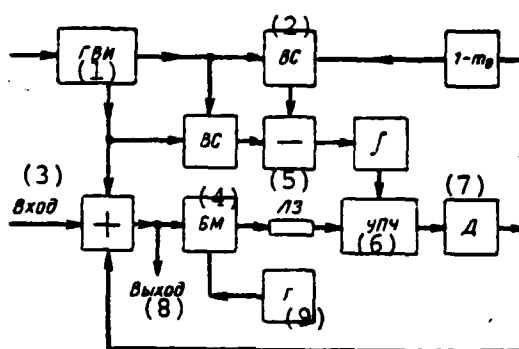


Fig. 11.2.3. Block diagram of storage device with automatic regulation of feedback coefficient.

Key: (1) Auxiliary video pulse generator; (2) Time selector; (3) Input; (4) Balanced modulator; (5) Delay line; (6) Intermediate-frequency amplifier; (7) Detector; (8) Output; (9) High-frequency generator.

The control circuit operates in a specially allocated time channel frequency of the effect of useful signals and is connected to the main circuit by two time selectors (VS) which are controlled by the auxiliary video pulse generator (GVI) started from the synchronizer. If a special time channel cannot be allocated to regulate the feedback coefficient of the storage device, then a special frequency channel is allocated for this purpose.

11.3. Effect of Multiple Spurious Reflections on Efficiency of Storage Device

Let us ascertain that multiple spurious reflections (i.e., those with delays $T_k = kT$, where k is an integer) contribute to signal storage through the main channel by increasing the equivalent feedback coefficient, the value of the stored signal and thus the gain provided by the storage device.

This is obvious for synchronous spurious reflection, which has delay T . In this case the combination of the main and auxiliary channels with identical delays and feedback coefficients and m and ma (Fig. 11.2.1) is equivalent to a single channel with the same delay and coefficient $m_3 = m(1 + a)$. The gain in the signal/noise ratio provided by the storage device increases if a sufficiently large number of pulsed signals is stored due to an increase of the equivalent feedback coefficient (if of course its value is less than 1 and there is no self-excitation).

384

Since the strongest spurious reflection is a tricircular echo, let us consider storage of the signal in a storage device containing one auxiliary channel with delay $T_k = 3T$ and attenuation a in addition to the main channel (Fig. 11.2.1). Let a sequence of N pulsed signals act on the input of the storage device, beginning at moment $t = 0$, and having repetition quasi-period T and pulse amplitude V_1 (Fig. 5.3.1, a). Let us assume that the useful signals are added to the multiple spurious reflections in phase, i.e., the useful signals and spurious reflections are coherent. It is easy to show by the induction method that the voltage at the output at moment $t = nT$, where $n \leq N - 1$, comprises

$$u_s(nT) = V_1 \sum_{l=0}^{E(n/3)} (ma)^l \sum_{k=1}^{n-2l} C_k^l m^{k-l},$$

where C_k^1 is the number of combinations of k components with respect to 1.

This expression can be converted to the following form:

$$\begin{aligned} \frac{u_s(nT)}{V_1} = & \sum_{k=0}^n [m(1+a)]^k - m^{n+1} \sum_{k=1}^{E(n/3)} \left(\frac{a}{m}\right)^k \sum_{l=1}^{2k-1} C_{n-m+1+l}^k - \\ & - (ma)^{E(n/3)+1} \sum_{k=E(n/3)+1}^n (ma)^{k-E(n/3)-1} \sum_{l=k}^n C_l^k m^{l-k}. \end{aligned}$$

If n is sufficiently large, the first term is considerably greater than the sum of the remaining terms and

$$u_s(nT) \approx V_1 \sum_{k=1}^n [m(1+a)]^k.$$

Accordingly, the signal is stored in the considered storage device by approximately the same law as in a storage device in which there is only one main channel with feedback coefficient $m_3 = m(1 + a)$.

Thus, multiple spurious reflections do not create false signals and contribute to storage of the useful signal. Therefore, their level can be permitted considerably higher than that of nonmultiple spurious reflections, which worsen the operation of the storage device by reducing its dynamic range (see section 11.4 below). However, the level of multiple spurious reflections should be taken into account when solving the problem of the value of the stable feedback coefficient through the main channel.

Due to the fact that auxiliary channels usually have irregular nature, due to which the coherence of useful signals and spurious reflections may be disrupted, a small total level of multiple spurious reflections is also desirable.

11.4. Effect of Nonmultiple Spurious Reflections on Dynamic Range of Storage Device

The dynamic range of a storage device is characterized by the ratio of the useful signal amplitude at its output to the amplitude of the greatest spurious reflection (expressed in decibels) (or to the total amplitude of all spurious reflections or to the mean square value of the amplitude of spurious reflections).

The dynamic range of the storage device is considerably below that of the ultrasonic delay line used in it. This is explained by the fact that the useful signals are stored in the storage device a considerably lesser number of times than the spurious reflections [152, 190].

To ascertain the validity of this conclusion, strange at first glance, let us consider a simplified circuit of a real storage device with main and one auxiliary channel with delays by T and T_k (where T_k is not a multiple of T) and with attenuation m and m_k (Fig. 11.2.1). As usual, $\alpha \ll 1$.

Let a sequence of N pulsed signals with amplitude V_1 and repetition quasi-period T be stored (Fig. 5.3.1, a). Then according to (5.4.1), the signal output voltage is

$$V_i(kT) = V_1 \frac{1-m^{k+1}}{1-m} \quad \text{at } 0 < k < N-1. \quad (11.4.1)$$

The spurious reflections are stored by a more complicated law. Let us take into account only those spurious reflections which were formed as a result of single passage through the auxiliary channel. The spurious reflections that passed two or more times through the auxiliary channel have considerably lower amplitude and they can be disregarded in the first approximation.

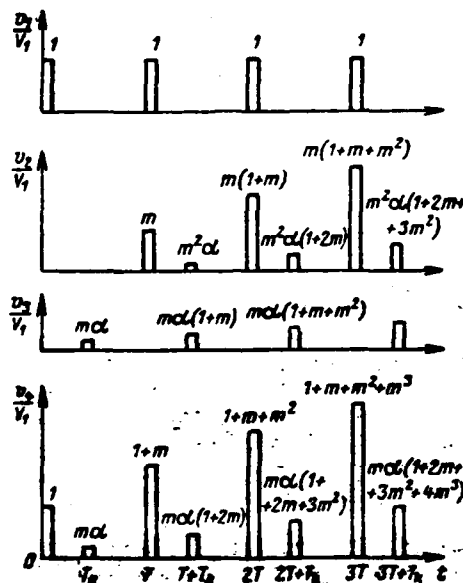


Fig. 11.4.1. Time diagrams of voltages in storage device.

The first impulse of the input channel (Fig. 11.4.1), passing through the adder, auxiliary channel and again through the adder, causes a spurious reflection $V_4(T_k) = m\alpha V_1$ at the output. A signal $V_4(T) = V_1(1+m)$, which causes a spurious reflection $V_3(T+T_k) = m\alpha V_1(1+m)$ at the output of the auxiliary channel and which is stored through the main channel, is fed to the auxiliary channel during the second repetition period. The spurious reflection coincides in time with the pulse at the output of the main channel caused by spurious reflection $V_4(T_k) = m\alpha V_1$ being fed to its input and having amplitude $V_2(T_k+T) = mV_1(T_k) = m^2\alpha V_1$. Obviously, $V_4(T+T_k) = V_2(T+T_k) + V_2(T_k+T) = m\alpha V_1(1+2m)$. In like fashion, $V_4(2T+T_k) = m\alpha V_1(1+2m+3m^2)$, and generally

$$V_1(nT + T_k) = maV_1[1 + 2m + \dots + (n+1)m^n] = \\ = ma \left[\frac{1-m^{n+1}}{(1-m)^2} - \frac{(n+1)m^{n+1}}{1+m} \right] V_1 \text{ at } 0 \leq n \leq N-1.$$

The peak value of the stored spurious reflections comprises

$$V_{so} = V_1[(N-1)T + T_k] = maV_1 \left[\frac{1-m^N}{(1-m)^2} - \frac{Nm^N}{1-m} \right]. \quad (11.4.2)$$

Accordingly, the ratio of the peak values of the useful signal and spurious reflections at the output of the storage device comprises

$$\mu = \frac{V_c}{V_{so}} = \frac{1-m}{ma} \frac{1-m^N}{1-m^N - N(1-m)m^N}. \quad (11.4.3)$$

Specifically, with a sufficiently large number of pulses when condition (5.4.19) is fulfilled,

$$\mu = \frac{1-m}{ma}. \quad (11.4.4)$$

Thus, the dynamic range of the storage device in decibels is

$$D_s = 20 \lg \mu = D_a - 20 \lg \frac{m}{1-m}, \quad (11.4.5)$$

where $D_a = 20 \lg \frac{1}{a}$ is the dynamic range of the ultrasonic delay line, while a decrease of the dynamic range due to storage of spurious reflections is

$$\Delta D = D_a - D_s = 20 \lg \frac{m}{1-m}. \quad (11.4.6)$$

This value comprises 12, 15, 19.1 and 25.6 dB, respectively, at $m = 0.8$, 0.85, 0.9 and 0.95.

Accordingly, the dynamic range of the storage device deteriorates more strongly, the greater its feedback coefficient, i.e., the higher its efficiency.

Thus, for example, if the dynamic range of the ultrasonic delay line is 55 dB, then the dynamic range of a storage device with $m = 0.9$ and 0.95 comprises 35.9 and 29.4 dB, respectively.

388

Some methods of reducing the harmful effect of spurious reflections are considered below.

11.5. Methods of Reducing Effect of Spurious Reflections

1. Periodic Variation of Signal Polarity During Different Repetition Periods

To reduce the effect of spurious reflections on the operation of a storage device, one can use periodic variation of signal polarity at the input and in the feedback circuit by means of balanced amplifiers BU (Fig. 11.5.1, a). Signal polarity at different repetition periods can be varied by different laws.

Specifically, double variation of polarity during three repetition periods yields good results (Fig. 11.5.1, b). In this case there is partial compensation for spurious reflections whose delay time differs considerably from that of the useful signal. Thus, when pulsed signals that delay the repetition period by time t_1 with respect to the beginning are stored, all spurious reflections whose delay time is not within the range $(T - t_1, 2T - t_1)$ are partially compensated.

As an example, let us take $t_1 = 0.5T$ and the delay time of the spurious reflection as $T_k = 1.75 T$. Two spurious reflections then coincide in time during the fourth repetition period at moment $t = 3.25T$. One of them is caused by the useful signal that has arrived during the first period and that has initially passed through the auxiliary channel and then the main channel of the delay line, while the second is determined by passage of the useful signal through the auxiliary channel during the first two periods. The amplitudes of these reflections are equal to $V_1 m \alpha$ and $V_1 (1 + m) \alpha$, respectively, while the polarities are opposite, due to which their sum has amplitude $V_1 m \alpha$. If there is variation of polarity, the spurious reflections have identical polarity and are added arithmetically, due to which the amplitude of their sum is $V_1 m \alpha (1 + 2m)$, i.e., $(1 + 2m)$ times greater.

It is recommended in [189] that variation of polarity (phase manipulation) be used by the law shown in Fig. 11.5.1, c to attenuate the tricircular echo. 389

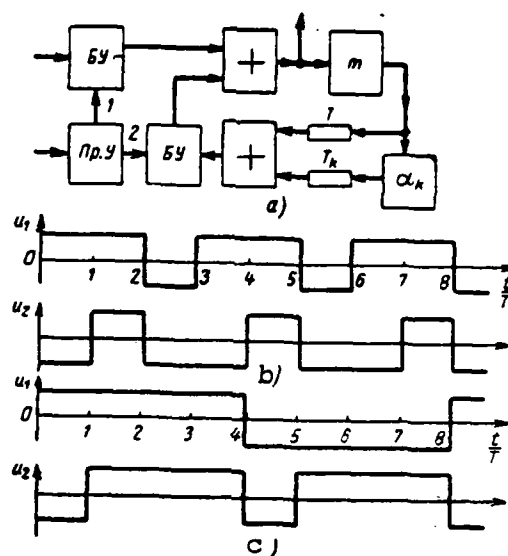


Fig. 11.5.1. Block diagram of storage device with variation of signal polarity and time diagrams of voltages in it.

Let us note that the methods described above for suppression and attenuation of part of the spurious reflections are based on time selection and therefore are effective only if the delay time of the spurious reflections differs considerably (by an average of the repetition half-period) from the delay time of the useful signal.

2. Use of Frequency-Modulated Storage Device

Spurious reflections in a storage device with amplitude modulation, which worsens the dynamic range of the storage device, are stored to a considerably less degree if amplitude modulation is replaced by frequency modulation. The blocks diagrams of two frequency-modulated storage devices are shown in Fig. 11.5.2, a and b.

390

The feedback circuit in the first storage device consists of a reactance tube, FM generator (ChMG), limiting amplifier (UO), delay line and FM discriminator (ChD). The advantages of this storage device are the capability of achieving feedback coefficients as close to one as desired and considerably lower instability of the amplification factors of the intermediate-frequency amplifier and other amplitude parameters and also instability of the feed voltages.

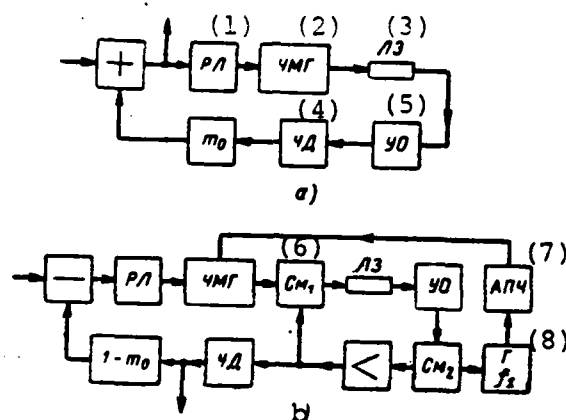


Fig. 11.5.2. Block diagram of frequency-modulated storage device.

Key: (1) Reactance tube; (2) FM generator; (3) Delay line; (4) FM discriminator; (5) Limiting amplifier; (6) Mixer; (7) Intermediate-frequency analyzer; (8) Frequency generator.

The pulses stored in this storage device are added on the video frequency. Therefore, its operation essentially does not differ from that of an AM storage device. The only difference is that the information on the arrival of a pulse to the input of the storage device and on its value is recorded in its frequency rather than in the amplitude of the oscillation delayed by the line.

There is direct addition of the frequency deviations caused by the pulsed signals to be stored in the second storage device (Fig. 11.5.2, b). Actually, if the first pulse is fed to the input of the storage device, the frequency of the FM generator varies from f_1 to $f_1 + \Delta F$, immediately changing the frequency of the output oscillation of the mixer Sm_1 from $f_2 = f_3 - f_1$ to $f_2 - \Delta F$ and after delay by T in the delay line, it changes the frequency of the output oscillation of mixer Sm_2 from $f_3 = f_1 + f_2$ to $f_3 - \Delta F$. After the pulse at the input ends, the frequency of the FM heterodyne returns to a value of f_1 . During the second period the pulsed signal, which delays with respect to the first by T , again changes the frequency of the FM generator by $f_1 + \Delta F$. In time it coincides with the frequency pulse $f_3 - \Delta F$ being fed to the second input of the first mixer. As a result a frequency pulse $f_3 - 2\Delta F$ and so on is formed at its output. Accordingly, the frequency deviations caused by the pulsed signals with weight equal to 1 are stored, i.e.,

the feedback coefficient of this (internal) storage device is equal to 1. Negative feedback with low coefficient $\beta = 1 - m_0$ is introduced between the output and input of the storage device to reduce the weight coefficient of storage to the desired value m_0 .

Thus, the considered FM storage device stores pulsed signals with optimum weight coefficient m_0 .

An important advantage of this layout of the storage device is the capability of reducing the effect of spurious reflections to the dynamic band of the storage device. This is explained in the following manner.

When the carrier frequency of the oscillations delayed in the delay line is constant, the spurious reflections that have passed through the main channel of the delay line will be in phase with the useful signals that have passed through the auxiliary channel and that have achieved the nature of spurious reflections due to this. Being in phase, they are added arithmetically as in an AM storage device, considerably reducing the dynamic range of the storage device.

However, the carrier frequency fluctuates due to natural fluctuations (for example, caused by hum in the reactance tube). This leads to addition of the spurious reflections in random phases, i.e., by power rather than by amplitude. Therefore, unlike an AM storage device and unlike the case when cophasal (coherent) addition of spurious reflections occurs in an FM storage device with noncoherent addition of them in an FM storage device, as Urkowitz pointed out [152], the dynamic range of the storage device is

39

$$D_s = D_a - 10 \lg \frac{m^2}{1-m^2} - 2. \quad (11.5.1)$$

It follows from (11.4.5) and (11.5.1) that the dynamic range is deteriorated less by the following value in an FM storage device due to noncoherent addition of spurious reflections than in an AM storage device

$$\delta D_s = 10 \lg \frac{1+m}{1-m} - 2. \quad (11.5.2)$$

This value comprises 7.5, 9, 10.8, 13.9 and 18 dB, respectively, at $m = 0.8, 0.85, 0.9, 0.95$ and 0.98 .

A specially run experiment showed [152] that the dynamic range of an FM storage device based on a delay line with dynamic range $D_n = 54$ dB and having $m = 0.98$, is equal to 21.5 dB with cophasal addition of spurious reflections and 38 dB with noncoherent addition of them, caused by the hum of the reactance tube. Thus, both the capability of a significant reduction of the effect of spurious reflections on deterioration of the dynamic range of an FM storage device and relations (11.4.5) and (11.5.1) that characterize this effect were confirmed experimentally.

Increased attention is now being devoted to development of this FM storage device due to its advantages.

3. Use of Phase-Modulated Storage Device

Information on pulsed signals and the accompanying noise being fed to the input of a storage device can be written not only in the form of the amplitude of radio pulses delayed in the delay lines or the frequency of the oscillation circulating through the feedback loop of the storage device, but in its phase as well. A phase-modulated generator (FMG), which changes the phase of the output oscillation by a value proportional to the instantaneous value of the input pulse voltage, is used for this purpose in the storage device (Fig. 11.5.3). Since the oscillation amplitude carries no information whatever about the input voltage, the oscillation can be subjected to amplitude restriction that eliminates the effect of instability of amplitude characteristics. Therefore, very low requirements are placed on the stability of these characteristics.

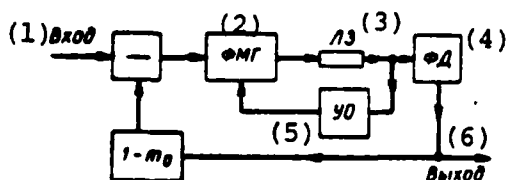


Fig. 11.5.3. Block diagram of phase-modulated storage device.
Key: (1) Input; (2) Phase-modulated generator; (3) Delay line; (4) Phase detector; (5) Limiting amplifier; (6) Output.

Phase shifts of the circulating oscillation caused by pulses located at different repetition periods with time shift by a value that is a multiple of T are added in a phase modulator. The latter is a phase-shift adder because of this.

Output voltage is taken from the load of the phase detector (FD) controlled by a special reference generator. As in the case of a frequency modulated storage device, negative feedback with coefficient $1 - m_0$ is introduced between the output and input of the storage device so that signals are stored with the desired weight coefficient m_0 .

A superregenerator can be used as the amplifier. Very simple in circuitry and having only one stage, it permits total compensation of signal attenuation in the delay line and automatic limitation of oscillation amplitude. In the storage device described in [192], delay lines by time $100 \mu s$ and a superregenerator are used that operate at a frequency of 40 MHz and have amplification of 60 dB. The stored pulses have length of $0.67 \mu s$. It is stated that the storage device permits storage of up to 2,000 pulses. This value was calculated as the product of the storage time (integration) by the repetition rate. The storage time was determined by the width of the bandpass of the spike of the frequency characteristic of the storage device rather than directly. We feel that the number of stored pulses indicated above is very exaggerated. Nevertheless, a phase-modulated storage device apparently permits one to store a considerably greater number of pulses than an AM storage device.

Urkowitz's investigations [193] showed that spurious reflections in a phase-modulated storage device can be stored both coherently (cophasally) and noncoherently (due to irregular variations of the carrier frequency). As in the case of a frequency-modulated storage device, the dynamic range of a phase-modulated storage device will be appreciably higher with noncoherent addition of spurious reflections than with coherent addition of them.

Since realization of analog storage devices is related to many technical difficulties, digital storage devices of pulsed signals, which have a number of advantages, are of great practical interest. They are also considered briefly in the next chapter.

DIGITAL STORAGE DEVICES

12.1. CHARACTERISTIC FEATURES OF DIGITAL STORAGE DEVICES

Digital storage devices of pulsed signals are devices based on digital computer equipment components and designed to separate repeated pulsed signals from the mixture with noise and other interference.

Since the digital equipment components operate with digital numbers, the received oscillations, which are analog, are converted to digital form prior to digital storage by means of special analog-digital converters (quantifiers). This quantification of the received oscillations is carried out both by level (amplitude) and in time.

In the simplest case of binary amplitude quantification,* one can use a threshold device as the converter (Fig. 1.2.2.). A voltage of some constant value, to which the value "1" is assigned, is generated at the output of this device when the received oscillation exceeds the threshold voltage. Otherwise, the output voltage is zero and the value "0" is assigned to it.

* Quantification of received oscillations for a large number of levels is not feasible since it permits one to reduce the threshold signal by only 1-2 dB and requires considerable complication of the storage device [202].

Since the received oscillation varies in time, it must also be quantified in time with a period selected from the condition of maintaining the basic information in the received oscillation to convert it to a number sequence. This converter can be a time selector (coincident circuit), to one input of which the received oscillation quantified in the threshold device is fed and to the other input of which control pulses with quantification period are fed. 39

Each of these pulses delays the system with respect to the beginning of the repetition period for a quite specific time. Therefore, the number generated by it corresponds to the previously known segment of range. Each repetition period of the system corresponds to some azimuth ("azimuth position"), in the direction of which the sounding pulses are emitted and from which the reflected signals come, with circular or sector scanning of space. The combination of segments of the same range at different azimuth positions comprises the so-called range circle in which digital storage of pulsed signals also occurs.

Unlike analog components, digital components are not invariant with respect to the delay time (see section 1.6) and therefore they do not have the natural multichannel nature in range. Because of this, digital storage devices that process signals coming from different distances must be made multichannel in range, which causes a sharp increase of their equipment. A large number of comparatively simple standard components of digital technology in circuitry and design, usually produced serially and therefore having low cost and high reliability, is used in digital storage devices.

Being more complex, digital storage devices require higher organization of their operation and accordingly of the entire information processing system. Having higher and more complex organization, digital storage devices are characterized by greater flexibility, which permits different operating complications of the radar system to be used—programmed scanning, sequential methods of analysis, pseudo-random modulation of the repetition period and so on—and also permit one to make it adaptive (self-tuned), which can permit a considerable increase of its capability with comparatively low complication of this system and improvement of its characteristics when operating in a complex and variable situation. 39

Digital storage devices are easily integrated with an automated information processing system. Their main advantage is that, working with numbers rather than physical values, they permit one to store an infinitely large number of pulsed signals and thus to separate very weak signals from their mixture with powerful noise and interference. A convincing example of the high efficiency of these storage devices is their use in planetary radar systems in the solar system, which made it possible to detect random signals on a noisy background with ratio of signal-noise output on the order of 100 [201]. However, digital storage devices can also be used successfully in ordinary target radar systems—aircraft, missiles, ships and so on.

12.2. Principle of Digital Storage

If a noise oscillation is being received, then a random flow of ones and zeros is formed as a result of its amplitude-time quantification. If a mixture of repeating pulsed signals and noise is being received, then the flow of quantified pulses becomes ever more random with an increase of the signal/noise ratio due to its greater regularity, which increases as the signal/noise ratio increases. Digital storage devices also determine by digital equipment methods the regularity (periodicity) of a pulsed flow formed as a result of quantification of a mixture of repeating pulsed signals and noise.

Let us consider the operation of a digital storage device in more detail. Let there be formed a sample $u_1, u_2, u_3, \dots, u_n$ as a result of quantification of the received oscillation in a fixed range circle during n adjacent repetition periods (i.e., at n adjacent azimuth positions). To solve the signal detection problem, it is required that the question of whether this sample was generated only by noise or a signal-noise mixture must be answered. Let us denote by p_u the probability of the event $u_i = 1$, observed when noise exceeds the quantification threshold in the i -th position in the range circle and let us denote by g_u the probability of an opposite event $u_i = 0$ (i.e., $g_u = 1 - p_u$). Let us denote similar probabilities by p_c and g_c when receiving a signal-noise mixture. Let us note that when storage occurs after a linear amplitude detector, then p_u and p_c are calculated by formulas (6.3.3) and (6.3.4) if F and D in them is replaced by p_u and p_c , respectively, and U_0 is assumed to be the quantification threshold.

Two hypotheses can be advanced with respect to the nature of the sample u_1, u_2, \dots, u_n : H_0 is a sample generated by noise and H_1 is a sample generated by a signal-noise mixture. The optimum procedure for making the decision (see section 1.2) is calculation of the similarity ratio $\Lambda(u_1, u_2, \dots, u_n)$ and comparison of it to threshold Λ_0 , whose value is determined by the given probability of a false alarm when using the Neymann-Pearson criterion.

In the considered case

$$\Lambda(u_1, u_2, \dots, u_n) = \frac{P_c}{P_u}, \quad (12.2.1)$$

where P_c and P_u are the probabilities that the sample is generated by a signal-noise mixture or by noise alone, respectively.

Because of the independence of events u_i ($i = 1-n$), the probability that a given noise sample contains k ones, which occupy quite specific positions, comprises $P_u = p_u^k g_u^{n-k}$.

In similar fashion, when receiving a mixture of a square-wave sequence of pulsed signals and noise, $P_c = p_c^k q_c^{n-k}$, since the probability of p_c is identical for all azimuth positions. Therefore, the similarity ratio is

$$\Lambda(u_1, u_2, \dots, u_n) = \frac{(p_c)^k (1-p_c)^{n-k}}{(p_u)^k (1-p_u)^{n-k}}. \quad (12.2.2)$$

Hypothesis H_1 is used if

$$\Lambda(u_1, u_2, \dots, u_n) = \left(\frac{p_c}{p_u}\right)^k \left(\frac{1-p_c}{1-p_u}\right)^{n-k} > \Lambda_0.$$

By taking the logarithm of this expression and solving it with respect to k , we find

39

$$k \geq \frac{\ln \left[\Lambda_0 \left(\frac{1-p_u}{1-p_c} \right)^n \right]}{\ln \frac{p_c(1-p_u)}{p_u(1-p_c)}} = k_0. \quad (12.2.3)$$

Accordingly, the optimum rule of signal detection by the sample of its n discrete values includes comparison of the number of ones in this

sample to the threshold number k_0 . If $k \geq k_0$, then the decision is made to receive the signal, otherwise it is absence.

As in the analog case, errors—false alarm and signal omission—are possible in this case. The probability of a false alarm and correct detection comprise, respectively

$$\left. \begin{aligned} F &= \sum_{k=k_0}^n C_n^k p_m^k (1-p_m)^{n-k}, \\ D &= \sum_{k=k_0}^n C_n^k p_c^k (1-p_c)^{n-k}. \end{aligned} \right\} \quad (12.24)$$

Analysis of the more complex case of receiving a sequence of pulsed signals with nonsquare-wave envelope leads to a similar result. In this case the weight sum of of sampled digital values $\sum_{i=1}^n \gamma_i u_i$, in which the weight coefficients γ_i are determined by the envelope of the sequence of pulsed signals at the input of the threshold device, is compared to the threshold [202, 203]. The use of optimum weight summation instead of weightless summation ($\gamma_i = 1$) permits one to reduce the threshold signal/noise ratios by only a value on the order of a decibel [202] and therefore it is usually unfeasible since it is related to complication of the digital storage device.

The detection algorithm considered above also remains valid in the case when the azimuth position of a sequence of pulsed signals is previously unknown. Similar to detection of a signal with unknown arrival time, the similarity ratio is calculated in this case for each azimuth position by n current sample values, which is equivalent to calculating the number of ones, which is compared to k_0 . This procedure is called the "sliding window" or "sliding cursor" algorithm (Fig. 12.2.1) [204].

40

This algorithm can be realized in a single range circle by using an amplitude quantifier and reversible counter. The indication of the latter upon conversion to the next azimuth position is increased by the number standing at this position and is decreased by the number which goes beyond the range of the "sliding window." Because of this, the counter indicates the number of ones in the range of the "sliding window." If this number exceeds the threshold value k_0 , then the decision is made about detection of the signal.

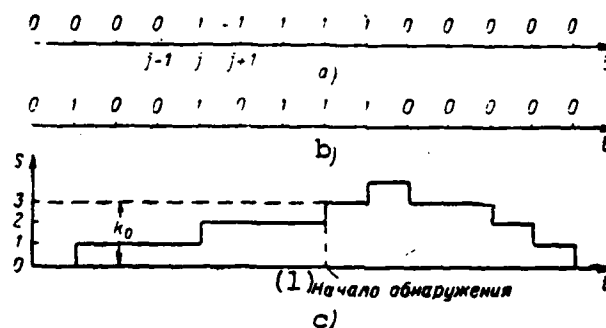


Fig. 12.2.1. Process of analyzing quantified voltage of received oscillation by "sliding window" algorithm at $n = 5$ and $k_0 = 3$: a—variation of quantified signals with number of azimuth position; b—variation of quantified signals for signal-noise mixture; c—dependence of number of ones in "window" on number of azimuth position.

Key: (1) Beginning of detection.

To receive minimum threshold signals, the threshold value k_0 should be selected as optimum [202, 205]:

$$k_{0, \text{opt}} \approx 1,5 \sqrt{n}. \quad (12.2.5)$$

The existence of an optimum value k_0 can be explained in the following manner. It is obvious from (12.2.4) that both the probability of a false alarm and the probability of correct detection decreases with an increase of k_0 with fixed values of probabilities p_w and p_c . To keep the probability of correct detection fixed, one must increase the probability p_c by increasing the threshold signal/noise ratio. On the other hand, to maintain the former value of the probability of a false alarm with an increase of k_0 , one should increase the probability p_w by reducing the level of the quantification threshold. In order that the latter not lead to an increase of probability p_c but accordingly lead to the probability of correct detection, one can reduce the threshold signal/noise ratio. 401

Thus, in the case of fixed probabilities of a false alarm and correct detection, an increase of k_0 leads on the one hand to a decrease of the threshold signal/noise ratio and on the other hand to an increase of this ratio. The first tendency predominates at the beginning of an increase of k_0 , due to which the threshold signal/noise ratio decreases,

while the second tendency that causes an increase of this ratio then begins to predominate.

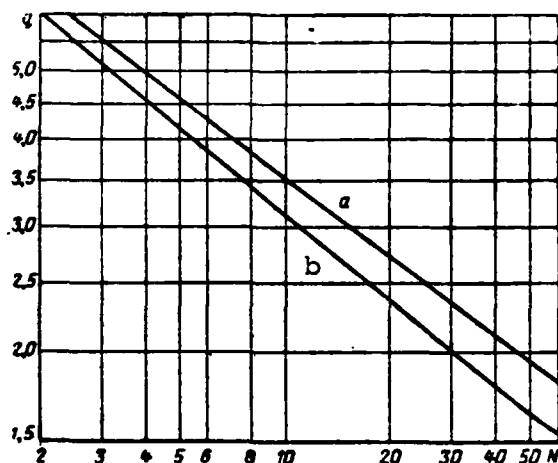


Fig. 12.2.2. Dependence of threshold signal/noise ratios on number of stored pulses with optimum noncoherent digital (a) and analog (b) storage.

This also explains the presence of an optimum value of k_0 and also the weak effect of slight deviations of k_0 from the optimum value by the threshold signal [205].

40

The optimum value of the threshold voltage of an amplitude quantifier during reception of weak signals is selected so that $p_{\text{ш}} \approx 0.2$ [205]. However, the threshold signal/noise ratio is weakly critical to the value of $p_{\text{ш}}$. Therefore, $p_{\text{ш}} \leq 0.1$ is frequently selected in practice. This permits a sharp reduction of the number of noise blips and thus a decrease of the storage capacity of the storage device (see section 12.5).

If the parameters of a digital storage device are selected as optimum, the gain in the threshold signal compared to an ideal noncoherent storage device is approximately 2 dB (Fig. 12.2.2) [202, 205].

12.3. Realization of Digital Storage Device

Let us consider one of the possible versions of realizing a digital storage device using shift registers (Fig. 12.3.1). The number of cells of each register is selected equal to the number of range circles, for

which the repetition period of the system T is quantified. The number of registers $n - 1$ is determined by the width of the sliding window. The width of the range circle is usually selected the same as the resolution of the range system. In the case of using optimum filtration and a noncoherent detector, the range system is determined by the autocorrelation function of the signal envelope, which coincides with that of the noise at the detector output. Because of the foregoing, the length Δ of the time segment corresponding to the range circle is usually selected as equal to the correlation time τ_k of the noise voltage at the detector output.

403

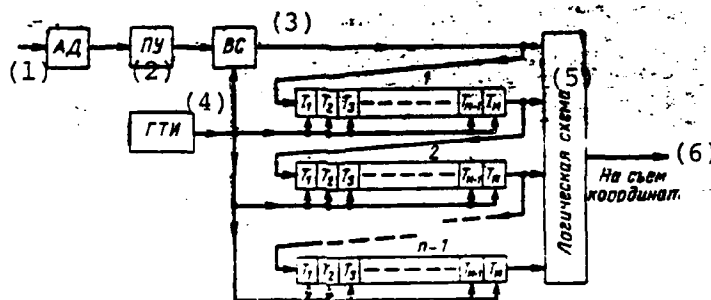


Fig. 12.3.1. Block diagram of digital storage device using shift registers.

Key: (1) Amplitude detector; (2) Threshold device; (3) Time selector; (4) Timing pulse generator; (5) Logic circuit; (6) To coordinate tap.

The register contents are shifted by timing pulses that follow the repetition period Δ . If the voltage at the input of the amplitude quantifier exceeds the threshold voltage in the i -th range segment, a one is written in the first cell of the upper shift register, which is then pushed to the right by timing pulses through the flip-flops of the shift register and is in the $(M - i + 1)$ -th cell of this register by the beginning of the next repetition period. This unit is fed through the repetition period after being fed to the input of the indicated register from the last flip-flop of the register to the inputs of the second register and the logic circuit and is fed through two repetition periods to the inputs of the third register and logic circuit and so on.

When receiving a sequence of signals following the repetition period T of the system, ones will be fed simultaneously to the inputs of the logic circuit with time selector v_s and from the outputs of different

registers, which may cause this circuit to be triggered, indicating a decision being made about detection of a signal.

It is easy to see that the considered system is a digital version of a delay line by time $(n - 1)T$ with $(n - 2)$ uniformly arranged leads in an optimum filter for the envelope of a sequence of n pulsed signals (Fig. 5.1.1, b) which is an ideal analog storage device.

A logic circuit that realizes a detection algorithm counts the number of ones in n range circles to be analyzed and makes a decision on detection of a signal when this number is greater than the established threshold k_0 . The range coordinate can be counted in this case from the range counter, while the azimuth coordinate can be counted from the azimuth counter.

In practice it is very difficult to make these digital delay lines in the form of shift registers with a large number of cells (on the order of 1,000). Therefore, instead of these registers, a matrix storage device with number of cells $M = T/\Delta$ and number of digits n is used, which is usually employed in digital computers and which is made on ferrite cores. 404

For precise realization of algorithm (12.2.3) for optimum detection of a sequence of pulsed signals, it is necessary that the width of the "window" be equal to the number of pulses in the sequence: $n = N$. In this case $(N - 1)M = (N - 1)(T/\Delta)$ flip-flops or some other storage cells should be used in the storage device (Fig. 12.3.1). Since $M = T/\Delta$ is on the order of 1,000 and since the number of N pulsed signals in the sequence may be sufficiently large, practical realization of this storage device is difficult. To simplify its realization, additional versions of realizing the detection algorithm are employed. The so-called " $k/n - 1$ " criterion is most frequently used as this algorithm [203, 206], with use of which no more than n adjacent azimuth positions are analyzed simultaneously, where $n < N$.

The rule for making a decision on this criterion includes fulfillment of two special criteria:

a) the criterion of the beginning of detection ϵ_k , which is assumed to be fulfilled in the i_H -th position if k ones in n adjacent positions with numbers from $i_H - n + 1$ to i_H are first recorded;

b) the criterion of the end of detection ϵ_1 , which is assumed fulfilled in position i_k if a series of 1 zeros following one after the other is first formed on 1 adjacent positions with numbers from $i_H - 1 + 1$ to i_k after fulfillment of criterion ϵ_k (Fig. 12.3.2).

The values of target azimuth α_H and α_k are determined by the azimuth positions i_H and i_k at the moment of the beginning and end of detection, which permits one to calculate the target azimuth:

$$\alpha = \frac{1}{2} [\alpha_H + \alpha_k - (k - 1 + 1) \Delta\alpha], \quad (12.3.)$$

where $\Delta\alpha$ is the angle between adjacent azimuth positions.

The presence of a subtrahend in formula (12.3.1) is explained by the fact that the decision on the beginning and end of detection of a strong signal is made with an error equal to $(k - 1)\Delta\alpha$ and $1\Delta\alpha$, respectively.

To simplify the circuitry realization, only logic criteria of type "k/n - 1" at $k \leq n \leq 5$ are used in practice. The criterion of the end of detection is usually selected from the condition $1 \geq n - k + 1$ [206

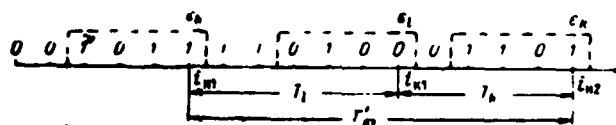


Fig. 12.3.2. Processing quantified noise voltage by "3/4 - 2" criterion in single range circle.

The "k/n - 1" criterion is called a whole criterion at $n = k$ and a fractional criterion at $n < k$. A whole criterion is most simply realized by a coincidence circuit at k inputs.

Other suboptimum processing algorithms are described in [206

12.4. Frequency of False Alarms and Detection Characteristics When Using "k/n - 1" Criterion

Let us first determine the mean frequency of false alarms for a single range circle. The sequence of ones and zeros formed in the circle as a result of amplitude quantification of noise oscillation can be regarded as a sequence of independent tests with probabilities of success (with fallout of a one) equal to p_w and failure (fallout of zero) equal to $g_w = 1 - p_w$. These tests are independent due to the independence of the values of noise separated by the repetition period of the system whose value is always much greater than the noise correlation time.

Let us use the results of recurrent event theory to determine the mean frequency of false alarms ν' in the range circle [137, 208]. The time interval between two sequential false alarms T'_{nT} is added from the delay T_1 of event ϵ_1 and the delay T_k of event ϵ_k (Fig. 12.3.2).

To determine the mean numbers of tests $\theta_1 = m_1(T_1)/T$ and $\theta_k = m_1(T_k)/T$ prior to the first realization of events ϵ_1 and ϵ_k , respectively, in a sequence of independent tests, let us consider the combination of probabilities $f_i (0 \leq i \leq \infty)$ of the onset of event ϵ first on the i -th test and function $h_n = \sum_{i=n+1}^{\infty} f_i$ that describes the probability of recurrent event ϵ in the first n tests.

The main number of tests before the first appearance of event ϵ is

$$\theta = \sum_{i=0}^{\infty} i f_i = \sum_{n=0}^{\infty} h_n. \quad (12.4.1)$$

If $Q(s) = \sum_{i=0}^{\infty} h_i s^i$ is a generating function for probabilities h_i [208], then $\theta = Q(1)$.

To compare the equation that permits one to determine $Q(s)$, let us use the method described in [137]. It follows from determination of values h_n and f_n that:

$$f_n = h_{n-1} - h_n. \quad (12.4.2)$$

And the probability f_n of the first realization of event ϵ for the first time on the n -th test can be expressed by probability h_p , where $p < n$, in the following manner.

For whole " $k/k - 1$ " criteria, event ϵ_k , which is a series of k ones one after the other, first begins on the n -th test with simultaneous fulfillment of the following conditions:

- a) ones fell out in k tests with numbers from $n - k + 1$ to n ;
- b) a zero fell out in a test with $n - k$;
- c) event ϵ_k did not begin once prior to the $(n - k - 1)$ -th test.

The probabilities of these events comprise p_w^k , g_w and h_{n-k-1} , respectively. Therefore, the probability of a complex event is

$$f_n = p_w^k g_w h_{n-k-1}. \quad (12.4.3)$$

By substituting (12.4.3) into (12.4.2) and replacing n by $n + k + 1$, 40 we find the recursion equation

$$h_{n+k+1} - h_{n-k} + p_w^k g_w h_n = 0 \quad (12.4.4)$$

with initial conditions

$$h_0 = h_1 = \dots = h_{k-1} = 1; h_k = 1 - p_w^k.$$

Multiplying (12.4.4) by s^{n+k+1} , adding from zero to infinity with respect to n and using the determination of the generating function, we will have

$$Q(s) - \sum_{i=0}^k h_i s^i - s \left[Q(s) - \sum_{i=0}^{k-1} h_i s^i \right] + p_w^k g_w Q(s) s^{k+1} = 0.$$

Substituting the initial conditions into this equation and assuming that $s = 1$, we determine

$$Q(1) = \theta_k = (1 - p_w^k) / (g_w p_w^k). \quad (12.4.5)$$

The expression for θ_1 has a similar form and can be found from (12.4.5), replacing p_w in it by g_w and k by 1:

$$\theta_i = (1 - g_{\text{m}}^i) / (p_{\text{m}} g_{\text{m}}^i). \quad (12.4.6)$$

Using these expressions, let us determine the average length of the period of false alarms in the range circle:

$$m_1(T'_{\text{m}}) = T(\theta_k + \theta_i) = \left(\frac{1 - p_{\text{m}}^k}{g_{\text{m}} p_{\text{m}}^k} + \frac{1 - g_{\text{m}}^i}{p_{\text{m}} g_{\text{m}}^i} \right) T. \quad (12.4.7)$$

Since usually $lp_{\text{m}} \ll 1$, expressions (12.4.6) and (12.4.7) are simplified:

$$\theta_i \approx T(1 + lp_{\text{m}}) \approx 1$$

and

$$m_1(T'_{\text{m}}) \approx \left(\frac{1 - p_{\text{m}}^k}{g_{\text{m}} p_{\text{m}}^k} + 1 \right) T \approx \left(\frac{1}{p_{\text{m}}^k} + 1 \right) T \approx \frac{T}{p_{\text{m}}^k}.$$

It follows from the last expression that the end criterion slightly affects the average length of the period of false alarms.

For fractional "k/n" criteria, θ_k is calculated in a similar manner, but the expression for f_n is complicated. 40

Possible situations that lead to the appearance of an event for the first time in the n-th test are shown for the "2/3" criterion in Table 12.4.1. The combination of ones and zeros in which event ε did not occur once during all i tests is denoted in it by C_i (i.e., in the considered case there were never two ones in three adjacent positions). Since the combination C_i appears with probability h_i , then

$$f_n = p_{\text{m}}^2 g_{\text{m}}^2 h_{n-1} + p_{\text{m}}^2 g_{\text{m}}^3 h_{n-2}.$$

Substituting this expression into (12.4.2), we find

$$h_{n+1} - h_{n+1} + p_{\text{m}}^2 g_{\text{m}}^2 h_{n+1} + p_{\text{m}}^2 g_{\text{m}}^3 h_n = 0. \quad (12.4.8)$$

The initial conditions for this equation are as follows:

$$\begin{aligned} h_0 &= h_1 = 1; \quad h_2 = 1 - p_{\text{m}}^2; \quad h_3 = 1 - p_{\text{m}}^2 - 2p_{\text{m}}^2 g_{\text{m}}; \\ h_4 &= 1 - p_{\text{m}}^2 - 2p_{\text{m}}^2 g_{\text{m}} - 2p_{\text{m}}^2 g_{\text{m}}^2. \end{aligned}$$

Solving (12.4.8), we determine

$$Q(1) = \theta_k = \frac{1 - p_w(1 + g_w)^2}{p_w^2 g_w^2 (1 + g_w)}.$$

This expression is simplified at sufficiently small value of p_w :

$$\theta_k \approx \frac{1}{2p_w^2 g_w^2}.$$

Table 12.4.1

Version of Situation	Number of Position					
	$n-5$	$n-4$	$n-3$	$n-2$	$n-1$	n
First		C_{n-4}	0	0	1	1
Second	C_{n-5}	0	0	1	0	1

Similar expressions for θ_k are presented in Table 12.4.2 in the case of more complex criteria. It is easy to show that for the considered criteria at sufficiently small value of p_w

409

$$\theta_k \approx \frac{1}{C_{n-1}^k p^k g^{n-k-1}}. \quad (12.4.9)$$

The expressions found above permit one to calculate the average frequency of false alarms by all M range circles:

$$\nu = \frac{M}{m_1(T'm_1)} = \frac{M}{(\theta_1 + \theta_k)T}. \quad (12.4.10)$$

The outlined method of calculation cannot unfortunately be used in those cases when a somewhat different method of processing is used in which range scanning is no longer divided into fixed range circles. In this case the frequency of false alarms can be calculated on the basis of the coincidence theory of pulses of independent flows [204, 206].

Systems with low probability level of false alarms in which the amplitude quantification threshold $U_0 \geq 1.5\sigma$, where σ is the effective voltage of noise, according to (6.3.3), are usually employed. And with this condition the noise blips form a Poisson flow [209], i.e., k flow pulses—noise blip with the following probability—are observed during time t

410

Several different algorithms that realize the " $k/n - 1$ " criterion can be suggested to process this flow. One of them includes the fact that a decision is made about detection of a signal at range r_0 if the following conditions are fulfilled simultaneously:

a) a normalized pulse in the i -th azimuth position corresponds to range r_0 ;

b) there are no pulses in the l previous positions which at least partially coincide ("or linked") with it;

c) the $(k - 1)$ -th pulse is "linked" to the pulse in the i -th position earlier in $(n - 1)$ -th subsequent azimuth positions than 1 "non-linking" is realized (Fig. 12.4.1). 41

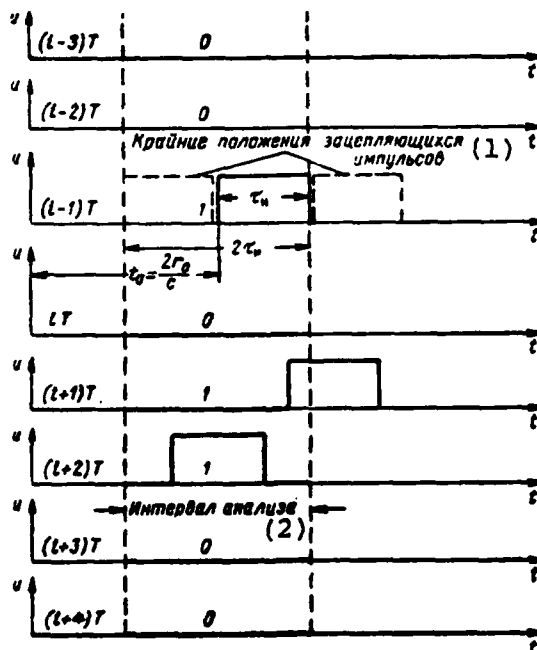


Fig. 12.4.1. Analysis of received pulse flows for coincidence by "3/4-2" criterion.

Key: (1) Extreme position of linked pulses to interval of analysis.

In this case the probability of "nonlinking" of $g_{\text{н}}$ is determined as the probability of the absence of a pulse front in an interval of length $t_0 = 2\tau_n$ (Fig. 12.4.1) and according to (12.4.13) comprises

$$g_m = 1 - p_m = \exp(-2\lambda\tau_m). \quad (12.4.15)$$

If overlapping of the pulses by a value not less than τ_3 is required for linking, then

$$g_m = \exp[-2\lambda(\tau_m - \tau_3)].$$

Let us determine the frequency of false alarms in the considered case [210].

If any pulse which is not linked to any of the pulses in the 1 previous scanning periods is fed to the input, analysis of this segment for fulfillment of the detection criterion begins. Therefore, the probability that the incoming pulse begins analysis is equal to the probability g_w^1 of the absence of noise pulses during the 1 previous periods. Because of this, if the average frequency of the pulse flow being fed to the input comprises λ , the flow of pulses that begin the analysis has mean frequency $\lambda_a = \lambda g_w^1$. This flow, as the initial flow of noise blips, is Poisson. Each of the pulses that begin analysis can cause a false alarm with probability F , due to which the mean frequency of false alarms comprises

$$\nu = \lambda_a F = \lambda g_w^1 F. \quad (12.4.16)$$

The probability of a false alarm F is obviously identical both in the considered case and for a single range circle. And in the latter case it is difficult to determine by using the results found previously. Actually, for a single range circle, we have a relation similar to the preceding

$$\nu = \lambda' F = \lambda' g_w^1 F,$$

from which it follows that:

$$F = \frac{\nu}{\lambda' g_w^1}.$$

On the other hand, the mean frequency of a flow of noise blips for a single range circle is $\lambda' = \frac{Dw}{T}$, while the mean frequency of false alarms is inverse to the mean period of false alarms (12.4.7):

$$v' = \frac{1}{m_1(T_{\text{ST}})} = \frac{1}{T(\theta_i + \theta_n)},$$

in view of which

$$F = \frac{v'}{\lambda g_{\text{W}}^l} = \frac{1}{p_{\text{W}} g_{\text{W}}^l (\theta_i + \theta_n)}.$$

Substituting this expression into (12.4.16), we find

413

$$v = \frac{\lambda}{p_{\text{W}} (\theta_i + \theta_n)}, \quad (12.4.17)$$

where θ_1 and θ_k are determined the same as above, while p_{W} and g_{W} are determined by formula (12.4.15).

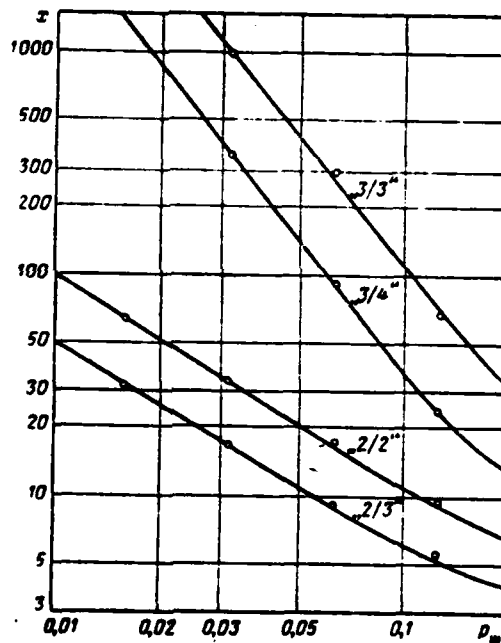


Fig. 12.4.2. Dependence of attenuation factor of frequency of false blips on probability of false blip for different detection criteria (o—experimental points found by the statistical modeling method on the Minsk-1 computer).

The effectiveness of this processing of noise pulses is characterized by attenuation factor of the frequency of false blips $x = \frac{\lambda}{v}$, whose value is higher, the less the value of p_{W} and the more rigid the detection criterion (Fig. 12.4.2).

The probability of correct detection D is determined by the probability of the first fulfillment of criterion "k/n" at azimuth

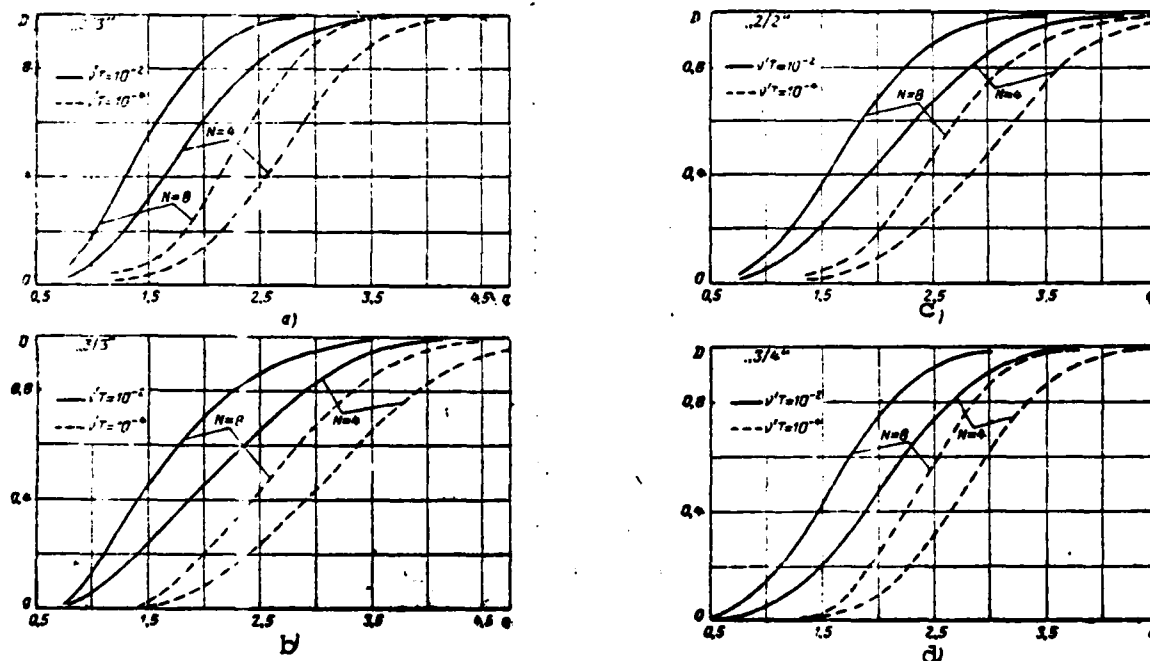
415

positions corresponding to the presence of a sequence of pulsed signals.

The probability of correct detection for a square-wave envelope of a sequence of N pulsed signals is calculated by the recursion equations described at the beginning of the given section and in which p_w is replaced by p_c , and

$$D=1-h_N. \quad (12.4.18)$$

This permits one to calculate the detection characteristics (Fig. 12.4.3).



414

Fig. 12.4.3. Detection characteristics with digital storage for different criteria.

The recursion equation with a nonsquare-wave envelope of the sequence has variable coefficients which depend on the probability p_{ci} that the threshold level on the i -th azimuth position determined by the shape of the envelope will be exceeded by the mixture [206]. As in analog storage (see item 1, section 10.6), the nonsquare-wave envelope of the sequence can be replaced by an equivalent square-wave envelope when calculating the detection characteristics and threshold signals, which simplifies this calculation.

415

12.5. Storage Capacity of Digital Storage Device

To realize the " $k/n-1$ " criterion on a digital computer, one must have a storage device (ZU) in which information is stored during n repetition periods of the system. As already indicated in section 12.3, this storage device can essentially be based on shift registers with number of cells $M = T/\Delta$ (Fig. 12.3.1). However, since M is on the order of 1,000 in practice, it is very difficult to make these registers.

Therefore, it is simpler to use a matrix storage device consisting of M cells, each of which has n binary digits, which is attached to a specific range circle and which realizes the sliding window in it, in digital storage devices. This type of storage device in which a single cell is allocated to each range circle, is called a storage device of first type (ZU-1). The characteristic feature of this storage device with low probabilities p_{w} consists in the fact that each cell of it will not contain useful information (ones) the majority of the time on the order of $1 - np_{\text{w}}$. Thus, for example, at $p_{\text{w}} = 0.01$ and $n = 3$ the cell will be filled with useful information during an average of 3% of operating time. 416

Rejecting the principle of attaching the cell of the storage device to a specific range circle permits one to reduce the total number of these cells by increasing their operating intensity. This principle of organizing the memory leads to the second type of storage device (ZU-2). Analysis of ZU-2 operation [137] shows that its functioning is described by queueing theory, which permits one to determine its capacity and other characteristics.

The operation of a digital storage device proceeds in this case in the following manner. If a pulse appears on some range circle, this circle becomes "suspicious" and its coordinate is stored in one of the free cells of the storage device. Analysis of the suspicious circle begins from this moment by the " $k/n-1$ " criterion, which is completed upon the appearance of 1 zeros one after the other, after which the cell is erased and can be engaged for analysis of pulsed flows in other circles. If the pulse arrives from a range circle that is already under analysis, the new cell is not occupied and a one is written in the

corresponding digit of the previously occupied cell. As a result the range code of the range circle being analyzed for the detection criterion is stored in this cell and the structural characteristic of the received sequence of pulsed signals is formed.

Thus, in order that analysis begin with the arrival of a pulse, it should be preceded by 1 zeros, the probability of which is g_{u}^1 . Continuation of the analysis, i.e., the delay of zeros, is a random value. The probability h_n that the analysis will continue for more than n periods is determined by formula (12.4.6), while the average time of analysis comprises

$$m_1(T) = \frac{1 - g_{\text{u}}^1}{p_{\text{u}} g_{\text{u}}^1} T.$$

If $p_{\text{u}} \ll 1$, function h_n is close to zero at $n \geq 1$. This means that 1 zero follows immediately behind the pulse of the beginning of analysis with high probability and analysis is completed within 1 periods.

417

As previously, we assume that the pulse flow being fed to the storage device is Poisson and has intensity (mean repetition rate) λ , which is easily determined from the expression for the average number of noise pulses during the repetition period of the system at M range circles

$$Mp_{\text{u}} = \lambda T. \quad (12.5.1)$$

The flow of pulses which begins the analysis is formed by thinning ("scattering") of the pulses of the input flow. As shown in the previous section, the flow intensity of the pulses that begin analysis comprises

$$\lambda_1 = \lambda g_{\text{u}}^1. \quad (12.5.2)$$

The probability distribution of the number of ZU-2 cells occupied for analysis with total number L in the steady mode is Erlang distribution [137]:

$$\left. \begin{aligned} P(m) &= \frac{\theta^m}{m!} / \sum_{i=0}^L \frac{\theta^i}{i!} \quad \text{at } 0 \leq m \leq L, \\ P(m) &= 0 \quad \text{at } m > L, \end{aligned} \right\} \quad (12.5.3)$$

where according to (12.4.6), (12.5.1) and (12.5.2) with sufficiently small value of p_{w} , the distribution parameter is

$$\theta = \lambda_m(T) = T \lambda g_m^l \frac{1 - g_m^l}{p_m g_m^l} \approx \lambda T l \left(1 - \frac{l-1}{2} p_m \right) \approx \lambda T l. \quad (12.5.4)$$

It follows from (12.5.3) that overflow of the storage device (i.e., the event when all the cells of the storage device are occupied upon arrival of a pulse from a "new" range circle, occurs with probability

$$P(L) = \frac{\theta^L}{L!} / \sum_{i=0}^L \frac{\theta^i}{i!}. \quad (12.5.5)$$

Normal operation of a digital storage device is possible only with low probability of overflow, for which in the case of large values of θ one must select the number of cells of the storage device from the condition 418

$$L \geq \theta + (2-3) \sqrt{\theta}. \quad (12.5.6)$$

In this case the finite sum in (12.5.5) can be replaced by an infinite series, Erlang distribution (12.5.4) changes to Poisson distribution, the probability of overflow is

$$P(L) = \frac{\theta^L}{L!} e^{-\theta}. \quad (12.5.7)$$

and θ has the meaning of the average number of occupied cells.

Having calculated the average number of occupied cells by formula (12.5.4) and having been given the probability of overflow, one can determine by means of the curves (Fig. 12.5.1) the required number of ZU-2 cells. This number is considerably less than the number of ZU-1 cells, which is equal to the number of range circles M.

However, not only the structural characteristic of the received oscillations during n repetition periods of the system, but also the 419

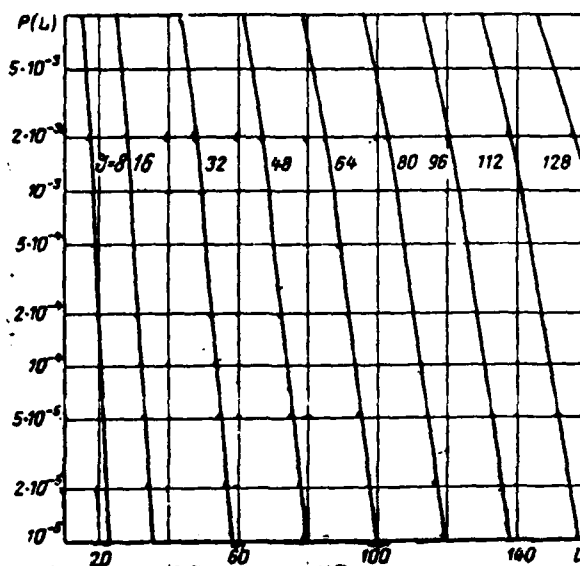


Fig. 12.5.1. Probability of overflow of ZU-2 as function of the number of its cells.

coordinate of the "suspicious" range circle are stored in each ZU-2 cell. Therefore, if the ZU-1 cell has n binary digits, the number of binary digits of each ZU-2 cell is equal to $n + E(\log_2 M) + 1 \approx n + \log_2 M$. Accordingly, total number of binary digits of the ZU-1 and ZU-2 comprises Mn and $L(n + \log_2 M)$. Their ratio

$$y = \frac{Mn}{L(n + \log_2 M)} = \frac{Mn}{z\theta(n + \log_2 M)} = \frac{n}{z\rho_{ul}(n + \log_2 M)} \quad (12.5.8)$$

is inversely proportional to the probability of a noise blip. The ratio of the number of ZU-2 cells to the average number of occupied cells was denoted above by $z = L/\theta$. Its value is easily determined by the curves (Fig. 12.5.1). This ratio lies in the range from 1.15 to 2.6 at $\theta = 10$ -100 and $P(L) = 10^{-5}$ to 10^{-2} .

It follows from (12.5.8) that ZU-2 has fewer binary digits than ZU-1 only with low probabilities of a noise blip. For example, the capacity of ZU-2 is less than that of ZU-1 only at $p_{ul} \leq 0.06$ -0.29 in the case of whole detection criteria and at $p_{ul} \leq 0.034$ -0.136 in the case of fractional criteria ($l = 2$ or 3) at $M = 1,024$ -2,048 and $n \leq 5$.

We note that only the noise blips were taken into account above when calculating the capacity of ZU-2 and the signal blips were not taken into account. This led to some underestimation of capacity. However, the number of expected targets on adjacent 1 azimuth positions is usually much less than the number of noise blips during time $1T$, corresponding to these positions. Therefore, the signal blips can be disregarded in the first approximation when calculating the capacity of the ZU-2.

AD-A115 395

FOREIGN TECHNOLOGY DIV WRIGHT-PATTERSON AFB OH
OPTIMUM FILTERS AND PULSED SIGNAL STORAGE DEVICES, (U)

F/6 9/5

MAY 82 Y S LEZIN

UNCLASSIFIED

FTD-ID(RS)T-0182-81

NL

5 11 5

7-82



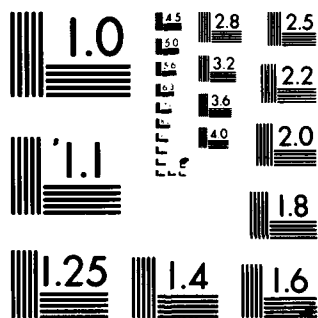
END

DATE

FILED

7-82

DTIC



MICROCOPY RESOLUTION TEST CHART

NATIONAL BUREAU OF STANDARDS-1963-A

Abbreviations of names of journals and publishing houses:

А и Т	—	"Avtomatike i telemekhanika" (Automatics and Telemechanics).
ЗРЭ	—	"Zarubezhnaya radioelektronika" (Foreign Radio Electronics).
Р и Э	—	"Radiotekhnika i elektronika" (Radio Engineering and Electronics).
Р и ЭЗР	—	"Radiotekhnika i elektronika za rubezhom" (Radio Engineering and Electronics Abroad).
ТИИЭР	—	"Trudy Instituta inzhenerov po elektrotekhnike i radioelektronike" (Transactions of the Institute of Electrical and Electronics Engineers).
ТППИ	—	"Trudy Gor'kovskogo politekhnicheskogo instituta" (Transactions of the Gor'ky Polytechnical Institute).
ТУИС	—	"Trudy uchebnykh institutov svyazi" (Transactions of Academic Institutes of Communications).
ICR	—	"IRE Convention Record".
IRET	—	"IRE Transactions".
JAP	—	"Journal of Applied Physics".
JFI	—	"Journal of the Franklin Institute".

1. Сифоров В. И. Развитие теории помехоустойчивости в СССР. Р и Э, 1957, т. 2, № 11, стр. 1413—1434.
2. Перих К. Обнаружение ракет радиолокационными станциями сверхдальнего действия. Р и ЭЗР, 1959, № 2 (50), стр. 85—95.
3. Холахан. Современное состояние радиолокации. Р и ЭЗР, 1959, № 4 (52), стр. 134—140.
4. Холахан. Роль теории информации в конструировании новых радиолокационных систем. Р и ЭЗР, 1959, № 3 (51), стр. 3—9.
5. IRET on Information Theory, 1960, vol. IT-6, № 3.
6. Голдман С. Теория информации, пер. с англ., под ред. В. В. Фурдуева. Изд-во иностранной литературы, 1957.
7. Лезин Ю. С., Оптимальные фильтры и накопители импульсных сигналов. Изд. 1-е. Изд-во «Советское радио», 1963.
8. Гуткин Л. С., Лебедев В. Л., Сифоров В. И. Радиоприемные устройства, ч. 2. Изд-во «Советское радио», 1963.
9. Гоноровский И. С. Радиотехнические цепи и сигналы, ч. 1. Изд-во «Советское радио», 1966.
10. Ширман Я. Д., Голяков В. Н. Основы теории обнаружения радиолокационных сигналов и измерения их параметров. Изд-во «Советское радио», 1963.
11. Вайнштейн Л. А., Зубаков В. Д. Выделение сигналов на фоне случайных помех. Изд-во «Советское радио», 1960.
12. Фалькович С. Е. Прием радиолокационных сигналов на фоне флюктуационных помех. Изд-во «Советское радио», 1961.
13. Гуткин Л. С. Теория оптимальных методов радиоприема при флюктуационных помехах. Госэнергониздат, 1961.
14. Бакут П. А., Большаков И. А., Герасимов Б. М., Курикса А. А., Репин В. Г., Тартаковский Г. П., Широков В. В. Вопросы статистической теории радиолокации, под ред. Г. П. Тартаковского. Изд-во «Советское радио», ч. 1, 1963, ч. 2, 1964.

15. Тихонов В. И. Статистическая радиотехника. Изд-во «Советское радио», 1966.
16. Вудворд Ф. М. Теория вероятностей и теория информации с приложениями в радиолокации, пер. с англ., под ред. Г. С. Горелика. Изд-во «Советское радио», 1955.
17. Миддлтон Д. Введение в статистическую теорию связи, пер. с англ., под ред. Б. Р. Левина. Изд-во «Советское радио», т. 1, 1961, т. 2, 1962.
18. Давенпорт В. Б., Рут В. Л. Введение в теорию случайных сигналов и шумов, пер. с англ., под ред. Р. Л. Добрушина. Изд-во иностранной литературы, 1960.
19. Хелстром К. Статистическая теория обнаружения сигналов, пер. с англ., под ред. Ю. Б. Кобзарева. Изд-во иностранной литературы, 1963.
20. Левин Б. Р. Теоретические основы статистической радиотехники, кн. 1. Изд-во «Советское радио», 1966.
21. Котельников В. А. Проблема помехоустойчивости радиосвязи. «Радиотехнический сборник». Госэнергоиздат, 1947, стр. 5-12.
22. Котельников В. А. Теория потенциальной помехоустойчивости. Докторская диссертация. МЭИ, 1946. Госэнергоиздат, 1956.
23. Ван дер Поль Б., Бреммер Х. Операционное исчисление на основе двухстороннего преобразования Лапласа. Изд-во иностранной литературы, 1952.
24. Лезин Ю. С. О помехоустойчивости при различных видах радиотелеграфии. «Электросвязь», 1957, № 4, стр. 40-47.
25. Лебедев Н. Н. Специальные функции и их приложения. Гостехиздат, 1953.
26. Харкевич А. А. Борьба с помехами. Физматгиз, 1963.
27. Ицхоки Я. С. Импульсные устройства. Изд-во «Советское радио», 1959.
28. Ризкин А. А. Основы теории усилительных схем. Изд-во «Советское радио», 1958.
29. Пугачев В. С. Теория случайных функций и ее применение к задачам автоматического управления. Гостехиздат, 1957.
30. Норс. Анализ факторов, определяющих обнаружение сигнала на фоне шумов в системах с импульсной модуляцией несущей. ТИИЭР, 1963, т. 51, № 7, стр. 1016-1029.
31. Ван Флек Дж., Миддлтон Д. Теоретическое сравнение визуального, слухового и инструментального методов приема сигналов в присутствии шумов. В сб. [196], стр. 7-84.
32. Турин Г. Л. Согласованные фильтры. ЗРЭ, 1961, № 3, стр. 30-63.
33. Фихтенгольц Г. М. Курс дифференциального и интегрального исчисления, т. 2. Гостехиздат, 1948.
34. Davis R. C. On the detection of sure signals in noise, 1954, JAP, vol. 25, № 1, p. 76-82.
35. Дворк В. М. Обнаружение импульсов, наложенных на флюктуационные шумы. «Вопросы радиолокационной техники», 1952, № 2 (8), стр. 9-15.
36. Лезин Ю. С. О синтезе оптимальных фильтров и взаимно корреляционных устройств. ТГПИ, 1960, т. 16, № 2, стр. 74-78.

37. Лезин Ю. С. Оснизе фильтров, оптимальных импульсам определенной формы. «Научные доклады высшей школы», Р и Э, 1958, № 2, стр. 23—28.
38. Лезин Ю. С., Синтез оптимальных фильтров в случае коррелированных шумов. ТГПИ, 1964, т. 20, № 2, стр. 55—58.
39. Стратонович Р. Л. Избранные вопросы теории флюктуаций в радиотехнике. Изд-во «Советское радио», 1961.
40. Zadeh L. A., Ragazzini I. R. Optimum filters for the detection of signals in noise. Proc. of the IRE, 1952, vol. 40, № 10, p. 1223—1231.
41. Харкевич А. А. Нелинейные и параметрические явления в радиотехнике. Гостехиздат, 1956, стр. 157—162.
42. Smith R. A. The relative advantages of coherent and incoherent detectors. Proceedings of the IEE, 1951, vol. 98, pt. 4, № 1, p. 43—54.
43. Китар Р. Когерентные и некогерентные детекторы. Чувствительность к сигналу и шуму. «Вопросы радиолокационной техники», 1957, № 5 (41), стр. 56—62.
44. Котельников В. А., Николаев А. М. Основы радиотехники, ч. 1. Изд-во «Советское радио», 1950.
45. Rochefort J. S. Matched filters for detecting pulsed signals in noise. ICR, 1954, vol. 2, pt. 4, p. 30—34.
46. Лезин Ю. С. О прохождении импульсного сигнала и шума через оптимальный фильтр. ТГПИ, 1958, т. 14, № 5, стр. 45—51.
47. Лезин Ю. С. О нечувствительности структуры согласованного фильтра к изменениям формы сигнала. ТГПИ, 1964, т. 20, № 2, стр. 59—62.
48. Гольдман С. Гармонический анализ, модуляция и шум, пер. с англ., под ред. Г. С. Горелика. Изд-во иностранной литературы, 1951.
49. Евтянов С. И. Переходные процессы в приемно-усилительных схемах. Связьиздат, 1948.
50. Грин, Моллер. Влияние нормально распределенных случайных фазовых ошибок на диаграммы направленности антенных решеток с синтезированным раскрытием. ЗРЭ, 1963, № 2, стр. 21—33.
51. Давенпорт В. Б., Джонсон Р. А., Миддлтон Д. Статистические ошибки при измерении случайных функций времени. В сб. «Определение параметров случайных процессов», под ред. В. И. Чайковского. Гостехиздат УССР, 1962, стр. 5—42 (пер. из JAP, 1952, vol. 23, № 4, p. 377—388).
52. Сифоров В. И. О влиянии помех на прием импульсных радиосигналов. «Радиотехника», 1946, т. 1, № 1, стр. 5—19.
53. Белоусов А. П. О наивысшей реальной чувствительности приемника. «Радиотехника», 1946, т. 1, № 5, стр. 18—27.
54. Евтянов С. И. Об эквивалентности усилителей высокой и низкой частоты. «Радиотехника», 1948, т. 3, № 4, стр. 26—33.
55. Тихонов В. И., Левиков А. А. О квазиоптимальных линейных фильтрах для импульсных сигналов. «Радиотехника», 1966, т. 20, № 1, стр. 10—17.
56. Колосов А. А. Резонансные системы и резонансные усилители. Связьиздат, 1949.
57. Семейов Н. А. Критерий выбора оптимальной частотной характеристики в приемниках импульсных сигналов. «Радиотехника», 1963, т. 8, № 2, стр. 38—50.

58. Сайбель А. Г. Основы радиолокации. Изд-во «Советское радио», 1961.
59. Сиверс А. П., Суслов Н. А., Метельский В. И. Основы радиолокации. Судпромгиз, 1959.
60. Урковиц Г. Фильтр для обнаружения слабых радиолокационных сигналов на фоне мешающих отражений. «Вопросы радиолокационной техники», 1954, № 2, стр. 52—65.
61. Ширман Я. Д. Способ повышения разрешающей способности радиолокационных станций и устройство для его осуществления. Авторское свидетельство № 146803 по заявке № 461974/40 от 25 июля 1956 г. Бюллетень изобретений, 1962, № 9.
62. Бычков С. И. Спектры одиночных радиопульсов при изменении несущей частоты. «Радиотехника», 1950, т. 5, № 1, стр. 42—53.
63. Клаудер, Прайс, Дарлингтон, Элберзгайм. Теория и расчет импульсных радиолокационных станций с частотной модуляцией. ЗРЭ, 1961, № 1, стр. 15—49.
64. Уорд. Анализ сжимающих фильтров с произвольной длительностью импульсного отклика. ТИИЭР, 1966, т. 54, № 4, стр. 281—283.
65. Krönert R. Impulsverdichtung. «Nachrichtentechnik», 1957, № 4, S. 148—152 und № 7, S. 305—308.
66. Справочник по радиотехнике, под ред. Б. А. Смирнина. Госэнергоиздат, 1950.
67. Мюллер, Гудвин. Широкополосный приемник со сжатием импульсов для разведки в сантиметровом диапазоне волн. ЗРЭ, 1963, № 3, стр. 29—44.
68. Эвелет. Обзор ультразвуковых линий задержки, работающих на частотах ниже 100 Мгц. ТИИЭР, 1965, т. 53, № 10, стр. 1588—1613.
69. Steward K. W. F. A practical dispersive network system. The Marconi Review, 1965, vol. 28, № 159, p. 254—272.
70. Meeker T. R. Dispersive ultrasonic delay lines using the first longitudinal mode in a strip. IRET, 1960, vol. UE-7, № 2, p. 53—58.
71. Fitch A. H. Synthesis of dispersive delay characteristics by thickness tapering in ultrasonic strip delay lines. Journal of Acoustical Society of America, 1963, vol. 35, № 5, p. 709—714.
72. Гор. Техника сжатия импульсов с большим произведением длительности на ширину спектра. ЗРЭ, 1963, № 12, стр. 31—38.
73. Тимис, Сайтрип, Лэвиола. Блок сжатия импульсов для РЛС сопровождения. ЗРЭ, 1964, № 11, стр. 26—40.
74. Фадеева В. Н., Терентьев Н. Н. Таблицы значений интеграла вероятностей от комплексного аргумента. Гостехиздат, 1954.
75. Хургии Я. И., Яковлев В. П. Методы теории целых функций в радиофизике, теории связи и оптике. Физматгиз, 1962.
76. Тимс. Коррекция боковых лепестков в канале дальности радиолокационной станции со сжатием импульсов. ЗРЭ, 1963, № 5, стр. 23—34.
77. Ди Франко, Рубин. Анализ искажений при обработке радиолокационного сигнала. ЗРЭ, 1963, № 9, стр. 35—50.
78. Cook C. E. Effect of phase-modulation errors on pulse compression signals. ICR, 1962, pt. 4.

79. Groginsky H. L., Wilson L. R. Effect of phase errors on pulse compression system. IRET, 1962, vol. IT-8, № 4, p. 321.
80. Bernfeldt M., Cook C. E., Paolillo J., Palmieri C. A. Matched filtering, pulse compression and waveform design. Microwave Journal, pt. II, 1964, vol. 7, № 10, p. 57—64; pt. 2, 1964, vol. 7, № 11, p. 81—90, pt. 3, 1967, vol. 7, № 12, p. 70—76; pt. 4, 1965, vol. 8, № 1, p. 73—81.
81. Рамп, Уингров. Принципы сжатия импульса. ЗРЭ, 1962, № 9, стр. 15—26.
82. Вакман Д. Е. Асимптотические методы в линейной радиотехнике. Изд-во «Советское радио», 1962.
83. Рихачек. Точность определения дальности с помощью импульсных сигналов с линейной ЧМ. ТИИЭР, 1965, т. 53, № 4, стр. 475—476.
84. Вакман Д. Е. Сложные сигналы и принцип неопределенности в радиолокации. Изд-во «Советское радио», 1965.
85. Зиберт В. Общие закономерности обнаружения целей при помощи радиолокации. «Вопросы радиолокационной техники», 1957, № 5 (41), стр. 3—35.
86. Кокэн, Цу. Теория и рабочие характеристики дифракционных линий задержки с перпендикулярными решетками. ТИИЭР, 1965, т. 53, № 6, стр. 674—684.
87. Кук. Повышение эффективности радиолокационных устройств за счет сжатия импульса. ЗРЭ, 1960, № 9, стр. 38—49.
88. Barker R. H. Group synchronizing of binary digital system. Book «Communication theory», edited by W. Jackson, London, Butterworth scientific publications, 1953, p. 273—287.
89. Турин Р. К. К вопросу о кодах Баркера четной длины. ТИИЭР, 1963, т. 51, № 9, стр. 1251—1252.
90. Иванова И. М., Кетков Ю. Л., Ямпольская Т. С. О существовании кодов Баркера. «Известия вузов», Радиофизика, 1960, т. 3, № 5, стр. 911—913.
91. Лезин Ю. С. О вычислении амплитудных спектров сложных сигналов с известной автокорреляционной функцией. «Электро-связь», 1966, № 9, стр. 62—66.
92. Градштейн И. С., Рыжик И. М. Таблицы интегралов, сумм, рядов и произведений. Физматгиз, 1962.
93. Хаффмен Д. А. Синтез линейных многотактных кодированных схем. В сб. «Теория передачи сообщений», под ред. В. И. Си-форова. Изд-во иностранной литературы, 1957, стр. 52—81.
94. Питерсон У. Коды, исправляющие ошибки. Изд-во «Мир», 1964.
95. Abramson N. M. A class of systematic codes for non independent errors. IRET, 1959, vol. IT-5, № 4, p. 150—157.
96. Golomb S. W., Baumert L. D., Easterling M. F., Stiller J. J., Viterbi A. J. Digital communication with space applications. Prentice-Hall, Inc., Englewood Cliffs, New-York, 1964.
97. Мешковский К. А., Кирялов Н. Е. Кодирование в технике связи. Связьиздат, 1966.
98. Виноградов И. М. Основы теории чисел. Гостехиздат, 1953.
99. Китов А. И., Криницкий Н. А. Электронные цифровые машины и программирование. Физматгиз, 1963.

100. Аллен, Уэстерфилд. Цифровые корреляторы со сжатием во времени и согласованные фильтры для активной гидролокации. ЗРЭ, 1964, № 12, стр. 32—62.
101. Кор. Кручфилд, Мергиз. Импульсная УКВ станция, использующая шумоподобные сигналы. ЗРЭ, 1966, № 4, стр. 20—31.
102. Ван Блэркэм, Сэрс, Фримэн. Анализ и моделирование приемника псевдощумовых сигналов с дискретным согласованным фильтром. ЗРЭ, 1968, № 1, стр. 57—71.
103. Кэн. Отношение сигнал/помеха в полосовых ограничителях. ЗРЭ, 1961, № 8, стр. 37—45.
104. Черняк Ю. Б. О линейных свойствах системы широкополосный ограничитель — фильтр. Р и Э, 1962, т. 7, № 7, стр. 1073—1076.
105. Черняк Ю. Б. Чувствительность, точности, разрешающая способность многоканального приемника с широкополосным ограничителем. Р и Э, 1962, т. 7, № 8, стр. 1302—1310.
106. Lerner R. M., Reiffen B., Sherman H. Delay-line specifications for matched-filter communications systems. IRET, 1959, vol. CP-6, № 4, p. 263—268.
107. Lerner R. M. A matched filter detection system for complicated Doppler shifted signal [5], p. 373—385.
108. Варакин Л. Е. Определение допусков на параметры согласованного фильтра. ТУИС, 1964, № 20, стр. 150—158.
109. Варакин Л. Е. Увеличение боковых лепестков на выходе согласованного фильтра при рассогласованиях. ТУИС, 1965, № 27, стр. 107—111.
110. Фишбейн, Риттенбэч. Корреляционная радиолокационная станция с псевдощумовой модуляцией. ЗРЭ, 1962, № 5, стр. 28—46.
111. Craig S. E., Fishbein W., Rittenbach O. E. Continuous-wave radar with high range resolution and unambiguous velocity determination. IRET, 1962, vol. MIL-6, № 2, p. 153—161.
112. Франк. Многофазные коды с хорошими непериодическими корреляционными свойствами. ЗРЭ, 1963, № 12, стр. 39—44.
113. Лурин. Метод цифрового сжатия импульса, использующий многофазные коды. ТИИЭР, 1963, т. 51, № 9, стр. 1258—1260.
114. Лезин Ю. С. Об оптимальных фильтрах для последовательностей импульсных сигналов. «Научные доклады высшей школы», Р и Э, 1958, № 3, стр. 20—24.
115. Рамлау П. Н. О частотных спектрах повторяющихся сигналов. А и Т, 1941, № 1, стр. 33—42.
116. Джордж С., Заманакос А. Гребенчатые фильтры в импульсных радиолокационных станциях. «Вопросы радиолокационной техники», 1955, № 1 (26), стр. 58—69.
117. Цыпкин Я. З. Теория импульсных систем. Физматгиз, 1968.
118. Макфарлан А. Анализ гребенчатых фильтров. ЗРЭ, 1960, № 10, стр. 87—111.
119. Фиксельштейн М. И. Гребенчатые фильтры. Изд-во «Советское радио», 1966.
120. Фиксельштейн М. И. Переходные процессы в гребенчатых фильтрах. «Радиотехника», 1967, т. 12, № 7, стр. 63—68.

121. Казаринов Ю. М., Толоконников С. В., Медыцев Л. Н. Расчет оптимальных параметров синхронного фильтра. «Известия вузов», Радиотехника, 1960, т. 3, № 1, стр. 49—59.
122. Лезин Ю. С. Сравнение систем многократного и двухэтапного накопления импульсных сигналов по эффективности. «Известия вузов», Радиоэлектроника, 1968, т. 9, № 6, стр. 13—17.
123. Лейхтер Л. Е. Многозвенное накопительное устройство импульсных сигналов. Авторское свидетельство № 144529 с приоритетом от 29.10.60 г.
124. Лезин Ю. С. Эффективность системы двухэтапного накопления импульсных сигналов. Р и Э, 1966, т. 11, № 1, стр. 25—31.
125. «Пороговые сигналы», пер. с англ., под ред. А. П. Сиверса. Изд-во «Советское радио», 1951.
126. Сегал Б. И., Семендяев К. А. Пятизначные математические таблицы. Физматгиз, 1959.
127. «Таблицы вероятностных функций», пер. с англ. Л. С. Барк, т. 1. ВЦ АН СССР, 1958.
128. Сиверс А. П. Радиолокационные приемники. Расчет и проектирование. Изд-во «Советское радио», 1959.
129. Бунимович В. И. Флюктуационные процессы в радиоприемных устройствах. Изд-во «Советское радио», 1951.
130. Барк Л. С., Большев Л. Н., Кузнецов П. И., Черенков А. П. Таблицы распределения Релея—Райса. ВЦ АН СССР, 1964.
131. Бунимович В. И. Приближенное выражение вероятности правильного обнаружения при оптимальном приеме сигнала с неизвестной фазой. Р и Э, 1958, т. 3, № 4, стр. 552—554.
132. Крамер Г. Математические методы статистики. Изд-во иностранной литературы, 1948.
133. Шварц М. Влияние флюктуаций сигнала на обнаружение импульсных сигналов в шуме. В сб. [199], стр. 232—245.
134. Сверлинг П. Вероятность обнаружения флюктуирующих целей. ЗРЭ, 1960, № 10, стр. 29—32.
135. Галвин. Система последовательного выделения радиолокационного сигнала. «Труды института радиотехников», 1961, т. 49, № 9, стр. 1643—1651.
136. Кобзарев Ю. Б., Вашаринов А. Е. Об эффективности алгоритмов поиска, основанных на методе пробных шагов управляемой длительности. Р и Э, 1961, т. 6, № 9, стр. 1411—1419.
137. Вашаринов А. Е., Флейшман Б. С. Методы статистического последовательного анализа и их радиотехнические приложения. Изд-во «Советское радио», 1962.
138. Эрих. Стейнберг. Панорамный анализатор спектра в реальном времени. ЗРЭ, 1960, № 1, стр. 3—12.
139. Соловьев И. В., Свириденко С. С. Новые методы спектрального анализа сигналов (обзор). ЗРЭ, 1961, № 8, стр. 3—36.
140. Brokner E. Synthesis of an arbitrary bank of filters by means of a time-variable network. ICR, 1961, pt. 4, p. 221—235.
141. Ellis R. E., Rohlfman W. C. Amplitude-modulated video integrator. ICR, 1959, pt 5, p. 263—271.
142. Сифоров В. И. Радиоприемники сверхвысоких частот. Воениздат, 1957.
143. Моруги Л. А. Импульсные устройства с запаздывающей обратной связью. Изд-во «Советское радио», 1961.

144. Крылов А. Н. Лекции о приближенных вычислениях. Гостехиздат, 1954.
145. Моругин Л. А. Накопление импульсных сигналов в устройствах с задержанной обратной связью при исключении времени эффективного запаздывания. Р и Э, 1962, т. 7, № 3, стр. 391—396.
146. Лезин Ю. С. Накопление шумов в устройствах с задержанной обратной связью. Р и Э, 1961, т. 6, № 2, стр. 187—192.
147. Лезин Ю. С. Еще раз о накоплении шумов в устройствах с задержанной обратной связью. Р и Э, 1962, т. 7, № 5, стр. 917—918.
148. Лезин Ю. С. Влияние параметров накопительных устройств на эффективность их работы. Р и Э, 1961, т. 6, № 4, стр. 529—535.
149. Лезин Ю. С. Об эффективности системы из частотного фильтра и накопительного устройства с задержанной обратной связью. Р и Э, 1962, т. 7, № 1, стр. 39—45.
150. Лезин Ю. С. Эффективность накопительной системы при любом числе импульсных сигналов. Р и Э, 1964, т. 9, № 6, стр. 966—974.
151. Харкевич А. А. Спектры и анализ. Гостехиздат, 1957.
152. Urkowitz H. Delay-line secondary responses in AM and FM sweep integrators. JFI, 1960, vol. 269, № 1, p. 1—23.
153. «Ламповые схемы для измерения времени», пер. с англ. под ред. А. Я. Брейтбарта, ч. 2. Изд-во «Советское радио», 1951, стр. 247.
154. Бакулев П. А. Радиолокация движущихся целей. Изд-во «Советское радио», 1964.
155. Сколник М. Введение в технику радиолокационных систем. Изд-во «Мир», 1965.
156. Бугров Г. М., Лезин Ю. С. Прохождение импульсного сигнала и шума через систему из частотного фильтра и двух накопительных устройств с задержанной обратной связью. ТГПИ, 1962, т. 18, № 2, стр. 33—41.
157. Лезин Ю. С., Бугров Г. М. О целесообразности применения второго накопительного устройства. Р и Э, 1963, т. 8, № 8, стр. 1355—1360.
158. Cooper D. C., Griffiths I. W. R. Video integration in radar and sonar systems. The Journal of the British Institution of Radio Engineers, 1961, vol. 21, № 5, p. 421—433.
159. Кузнецов П. И., Стратонович Р. Л., Тихонов В. И. Прохождение некоторых случайных функций через линейные системы. А и Т, 1963, т. 14, № 2, стр. 144—163.
160. Поляк Ю. В., Кельзон В. С. К теории обнаружения периодических импульсных сигналов в гауссовом шуме при некогерентном накоплении. Р и Э, 1958, т. 3, № 6, стр. 764—769.
161. Каплан Е. Л. Исследование обнаружения сигналов и некоторые применения. В сб. [199], стр. 191—231.
162. Маркум. Статистическая теория обнаружения целей импульсной радиолокационной станцией. ЗРЭ, 1960, № 10, стр. 3—10.
163. Трубацки Е. Г. Последетекторное интегрирование в радиолокационных станциях. ЛКВВИА им. А. Ф. Можайского, 1957.
164. Лезин Ю. С. О пороговых сигналах при некогерентном накоплении с экспоненциальной весовой функцией. Юбилейный сб. «100 лет со дня рождения А. С. Попова». Изд-во АН СССР, 1960.

165. Лезин Ю. С. О некогерентном накоплении с экспоненциальной весовой функцией. «Известия вузов», Радиотехника, 1961, т. 4, № 2, стр. 148—154.
166. Конт орови ч М. И. Операционное исчисление и нестационарные явления в электрических цепях. Гостехиздат, 1949, стр. 171.
167. Лезин Ю. С. О законе распределения случайных напряжений на выходе квадратичного накопителя с экспоненциальной весовой функцией. ТГПИ, 1960, т. 16, № 2, стр. 79—81.
168. Лезин Ю. С. Жуков О. В. Об интегральной функции распределения шума на выходе квадратичного экспоненциально-весового накопительного устройства. ТГПИ, 1962, т. 18, № 2, стр. 42—45.
169. Слуцкий Е. Е. Таблицы для вычисления неполной Γ -функции и функции вероятностей χ^2 . Изд-во АН СССР, 1950.
170. Pachages J. A table of bias level useful in radar detection problems. IRET, 1958, vol. IT-4, № 1, p. 38—45.
171. Митропольский А. К. Техника статистических вычислений. Физматгиз, 1961.
172. Tables of the error function and of its first twenty derivatives. Harvard University press, Combridge, Massachusetts, 1952.
173. Лезин Ю. С. О распределении случайных напряжений на выходе некогерентного накопительного устройства с экспоненциальной весовой функцией. «Известия вузов», Радиотехника, 1960, т. 3, № 6, стр. 592—597.
174. Маркум. Математическое приложение к статистической теории обнаружения цели импульсной радиолокационной станцией. ЗРЭ, 1960, № 10, стр. 11—30.
175. Деч Р. Нелинейные преобразования случайных процессов, пер. с англ., под ред. Б. Р. Левина. Изд-во «Советское радио», 1965.
176. Дунин-Барковский И. В., Смирнов Н. В. Теория вероятностей и математическая статистика в технике. Гостехиздат, 1965.
177. Питерсон В. В., Бердсал Т. Дж., Фокс В. К. Теория обнаружения сигналов. В сб. «Теория информации и ее приложения», под ред. А. А. Харкевича. Физматгиз, 1959, стр. 210—274 и в сб. переводов (198), стр. 85—151.
178. Лезин Ю. С., Штернов А. А. О некогерентном экспоненциально-весовом накоплении последовательностей импульсных сигналов с непрямоугольной огибающей. «Радиотехника», 1964, т. 19, № 4, стр. 46—51.
179. Лещинский М. М. К определению вероятностных характеристик сложных некогерентных накопителей. Р и Э, 1968, т. 13, № 1, стр. 51—60.
180. Лещинский М. М. Статистические характеристики двухкратного некогерентного накопителя. ТГПИ, 1968, т. 24, № 1, стр. 50—54.
181. Emerson R. C. First probability densities for receivers with square law detectors. JAP, 1963, vol. 34, № 2, p. 1168—1178.
182. Крайзер Л. П. Устройства хранения дискретной информации. Госэнергоиздат, 1961.
183. Кволя М., Казан В. Электронно-лучевые трубки с накоплением зарядов, пер. с англ., под ред. М. М. Вейсбека. Госэнергоиздат, 1966.

184. Раков В. И. Индикаторные устройства радиолокационных станций. Судпромгиз, 1962.
185. Фельдбаум А. А. Вычислительные устройства в автоматических системах. Физматгиз, 1959.
186. Иоффе А. Ф. Применение магнитной записи. Госэнергоиздат, 1959.
187. Уинклер С., Нозик С. Ограничение применений электронно-лучевых трубок с накоплением, обусловленное помехами. «Вопросы радиолокационной техники», 1955, № 1, стр. 18—28.
188. Соколинский А. Г., Сухаревский Ю. М. Магнитные ультразвуковые линии задержки. Изд-во «Советское радио», 1966.
189. Baumann R. H. Transposition frequency-times pour la mesure d'une fréquence inconnue. «Annales de radioelectricite», pt. 1, 1960, t. 15, № 62, p. 309—329; pt. 2, 1961, t. 16, № 63, p. 69—92.
190. Cooper D. C. Delay line secondary responses, JFI, 1960, vol. 270, № 5, p. 397—400.
191. Фаулер, Уззо, Равин. Обработка сигналов обзорного радиолокатора. ЗРЭ, 1962, № 3, стр. 55—66.
192. Циммерман, Эрих, Сунстейн. Рециркулятор на линии задержки с длительной памятью. ЗРЭ, 1960, № 1, стр. 13—23.
193. Urkowitz H. Delay line secondaries in phasemodulated sweep integrators. IEEE Transaction, 1965, vol. MIL-9, № 3—4, p. 189—196.
194. Бенджамин. Последние достижения в технике генерирования и обработки радиолокационных сигналов. ЗРЭ, 1965, № 7, стр. 22—48.
195. Stanek M. Optimalni filtrace impulsovych signalu. «Slaboproudny obzor», 1964, sv. 25, čís. 5, L. 37.
196. Мей Дж. Волноводные ультразвуковые линии задержки. В кн. [200], стр. 488—565.
197. Мэзон У. Ультразвуковые линии задержки с многократными отражениями. В кн. [200], стр. 566—585.
198. «Прием импульсных сигналов в присутствии шумов», пер. с англ., под ред. А. Е. Башаринова и М. С. Александрова. Госэнергоиздат, 1960.
199. «Прием сигналов при наличии шума», пер. с англ., под ред. Л. С. Гуткина. Изд-во иностранной литературы, 1960.
200. «Физическая акустика», т. 1. Методы и приборы ультразвуковых исследований, ч. А, под ред. У. Мэзона, пер. под ред. Л. Д. Розенберга. Изд-во «Мир», 1966.
201. Морозов В. А., Трунова З. Г. Анализатор слабых сигналов, использовавшийся при радиолокации Венеры в 1961 г. Р и Э, 1962, т. 7, № 11, стр. 1881—1889.
202. Ключев Н. Ф. Обнаружение импульсных сигналов с помощью накопителей дискретного действия. Изд-во «Советское радио», 1963.
203. Кузьмин С. З. Цифровая обработка радиолокационной информации. Изд-во «Советское радио», 1967.
204. Седякин Н. М. Элементы теории случайных импульсных потоков. Изд-во «Советское радио», 1965.
205. Харрингтон Д. В. Исследование обнаружения повторяющихся сигналов в шуме при помощи двойного накопления. В сб. [199], стр. 246—268.

206. Ицхоки Я. С., Овчинников Н. И., Фирсов Л. П. Логические схемы устройства первичной обработки радиолокационной информации. Изд-во ВВИА им. проф. Н. Е. Жуковского, 1963.
207. Диннин Г., Рид И. Исследование обнаружения и локализации сигналов при помощи счетчиков. В сб. [199], стр. 269—293.
208. Феллер В. Введение в теорию вероятностей и ее приложения, пер. с англ., под ред. Е. Б. Дынкина. Изд-во иностранной литературы, 1952.
209. Тихонов В. И. О выбросах флуктуаций и их коррелированности. «Электросвязь», 1957, № 6, стр. 10—14.
210. Лешинский М. М. Средняя частота ложных тревог при реализации логической схемы « $k/r-a$ » на ЦВМ. ТГПИ, 1967, т. 23, вып. 5 (90), стр. 35—37.
211. Лезин Ю. С. О критичности структуры оптимального фильтра к случайным вариациям амплитуды и фазы сигнала. Сб. докладов «Третья конференция по теории передачи и кодирования информации» (секция 4), 1967, стр. 67—72.
212. Москва. Уменьшение уровня боковых лепестков в РЛС со скачком фазоманипулированного сигнала. ЗРЭ, 1968, № 3, стр. 68—74.
213. Гоноровский И. С. Радиотехнические цепи и сигналы, ч. 2. Изд-во «Советское радио», 1967.
214. Вакман Д. Е. Регулярный метод синтеза ФМ сигналов. Изд-во «Советское радио», 1967.
215. Bagley G. C. Radar pulse-compression by random phase coding. Radio and Electronic Engineer, 1968, vol. 36, № 1, p. 5—15.
216. Пантелеев Ю. В. О вычислении порога решающего устройства в многоканальных схемах обнаружения сигналов при экспоненциально-весовом накоплении. ТГПИ, 1968, т. 24, вып. 5, стр. 47—49.
217. Пантелеев Ю. В. Выигрыш в отношении сигнал/шум при экспоненциально-весовом накоплении многочастотных радиолокационных сигналов. ТГПИ, 1968, т. 24, вып. 6, стр. 38—40.
218. Лешинский М. М. Определение объема запоминающего устройства обзорной РЛС с накоплением дискретного действия. ТГПИ, 1968, т. 24, вып. 1, стр. 55—58.
219. Белецкий А. Ф., Лебедев А. Т. Синтез согласованных фильтров на пассивных элементах. «Электросвязь», 1966, № 3, стр. 3—10.

A list of the notations together with their designations used in the preceding text is presented below. The chapter, paragraph and item in which these notations are introduced are indicated in the parentheses and a brief explanation of them is given. In some cases the notations have several interpretations and ambiguity is eliminated in the text where these notations are used. Many of the notations are found throughout the book, whereas others (mainly not presented in this list) are either generally accepted and therefore obvious or have limited use within one section.

- $A(t)$ — transfer function (2.3.1).
- a — half of spectral white noise intensity (1.2).
- B — power gain in signal/noise ratio compared to optimum filter for single signal (5.4.1); storage effect (10.3.3).
- b — product of bandpass by pulse length (2.5) and (7.4).
- C — constant multiplier (1.3).
- D — probability of correct detection (1.2); compression coefficient of linear frequency-modulated pulse (3.2).
- D_M — dynamic range of storage device (11.4).
- d — read level of pulse response of filter and of its bandpass (7.1).
- d_i — elements of Barker's code (4.1.1) and binary pseudo-random sequence (4.2.1).
- E — signal energy (1.2).
- $E(x)$ — whole part of number x (2.2.2).
- F — probability of false alarm (1.2) and Doppler frequency (3.8) and (6.5.1).
- $F(\omega)$ — energy spectrum or spectral intensity of noise (1.2).
- G — loss in signal/noise ratio (2.4.2).
- g — transfer coefficient of peak value of signal (3.3.2) and (7.2); signal storage coefficient (5.4.2).
- $g_c(g_w)$ — probability that signal-noise mixture (or noise) will not exceed quantification threshold (12.2).

$\bar{H}(t)$	— complex amplitude of pulse characteristic (1.3).	
h_n	— probability of absence of recursion event in first n tests (12.4).	
$h(t)$	— pulse characteristic (1.3).	
$\bar{K}(\omega)$	— transfer function of filter (1.5).	
$K(\omega)$	— amplitude-frequency characteristic of filter (1.5).	
k	— asymmetry coefficient (10.3.1); number of ones in n samples of random quantified voltage (12.2).	
" $k/n-1$ "	— logic detection criterion (12.3).	432
L	— total number of memory cells (12.5).	
$L_k^{\bar{a}}(x)$	— generalized k -order Laguerre polynomial (10.3.2).	
l	— relative response threshold of threshold device (1.3) and (10.2); number of zeros with digital detection required to make decision on end of signal detection (10.3).	
M	— ratio of length of delay in second and first recirculators of two-stage storage device (5.4.4) and (9.1); number of range circles with digital detection (12.2); number of ZU-1 cells (12.5).	
m	— recirculator feedback coefficient (5.4.1).	
m_{nk}	— initial n -order moment of voltage distribution u_k (1.2) and (10.4.1).	
$m_1(x)$	— mean value of random value x (1.2).	
N	— number of pulsed signals in sequence (5.1.2); number of elements of Barker code (4.1.1), number of period of binary pseudorandom sequence (4.2.1) and number of multiphase code (4.3).	
N_a	— active number of stored pulses (5.4.1).	
n	— ratio of bandpasses of prestorage filter and recirculator feedback circuit (7.1).	
$n_k(t)$	— instantaneous value of noise voltage at point k of block diagram (1.2).	
$P(U)$	— integral probability distribution function (10.3.2).	
$P_C(P_W)$	— probability of signal-noise mixture (or noise) exceeding quantification threshold (12.2).	
Q	— noise output transfer coefficient (2.3.4) and (5.4.1), noise output storage coefficient (7.3).	
q	— ratio of peak value of signal to effective value of noise (1.2) and (7.2).	

R	— additional gain in signal/noise ratio (5.4.4).
$R(x)$	— fractional part of number x (2.2.2).
$R_a(t),$ $R_B(t)$	— auto- and cross-correlation functions of noise (1.2).
$r(t)$	— normalized correlation function of noise (2.3.3).
$\bar{S}(\omega)$	— spectral density of signal (1.5).
$S(\omega)$	— amplitude spectrum of signal (1.5).
T	— repetition quasi-period of pulsed signals (5.1.2).
U_0	— response threshold voltage of threshold device (1.2).
$u_k(t)$	— instantaneous value of voltage at point k of block diagram (1.2).
$V_k(t)$	— signal amplitude at point k of block diagram (1.3).
$v_k(t)$	— instantaneous value of signal voltage at point k of block diagram (1.2).
$v(t, \tau)$	— bell pulse (7.1).
$W(u)$	— probability distribution density of voltage u (1.2) and (10.2).
α	— parameter of bell filter (3.6) and (10.2).
β	— time constant of integrating device (2.3.1) or of amplifier (2.5).
β_k	— mean square value of noise frequency n_k (10.2).
$\Gamma(x)$	— γ -function (10.3.2).
γ	— relative value of side blip of signal (3.6); excess coefficient (10.3.1).
Δ	— time corresponding to width of range circle during digital processing (12.3).
ΔF	— amplifier (2.5) or filter (3.6) and (7.1) bandpass; frequency resolution of system (3.9).
$\Delta\omega$	— frequency deviation (3.2); frequency shift in recirculator circuit (6.5.2).
$\delta(t)$	— single pulse (1.3) and (7.1).
ϵ_k and ϵ_1	— criteria of beginning and end of signal detection (12.3).
η^2	— mean output of fluctuating signal (6.4.1).
θ	— average number of tests until appearance of event (12.4).
ϕ	— average number of occupied ZU-2 cells (12.5).
x_{nk}	— n -order voltage distribution cumulant u_k (10.3.1).

Λ	— similarity ratio (1.2).
λ	— mean pulse recurrence frequency of flow (12.4).
λ_0	— mean wavelength (3.8).
μ_k	— weight multipliers for processing frequency-modulated signal (3.6).
ν	— frequency of false alarms (10.2) and (12.4).
ξ	— coefficient of exponential weight function of storage device (10.1.2).
ρ^2	— ratio of mean outputs of fluctuating signal and noise (6.4.1).
σ^2	— frequency difference (output) of noise (1.2).
τ	— length of pulsed signal (1.4) and (2.1.2).
τ_0	— length of elementary pulse of complex signal (4.1.1) and (4.2.1).
$\Phi(x)$	— probability integral (1.2).
$\phi(x)$	— Euler function in number theory (4.2.1); Gauss function (10.3.2).
$\phi(\omega)$	— phase spectrum of signal (1.5).
χ	— angle of phase rotation of by phase-shifting device (2.2.2) and (6.5.2).
$\psi(t, F)$	— joint correlation function of signal modulation (3.9).
$\psi_0(t)$	— normalized autocorrelation function of complex envelope of signal (4.1.1).
$\psi(\omega)$	— phase characteristic of filter (1.5).
Ω	— angular Doppler frequency (6.5.1).

Abbreviations Used in Text and on Block Diagrams

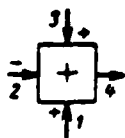
AD	— amplitude detector.
BM	— balanced modulator.
VIRU	— highly selective tuned amplifier.
VKU	— cross-correlation device.
VS	— time selector.
G(GVCh)	— high-frequency generator.
GOI	— single video pulse generator.
GTI	— timing pulse generator.
DULZ	— dispersion ultrasonic delay line.
KV	— square-law generator.
KVD	— square-law detector.

KGD	— coherent detector.
LZ	— delay line.
NIS	— pulsed signal storage device.
NU	— video frequency storage device.
OF	— optimum filter.
OFOP	— video frequency optimum filter for envelope of pulsed signal sequence.
PU	— threshold device.
RNU	— radio-frequency storage device.
ROFOP	— radio-frequency optimum filter for envelope of pulsed signal sequence.
ROFOS	— radio-frequency optimum filter for single pulsed signal.
RF	— radio-frequency filter.
Sm	— frequency mixer.
T	— flip-flop.
UO	— limiting amplifier.
F	— filter.
D	— differentiating device.

Notations of Block-Diagram Components Used in Figures



Integrating device.



Adder of voltages taken with indicated signs ($u_4 = u_1 + (-u_2) + u_3 = u_1 - u_2 + u_3$).



Subtraction device.



Nonequivalence circuit (adder modulo 2).

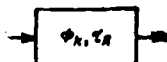
43



Delay device by time t_s



Frequency generator f_k .



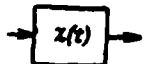
Filter F_k with length of pulse reaction τ_R .



Attenuator with transfer coefficient $m(m < 1)$.



Amplifier with amplification factor A .



Phase rotation device by angle $\chi(t)$.